



UNIVERSITÄT ZU LÜBECK
INSTITUT FÜR TECHNISCHE INFORMATIK

From the Institute of Computer Engineering
of the University of Lübeck

Director: Prof. Dr.-Ing. Erik Maehle

Robotic Rehabilitation After Stroke

A Modular System for Training Distal Upper Limb Functions

Dissertation
for Fulfillment of
Requirements
for the Doctoral Degree
of the University of Lübeck

from the Department of Computer Sciences

Submitted by

Patrick Weiß
from Düsseldorf (Germany)

Lübeck 2014

IM FOCUS DAS LEBEN

First referee: Prof. Dr.-Ing. Erik Maehle
Second referee: Prof. Dr.-Ing. Alexander Schlaefer
Date of oral examination: 16 January 2015

Approved for printing. Lübeck, 30 April 2015

Acknowledgements

Ich sage nur ein Wort: "Herzlichen Dank!"

(Horst Hrubesch)

Während meiner Promotion erfuhr ich von verschiedensten Seiten hilfreiche Unterstützung, ohne die diese Arbeit nicht solch einen positiven Verlauf genommen hätte. Mein Dank gilt all jenen, die mich bei der Durchführung der Promotion unterstützt haben, wobei einige Personen und Gruppen besonderer Erwähnung verdienen.

An erster Stelle danke ich meinem Doktorvater, Herrn Prof. Dr.-Ing. Erik Maehle, für das mir entgegengebrachte Vertrauen in den vergangenen Jahren und die mir eingeräumten Freiheiten bei der Bearbeitung des Promotionsthemas. Auch Prof. Dr. med. Thomas F. Münte und Prof. Dr.-Ing. Achim Schweikard danke ich für die Übernahme ihrer Rollen im Rahmen des Graduiertenprogramms. Weiterhin möchte ich den Physiotherapeuten des UKSH für die Rückmeldungen und vielen hilfreichen Informationen zur Verbesserung des Rehabilitationssystems danken.

Ein herzlicher Dank gilt auch meinen Kollegen, die für eine gute und kollegiale Stimmung gesorgt und in Diskussionen zur Lösung offener Fragestellungen beigetragen haben. Dabei möchte ich insbesondere den Kollegen danken, die mich beim Korrekturlesen unterstützt haben. Die Arbeit wurde weiterhin durch die tatkräftige Unterstützung einiger Studenten bereichert, denen ich an dieser Stelle auch vielmals danken möchte.

Since I did not write my thesis in my mother tongue, I am particularly thankful for the help of some of my native speaker friends. Their proofreading helped a lot to improve the quality of my work and further to advance my English proficiency.

My stay as a visiting researcher in Toronto was an amazing time and a valuable experience. I would like to thank Dr. Alex Mihailidis for giving me the opportunity to work at the exiting environment of Toronto Rehab with his team at IATSL, University of Toronto. Thanks to all for welcoming me warmly and supporting me in academic as well as private matters. Especially, I would like to thank Rosalie Wang who initiated the visit together with Jen Boger and supported me a lot before, during, and after my stay.

Um die Promotion gut zu überstehen ist auch das soziale Netz sehr wichtig. Dabei möchte ich mich bei allen Leuten bedanken, die die Zeit in Lübeck zu einer unvergesslichen gemacht haben. Insbesondere in den schwierigen Phasen war ich über die Unterstützung meiner engen Freunde sehr dankbar. Dazu gehört auch Hamid

Hadjar, der mir immer ein guter Freund war und sogar den weiten Weg aus München zum Besuch meiner Verteidigung gemacht hat.

Ein besonderer Dank geht an die deutsche Fußballnationalmannschaft, die in der Endphase meiner Promotion die Weltmeisterschaft in Brasilien gewonnen hat. Somit war die Zeit, die ich während der heißen Phase mit Fußball schauen verbracht habe, mehr als gerechtfertigt.

Auch meinem Vater möchte ich für das Korrekturlesen und die Geduld bei meiner vereinzelt verzweifelten Formulierungssuche danken. Aber viel mehr noch muss ich meinen Eltern über alles für die bedingungslose Unterstützung danken, die ich mein ganzes Leben erfahren habe. Ohne sie wäre ich niemals so weit gekommen und deswegen widme ich diese Arbeit meinen Eltern.

Zusammenfassung

Schlaganfall ist die führende Ursache für erworbene Behinderungen. Dabei besteht ein Bedarf an neuen Behandlungsmöglichkeiten für eine effektivere Rehabilitation bei akzeptablen Kosten. In der vorliegende Dissertation wird ein neuartiges Rehabilitationssystem beschrieben, das eine kostengünstige, portable und patientenspezifische robotische Rehabilitation ermöglicht und die traditionellen Therapiemöglichkeiten auch beim Einsatz in der Heimrehabilitation erweitert. Das entwickelte System ist modular aufgebaut und besteht aus zwei Hauptmodulen, welche das Training einer Vielzahl von wichtigen Bewegungen der distalen oberen Extremitäten ermöglichen, die üblicherweise nach einem Schlaganfall beeinträchtigt sind.

Das erste Modul namens m-ReS^R trainiert Supination/Pronation, Dorsalextension und fingerbezogene rotatorische Bewegungen. Die erste Designiteration umfasst die Implementierung einer Reibungs- und Trägheitskompensation und wurde in einer vorläufigen Studie zur Bestimmung wichtiger Parameter für die Anwendung eines Rehabilitationsparadigmas angewendet. Patienten- sowie Therapeutenrückmeldungen unterstützten die Weiterentwicklung. Maßgefertigte Elektronik erlaubt in der zweiten Iteration eine Verbesserung der Drehmomentmessung und -regelung. Ein damit verbundener Verzicht auf teure Kraftmomentensensoren reduziert die Systemkosten erheblich. Die hohe Flexibilität des modularen Aufbaus der Hard- und Software ermöglicht es, m-ReS^R für die Erweiterung eines Rehabilitationsroboters des Toronto Rehabilitation Institute anzupassen, um diesem einen weiteren Freiheitsgrad zu ermöglichen.

Das zweite Modul namens m-ReS^X ist ein Exoskelett, das sich auf das Training von Greifbewegungen und Feinmanipulation spezialisiert und eine innovative Parametrisierung zur Größenanpassung des Exoskeletts an Handformen beinhaltet. Die Einführung geeigneter Parameter in das CAD-Modell und die Verwendung von 3D-Druckern ermöglichen die Herstellung individualisierter Exoskelette. Präzise angepasst an die Anatomie des Benutzers können Fehlansichtungen reduziert werden ohne mühsame mechanische Anpassungsvorrichtungen verwenden zu müssen. Die Anpassungsqualität kann bereits vor dem 3D-Druck durch eine neuartige Evaluationsmethode untersucht werden. Neben einer quantitativen Untersuchung der Parametermessungen konnten Projektionen von 2D-Darstellungen der CAD-Modelle auf Bilder der Hände schon eine gute Abschätzung über das Endresultat liefern. Die erfolgreiche Vorevaluation wurde durch das Anprobieren der hergestellten Exoskelette an einer Schlaganfallpatientin und einem gesunden Probanden bestätigt. Desweiteren wurden verschiedene Gelenkwinkelsensoren evaluiert. Mit einem Maximalwert der Wurzeln der mittleren quadratischen Fehler aller Experimente von $1,89^\circ$ zeigte die

Evaluierung, dass die Sensoren sehr genau sind und sogar eine höhere Genauigkeit als ein spezialisierter Goniometer für die Gelenkwinkelmessung von Fingern aufweisen. Seilzüge werden zur Übertragung der Kraft von entfernt platzierten Motoren eingesetzt. Die Seilkraft kann akkurat geregelt werden, so dass Unterstützung und Widerstand auf die Finger an die Fähigkeiten der Patienten angepasst werden können. Dazu wurde ein Modell aufgestellt, um die Motorencoder zur Messung von Gelenkwinkeln einzusetzen. Um die Anzahl der kostenintensiven Aktoren zu reduzieren, wurde ein spezielles Getriebe entwickelt, das die Verteilung des Drehmoments von einem Motor auf vier Finger mit unabhängigem Bewegungstraining ermöglicht. Für dieses Erweiterungsmodul wurde ein Patent beantragt.

Abstract

Stroke is the leading cause of acquired disabilities, while new ways of treatment are needed to provide effective rehabilitation at acceptable costs. This thesis deals with the development of a novel modular system for inexpensive, portable, and patient-specific robotic rehabilitation, augmenting traditional therapy with a focus on home rehabilitation. The developed system consists of two main modules allowing for training several distal upper limb functions that are commonly impaired after stroke.

The first module called m·ReS^R focuses on training supination/pronation, dorsiflexion, and finger-focused rotational movements. The first design iteration was applied in a preliminary study to determine important parameters for a rehabilitation paradigm, improved backdrivability with a developed friction and inertia compensation, and provided feedback from patients and therapists. The gained experience was incorporated in the further development. Custom-made electronics in the second iteration improve the torque measurement and control, making it feasible to omit expensive force/torque sensors. The high flexibility and modularity of m·ReS^R's hard- and software allowed it to be applied for the enhancement of a robot for reaching training, developed at the Toronto Rehabilitation Institute, with an additional degree of freedom.

The second module m·ReS^X is an exoskeleton for grasping and pinching exercises, incorporating an innovative parametrization method for size customization. The introduction of parameters in the CAD model and the use of 3D printing allows to precisely fit individualized exoskeletons to different hand sizes, thereby reducing misalignment with the patients' unique anatomical features and avoiding tedious mechanical adjustments. The fitting quality could already be estimated before 3D printing with a novel pre-print evaluation. Apart from analyzing the measurement data, projected 2D representations of the models overlaid onto images of the hands already indicated the good fitting. This was confirmed with the manufactured exoskeletons fitted to both a stroke patient and a healthy subject. Furthermore, different sensor types were implemented and evaluated. With a maximum root-mean square error of 1.89°, the evaluation showed that the sensors are very accurate and even perform better than a specialized goniometer for joint angle measurements of the finger. Tendon-based transmission is used to transmit forces from remotely placed motors. The force on the cables can be accurately controlled to adapt the assistance or resistance to the patient's abilities. A model was developed to exploit the motor encoder measurements for an additional joint angle estimation. A special gearbox to distribute the torque of one motor to four fingers, reducing the number of expensive actuators while providing independent movement training, was developed and filed for patenting.

Contents

Acknowledgements	v
1 Introduction	1
1.1 Motivation	1
1.2 Aim	3
1.3 Structure of this work	4
2 Background and related work	7
2.1 Medical background	7
2.1.1 Stroke	7
2.1.2 Neuroplasticity	8
2.2 Anatomy of the hand	9
2.3 Rehabilitation of hand and wrist functions after stroke	10
2.3.1 Traditional stroke rehabilitation	10
2.3.2 Virtual reality rehabilitation	12
2.3.3 Robotic rehabilitation systems	12
2.3.4 Tests and scales for progress evaluation	18
2.4 Chapter conclusions	19
3 Concepts and requirements	21
3.1 Trainable movements	21
3.2 Exercise modes	22
3.3 Modularization of rehabilitation devices	23
3.3.1 Training of rotational movements (m·ReS ^R)	25
3.3.2 Actuated hand exoskeleton (m·ReS ^X)	25
3.4 Requirements	26
3.4.1 General requirements	26
3.4.2 Specific requirements for m·ReS ^R	29
3.4.3 Specific requirements for m·ReS ^X	30
3.5 Design process	31
4 Implementation of a Training Device For Rotational Hand Move- ments	33
4.1 Introductory system description	33
4.2 Actuation and sensing	33

4.2.1	Selection and dimensioning of the actuators	34
4.2.2	Torque measurement and control	37
4.2.3	Angle measurement and position control	39
4.3	Electronics	39
4.4	Friction and inertia compensation for improved backdrivability of m·ReS ^{R1}	43
4.5	Mechanical design	45
4.6	Extension modules and accessories	48
4.6.1	Passive Motion Cube	48
4.6.2	Handles	48
4.7	m·ReS ^{R2} -based extension of a rehabilitation robot at TRI	49
4.7.1	Toronto Rehabilitation Institute robotic rehabilitation system	49
4.7.2	Motivation for the extension module	50
4.7.3	Design and implementation of the extension module	50
4.7.4	Electronics and sensing	52
4.8	Discussion on iteration improvements	53
5	Implementation of parametrizable actuated hand exoskeletons	55
5.1	Introductory system description	55
5.2	Mechanical design	55
5.2.1	Base	56
5.2.2	Joints	56
5.2.3	Preliminary thumb design	57
5.2.4	Assembly	58
5.3	Parameterization	59
5.4	Actuation and transmission	61
5.4.1	Tendon-based transmission	62
5.4.2	Configurations to train different movements	63
5.4.3	Motor selection	64
5.4.4	Actuation module	65
5.5	Angle sensing	66
5.5.1	Hall-effect based angle sensing	67
5.5.2	Multi-pole magnet strip encoder for MCP joint angle sensing .	70
5.5.3	Motor encoder for angle estimation using Denavit-Hartenberg convention	71
5.6	Current limiting for force control	75
5.6.1	Current sensing	75
5.6.2	Current limiting	77
5.7	Two-stage differential gear for force distribution of one motor	78
5.8	Discussion on iteration improvements	82
6	Software and communication	85

6.1	Communication architecture	85
6.1.1	Communication hardware	85
6.1.2	Data transmission	87
6.1.3	Command set	89
6.2	Low-level microcontroller program	89
6.3	High-level software and graphical user interface	90
6.3.1	m·ReS GUI with C++ and Qt	91
6.3.2	Toronto Rehabilitation Institute extension GUI in Java	98
7	Evaluation and studies	101
7.1	Evaluation of m·ReS ^R	101
7.1.1	Friction and inertia compensation with m·ReS ^{R1}	101
7.1.2	Torque measurement and control	105
7.1.3	Preliminary study on the just noticeable difference with m·ReS ^{R1}	113
7.1.4	Clinical study with the extension module for the TRI rehabilitation robot	117
7.1.5	Application experience	118
7.2	m·ReS ^X	118
7.2.1	Tendon displacement measurements for angle estimation	119
7.2.2	Finger joint angle measurement accuracy using Hall effect based sensor	122
7.2.3	MCP joint angle measurement accuracy using a multi-pole magnetic strip encoder	126
7.2.4	Current Limiting for Force Control	129
7.2.5	Parametrization	134
7.2.6	Application Experience	137
8	Conclusion and future work	141
8.1	Conclusion	141
8.1.1	Training of rotational movements with the module m·ReS ^R	142
8.1.2	Grasping and pinching trained with the exoskeleton m·ReS ^X	143
8.2	Future Work	145
A	Abbreviations	149
B	Command set for communication	151
C	Parametrization measurements	153
C.1	Stroke patient	153
C.1.1	Unimpaired right hand	153
C.1.2	Impaired left hand	155
C.2	Healthy subject	i

List of Figures	iii
List of Tables	vii
Bibliography	ix

Chapter 1

Introduction

1.1 Motivation

Stroke belongs to the most common neurological diseases with 15 million people suffering a cerebrovascular accident worldwide each year. Of these, five million die and another five million are permanently disabled [142]. In Germany, stroke is the third most common cause of death (11.4%) after cardiovascular diseases and cancer. It is the leading cause of severe disabilities and need for caregiving [55].

Stroke leads to different impairments depending on which area of the brain is affected. Often, the upper limb is affected leading to significant problems in fine and gross motor skills. Hand impairments are among the most common deficits after stroke, occurring in approximately 60 % of the cases [135]. The hand is ubiquitously used in daily life, which is why impairments have a huge impact on the sufferer. Six months after stroke, about 65 % of patients are not able to incorporate the impaired hand into their usual activities [44]. Currently, even extensive therapeutic interventions in acute rehabilitation only achieve a low probability of regaining functional use of the impaired hand [94]. 15 % to 30 % of patients with stroke remain permanently disabled even with rehabilitation including intensive task-specific training and physical activity [105]. Initial treatment focuses foremost on walking whereas hands and fingers are mostly not recovered by the time the patients are dismissed [45].

After treatment in acute-care hospitals, patients are usually sent back home even if they have not recovered completely [45]. In the US, the current median length of stay in inpatient rehabilitation facilities is only 16 days [144]. Afterwards, rehabilitation centers provide ongoing training mostly in outpatient sites. However, the intensive and long-lasting care necessary can rarely be provided due to high cost and limited labor force. Current resources are unable to fulfill the intensity requirement for optimizing post-injury neuroplasticity [93], although it already absorbs a considerable proportion of healthcare budgets [15].

New ways of treatment are being developed to improve rehabilitation. Haptics and virtual reality technology can enhance patient attention and motivation and the instant feedback may help to exploit motor recovery through neuroplasticity [109]. The use of robotics further increases the rehabilitation possibilities, offering several advantages over traditional therapy. It enables longer training sessions while decreasing

the workload on therapists [151]. Sensors and actuators enhance training possibilities and allow for very precise progress measurement and instant intensity adaptations. Novel modes of exercise not currently available and more detailed studies on motor learning are, thus, enabled [156].

Robotic therapy was shown to be an effective tool in some applications [113, 117, 177]. Robots potentially improve and facilitate training, since treatment frequency and intensity correlate with the recovery [96, 172]. However, other studies could not clearly prove a positive effect of robotic therapy on the rehabilitation outcome [95]. A study by Lo et al. found no significant improvement over 12 weeks but did so over 36 weeks as compared with usual care but not with intensive therapy [107]. This shows the necessity for more research on motor therapy and robotic rehabilitation to increase effectiveness.

Even if robotic therapy shows only comparable results in outcome, robots can be a valuable tool for enhancement of the therapy. Specialized care centers provide effective therapy but only an insufficient amount can be given in most cases due to the high cost. More frequent therapy improves the results in terms of rehabilitation outcome, where patients receive more therapy per day for extended periods of time [39]. Therefore, a cost-effective extension of the therapy seems promising. Systems tailored for the home environment are a potential tool to reduce cost, facilitate virtual therapeutic visits, and motivate stroke survivors to engage in under-supervised therapeutic activity at levels necessary for motor learning and generalization to occur [74]. This environment is often characterized by low supervision of healthcare professionals and low extrinsic motivation. There is a need to improve semi-autonomous stroke therapy in home environments to deal with these circumstances. The rehabilitation approaches have to be affordable yet effective to maximize the independence of persons experiencing disability after stroke [73]. The goal is not to replace labor but to increase the amount of time and to enhance therapeutic possibilities. Cost-effective and portable systems are also an asset for rehabilitation centers, where they can accompany and extend traditional therapy with therapists. The findings of a survey for identifying clinical practices and design requirements for stroke rehabilitation robotics suggest that therapists would like to have a device that may be used both with the therapist in a clinical setting and for stroke survivors to use at home [111].

However, the majority of available systems are not suitable for home rehabilitation due to high cost, complexity in design and use, and a lack of portability [81]. High complexity is the reason why 75 % of recent research projects in hand rehabilitation have not even undergone any testing [11]. Therefore, the development of affordable rehabilitation systems for outpatient centers and low-cost solutions for domestic environments belong to current challenges [82].

The specificity of the rehabilitation training with respect to the deficits and desired functional outcomes has an impact on the recovery [90]. Therefore, robotic systems should allow to train different movements with adaptable assistance or resistance tailored to the patient's needs. Successful robotic upper arm therapy requires focus

not only on the proximal joints of the arm, but also on the distal joints of the hand for patients to perform activities of daily living (ADLs) [168].

Robotic rehabilitation may also be a valuable tool for progress evaluation. The success of a therapy is measured with a wide variety of scales and assessments. However, the tests performed by clinical staff are often lengthy and mostly require hours of training before a physiotherapist is competent in their use [35]. They are foremost based on subjective and qualitative metrics judged by the therapist and their results are often not easily communicated to other professionals who are rarely familiar with the test procedure [35]. Computer-aided rehabilitation may help to automate the documentation of patient performance. It can compute key values from the training data, achieving a means of progress evaluation. It could potentially measure outcome of dexterity of the paretic arm and hand, which is a measurement mostly not performed in studies reviewed by Kwakkel et al. [95]. Robotic rehabilitation quantifies the progress by giving objective feedback on the patient's performance in therapy, making it a valuable complement to functional progress tests.

In summary, robotic rehabilitation can be an effective and valuable tool for therapy. The objective sensors and actuators provide new ways of exploring rehabilitation paradigms, however, more research is necessary since many uncertainties exist on how motor learning works and which are the best techniques to be applied. The major focus of research of robotic rehabilitation has not been on forearm, wrist, and hand functions although they are often impaired after stroke and they are particularly important for performing activities of daily living. Furthermore, the literature reveals a lack of inexpensive hardware for rehabilitation, particularly portable systems for extending therapy to the home environment although it is a promising tool to provide extended training for better functional outcome and to reduce therapy cost. However, the increased complexity of training several movements works against the goal of a simple, inexpensive design.

1.2 Aim

The literature reveals that a cost-effective device that allows for patient-specific training of several movements with adaptable assistance or resistance focusing on the distal joints would be a valuable contribution to the state-of-the-art. This work intends to pave the way to inexpensive, portable and effective upper-limb robotic rehabilitation technology that can be deployed at home, augmenting traditional therapy. The system shall focus on the training of several hand and wrist functions that are commonly impaired after stroke. Besides being used as a training device on patients, it is intended to be a means of studying rehabilitation paradigms and deepening the understanding of motor learning.

The device shall be cost-effective while allowing for the training of several different movements. A modular design with small configurable components, relatively simple motor-gear-drives, and integrated sensors offers the advantage of faster and cheaper

design and manufacturing compared to complex multi-functional devices. In clinical use, they are potentially less prone to errors and easier to operate and set up. The functional distribution on different components may reduce complexity and, in a clinical setup, the individual modules can be used simultaneously by several patients. Moreover, by providing optional components, potential customers could choose the functionality according to their needs. Therefore, modularization is a promising path to be pursued.

1.3 Structure of this work

This work is structured as follows:

Chapter 1 describes the motivation and the aim of this work.

Chapter 2 provides more detailed information on stroke and its rehabilitation including traditional and robotic therapy. Furthermore, the section gives an overview of current approaches to improve stroke rehabilitation.

Chapter 3 contains the concepts and the requirements for the system to be developed. The concepts represent preliminary design considerations that narrow down the requirements that are set up afterwards. No details on the implementation are provided in this chapter.

Chapter 4 presents the implementation of the first module for training of rotational movements called $m\text{-ReS}^R$. It contains details on the different parts of the development like design, actuation, and sensing. The system is developed in two design iterations, which are described and compared in this chapter.

Chapter 5 describes the implementation of the second module called $m\text{-ReS}^X$, an exoskeleton for the training of grasping and pinching. The differences of the development iterations are compared within the sections dealing with different aspects of the design. A focus is on the parametrization of the exoskeletons, which is used for the adaptation to different hand sizes.

Chapter 6 unites the description of the software and communication implementation of both $m\text{-ReS}^R$ and $m\text{-ReS}^X$ due to a vast overlap in the architecture.

Chapter 7 presents the performance evaluation of both modules and a preliminary study with the first iteration of the rotational training module. This chapter includes the discussions of the results.

Chapter 8 summarizes the achievements and contributions to the field of rehabilitation robotics and provides a conclusion about this work. Finally, an outlook to future challenges is presented.

Chapter 2

Background and related work

2.1 Medical background

This thesis deals with a device intended for, but not limited to rehabilitation following a stroke. Therefore, basic background about this medical condition is given first. The subsequent subsection deals with plasticity, which is an important factor in stroke rehabilitation. Next, an anatomical background will help to display the complexity and biomechanics of the hand, which is important for the design of devices for training hand functions. Finally, traditional rehabilitation methods will be described, followed by virtual and robotic rehabilitation systems for the hand.

2.1.1 Stroke

Cerebral Vascular Accident (CVA), also referred to as stroke, occurs when the blood supply to the brain or other regions of the central nervous system is interrupted. This interruption causes some parts of the brain to not receive sufficient oxygenated blood, leading to neuronal death in that region [109]. Although stroke usually occurs in the brain, occurrence in other regions of the central nervous system like the spinal cord is possible [199]. Stroke is classified into two major categories: ischemic and hemorrhagic. The most common kind is ischemic stroke, responsible for 80 % to 85 % of the cases [157], which is caused by a disturbance in the blood supply. The resulting oxygen shortage leads to necrosis of brain tissue and dysfunction of the affected area. The second kind is the hemorrhagic stroke, which can be accounted for around 15 % of the cases [157]. It is inflicted by an accumulation of blood either within the brain or within the skull but outside of the brain. The increased blood pressure harms the blood vessels, eventually leading to rupture. The internal hemorrhaging destroys and displaces brain tissue leading to dysfunction.

In 2005, stroke caused an estimated 5 - 7 million deaths, and without intervention, the number of global victims is projected to rise to 7-8 million in 2030 [176]. The incidence rate per year between 1994 and 1996 was 134 out of 100,000 inhabitants [87]. In Germany alone, there occur around 196,000 new and 66,000 recurring strokes each year based on data from 2008 [63]. For specialized treatment, 163 certified stroke

units exist with a total of 950 beds. However, only 45 % to 50 % of affected persons are treated in a stroke unit [63].

After cardiovascular diseases and cancer, stroke is the most common reason for death and leads to more long-term disability than any other disease process [42]. A number of neurological dysfunctions are associated with stroke, the most common of which is motor disability contralateral to the side of the lesion [57], in most cases including incoordination and spasticity [169]. Control, sensory, or cognitive functions may be lost or impaired [109]. The symptoms depend on severity, localization and extent of the affected brain area and temporal course. Ischemic and hemorrhagic stroke can result in similar symptoms. Stroke is expected to rise from the sixth leading cause of lost disability adjusted life years (DALY's) to the fourth in the world by the year 2020 [129]. The expected increase in stroke survivors, from which the majority cope with disabilities, will place a social and financial impact on the survivor's family, the community, and the healthcare system.

Often, the upper limb is affected leading to significant problems in fine and gross motor skills. Three months after stroke, only 20% to 56% of all survivors regain useful upper limb functions [130]. In about 60 % of the cases, the hand is affected for longer periods and estimated 5 % to 20 % do not recover completely [94]. Due to the ubiquitous use of the hand, impairments significantly restrict the patient's independence and cause problems in coping with activities of daily living.

2.1.2 Neuroplasticity

Although significant regeneration does not occur in the brain after the necrosis inherent to stroke, functional compensation does occur, enabling spontaneous and longer term rehabilitation [154]. The discovery of nerve growth factors [34] and the demonstration that neurogenesis can occur even in the adult brain [5] indicates that exogenous treatments that stimulate neurogenesis could improve recovery after stroke [13, 28]. The process of the central nervous system's attempt to repair itself has been termed neuroplasticity [204]. It is an intrinsic property of the human brain to adapt to rapidly changing environments, physiologic changes, and experiences. The continuous, rapid changes may be followed by new connections that are established through dendritic growth and arborization. Due to this mechanism, brain activity associated with a given function can move to different locations, either as a result from normal experience or in the process of recovery from brain injury. However, the mechanisms behind the brain's ability to reorganize and adapt to overcome the disorder are not completely understood. [146].

The degree of damage to the corticospinal tract after a focal brain injury correlates well with motor recovery. Exploiting mechanisms underlying the recovery of motor function, like neural reorganization, might also lead to the development of new interventions to promote poststroke rehabilitation [189]. For some forms of therapies, including constraint-induced movement therapy, functional electrical stimula-

tion, treadmill training with body weight support, and virtual reality therapy, the mechanism of change could be traced back to cortical reorganization. Robot assisted therapy is hypothesized to work based on neuroplasticity as well, although there is currently insufficient evidence to determine the exact mechanisms of change when using this method [204].

After describing the anatomy of the hand, the subsequent section explains in detail the different forms of therapy ranging from traditional methods to robotic means of rehabilitation.

2.2 Anatomy of the hand

The human hand consists of 27 bones belonging to the carpus, metacarpus, and the phalanges (bones of the fingers) (Fig. 2.1). The carpus is comprised of eight bones that are connected by an amphiarthrosis. The carpals together with the ulnar and the radius form the wrist. Its main role is to facilitate positioning of the hand and to powerfully use the extensors and flexors of the forearm. Additionally, the mobility of individual carpal bones increases the freedom of movements at the wrist [85].

The metacarpus is connected to the carpus over the carpometacarpal joints (CMC). The joint of the index finger is firmly fixed, and the middle ones are tightly united, while the thumb's CMC joint is highly movable. This enables opposition of the thumb to the fingers, which is necessary for pinching and grasping [119]. The thumb in relation to the index finger is longer than the thumb of other primates [131], which allows to grasp and manipulate small objects [72]. In contrast to the other fingers, it only has two phalanges and is attached to the mobile first metacarpal. The carpometacarpal joint produces most of the opposability.

More distally, the phalanges follow. The thumb consists of two phalanx bones (proximal, distal), whereas the phalanges of the four fingers each consist of three bones (proximal, middle, distal). The proximal interphalangeal joint (PIP) between the proximal and intermediate phalanges, and the distal interphalangeal joint (DIP) between the distal and intermediate phalanges are anatomically very similar. They both only permit flexion and extension movements. Their major differences are the smaller dimension and reduced mobility of the distal joint [106]. The heads of the metacarpal bones articulate with the bases of the proximal phalanx of the phalanges, resulting in the formation of the metacarpophalangeal joints (MCP). These joints allow flexion and extension movements as well as more limited adduction and abduction movements.

The complex musculature of the hand consists of 33 muscles, which are divided into extrinsic and intrinsic muscles. The majority of the muscles are extrinsic, meaning that they consist of long flexors and extensors with their muscle belly located in the forearm. The intrinsic muscles are organized into three different groups depending on their location. The thenar muscles are located close to the thumb, and the hypothenar muscles at the little finger. The interosseous muscles originate between the metacarpal

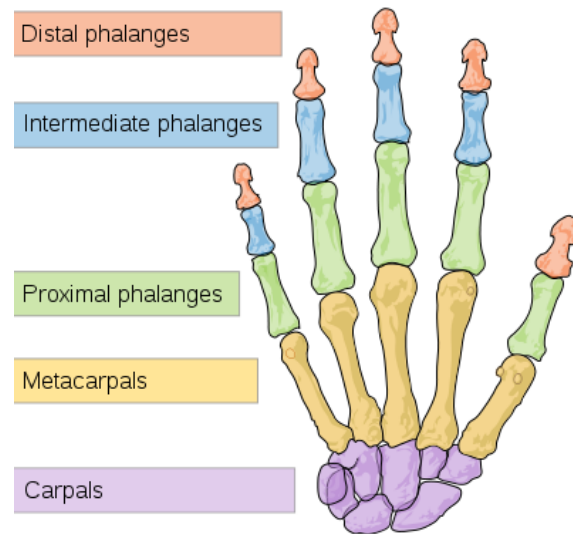


Figure 2.1: Bones of the human hand [118]

bones, and the lumbrical muscles flex the metacarpophalangeal joints and extend the interphalangeal joints.

2.3 Rehabilitation of hand and wrist functions after stroke

In this section, several rehabilitation concepts are described ranging from traditional methods to virtual reality-based and robotic rehabilitation.

2.3.1 Traditional stroke rehabilitation

After a physician has stabilized the patient following a stroke, rehabilitation should begin as soon as possible. Motor relearning and self-care skills in upper limbs are mostly rehabilitated under guidance of physical and occupational therapists. Training-based techniques with both physical and occupational therapy remain the gold standard for poststroke motor rehabilitation [43].

Physiotherapists focus on evaluating, maintaining, and restoring movement dysfunction. Occupational therapists look at physical functions as well, but more with respect to how it affects the ability to perform activities or occupations that are important to the patient [140]. The relearning of performing activities of daily living belongs to common exercises. Furthermore, frequent movement repetitions are important for motor rehabilitation of the paretic hand. Conventional physiotherapeutic strategies

that focus on spasticity reduction instead of early initiation of active movements may not be as effective [27].

In physical and occupational therapy, conventional concepts like Bobath and proprioceptive neuromuscular facilitation (PNF) are the primary strategies for inpatient and outpatient treatment [136]. The Bobath concept is a widespread accepted form of stroke rehabilitation. It is supposed to be based on the plasticity of the brain, however limited knowledge and a lack of scientific studies were available in 1943 when it was developed by Berta and Karel Bobath. Recent studies could not find evidence for the superiority of this concept in comparison to other treatments [86].

PNF is a stretching technique designed to enhance active and passive range of motion for treatment of different motor performance impairments. It has shown promising results for stroke rehabilitation, but it is more commonly used in gait therapy [3].

Constraint-induced movement therapy Constraint-induced movement therapy (CIMT) is a form of therapy that deals with learned non-use, a condition which is caused when the patient stops using the affected limb after being discouraged by the difficulty [180]. The therapy works by constraining the unaffected limb to force the usage of the affected limb. Applying this therapy, patients who have suffered a stroke within the previous 3 to 9 months produced statistically significant and clinically relevant improvements in arm motor function that persisted for at least one year [200]. In a study by Lin et al. even long-term patients could regain motor control in goal-directed reaching after wearing a restrictive mitt or sling for 6 hours a day for 2 to 3 weeks and performing massed practice for 2 hours a day for 10 days [104].

Splints and orthoses High tone and severe weakness can limit mobility and create contractures of soft tissue. Therapists often apply splinting in order to provide static positioning to reduce the chance of flexion contracture. However, a preliminary study by Andringa et al. suggests that a number of patients cannot tolerate a static orthosis over a long-term period because of discomfort, potentially leading to a clenched fist and problems in coping with daily life activities [6]. Furthermore, literature suggests that static orthoses show no effect on upper limb function, range of motion of the wrist, fingers, thumb, nor on pain [184].

Dynamic orthoses apply prolonged low-loads with a constant force, ensuring slow, passive stretches [7]. Saeboflex is a dynamic custom-fabricated wrist, hand, and finger orthosis. It includes a forearm shell to which resistive springs are attached, exerting forces onto the fingers and supporting extension movements. Springs with different force/displacement ratios are available, and are selected according to the abilities and degrees of spasticity. In contrast to CIMT, the orthosis has the advantage that even patients with limited or no hand and arm function can be treated [65]. A study by Heise et al. with patients in chronic stage showed improvement in Fugl-Meyer score [58]. A pilot study by Barry et al. revealed improvements after therapy with

SaeboFlex, although not significantly more than in the manual-assisted therapy control group [12]. Despite advantages compared to passive orthoses, dynamic systems still lack adaptive, controlled actuators and sensors for robotic and virtual reality rehabilitation.

2.3.2 Virtual reality rehabilitation

Virtual reality (VR) is a computer-based technology that allows users to interact with a simulated environment. The potential of VR technology for rehabilitative assessment and treatment purposes was first presented in the 1990s [159]. With this technology, the patients can receive instant feedback on performance based on input devices and sensors. VR exercises open up the potential to enable the application of concepts of neuroplasticity, such as repetition, intensity, and task-oriented training of the paretic extremity [100].

This training has been enhanced by means of haptic devices [10, 22, 23]. The cost of such devices can be reduced by using inexpensive gaming hardware and free 3D frameworks [76, 99, 127]. Employing games may increase the training motivation and improve the training effect. These "serious games" have experienced a growing interest. Preliminary evidence indicate that interactive computer games may increase stroke subjects' motor and cognitive skills [21]. Based on a modified version of the SaeboFlex (compare Section 2.3.1) that has been equipped with several sensors to measure joint rotations, applied torques, and forearm posture, the orthosis can interact with an interactive gaming environment [9].

A review by Henderson et al. concluded that the effectiveness of VR in stroke rehabilitation is limited yet sufficiently encouraging to justify additional clinical trials [59]. A more recent comprehensive meta-analysis including five randomized clinical trials and seven observational studies with a pre-/postintervention design showed a significant benefit towards VR for selected outcomes in eleven studies. This lead to the conclusion that VR and video game applications are potentially useful technologies that can complement conventional rehabilitation for upper arm improvement after stroke [166].

However, most virtual reality rehabilitation systems have no actuators or only ones with low forces for haptic experiences [37]. Without actuation, patients who have not sufficient residual abilities to initiate movements are not able to carry out the exercises. Robotic rehabilitation systems, in contrast, incorporate manipulators that may assist the patients in performing a movement.

2.3.3 Robotic rehabilitation systems

As a means of rehabilitation for post stroke patients, mechatronic systems have been proposed [115]. It has been shown that therapies using these devices showed improvement in hand motor function after chronic stroke. These systems offer more

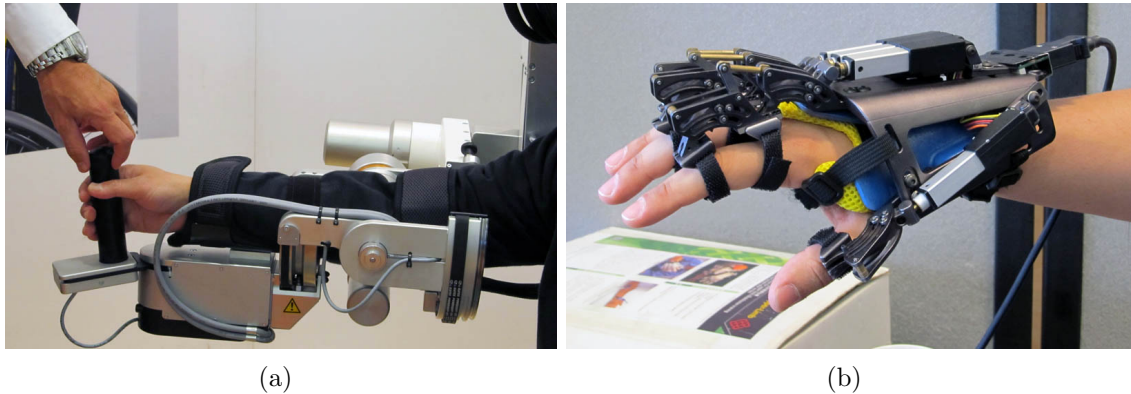


Figure 2.2: Typical end-effector and exoskeleton. (a) End-effector Armeo Power [133]
 (b) Exoskeleton [141, 181]

possibilities in comparison to traditional treatments with therapists, such as home rehabilitation or small groups therapy supervised by single therapists. This facilitates and reduces the cost for therapy, particularly over longer periods with shorter sessions, which has been proved to be more effective for stroke rehabilitation [186].

In this work, the state-of-the-art of robotic rehabilitation is restricted to systems focusing on rehabilitation of the distal part of the upper limbs involving forearm, wrist, hand, and finger functions. Hand rehabilitation devices are structured into two main approaches: end-effectors and exoskeletons. End-effectors usually recreate movements corresponding to activities of daily living, and interact distally with the user's joints. In contrast, exoskeletons guide hand movements using a frame that can be controlled in certain ways. This means that the movement is constrained to the mechanical degree of freedom (DOF) [11]. Typical examples of each type are shown in Fig. 2.2. The rest of this section is organized, accordingly. Additionally, a rehabilitation paradigm called visual feedback distortion is described.

2.3.3.1 End-effectors

End-effectors assume that the patient's biomechanics and central nervous system will determine the movements at the joint level and that the alignment with the patient's joint rotation axis is resolved distally [11].

The renowned MIT-MANUS [2, 31, 91] revolutionized rehabilitation by introducing robotics into the field. Masia et al. complemented the system with a 1-DOF mechanism hand-module which enables the rehabilitation of grasping. The system is commercialized by InMotion robotics as an add-on for the arm module based on the MIT-MANUS. A wrist module is available, but it may be limited by a small range of motion, and size and cost impede its potential use for home rehabilitation [121].

Yeong et al. presented the ReachMAN, a rehabilitation system with three degrees of freedom (DOF) combining reaching, forearm supination/pronation and grasping in one device. A 6 DOF force/torque sensor measures interaction forces and torques during arm movements [203].

The Universal Haptic Pantograph (UHP) allows training of shoulder, elbow, and wrist with the same robot by locking joints. The innovative variable structure pantograph mechanism can change the DOF between zero and three. Although it is a cost-efficient system for upper limb training, it does not feature modularity. To train only the wrist requires the use of the whole device, which is not very portable and may not be suitable for home rehabilitation.

HandCare is a cable-actuated rehabilitation system to assist in opening and closing movements [45]. A clutch system allows switching between fixed, free running, and active modes for each of the five fingers. One actuator applies forces onto the fingers in active mode. Although the clutch can be used to set different fingers to free running mode for independent movements, this is not possible if more than one finger is in active mode.

The RehapticKnob [125] is the successor of the haptic knob [97]. The device has two degrees of freedom which allow independent control of hand opening/closing and forearm rotation. The compact design with high-fidelity instrumentation allows for precise assessment and dynamic interaction. However, the sensors, especially force/torque sensors, are costly.

Hesse et al. developed a bilateral system with one degree of freedom (DOF) for the training of forearm pronation/supination and wrist flexion/extension. Including the non-affected upper limb in the training may stimulate ipsilateral cortico-spinal projections to the paretic muscles that are regarded to be relevant for recovery from hemiplegia. This has been shown in functional imaging studies, where an increased activation of the ipsilateral sensorimotor area and subsequent motor recovery of the affected extremity after stroke were observed [62]. This simple device, called the Bi-Manu-Track, has been commercialized and is suitable for home rehabilitation [155]. However, it lacks an interface to a computer for virtual and tele rehabilitation. Rashedi et al. proposed a similar design emphasizing force feedback that provides a real-time dynamic sensation of the paretic hand in the healthy hand [153].

Besides the Bi-Manu-Track, several other devices have been developed in companies or were transferred from university to corporate structures. The Austrian company Tyromotion offers several rehabilitation devices that are used with serious games and performance evaluation software. Finger functions are trained with the Amadeo system, with either passive, assistive, or active exercises measuring the range of motion (ROM) and finger forces in extension and flexion direction [182]. Pablo is a passive, modular system that includes a handle for measuring the gripping forces and ROM of the arm, a ball-shaped end-effector for pronation/supination and extension/flexion of the wrist, and a multiboard for upper limb training [183].

ReJoyce is a passive upper extremity rehabilitation workstation offering rehabilitation of tasks of daily living, fitness training, and client performance measurement. It

allows for the continuation of the ReJoyce exercises in the home environment after leaving the clinic, tele-supervised over the internet [66, 88].

The Reha-Digit device for finger training excludes the thumb with an actuated camshaft, moving the four fingers in a physiological range of movement [61]. The device is for patients without functional movements in the affected hand and provides only continuous passive motion training without an interface to a computer.

2.3.3.2 Exoskeletons

Exoskeletons are amongst the most complex rehabilitation devices due to the high number of degrees of freedom (DOF) of the hand. The complexity depends on the number of actuated joints, measured joint angles, and the availability of bi-directional movement amongst other variables.

Kawasaki et al. presented a hand motion assist robot, which belongs to the most elaborate developed devices with 18 DOF. It assists not only the flexion/extension and abduction/adduction of each hand joint independently, but also the opposability of the thumb. Moreover, it assists the palmar flexion/dorsiflexion of the wrist and the pronation/supination of the forearm so as to allow hand rehabilitation therapy in coordination with wrist motion [79, 80]. The high number of DOF leads to an inherently complex and expensive design. Further drawbacks are the limited range of force (0 N to 5 N) that may not be sufficient for patients with severe spasticity, and friction that may reduce the smoothness of movement [45].

Besides complexity and cost, further challenges are that little space is available for actuators, and the weight has a strong effect on the performance or ergonomics. Tendon-based transmission allows for the reduction of weight by putting actuators from the actuated joints remotely. They transmit loads over distances with low friction and zero backlash, which is advantageous in comparison to gears. The power is transmitted over tendons, also named wires or cables, and guided via pulleys or sheaths to the attachment point. Therefore, tendon-based systems are of high interest and are commonly used for exoskeletons [45, 49, 75, 201, 202].

Most developers decide to further reduce the complexity and cost through both the mechanical design and the actuation. Several exoskeletons have been developed that cover only one finger. Wege et al. proposed an exoskeleton for rehabilitation after hand injury, supporting bidirectional motion in all joints with a dorsal lever construction and actuation via Bowden cables [191]. The Actuated Finger Exoskeleton (AFX) is intended to assess strategies for optimizing rehabilitation of pinch and reach-to-pinch following stroke. It allows independent actuation of each of the finger joints at levels of velocity and torque comparable to the performance of everyday hand manipulation tasks [75, 201]. Li et al. developed an index finger exoskeleton for active and passive motion training with a simple parallelogram mechanism. The reason for restraining the training to the index finger was not given. Other issues include the high weight of 160 g per finger, and the tedious adjustments required to fit the exoskeleton to different hand sizes using screws [103, 188]. The exoskeleton

developed by Cempini et al. consists of an index finger module and a thumb module. One key feature is the self-aligning mechanism of the metacarpophalangeal (MCP) joint. Despite the remote placement of the actuators, the weight remains very high at 500 g for two fingers [30]. 350 g is already considered too high [16].

HANDEXOS aims to provide a full exoskeleton, but so far has developed only the index finger module. It focuses on functional and safe user interaction based on anthropomorphic kinematics and the minimization of the human/exoskeleton rotational axes misalignment. The extension of the MCP, PIP, and DIP joints is achieved by pulling the tendon cable with a single linear slider driven by a DC motor, whereas the flexion consists of three antagonist cables for each joint connected to passive compression springs [32, 33]. Due to the lead screw mechanism in the extension unit, the system is, however, not backdrivable. Backdrivability is, however, considered important both by healthcare professionals and engineers [147].

Other systems allow training of the whole hand but simplify the design by actuating several fingers together. The Hand EXOskeleton Rehabilitation Robot HEXORR couples the rotations of the MCP and PIP joints of all the fingers. It incorporates a thumb actuator that allows for a variable thumb plane of motion to incorporate different degrees of extension/flexion and abduction/adduction [168]. Some devices involve every finger, but simplify the design by using one bar for the four fingers counteracting the thumb [168, 177]. The Hand-Wrist Assisting Robotic Device (HWARD) also combines the four fingers to a single unit that counteracts the thumb. It is a 3-DOF pneumatically-actuated and backdrivable system that assists functional grasping and releasing movements of the stroke-impaired hand. One actuator drives the bar with the four fingers while the other two degrees of freedom are for the thumb and the wrist [177, 178]. Fischer et al. tested a cable orthosis and a pneumatic glove on stroke patients. The body powered orthosis (BPO) was simplified by conjoining the five cables from the fingers at the wrist to form one single actuated cable. The pneumatic-powered device (PPD) assists in extension of the digits by inflating an air bladder thereby forcing them to be straightened over each of the fingers without regard to the joints [47, 114]. Pneumatics have, however, the disadvantages that precise control is hardly achievable, that the operation is noisy, and that a pressure supply is required.

The Rutgers Master II is a force-feedback glove for haptic and VR applications [16]. Due to force exertion from the palmar side of the hand, the glove is not suitable for stroke rehabilitation since it obstructs the natural closing of the hand. The CyberGrasp is another system mainly intended for haptic and virtual reality applications that, in contrast, has been applied to the field of rehabilitation [1, 158]. It is donned over the CyberGlove, which is a data glove that measures the joint angles. Forces against the closing direction of the hand can be controlled independently for each finger. The CyberGrasp belongs to the earliest commercialized exoskeletons. However, the excessive cost of about € 85,000 limits widespread use in clinics and home rehabilitation.

Other commercialized systems specialize in stroke rehabilitation and are often cheaper due to the simpler design. The Hand Mentor is the first commercial hand rehabilitation therapy system with active repetitive motion [167]. It trains upper extremity functions in patients with chronic stroke with minimal finger and wrist movement. It is limited to wrist flexion and extension, focusing on improving active range of motion, wrist control, and initiating movement distally [162]

An increasing number of exoskeleton systems are manufactured using 3D printers. Iqbal et al. used this technology for a one-fingered bi-directional underactuated prototype for daily life activity training [70]. Burton et al. used rapid prototyping to customize their exoskeleton to the patient's hand dimensions based on a parametric kinematic model of the hand. However, the parameters and the extent of their parametrization are not described and evaluated [25, 26].

Several systems use surface electromyography (sEMG) to estimate the intentions when moving the hand [112, 128, 181]. The additional cost and the correct placement of the electrodes speak against the use of such systems in the home environment. Furthermore, backdrivability is usually not given, since the control signal does not come from the movement but from the sEMG signal.

2.3.3.3 Visual feedback distortion

The use of robotics enables a more precise training with higher standardization and allows for feedback about the patient's performance. This promotes an extension of novel neurorehabilitation strategies. Matsuoka et al. proposed a paradigm called visual feedback distortion to address patients' cognitive or perceptive deficits, which may cause a false perception of their own ability. It may be especially suitable for stroke patients with learned nonuse [123], with about 25 % of stroke patients being affected by this condition [179]. The patient's underestimation may restrict the motor recovery, since patients may be reluctant to move beyond their perceived limits [19]. This part of rehabilitation has not been addressed before in rehabilitation robotics research, although it has been implicated as a potential factor in inhibiting motor recovery [123].

The paradigm is based on the hypothesis that the internal somatosensory representation of a movement goal changes along with distortion of the visual feedback. Since the proprioceptive sensors are less accurate than visual sensors, deviations between the actual position or force level and the visual representation on a screen are not perceived.

The rehabilitation protocol works by gradually distorting the visual representation of force and position in imperceptible steps to encourage the patient to exceed in their performance. In a first step, the just noticeable difference (JND) for specific movements is determined below which the patient does not detect the distortion in a single step [4, 17, 123]. The gradual change allows cumulated distortions that are significantly larger than the JND [20].

This form of therapy may be especially suitable for patients that live with their deficits for long periods of time and have psychological or habitual barriers. It helps to reach beyond their self-assessed abilities, making further functional improvements. Subjects in a study, in which reaching tasks were conducted distorting the distance between the tip of the index finger and the tip of the thumb, showed clinically important improvements [18]. Given the fact that pinching training using visual feedback distortion shows improvements on the rehabilitation outcome, an extension of the trainable movements promises to be beneficial on motor recovery.

2.3.4 Tests and scales for progress evaluation

Reliable and valid assessment of sensorimotor skills is required for clinical decision-making and research purposes. Several tests that focus on assessing different motor skills and activities are applied to measure the status of rehabilitation.

2.3.4.1 Common tests used in clinical practice

The Box-and-Block test evaluates individuals with suspected impairments in gross manual dexterity. Blocks have to be moved from one side of a box to the other, making it a simple, low-cost and efficient test [122]. Fine motor skills and fine manual dexterity are either tested with the Nine-Hole-Peg test [54] or the grooved pegboard test [164]. Both measure the time that a patient needs to put pegs into a board. The grooved pegboard test additionally requires the turning of the pegs in a correct orientation. A virtual version exists that extends the time measurement with more metrics such as the trajectory [48].

The Action Research Arm Test (ARAT) was designed to assess recovery in the upper limb following cortical damage [124]. A practical test of upper extremity function in patients with stroke confirmed the high intra- and interrater reliability of the ARA test [102].

The Ashworth and modified Ashworth scales are the primary clinical measures of spasticity. Although it has been reliably applied to poststroke spasticity assessment [53], this test also lacks standardization [14].

The TEMPA (Test Évaluant les Membres supérieurs des Personnes Âgées) is an upper extremity function test specifically designed for the elderly [41]. It is also used for the evaluation of stroke rehabilitation [126].

Besides testing specific functions, it is important how well patients cope with activities of daily living (ADLs). These tests don't rely on objective metrics like the time, but rather on subjective evaluation of the performance in exerting specific tasks. The Barthel ADL Index is a reasonable, robust, and reliable clinical measure for use with head-injured and stroke patients, provided its limitations due to the subjective nature of the test are recognized [36]. The Fugl-Meyer assessment evaluates motor function, balance, some sensation qualities, and joint function in hemiplegic patients [50]. It is among the most extensively used and discussed metrics of physical performance [51].

The Functional Independence Measure is used to rate the severity of care-recipients' functions and impairments. It contains 13 items that assess motor functioning and 5 items for measuring cognitive functioning rated on an ordinal scale from 1 to 7 [56]. It demonstrated acceptable reliability across a wide variety of settings, raters, and patients [143].

The Chedoke-McMaster Stroke Assessment measures both the physical impairments and disabilities of patients with stroke and other neurological impairments. It is made up of two parts; a physical impairment inventory and a disability inventory. It assesses the recovery stage of the arm, hand, leg, and foot, postural control and shoulder pain. Each item is measured on a 7-point scale. Studies have confirmed that the tests yield both reliable and valid results. The impairment inventory correlates with the Fugl-Meyer assessment and the disability inventory with the Functional Independence Measure [52].

2.3.4.2 Computer and robotic-aided assessment

Commonly used tests and scales in clinical practice have several shortcomings, including ceiling and floor effects, and reliance upon subjects' effort. Moreover, the subjectiveness of observer ratings is prone to bias, especially in trials in which a double-blind protocol is not possible [89].

Measurements taken by a robot and the analysis of data by a computer offers several benefits. First, the measurements (e.g. ROM, torque, force, velocity, smoothness of movements etc.) provided by the sensors are objective. The assessment is performed automatically during the whole therapy, which increases the sample size without additional cost. This may contribute to improving the clinical rehabilitation practice [11].

However, this form of assessment also has some shortfalls. Ceiling and floor effects as well as influences on the subjects' efforts may also occur. The multitude of data needs to be reduced to a few metrics which are comprehensible by therapists and patients. The question is how to condense the sampled data to identify the key factors to be extracted. Nevertheless, some robotic measurements have been shown to correlate well with standard clinical measures such as the Fugl-Meyer assessment [29, 98]. The correlation is stronger for robotic measurements focusing on movement quality, such as smoothness of movement and trajectory error, rather than on speed [29].

2.4 Chapter conclusions

Virtual reality (VR) and robotic rehabilitation offer the potential to employ concepts of neuroplasticity and to improve functional outcome, making it a valuable tool to add to traditional therapy. VR rehabilitation has been shown to be an effective tool in some applications, but the lack of actuators does not allow for assistive therapy and excludes a wide group of patients from using the training device. The efficacy

of robotic intervention varies in different studies, ranging from more to less effective in comparison to traditional therapy. The disadvantage of the latter is that sufficient rehabilitation over a longer period of time can rarely be provided due to costs and limited labor.

Robotic systems have great potential to extend therapy to the home environment. Therefore, inexpensive, portable, and easy to use systems are required that can be deployed in an unsupervised setting. However, current robotic devices for hand rehabilitation are often not portable enough and use expensive hardware that impedes wide distribution into decentralized rehabilitation centers or home environments. Simpler non-actuated systems or continuous passive motion (CPM) devices do not allow for the control of the force or train active movement training. Little emphasis has been put on the distribution of movement training for different components.

Exoskeletons for the hand are inherently complex if they follow the full anatomy. The systems that try to measure and actuate each joint are mostly reduced to one finger to prevent excessive complexity. Other systems have been strongly simplified limiting their use. Besides, mechanical adjustment mechanisms that fit the exoskeleton to different hand sizes, impede the usage. Only few systems focus on home-based usage of these exoskeletons. For the use of such systems at home, cost, complexity, portability, setup time, and self-dependency are major concerns.

In conclusion, more research is required to find suitable approaches for the different applications, patients, and movements to be trained.

Chapter 3

Concepts and requirements

The literature review in section 2.3 showed that many problems are still unaddressed. In this chapter concepts are presented that approach some of the shortcomings. Based on guidelines by cooperating neurologists, the first two subsections define the movements that shall be trainable, as well as exercise modes. Then, preliminary considerations are set up to limit design possibilities and narrow down requirements.

3.1 Trainable movements

The developments described in this work focus on the training of distal upper limb functions involving the forearm, wrist, and hand. This section clarifies more in detail the particular movements. In collaboration with cooperating neurologists, a catalog of trainable motions was created (Table 3.1).

These more distal movements are a crucial part for performing activities of daily living (ADLs), such as drinking and eating [62]. Therefore, they are commonly trained with physical and occupational therapists (PTs, OTs).

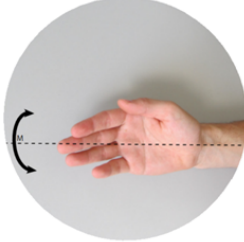
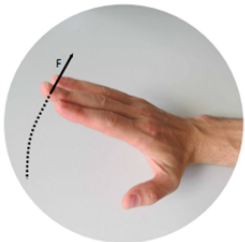

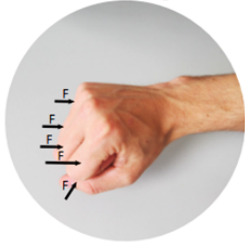
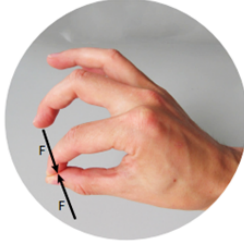

Supination / pronation and dorsiflexion are, for instance, important for orienting the hand to grasp an object [101, 102]. The final hand posture or orientation has a major impact on the hand transport in reaching and grasping and is related to comfortable end posture [160, 161].

Fine finger movements are used to handle smaller objects, for example, the manipulation of a lid while opening a bottle. These movements are more advanced and the exercises are intended for the progressed rehabilitation phase.

Grasping is based on two basic patterns, power grip and precision grip. Other specialized movements can be derived from them. The recovery of these motions allows for a greater level of independence and quality of life [26].

Stroke patients often suffer from flexed fingers being unable to open or control the hand due to extensor muscle weakness. Therefore, a training device should initially focus on finger extension training. Later, finger flexion exercises can help to strengthen weak muscles and reduce effects of synergies [45]. Finger adduction and abduction play a part in grasping by adapting the area of the opened hand to the size of the object. It does not need specialized training, but it should not be constrained in grasping training. Patients showing finger strength and workspace close to normal,

Table 3.1: Overview of movements to be trained with the device

Supination / Pronation		Dorsiflexion (or dorsal wrist extension)	
Fine finger movement extension		Grasping (Hand opening / closing, power grip)	
Pinching (Precision grip)		Independence of finger movements	

still exhibited deficits in task performance, particularly tasks including finger individuation [38]. Therefore, training and measurement of the independence of finger movements is important in the progressed stage of rehabilitation.

3.2 Exercise modes

The movements above can be trained in different ways. Based on specifications from the collaborating neurologists and related work, the training modes are specified. The following list shows the various modes to be developed:

Passive In this mode the patient is passively moved. Therefore, it is also known as assisted training. It is among the conventional mobilization techniques to improve muscle, joint and tendon mobility while reducing muscle tone [27]. This mode aims to improve mobilization and to reduce muscle tone. A study by Hu et al. indicated that passive training reduces the spasticity in the wrist flexor [67].

Active This exercise demands that the patient actively exerts forces either without motor resistance, or with adaptable resistive or assistive forces. Torque profiles should also be implemented, such as a linear increase of the force with the angular position. For wrist movements, the combination of passive and active training of the paretic side was more effective than conventional rehabilitation of upper-limb motor function in subacute stroke survivors [62].

Calibration The assistance or resistance may be determined within an initial time period. Training parameters measured over a specific time period are used to determine the challenge of the subsequent exercise. Patient-specific training improves motor learning [90].

Progress Evaluation Movement assessment can be performed automatically and objectively throughout the whole therapy without additional cost [11]. The data created by sensors serves as a metric for determining the progress of rehabilitation. By comparing for example range of motion (ROM) or maximum forces exerted by the patient over several sessions, a trend may allow inferences about the success of the therapy.

Visual feedback distortion The rehabilitation paradigm has already been introduced in the background chapter (Section 2.3.3.3). Sensors and their representation in a graphical user interface (GUI) together with adaptable actuators enable the implementation of visual feedback distortion. The GUI shall offer the necessary functionality, including convenient manipulation of the involved parameters.

Independence of finger movements The loss of fine movements is reflected in the inability to perform relatively independent finger movements. Movements are slowed down and the mobilization of the force is delayed [137]. Therefore, an exercise shall be implemented that tests for independence of finger movements.

Rehabilitation Games The system shall be used as an input interface for playing motivating games to train the movements, since attention and motivation are key factors for motor relearning following stroke [109]. Optionally, visual feedback distortion could be incorporated into the games for potential benefits.

3.3 Modularization of rehabilitation devices

Stroke causes a wide spectrum of disabilities. In the case of hand functions, there are several common impairments, but the extent varies between patients (Section 2.1.1) Therefore, a training device requires exercising several different movements with strongly varying ranges of strength. However, the increased complexity is contrary to cost-effectiveness, which is necessary to make the system affordable for home rehabilitation and health care centers with lower budgets. High complexity is the reason

why 75% of the recent research projects in the field of hand rehabilitation have not undergone any testing [11].

A modular design regards both contradictory requirements of necessary functionality and cost. The distribution of movements and functionality on different components can potentially reduce complexity. Smaller modules are advantageous in comparison to complex multifunctional devices for several reasons: The single module may be designed and manufactured faster and cheaper. In clinical use, they tend to be less prone to errors, easier to setup and operate, and the single modules can be used simultaneously by several patients. Also, during development, multiple devices facilitate parallel development and synergy effects may arise due to overlapping components or functionality. Finally, providing optional components allows potential customers to select the functionality according to their needs.

The modularization is mostly determined by the set of trainable movements (Section 3.1). It is desirable to train as many motions as possible with one device as long as this does not contradict with the aforementioned points of complexity, cost-effectiveness, and portability. These considerations led to the distribution of movements on two devices forming together the **m**odular **R**ehabilitation **S**ystem called **m·ReS**:

m·ReS^R The resembling nature of the movements suggests to realize the training of the rotational movements (supination/pronation, dorsiflexion) within one device. This also includes fine finger movements since the main focus of these exercises is on manipulation of rotating knobs, which are commonly encountered in activities of daily living. This requires one actuator in an end-effector design. The module is called **m·ReS^R** with the **R** indicating rotational movement training.

m·ReS^X Grasping and pinching are related to finger opening and closing, and therefore, are grouped together to be trained by a second device. It shall be possible to train the movements of each finger independently. This device should constrain abduction and adduction as little as possible. The **eX**oskeleton to be developed is called **m·ReS^X**.

The movements to be trained (Section 3.1) are diverse but still can be covered by these two devices only. By using both an end-effector and an exoskeleton approach, the systems complement each other and the advantages of each approach can be exploited. Optional submodules shall increase the versatility of the devices. A closer look at the concepts of both devices is given in the following subsections. They represent preliminary considerations that narrow down the endless possibilities of the requirements. After establishing the requirements, the implementation is described in detail in Chapter 4 and 5 .

3.3.1 Training of rotational movements (m·ReS^R)

The wrist is important for orienting the hand to grasp objects (compare Section 3.1). Moreover, the wrist joint is considered to play a more significant role in physical therapy than other parts of the upper extremity, since motor recovery after stroke is more effective extending the training from distal to proximal joints [27]. For the training of supination/pronation, dorsiflexion and fine finger training an end-effector design is used. This approach exhibits advantages in reducing cost and complexity by using different configurations with the same hardware. We intend to use only one actuator and exploit the variability of its orientation to the wrist for different functionalities. Although the movements cannot be trained at the same time, repetitive training of isolated movements improves the outcome of motor rehabilitation [27]. Similar to traditional therapy, the use of several handles with different functionality, size and haptic properties is desired. The contact between device and patient over a handle is also inherent to the end-effector approach.

In contrast, an exoskeleton requires the same amount of mechanical DOF as anatomical for performing complex movements without constraints. In particular, fine finger manipulation is so complex that exoskeletons would require excessive mechanical complexity for training. Therefore, we restrict the training and assessment to specific tasks like a bottle opening movement imitated by the device. This means that it does not need all the DOF involved to allow training of complex hand movements. On one hand, this allows more freedom in choosing how to perform the exercise, on the other hand, it does not allow for the forcing of a specific movement.

Safety aspects have to be considered, particularly in case of supination/pronation, where high motor torques are required to work against the strong muscles of the forearm. In common use, the hand grasps the end-effector without attachment. Since the hand could then release the end-effector in case of an emergency, safety issues are less critical in comparison to exoskeletons.

Finally, the efficacy of robotic rehabilitation with end-effector-based training of supination/pronation and wrist extension/flexion has been shown [60]. The arguments in the preliminary design considerations speak for building upon the end-effector approach for the training of supination/pronation, dorsiflexion, and fine finger movements.

3.3.2 Actuated hand exoskeleton (m·ReS^X)

m·ReS^X focuses on the training of grasping and pinching. The interaction of the fingers in performing these movements involves a high number of degrees of freedom. Even more DOF are needed so that abduction/adduction is not constrained as stated in Section 3.1. The complexity could be reduced by using another kind of end-effector. However, several reasons justify the development of an exoskeleton.

As argued in Section 3.1, the independence of fingers is an important factor in rehabilitation. End-effectors that allow independent but guided finger training also

posses higher mechanical complexity. Therefore, the advantage of a simpler design in comparison to exoskeletons, as reasoned for m·ReS^R, is not given for the intended purpose of this module. The second module is intended to complement the first one beyond the mere distribution of movements. The attachment of the exoskeleton to the anatomy can be positively employed by giving more freedom of where forces are applied and where angles and forces are measured. This facilitates capturing individual finger joint angles that are important to determine degrees of impairment [71, 78]. Furthermore, safety concerns are lower due to smaller forces on the anatomy for finger training in comparison to forearm and wrist training. A fixed connection between the actuated mechanical parts and the anatomy is less critical.

However, due to the high number of degrees of freedom of the hand, these training devices belong to the most complex rehabilitation systems. In order to prevent excessive complexity, trade-offs have to be accepted. One possibility is to apply under-actuation, which means having less actuators than mechanical DOF. Exoskeletons offer various ways to follow the principle of using the same actuators to train different movements [33, 69]. In conjunction with cable-based transmission, they open up multiple configurations by changing the force transmission via the routing and the attachment points of the tendons. This can potentially reduce complexity by using different configurations to vary kinds of training. Following the modular approach, exoskeletons in combination with a cable-drive facilitate the sourcing out of the actuation into a separate module. Further advantages have already been provided in Section 2.3.3.2. Finally, we recognize a need in research to exploit the advantages of exoskeletons with cost-efficient designs. These preliminary considerations determine the following of an exoskeleton approach and guide the requirements upon which the final design is based.

3.4 Requirements

The fundamental requirements and design decisions described above lead to modularization into two devices. This section gives a more detailed overview of the requirements set up for the development of such devices. First, general requirements are given that count for both modules before the specific ones for each of them are carved out.

3.4.1 General requirements

Based on the goal of developing a home rehabilitation system, the following fundamental requirements were outlined, forming a basis for further development.

Functionality Virtual reality interaction and progress evaluation shall be enabled by the use of sensors for forces and range of motion. Actuators allow for support

or resistance in motor training. Natural hand, wrist, and forearm movements should be impeded as little as possible.

Affordability The system should be cost-effective in order to make it affordable for home rehabilitation and clinics with lower budgets. It should incorporate optional components to adapt the functionality to the user's needs and available funds.

Safety Safe operation without risk to the user's health has to be ensured. Therefore, a number of measures to increase safety for the user have to be taken that are described more in detail in the subsection below.

Usability The system shall be intuitive and easy to use. Even without the presence of a therapist, e.g. at home, the patient shall be able to use it self-dependently.

Modularity The system should be split into several modules and submodules. This is beneficial in many ways: It allows for the simplification of the components, for simultaneous use in different exercises, and adaptation of functionality to the patient's needs and the availability of funds.

Portability Usage in a home environment requires the device to be small enough for transport. It should fit into a suitcase and weigh less than 5 kg.

Simplicity A simpler design is preferred as long as it fulfills the required functionality. Simplification also positively influences the manufacturing effort, cost, development time, and proneness to errors.

The requirements of some aspects of development are described more in-depth in the subsections below.

3.4.1.1 Hardware

The system shall allow for training with adaptive assistance or resistance (Section 3.2), which requires the use of actuators producing adequate forces. An appropriate motor driver with necessary control has to be provided to adapt the torque. This enables force feedback and adaption of the exercise difficulty to the patient's capabilities for a subset of the motions. The interaction between the user and motor demands backdrivability of the actuator. This means that low user-driven torques are sufficient to execute movements. Most servos and geared motors with high reduction gear ratios consequently have low backdrivability, and are thus not applicable. A simple setup with a low amount of additional hardware to drive the motor is preferred.

Sensors extend the functionality beyond possibilities of traditional therapy. They should be low-cost but still be sufficiently accurate to be a valid tool in rehabilitation. The measurement of two variables is required, ROM, and torque or force, respectively. The accuracy of the joint angle measurements is required to have a mean error below

the 5° limit accepted by the American Medical Association to consider the measurements reliable for the evaluation of movement impairments in a clinical context [206]. The measurements differ between both modules and are described in more detail in the related subsection.

3.4.1.2 Safety

Safety is a crucial aspect in rehabilitation robotics. Therefore, a number of measures to increase safety for the user have to be taken. First, alternating current (AC) to power the system should be omitted due to the higher risk of severe injuries. Direct current (DC) is advisable, preferably with low voltages. This overlaps with a requirement to limit motor power. In contrast to usual motor applications, this application demands rather high torque at low to zero velocity. However, the stall torque of DC motors can be far above the nominal torque. At nominal voltage, the motor is capable of exerting high peak torques over the nominal torque that creates a potential health. Moreover, the current during stall may cause over temperature and risks the motor's functioning. Therefore, the maximum motor torque should be restricted by the supply voltage, so that operation during standstill does not lead to failures. The armature current could also be limited by means of software, but this should only be done as an additional measure to the voltage limitation since the software approach is more prone to errors. Electrical shocks have to be prevented by a ground connection to the casing of the system. Mechanical stops or software-controlled safety mechanisms have to be included to prevent actuator movements exceeding the anatomical limits. Additionally, an emergency switch in reach of both patient and physiotherapist has to be provided to interrupt power in case of an emergency.

3.4.1.3 Software and communication

Following the hardware design approach, the software shall show modularity as well. In particular, the access to hardware functionality shall not be constrained to a software which runs only on one device or operating system (OS).

The requirements differ for the low-level code on the microcontroller and the high-level software with which the user interacts. The microcontroller has direct access to the hardware, which is necessary to fulfill real-time constraints. In normal operation, soft real-time is sufficient since no emergency is caused when e.g. sensor samples are delayed. However, safety relevant aspects, particularly those related to motor control, underlie hard real-time constraints. The system's absolute minimum update rate shall be twice the human motion's mechanical bandwidths of 2 Hz for normal speed movements [45]. However, higher rates may be desired or necessary for the control part. The low-level part requires an interface by which the functionality is accessed in a convenient way for the user.

A comfortable access to the hardware functionality shall be achieved by a graphical user interface (GUI). Moreover, it gives a visual representation of sensor values to the user. This is necessary to make some of the exercise modes possible. The visual feedback can be distorted, the data for the progress evaluation presented, and rehabilitation games provided. The parameters shall be conveniently made available in the software. Studies may need a specialized interface. Since stroke usually occurs at higher ages, the GUI needs to be usable by elderlies. This includes readable buttons and directions as well as consideration of the degradation.

From the technical point of view, one important requirement is cross-platform compatibility. First, this supports the aspect of modularity and deployment of the software on different devices. Major focus shall be on the Windows platform due to its wide distribution. In addition, it shall be runnable on Linux because it is the most widely used free and open-source platform and is the recommended operating system for use in conjunction with the Raspberry Pi. This single-card computer is cheap, small, and capable of providing the necessary functionality for communication with the microcontroller and running a GUI. This makes it an ideal fit for use in the present application, which is why the software shall be made compatible with it. Furthermore, the ability to compile the code to native binaries is preferred so that no virtual machine is required, making the execution inherently faster.

The GUI and the low-level layer has to be interfaced with some form of communication architecture. It shall be flexible and extendable to allow communication between the hardware and several different modules and devices. Industrial automation hardware as well as custom-made microcontroller-based solutions shall be supported and communication with a PC shall be made available, avoiding additional hardware. Thus, proprietary motion controllers can be used that facilitate the development, as well as custom-made microcontrolled circuits that allow for a more flexible design. An interface with a PC allows for debugging and the use of a GUI for access to functions and visualization.

3.4.2 Specific requirements for m·ReS^R

The preliminary considerations (Section 3.3.1) determined to reuse the same hardware for several configurations. Still, supination/pronation, dorsal extension and finger training shall be enabled by using one actuator only. The effort required to change these configurations shall be at a reasonable level.

The sensors provide measurements of the angular position and torque. A position sensor shall have sufficient resolution to provide accurate angle measurements from which velocity signals can be derived. The maximum anatomical ranges of motion have to be recorded and measures have to be taken to prevent motor movements exceeding these limits. In the prototype phase, the user shall be able to release the handle in case of an emergency. Patients who need attachment due to spasms may be incorporated into the user group after intensive testing and redundant safety measures.

Expensive sensors shall be avoided to keep the system cost-efficient. Commercial force-torque sensors are not feasible due to their high cost.

Optional submodules shall enhance the functionality. Different handles shall be provided according to the training mode, hand size, and to patients' needs. Therapists neither should feel inconvenienced by changing the handle nor hesitate to use a more suitable handle due to increased time consumption. Therefore, the ability to change handles shall be fast and not require the use of additional tools.

3.4.3 Specific requirements for m·ReS^X

One of the major problems of exoskeletons are misalignment of the joints with the anatomy. It can cause unwanted reaction forces and make the usage uncomfortable or even painful. Soreness and incorrectly trained motions have to be prevented. Therefore, good alignment with the anatomy is among the major requirements. To facilitate high acceptance of health care professionals, usability is an important point. Therefore, adaption mechanisms or time consuming adjustments should be avoided. Some systems use orthotic material to increase compliance and compensate rigid mechanical motion [177], which could, however, lead to soreness and incorrectly trained motions [25]. Furthermore, the device should be easy to apply and remove, particularly so because patients in a home environment would have to be able to use it without assistance. Strain and movement limitations while wearing the exoskeleton shall be minimized. This means the exoskeleton must be lightweight and the movable parts shall have low inertia and friction. Minor movements of the arm shall be possible.

The placement of the exoskeleton inherently involves unwanted disadvantages and contradictory requirements. Therefore, the requirements are prioritized in the order of their appearance in this paragraph. Interference with the real hand should be reduced to a minimum. Therefore, the palm shall be kept free so that grasping or closing movements are not impeded. This results in a necessity to shift the exoskeleton to the side or to the dorsal part of the hand. However, placement at the side of the fingers reduces adduction/abduction movements which should be avoided as well. Dorsal placement also impedes free movements of the hand. Excessive dimensions may lead to reduced usability and could possibly intimidate the patient.

The complexity of the hand can be encountered with a multitude of actuators and sensors. Due to cost and issues with mechanical complexity like proneness to errors and less intuitive use, limitations have to be accepted. Because of this argument in combination with the independence of fingers called for in Section 3.1, we limit the number of actuators to one per finger. The device is intended to allow passive and active training with adaptable forces. Typical force levels to accomplish many activities of daily living are around 10 N to 15 N [70]. This range is also taken as a reference value for dimensioning the actuation and transmission. The forces on the fingers must not harm the patient, which is why mechanical stops in extension direction have to be included into the design.

The actuators are the major cost-drivers of the system. Following the modular approach, it shall be possible to reduce the number of actuators while still allowing limited use of the exoskeleton. This allows for the adaptation of the functionality to available funds as well as the capabilities and necessities of the patient. The preliminary concepts introduced the idea of changing the routing of the cables in order to make different configurations possible (Section 3.3.2). This requires the ability to easily change routing.

In the case of the exoskeleton, the range of motion relates to the finger joint angles. Sensors are cheaper and more easily integrated, which is why the number is not limited as in the case of the actuators. However, depending on the aim of the training, a different amount of sensors may be necessary. The motor encoder shall be used as a means of measurement in the case that no sensors are employed in the exoskeleton itself. Friction is an important property in haptic devices due to its effect on sensitivity and dynamic range of the interface [16]. Therefore, the use of friction-inducing sensors shall be avoided.

The thumb has great flexibility and range of motion, which allows its opposition to the other fingers and facilitates grasping. This imposes additional complexity to the training device that counteracts simplicity and cost-efficiency. It remains a requirement for training pinching movements, however extensive capturing of data and guidance of the trajectory may be omitted.

3.5 Design process

Since the devices to be developed are intended to mirror the needs of the patients, practical experience is paramount. However, no rehabilitation robotics device or background knowledge in this field had existed at the institute before the project related to this thesis. Therefore, cooperation with the clinical side is important. Practical experience shall be gathered by developing in fast iterations, which is why two prototypes are planned and developed for each major module. After testing the first prototype on patients, the experiences can be used for the second iteration.

The implementation chapter 4 of m-ReS^R will mostly describe general design decisions and developments while pointing out the differences between the iterations. A more detailed discussion of the differences and how the experiences from the first prototype improved the development of the second one is provided in Section 4.8.

Chapter 5 describes the implementation of the exoskeletons. Major differences between the iterations lie in the mechanical design and the sensing. As before, this chapter describes the differences of the iterations within the sections with an additional discussion at the end of the chapter. Due to many overlaps between both modules in software and communication, the description is bundled in Chapter 6.

Chapter 4

Implementation of a Training Device For Rotational Hand Movements¹

In this chapter, a system to train rotational movements named m·ReS^R is described. It focuses on training supination/pronation, dorsiflexion, and fine finger movements, e.g. necessary for opening a bottle. The design and implementation of the system is based on the concepts and requirements in Chapter 3 and developed in two iterations. The chapter is not structured according to the iterations, but each section highlights the differences of the two designs.

4.1 Introductory system description

The system is designed as an end-effector with one degree of freedom. The patient interacts with an actuator that may assist or resist the movement in smooth gradation. In the concepts, it was proposed to use one actuator for several exercises (Section 3.3.1). Therefore, the actuator can be oriented in different angles to the forearm. For supination/pronation training it is horizontally oriented and the patient can use the stronger muscles lying at the forearm and upper arm. When the motor axis is orientated vertically it stands perpendicular to the forearm. Thus, only a small amount of the torque can be exerted by the muscles of the forearm. Depending on the handle, two different major movements can be trained. A longer handle can be grasped with the whole hand and the rotation counteracts with the dorsiflexion of the wrist. A small handle forces the use of the fingers, training fine finger movements similar to opening a bottle or other knob-related activities of daily living. A computer-aided design (CAD) drawing is shown in Fig. 4.1 to give an idea about the design and use of the system.

4.2 Actuation and sensing

The challenge of the actuation of m·ReS in contrast to classical motion control lies in the unknown torques induced by the patient. Commonly, the motor is dimensioned

¹Parts of this chapter have been published in [194, 198]

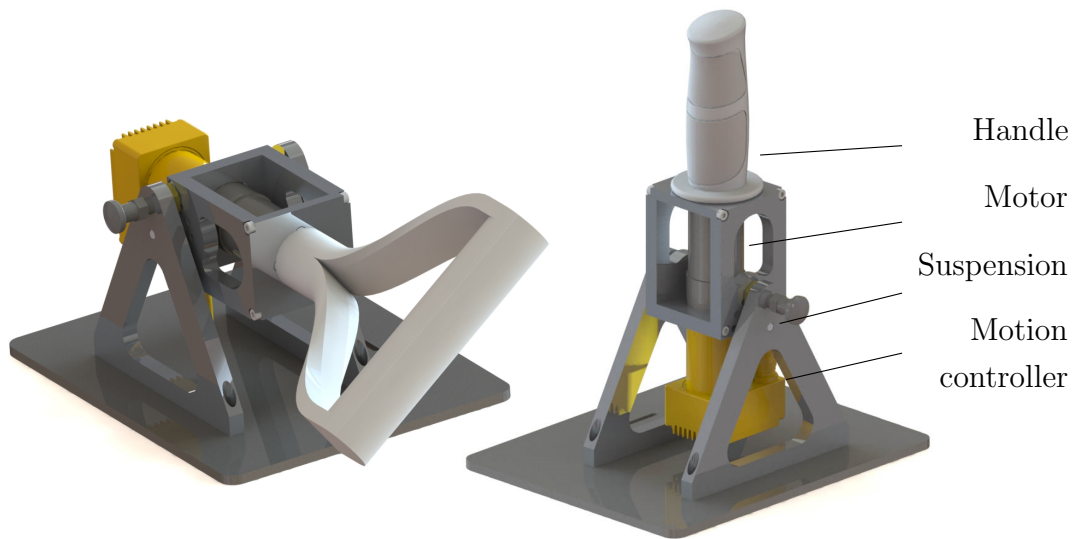


Figure 4.1: Rendered image of the CAD draft of m-ReS^{R1}

for a specific operating point, disregarding the reverse load of an active force. In this application, high torques from the user onto the device have to be regarded, which is especially challenging for spastic hands. At the same time the motor shall react sensible to user-induced torques, meaning that it requires high backdrivability.

4.2.1 Selection and dimensioning of the actuators

A preliminary experiment that gives guideline values for the dimensioning is described before the selection of the actuators is presented.

4.2.1.1 Preliminary dimensioning experiments

To estimate the maximum torques and forces onto a rehabilitation device in use, a simple experiment with three healthy subjects (male, age between 27 and 32) was conducted. A force-torque sensor was positioned in vertical and horizontal orientation similar to the intended orientation of the motor in later use. For both configurations a new run was started and the three subjects performed the test subsequently, while the sensor sampled the forces and torques in x,y, and z-direction (Fig. 4.2).

Table 4.1 shows the maximum absolute values of forces and torques, since the sign is not relevant and only the peaks are of interest for the dimensioning. The z-direction is colinear to the rotational axis of the handle, meaning that it is the axis of torques relevant for rehabilitation. The x- and y- directions are radially directed and the Pythagorean equation is applied to get a single combined radial force or torque.

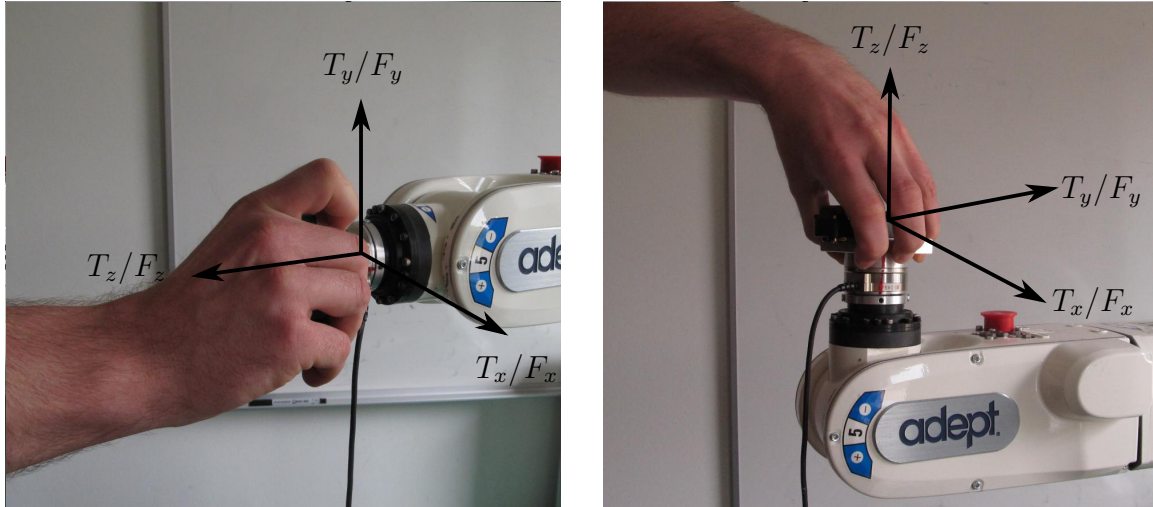


Figure 4.2: Horizontal and vertical orientation of the force-torque sensor

Direction	Force (N)		Torque (Nm)	
	X,Y	Z	X,Y	Z
Horizontally oriented	37.42	16.38	1.69	4.45
Vertically oriented	14.68	7.29	0.52	2.1

Table 4.1: Absolute maximum forces and torques acting on a sensor during different grasps performed by three healthy subjects

As expected, the results show higher torques for supination/pronation than for the bottle opening motion, which was taken to dimension the torque of the motor/gear-combination.

The experiment was conducted with healthy subjects who exerted the highest torque they were capable of on the sensor. Therefore, the torque result represents an upper bound for the dimensioning. The forces and torques in x- and y-direction are used to determine the load on the shaft of the gearbox. In case of exceeding the maximum shaft load, the gearbox might get damaged.

4.2.1.2 Selection

First the motor type to be used is discussed, followed by specific actuators selected for m-ReS^{R1} and m-ReS^{R2}.

Motor types and gear A huge variety of different kinds of motors exists. Due to size, controllability, cost, and availability we restrict the considerations to electric motors. Further, asynchronous motors are ruled out due to the requirement of using direct current (Section 3.4.1.2), but also since they are more suitable for high power applications or in fixed-speed services. The requirement of having an adaptable torque would require variable-frequency drives. Although prospective positive effects on the energy efficiency are expected, they do not outweigh the simpler setup of DC motors. Another kind of actuators are stepper motors, typically used for positioning tasks since they allow to move in equal steps without any feedback sensor. However, in our application high torques occur, which may cause the open-loop positioning to fail. Moreover, this type is often not suitable for torque control or requires unnecessary complex motion control. This disadvantage suggests the use of other types of DC motors that allow for simpler torque control.

There are two ways to provide the demanded torque; by increasing either the motor power or the gear reduction ratio. Since high torques with very low velocities are required, the use of a gearbox is reasonable. However, high reduction gear ratios lead to poor backdrivability due to the resulting friction. This means that high torques must be overcome to initiate user-driven movement. Planetary gears are used due to widespread availability and the ability of bi-directional use.

m·ReS^{R1} uses a brushless DC (BLDC) servomotor from Dr. Fritz Faulhaber GmbH that provides a maximum torque of $96 \times 10^{-3} \text{ N m}$ and a gearbox with a reduction ratio of 43:1. The motor-gear combination can provide a total torque of 2.9 N m. This is below the upper bound torque of 4.45 N m (table 4.1) but is expected to be sufficient for impaired patients even if spasms are present. The gearbox owns high resistance against axial force in z-direction and radial forces and torques in x- and y-direction so that no additional bearing or clutch is required. This simplifies the mechanical design and means at the same time a cost reduction. The gear's maximum allowed axial force is 150 N which is far below the maximum force in z-direction in the force-torque test (16.38 N). The maximum combined moment in x- and y-direction (1.69 N m) is within the limits of the gearbox (2.25 N m) as well.

m·ReS^{R2} The industrial motion controller used for m·ReS^{R1} allows the fast creation of a working prototype. It also provided electronic commutation to easily use a BLDC motor, which exhibits some advantages over brushed DC motors. However, the major drawback of the motion controller is its limitation in control, communication, and functionality. For instance, it does not natively support torque control. Therefore, a microcontroller in conjunction with custom-made electronics and motor control replaces the former proprietary motion controller. A brushed DC motor is used since they can be controlled by only adjusting the voltage and maximum current. While the motion controller for the first prototype allowed the use of BLDC motors without additional effort, their implementation complicates custom motor control.

The simplification of the motor control justifies to relinquish the advantages of BLDC motors. Since the motor torque is proportional to the armature current of DC motors, torque control can be achieved by restricting the maximum current. The required electronics and microcontroller part are described later in Section 4.3 and 4.2.2.

The actuator of the first prototype was able to exert torques close to the maximum ratings of healthy subjects (Table 4.1). The advantage is that it provides sufficient torque to work against increased muscle tone, which is common for stroke patients. The field tests of $m\cdot ReS^{R1}$ revealed that subjects tend to exaggerate exercises leading to discomfort and pain in the wrist. Moreover, safety is an even bigger concern for $m\cdot ReS^{R2}$, since more custom-made components are implemented leading to more sources of malfunctions. Therefore, decreasing the maximum motor torque reduces the risk for severe injuries and inherently improves safety. Less maximum torque requires a lower reduction gear ratio, which improves backdrivability resulting in better control, current sensing, and haptical feedback. The ideal case would be to omit a gear. $m\cdot ReS^{R1}$ could, then, only exert a torque of 96 mNm, which is far below the torques exertable by humans. $m\cdot ReS^{R2}$ uses a stronger motor with 270 mNm (Dunkermotoren GR 63x55), which still would not allow to omit the gear. Therefore, a gear is used with a lower reduction ratio of 7:1 reaching a total torque of 1700 mNm. A stronger motor in combination with low terminal resistance has also the advantage that higher currents occur especially during stall, which facilitates torque measurement and control.

4.2.2 Torque measurement and control

Omitting additional force/torque sensors, the torque measurements have to be derived from the motor-inherent metrics. The technique for measuring the torque differs between the two iterations. $m\cdot ReS^{R1}$ is limited to the functions of the motion controller, while $m\cdot ReS^{R2}$'s customization allowed to tailor the components to the application.

$m\cdot ReS^{R1}$ relies on the functions provided by the industrial motion controller. Although a command exists to read-out the current, the results were influenced by the direction of the voltage applied on the motor. This results in deviating current measurements for the same torque in different directions. Therefore, torque is determined in position control mode using a predetermined mapping of the torque-dependent motion controller's position control parameter [193]. The disadvantage is that the motor has to remain at a constant position. The current or torque, respectively, can be limited with a dedicated command, which is sent over the RS-232 interface. Since direct access of the hardware is prohibited, exercises where the torque is continuously adapted, can only be controlled over the serial interface. This slows down the communication and strongly limits the flexibility. Torque measurements in motion and adaptive torque control are not possible.

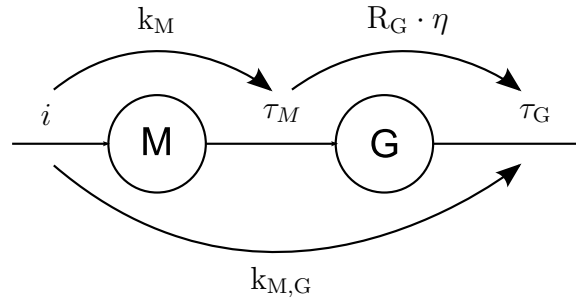


Figure 4.3: Relations between the motor current i , motor torque τ_M , torque constant k_M , gear ratio R_G , efficiency rate η , and torque output τ_G .

m·ReS^{R2} Accurate sensing of the current is crucial for exact determination of the motor torque. In contrast to the first iteration, the custom electronics allow the torque to be determined by the linear relation between the motor’s armature current i and the motor torque τ_M .

They are related with each other is connected over the torque constant k_M according to

$$\tau_M = k_M i. \quad (4.1)$$

k_M unites the influences of the magnetic field B of the stationary set of magnets in the stator, the number of armature current-carrying wires, and the motor geometry. The constant is provided by the motor’s data sheet. By measuring the current through the motor, the torque can be estimated.

To summarize, the relations between armature current, motor torque, gearbox, and torque output are depicted in Fig. 4.3.

After establishing the measurement, the next step is to control the torque. This can be achieved by limiting the armature current. Given that the magnetic field is constant, the armature current can be controlled by applying an adjustable voltage as a manipulated variable. The current is measured to close the loop, a setpoint is defined, and the current is controlled accordingly. The adjustable voltage uses pulse-width modulation (PWM), which is supported by the microcontroller and allows to control the motor after amplification of the signal.

In comparison to common motor control applications, the motor is not or only slowly moving during the exercises. To simplify, we dimension the control system at standstill so that counter EMF is not regarded and the relation between voltage and current follows Ohm’s law. Therefore, no 1st-order lag (PT1) behavior is expected, which is typical for free-running motors, but proportional behavior and so we model the plant accordingly. A suitable controller for this has integral behavior, optionally together with low proportional gain. System stability is paramount because it is necessary for safe operation. Derivative action is, therefore, not used due to the variable impact on system stability [8]. Strong disturbances are expected due to the user’s input that support or work against the direction of the motor. To avoid amplification

of the strong changes of the error, an integral controller without proportional gain is used.

A low setting of the integral term leads to slow response of the current to disturbances or changes of the setpoint. A controller with a high integral parameter responds quickly but tends more to oscillations. The parameter was determined by observing the control behavior when a user works with the motor. The integral gain value K_I was set to the highest value possible without oscillations when working against the maximum torque. A K_I of 1.7 was determined, which is multiplied with the sampling time T (in most cases 10 ms) for the discrete controller.

4.2.3 Angle measurement and position control

Virtual rehabilitation and the implementation of visual feedback distortion requires exact angular position measurements. The accuracy depends on the resolution of the encoder and the gear ratio. $m\text{-ReS}^{\text{R1}}$ has a higher theoretical resolution of 0.00056° on the speed reduced side than $m\text{-ReS}^{\text{R2}}$. The accuracy is, however, limited by mechanical effects like backlash ($\leq 1^\circ$ according to the gearbox's datasheet). The encoder used in $m\text{-ReS}^{\text{R2}}$ achieves 1024 impulse per revolution per channel. Capturing both channels' rising and falling edges, respectively, and including the gear ratio of 7:1 leads to an accuracy of 0.0125° . The lower resolution is sufficient and less interrupts have to be detected by the microcontroller, saving its resources.

Whereas $m\text{-ReS}^{\text{R1}}$'s motion controller provides a position controller, this functionality has to be implemented on the microcontroller for $m\text{-ReS}^{\text{R2}}$. The heuristic tuning method by Ziegler and Nichols gives a first estimate [207]. According to this method, the proportional gain K_P is set to half the ultimate gain $K_{P,u}$. The ultimate gain was found to be $K_{P,u} = 38$ so that

$$K_P = \frac{K_{P,u}}{2} = 19. \quad (4.2)$$

A proportional controller generally operates with a steady-state error. Therefore, an integral term K_I shall be introduced. The parameter is tuned based on the ratio between K_P and the oscillation period at ultimate gain T_u . However, the period was so short, so that the integral term resulted to be magnitudes too high for stable control. Therefore, it was manually tuned such that no steady-state error as well as no instability occurs, and good behavior in following a setpoint trajectory can be achieved ($K_I = 1.89 \cdot T$).

4.3 Electronics

The electronics between both iterations strongly differs since $m\text{-ReS}^{\text{R1}}$ focuses on rapid development and testing with industrial hardware and $m\text{-ReS}^{\text{R2}}$ extends the possibilities with custom-made circuits.

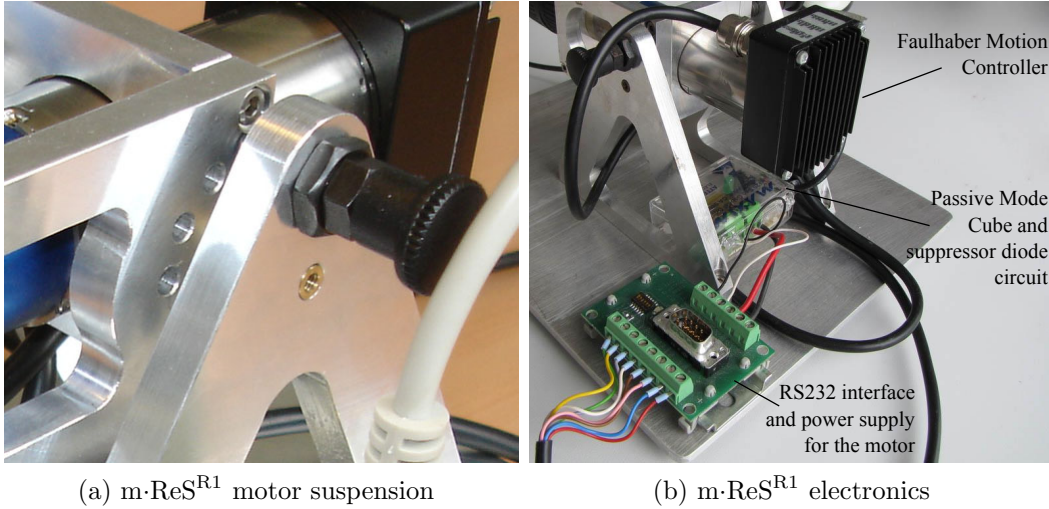


Figure 4.4: m-ReS^{R1} motor suspension and electronics

m-ReS^{R1} was intended to be applied quickly to use feedback for further developments. Therefore, an industrial motion controller is integrated into the actuator facilitating the motor control and sensor acquisition. It takes care of the electronic commutation of the brushless DC motor. Position and velocity control as well as overheating prevention are provided straight out-of-the-box.

An included circuit board provides connectors for the power supply and a D-Sub socket for the RS-232 communication (Fig. 4.4b). The circuit was extended with a transient-voltage-suppression diode to protect the power supply from motor-induced voltage spikes. Furthermore, circuitry was developed that enables to exploit one of the motion controller's function to control the motor position with an externally applied voltage (Fig. 4.5). It cuts off the supply voltage to 20 V and shifts it to a range between 10 V and -10 V. An additional potentiometer adjusts the voltage at the analog in pin (AnIn) in comparison to the analog ground (AGND). This permits the motor's position to be controlled with the potentiometer forming the basis for one the extension module called Passive Motion Cube (Section 4.6.1).

The use of an industrial controller in the first prototype saved time in the development and allowed to quickly proceed into the testing phase. It was tried on different patient, used for a study, and helped to gain insights into friction and inertia compensation. However, it restricts the possibilities due to the predefined set of commands and the limitations of the RS232 communication. Torque measurements can only inaccurately be performed. Therefore, a microcontroller and custom-made electronics are introduced for the second prototype.

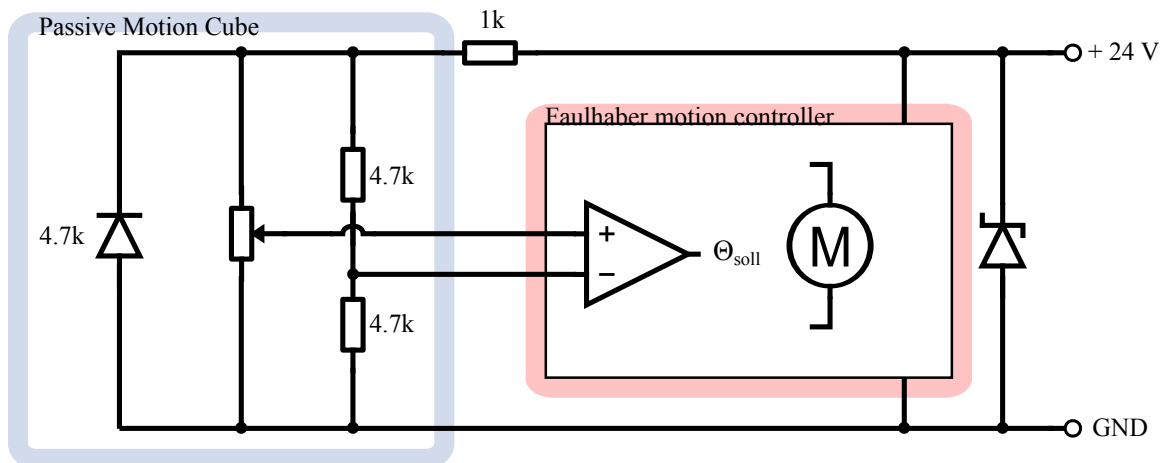


Figure 4.5: Schematic for the motion controller with functionality for an extension module called Passive Motion Cube (Section 4.6.1)

m·ReS^{R2} A microcontroller with our own firmware was introduced in the new version that allows for greater flexibility. It controls the actuators using a motor driver, takes care of gathering sensor data, and sends and receives data over a serial connection. Due to the closeness to the hardware layer, this approach is inherently faster. The 8-bit AVR RISC-based Atmel ATmega328P microcontroller has 23 general purpose I/O lines, three flexible timer/counters with compare modes, internal and external interrupts, serial programmable Universal Synchronous and Asynchronous Serial Receiver and Transmitter (USART), 2-wire serial interface, SPI serial port, and a 6-channel 10-bit A/D converter. Its compatibility to the majority of the Arduino families would allow to reuse the code with the very popular open-source hardware. The same chip is also used for two different microcontroller modules that we used to reduce the hardware prototyping effort. The boards provide the basic components to put the microcontroller into operation, but differ in the way of transmitting the serial communication. One incorporates an UART-to-USB bridge for a tethered connection while the other includes a Bluetooth module for wireless connection.

The 25 W switching power supply provides 5.5 V, which supplies the motor driver as well as the microcontroller and other integrated circuits (ICs). A shunt regulator using a LM4040 precision micropower shunt voltage reference regulates the supply voltage to 5 V, which is used for the Hall-sensor and the potentiometer of the Passive Motion Cube.

A common actuation solution is pursued using a fully integrated H-bridge motor driver IC [83] (Fig. 4.6). We apply the VNH2SP30-E chip, which is typically used in automotive applications. It is dimensioned for currents up to 30 A, which is why the maximum necessary 4.9 A continuous current for the motor can be provided with a low temperature increase. The IC interacts with the microcontroller with logic level compatible inputs and amplifies a PWM signal of up to 20 kHz. The high frequency

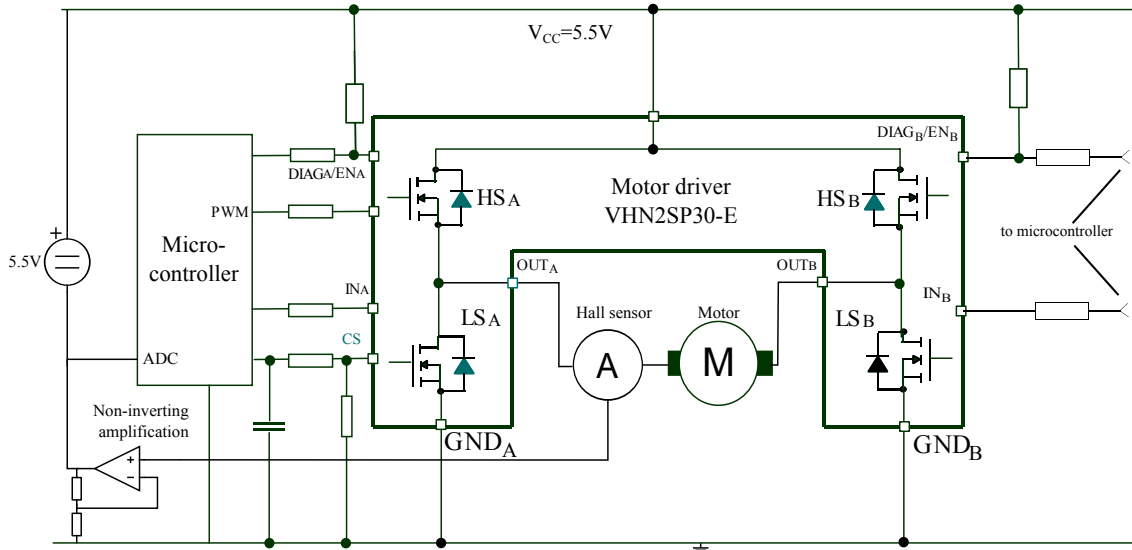


Figure 4.6: Simplified schematic of the m-ReS^{R2} circuit focusing on the actuation. Connectors for the Passive Motion Cube, the motor encoder, power supply, and the navigation switch were omitted.

is above the audible range so that less noise is generated in operation. Another important property is that it is possible to switch into coasting state where high impedance is applied on the H-bridge outputs by turning off all MOSFETs improving backdrivability. In contrast, many other motor drivers short-cut the leads causing the motor to break by converting the mechanical energy to electrical power and finally dissipating it to heat.

The motor driver features an integrated current sensing. However, the quality is limited, which is why a carrier board with a Hall effect-based ACS714 current sensor and low-pass filter is serially connected to the motor driver. It converts the armature current to a voltage that is sampled by the microcontroller. A supply voltage of 5 V results in a centered sensor output voltage of 2.5 V for 0 A and changes by 185 mV per Ampere of input current. Positive or negative currents increase or decrease the output voltage, respectively. The current sensor board can optionally be plugged into the main circuit board, if higher accuracy of the current sensing is desired. An operational amplifier circuit shifts the sensor output to the measurement range of the microcontroller for higher accuracy. The Passive Motion Cube (Section 4.6.1) is almost completely compatible to the new circuit allowing for the same functionality.

4.4 Friction and inertia compensation for improved backdrivability of m·ReS^{R1}

The technique described in this section is implemented and tested on m·ReS^{R1} to reduce unwanted effects of the gear. It can be transferred to m·ReS^{R2} regarding the differences in hardware.

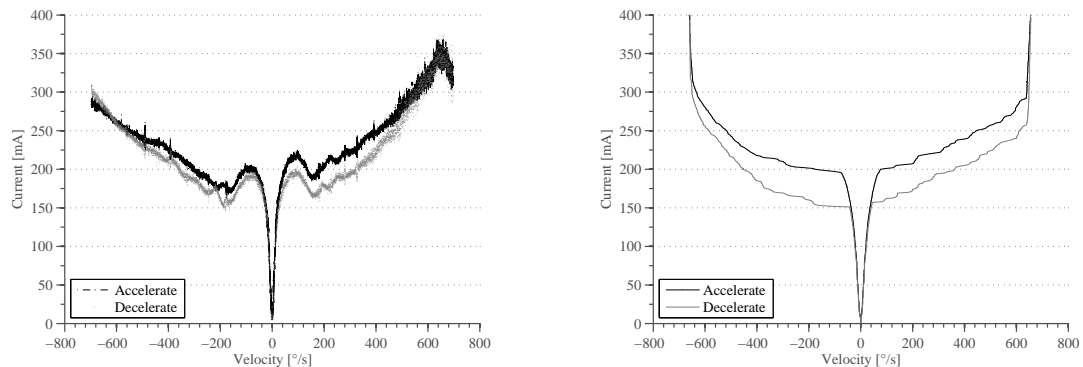
Backdrivability is an important property, since it is required that the motor measures and reacts on user-driven torque. However, motors and gears introduce friction and inertia that impede movements of the user on the motor. As described before, expensive force-torque sensors are avoided to keep the cost low. Without the feedback of such a sensor, the loop for user-experienced torque cannot be closed in order to control the motor for increasing backdrivability. As an alternative, feed-forward control can help to improve backdrivability by directly linking the control variable to the disturbance.

We model the friction to be composed of a breakaway part that has to be overcome to initiate movements from standstill and a velocity-dependent part. Breakaway friction causes increased resistance in initiating user-driven movements from standstill. Since bi-directional movement is required in our application, we investigate the influence of the breakaway friction on bi-directional movement.

In order to determine the breakaway friction torque, the armature current was increased in steps of 1 mA and applied on the motor of m·ReS^{R1} until it starts moving. The procedure was repeated 240 times and averaged, resulting in a breakaway threshold of 7 mA after rounding down. The lower value is taken, so that the motor does not start unintentionally. The corresponding torque is a surmountable threshold, so that breakaway friction compensation is not regarded for the used motor-gear combination and application and will not be used for the subsequent implementation of the compensation.

The kinetic friction compensation depends on the relation between the velocity and the kinetic friction torque. A mapping can be measured by generating a lookup table between the velocity and the current and applying it in application as a feed-forward input. Either the velocity is the independent variable and the armature current is measured or vice versa. Both ways were tested. First, the velocity was kept constant over 80 samples for each step in order to avoid dynamic friction components. The samples were averaged and written into the lookup-table visualized in Fig. 4.7a. Second, currents were applied and the velocity was measured avoiding influences of the controller. For each step of 1 mA from 0 mA to 400 mA, three passes with 80 measurements were taken and averaged and written into a second lookup table (Fig. 4.7b).

In both graphs hysteresis occurs leading to two different armature current values for acceleration and deceleration at the same velocity. The oscillations in the velocity result in a change of the sign of the derivative. This causes switching between the lookup tables and undesired behavior in the motor control. Therefore, a factor is



(a) Setting the velocity and measuring the resulting current (b) Setting the current and measuring the resulting velocity. Used as a lookup table for the kinetic friction compensation

Figure 4.7: Mapping between current and velocity. The black curves were generated by increasing the velocity or current, respectively, and measuring the dependent variable and the grey curve by decreasing velocity or current [198] ©Springer.

introduced that divides the transition between the two values of the lookup table in parts of 20% per cycle of the difference.

The graph generated using velocity control exhibits local minima while there are none for the armature-dependent trial. Therefore, the second lookup table (Fig. 4.7b) is used for the kinetic friction compensation.

The inertia compensation depends on the acceleration of the motor a together with the moment of inertia I . The acceleration is the discrete derivative of the velocity output and the constant I depends on the mass distribution of the rotating parts. The induced torque τ_I depends on the inertia and the acceleration according to

$$\tau_I = I \cdot a. \quad (4.3)$$

The control diagram in Fig. 4.8 depicts the use of the compensations. In contrast to the lookup tables (Fig. 4.7), the unit in the equations is rpm since it is used by the motion controller. The motor is represented as admittance control since the user exerts torque on it and the motor reacts with a proper displacement. The velocity output is input for the impedance modeled human who reacts on the displacement and exerts the torque τ_U used to determine the torque necessary to compensate the friction. The kinetic friction compensation is either zero for $\omega = 0$ rpm or uses the mapping above. The sum of friction and inertia compensation torques are converted to the corresponding currents by dividing it with the torque constant k_M and adding

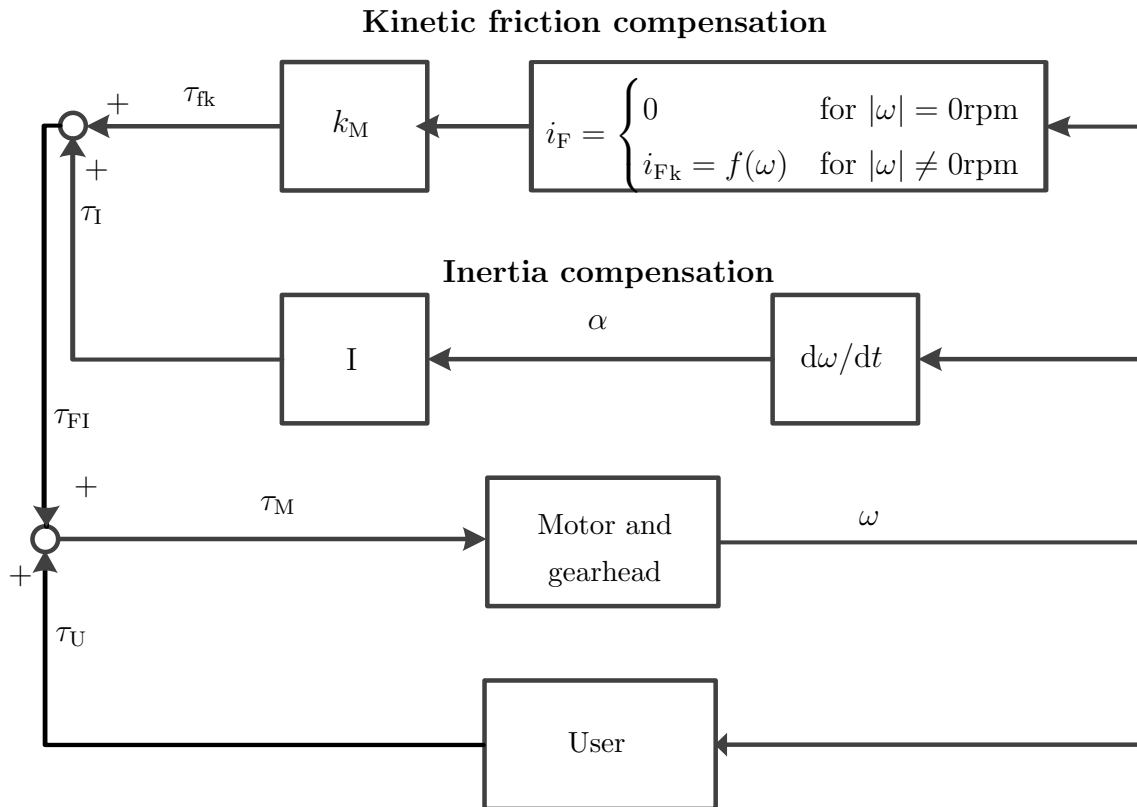


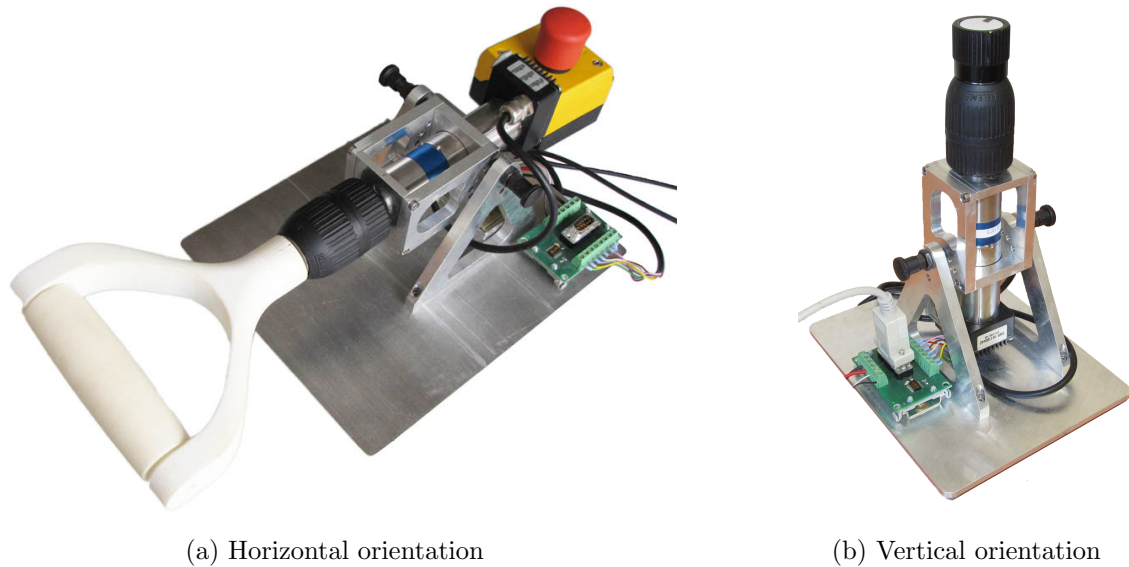
Figure 4.8: Block diagram of the friction compensation

it up to i_{FI} and applied to the motor, so that a corresponding torque τ_{FI} is exerted. It sets off against the user-driven torque τ_U resulting in τ_M . The torque is the input to the admittance control modeled motor resulting in a new velocity. The friction and inertia compensation was partially developed as part of a bachelor thesis, which gives more details on the implementation [205].

4.5 Mechanical design

The concepts in Section 3.3.1 proposed to use one actuator in different orientations to combine the supination/pronation, dorsiflexion, and finger function exercises in one device. The implementation differs between both iterations.

m·ReS^{R1} In the first iteration, the motor is kept in an open casing that is suspended so that it can be rotated and fixed at different angles. Orientated horizontally, supination/pronation movement can be trained (Fig. 4.9a). In vertical orientation, dorsiflexion and finger functions can be exercised (Fig. 4.9b). Further angles in 30° offsets can be adjusted and fixed with a locking pin (Fig. 4.4a). The cables for the power supply and motor electronics rotate with the motor (Fig. 4.4b).



(a) Horizontal orientation

(b) Vertical orientation

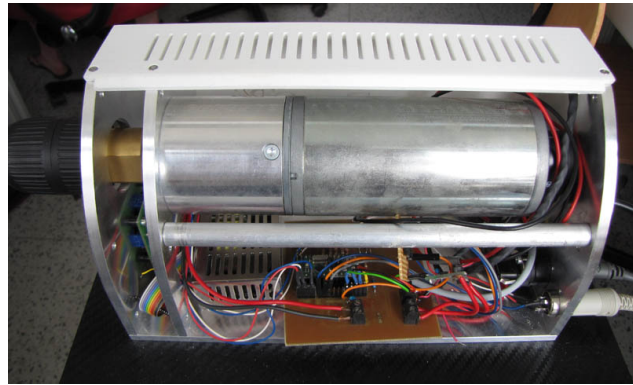
Figure 4.9: Image of $m\cdot\text{ReS}^{\text{R}2}$ in horizontal orientation for supination/pronation and vertical orientation for dorsiflexion and fine finger training.

$m\cdot\text{ReS}^{\text{R}2}$ The new iteration follows the same concept as for $m\cdot\text{ReS}^{\text{R}1}$. Some design aspects of the first prototype such as the exposed electronics still exhibit a prototype-like look. The second iteration shall be pushed further towards clinical application and also the design shall be revised. The motor and the electronics are not freely visible anymore, but integrated into a casing with ports for the supply voltage, HDMI, USB for communication, and a plug for the extension modules (Fig. 4.10a). The weight is increased due to the use of a stronger and bigger motor. Although this means a marginal disadvantage in terms of portability, the stability of the unfastened table-top system is increased. The higher length impedes a similar suspension of the motor as in $m\cdot\text{ReS}^{\text{R}1}$ to allow different orientations. Also the beforementioned integration of the system into a casing hinders this suspension. Therefore, a table that is adaptable in height and can rotate the whole device has been introduced. Besides changing the orientation, the table allows to adapt the height in relation to the user's arm which gives more freedom in finding a comfortable training position (4.11). Alternatively, $m\cdot\text{ReS}^{\text{R}2}$ can be used as a table-top system as well.

$m\cdot\text{ReS}^{\text{R}1}$ does not have any input elements and relies therefore on the commands send over the RS-232 interface. It is mostly used in conjunction with a touchscreen to control the device. The experience from the use with patients showed that especially elderlies have problems to switch the focus between the input device and the training region. Therefore, $m\cdot\text{ReS}^{\text{R}2}$ features an additional control element that sits below the motor. This position close to the impaired hand together with the tactile response



(a) Backside of m-ReS^{R2}



(b) Look inside of m-ReS^{R2}

Figure 4.10: m-ReS^{R2} input interface and connectors

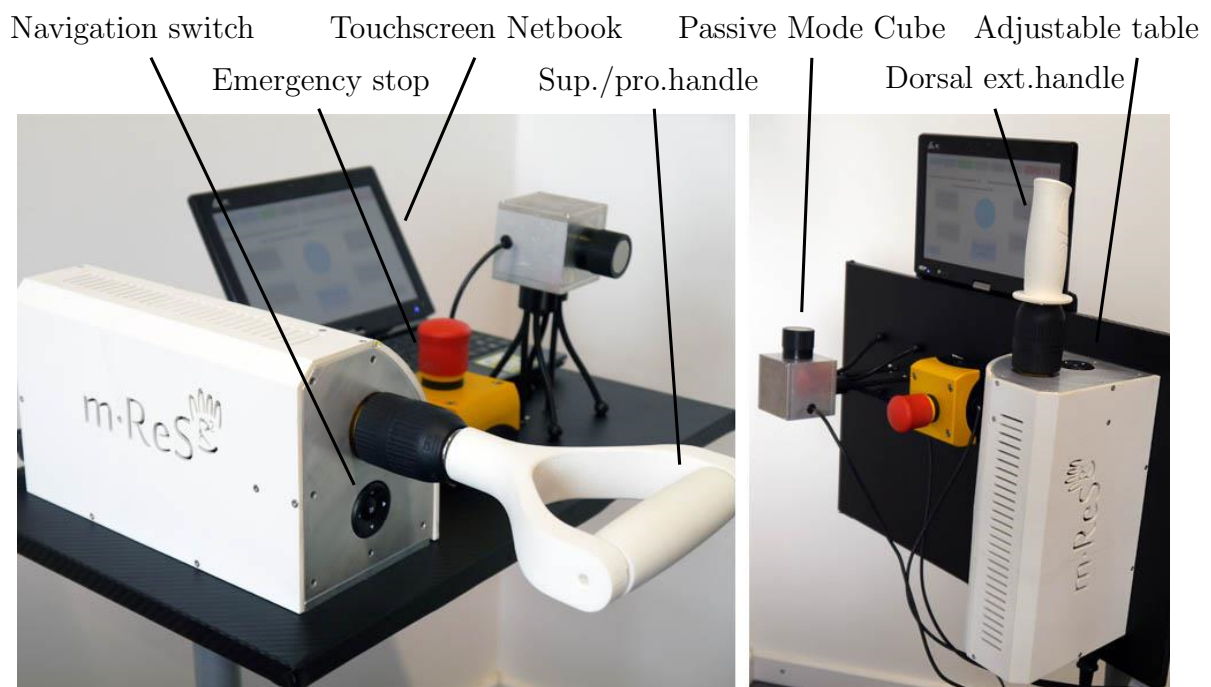


Figure 4.11: Horizontal (l.) and vertical (r.) orientation of m-ReS^{R2} using the adjustable table

of the buttons enables the patient to control the software without losing focus on the training.

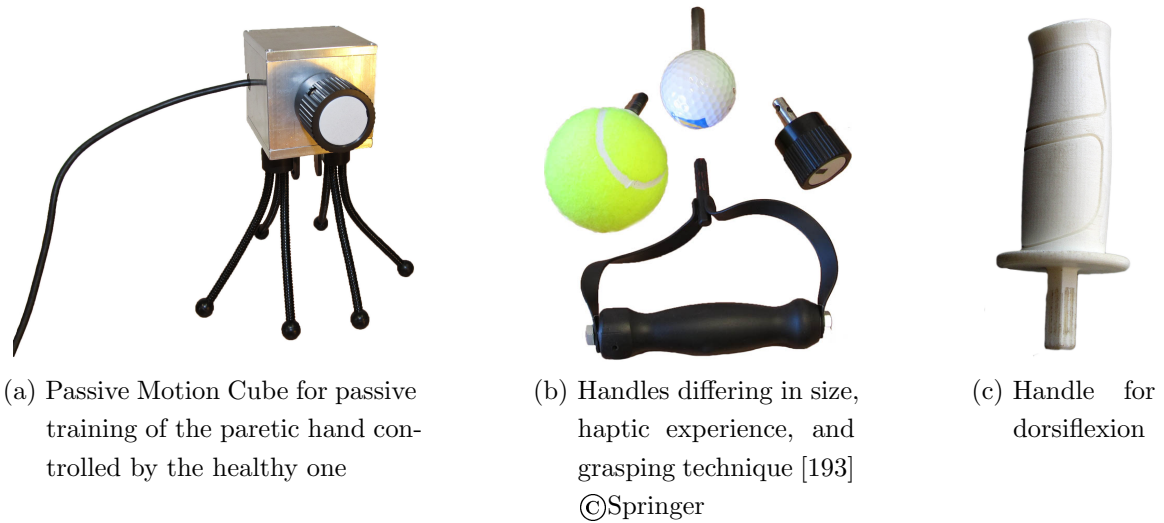


Figure 4.12: Extension modules and handles

4.6 Extension modules and accessories

4.6.1 Passive Motion Cube

The Passive Motion Cube extends the functionality of the device to bi-manual passive training (Fig. 4.12a). Including the non-affected upper limb in the training has a facilitatory effect on the affected extremity [62]. The extension module allows hemiparetic patients to control the motor with their healthy hand in order to mobilize the paretic one. It consists of a potentiometer that sets the motor's position by applying a voltage to the analog input of the main device's motor for m-ReS^{R1} (Fig. 4.5) or the microcontroller's ADC pin for m-ReS^{R2}. The patient's position limits have to be defined first, so that the motor cannot exceed the joint range of motion. Then the non-paretic hand turns the handle of the Passive Motion Cube that controls the motor moving the impaired hand attached to the motor within the limits [193].

4.6.2 Handles

Different exercises or movement trainings need specific handles. They are required to be changed easily and swiftly avoiding the use of screws or special tools. Therefore, we adopted a keyless three-jaw chuck, which is connected to the motor shaft by a custom-made adapter. This allows to attach all cylindrical or multi-sided shafts with diameters from 2 to 13 mm, giving high flexibility in the tools and handles used. Examples are shown in Fig. 4.12b depicting handles that are specifically useful for different grasps or training modes.

A safety handle for supination and pronation exercises, which has been developed at the Toronto Rehabilitation Institute, can be used with the shoulder and elbow rehabilitation robot in Toronto as well as with m·ReS^R. It is described more in detail in Section 4.7.3 about the research visit.

After orienting m·ReS^R vertically, another kind of handle is more suitable for dorsiflexion exercises (Fig. 4.12c). It has to be grasped in the semi-supinated grip so that the motor axis is colinear to the handle's axis. If grasped, the motor torque is transferred over the hand to the wrist joint. Simultaneously, the wrist joint's axis moves around the motor axis and is extended or flexed depending on the motor direction and the side of the hand.

4.7 m·ReS^{R2}-based extension of a rehabilitation robot at the Toronto Rehabilitation Institute

The research described in this section was conducted in cooperation with the Intelligent Assistive Technology and Systems Lab (IATSL) located at the Toronto Rehabilitation Institute (TRI), which is affiliated with the University of Toronto. The goal was to extend an existing stroke rehabilitation robot for shoulder and elbow-based reaching exercises with an additional degree of freedom to train forearm and wrist functions. This work is based on m·ReS^{R2} with an adapted mechanical design and hardware.

This section capsules the motivation, concept and implementation of the extension module, since the research stay arose after the concept phase of m·ReS. The software and communication, however, strongly overlap so that this part is described later together with the whole m·ReS software in Chapter 6. First, the existing robot is described followed by the motivation to extend it to forearm and wrist functions. Then the concepts and implementation are described.

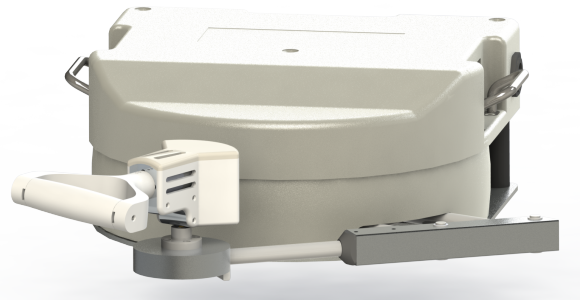
4.7.1 Toronto Rehabilitation Institute robotic rehabilitation system

The existing upper limb stroke rehab robot features an actuated two DOF robot arm that allows training of reaching on a planar workspace with adaptable assistive or resistive forces on the user's hand [110, 111]. After the calibration process, different exercises like waypoint reaching or games can be pursued, while the therapists set and adapt goals on a second screen. Based on an adaptive algorithm the actuators allow assistive and resistive forces depending on the patient's performance [68] (Fig. 4.13a).

The hardware and low-level programming was developed by a company named Quanser based on requirements and user-centered design specifications from IATSL. The robot with an included DAQ card is used for the real-time data acquisition and



(a) Stroke Rehab Robot at IATSL



(b) Rendered image of a CAD design of the stroke rehab robot with the developed extension module attached

Figure 4.13: m·ReS^{R1} motion controller

control of the robot arm. The high-level software is being developed by IATSL comprising two parts: The robot is controlled with Quanser's Rapid Control Prototyping software QuaRC [152], which can be programmed in a Simulink environment. It is connected to a computer via USB. A graphical user interface (GUI) written in Java communicates with the Simulink model and provides user interfaces for the therapist and the user.

4.7.2 Motivation for the extension module

The related works show several arguments and studies that speak for the training of distal upper limb functions (Chapter 2 and Section 3.1). Particularly relevant for the extension of the TRI robot is a work by Krebs et al. They extended an upper limb robotic therapy system for the shoulder and elbow with a module for forearm and wrist movements. A clinical trial with 52 stroke patients showed further increased rehabilitation outcomes concluding that an extension of the training to other limbs allows for further functional improvements [92]. Moreover, supination and wrist extension movement practice is paramount to allow progress towards more functional whole upper extremity movements [139]. Also important for the specific application, the extension module may also be used to control the posture during reaching exercises with the TRI robot.

4.7.3 Design and implementation of the extension module

The aim of the project was to develop a module to extend the robot with an additional DOF for training of forearm and wrist functions. The extension shall be attachable and detachable so that normal operation with the robot's old hand support remains possible without much effort in reconfiguration. In the first step, the

requirements for the extension module had to be set up. They were mostly based on specifications of the developers, discussions with occupational therapists at TRI, and mechanical constraints determined by the TRI robot design. The therapists re-confirmed that the most useful movement training for distal upper limb functions is supination / pronation, which coincides with m·ReS^R. Importantly, the therapists preferred a stronger motor with lower backdrivability, but with the ability to fix the patient's hand in a certain position, over a highly backdrivable weaker motor. The motor selection was limited to the available hardware. According to the therapists' preference, a Faulhaber 3042C motor was taken together with a planetary gearhead that has a reduction ratio 66:1. The nominal power of the motor is 16 W, from which the torque can be estimated according to the following equation

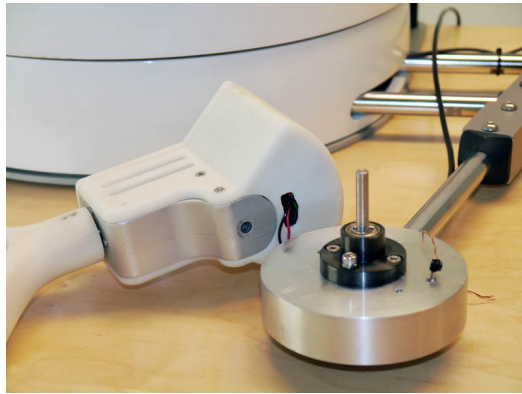
$$\tau_{M_n} = \sqrt{\frac{P_n}{R}} \cdot k_M \cdot R_G \cdot \eta \quad (4.4)$$

where P_n is the nominal power, R is the terminal resistance, k_M is the torque constant, R_G , the reduction factor, and η the efficiency rate. This motor-gear combination has a nominal torque of about $\tau_{M_n} = 2624 \text{ mN m}$.

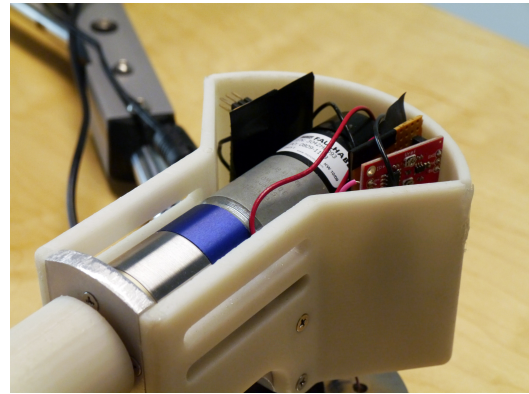
The design of the extension module originates from m·ReS^R with adaptations necessary to meet the requirement of the new application. It consists of a motor with a suitable driver, a microcontroller, and a current sensor packed together in a casing. It can be mounted to the robot together with a special handle, and interacts with the user controlled by a software.

The motor has to be mounted onto the robot's arm the patient grasps for training. The additional weight of the motor may be problematic for the robot's bearings. Additionally, the handle and its attachment cause an increase of the lever arm leading to higher forces onto the robot arm mount. The developers could not provide a guide value for the maximum load. Therefore, careful dimensioning was advised, keeping the distance between the attachment and the grasp as small as possible. Restrictions applied to the dimensions of the casing. It must not touch the robot within the workspace. Therefore, a round form for the casing is chosen.

Based on the requirements, the module was designed in Solidworks. A rendered image together with a CAD model of the robot is shown in Fig. 4.13b. The motor mount is made of aluminum to resist the forces lasting on the motor from the arm. The robot's end-effector shaft is put into a hole in the aluminum that works as a passive pin joint. This allows the extension module to orient in the direction of the user independent of the position of the end-effector (Fig. 4.14a). The casing holds the electronics and hides the parts due to appearance and safety (Fig. 4.14b). Low forces last on the part, which is why it was 3D printed with an stereolithography (SLA) machine. The training of dorsiflexion, similar to m·ReS^{R2}, is feasible to implement with little modifications in the design. A second hole in a 90° angle in the aluminum part would be sufficient for a functional system. However, the casing's design would have to be adapted.



(a) Bottom side of the extension module revealing the hole for the end-effector's shaft



(b) View into the casing showing the electrical components

Figure 4.14: Bottom side and look inside of the extension module

The position controller, in combination with the strong motor, is capable to maintain the patient's hand in an orientation prescribed by the therapist. This may improve body posture while performing the reaching exercises. Besides, the hardware allows to implement the same training modes as for $m\text{-ReS}^{\text{R}2}$ (Section 3.2).

Along with the motor mount and the casing, a safety handle was tailored to the application. It transmits rotational torque from and to the actuator but, in case of an emergency, it can be quickly released by pulling back (Fig. 4.15). For rotational movements the forces are transmitted from the hand piece over the material to the shaft and the motor. In the direction of a translatory pull-back movement, the hand piece is only fastened by steel ball plungers that release after overcoming a defined force, which depends on the strength of the spring in the ball plunger (Fig. 4.15c).

4.7.4 Electronics and sensing

The electronics that were selected in a way such that they remain compatible with former works for reusing the developments bidirectionally. It consists of a microcontroller, a motor driver, and a current sensing board amongst other circuitry. The ATmega168P microcontroller is compatible to the before written code. The motor driver is a different one but the necessary adaptations of the code are marginal. In comparison to $m\text{-ReS}^{\text{R}2}$, the motor is dimensioned for lower currents, which is why another sensor board with an operational amplifier gain stage amplifies the current measurements. The sensing principle is based on the Hall effect and the method of measuring resembles the one used for $m\text{-ReS}^{\text{R}2}$. Therefore, the code is interchangeable between the projects and only a few parameters have to be adapted.

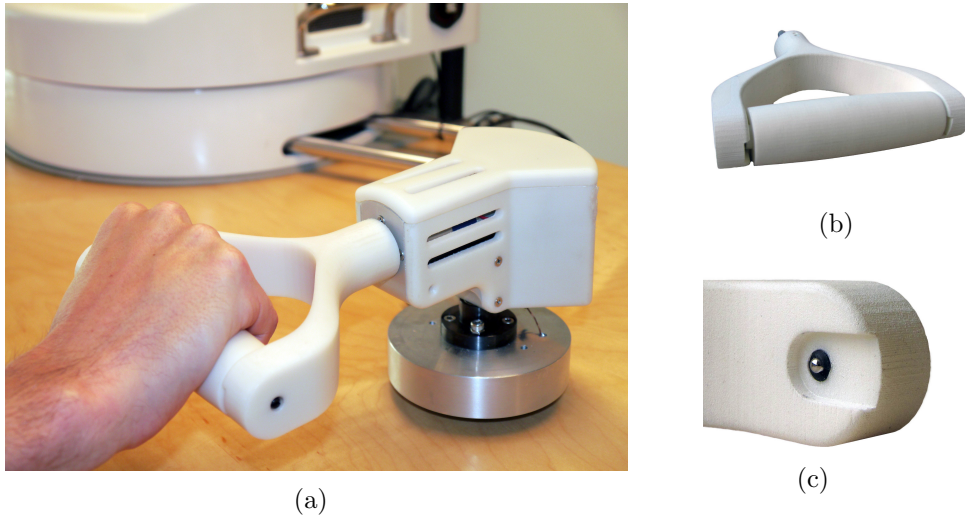


Figure 4.15: (a) Final design of the extension module in use with the upper limb rehabilitation robot in the background; (b) Supination/pronation safety handle; (c) A close-up of the steel ball plunger release mechanism

4.8 Discussion on iteration improvements

The quick iteration process allowed to develop a second prototype that builds upon the experiences from the first one. Especially, the demonstrations and practical tests with the neurologists, physiotherapists, and stroke patients helped to detect issues and problems in clinical use. For instance, we observed that elderlies had problems to switch their attention between the impaired hand for training and the touchscreen computer for proceeding in the steps in the GUI. Therefore, we integrated a navigation switch in $m\text{-ReS}^{\text{R}2}$, which is placed close to the impaired hand (Fig. 4.11). The motor of $m\text{-ReS}^{\text{R}1}$ was suspended to rotate it for the different exercises. However, the height was not adjustable, leading to uncomfortable use or making it necessary to support the arm with several cushions. $m\text{-ReS}^{\text{R}2}$ can either be placed onto the table-top or adapted in height and orientation using an adjustable table. The advantages are that the mechanical design of the device is kept simpler, the height can be changed, and the table can be omitted, if a table-top use is sufficient. Furthermore, the therapists and patients were intimidated by the setup and hesitated to use the system on their own. This led to the decision to provide a version where the computer is already integrated into the system using the Raspberry Pi (Chapter 6). Alternatively, the USB connection to an existing PC may be used, which was developed towards "plug-and-play" behavior for the second prototype.

Also the technical side showed several improvements. First, the custom-made electronics allow for more flexibility and faster control rates. The torque estimation based on current sensing is expected to be more accurate. Many limitations of the commercial motion controller could be overcome. In $m\text{-ReS}^{\text{R}1}$ decreased backdrivability was

observed when the motor is connected to the Faulhaber motion controller. The motor driver in m·ReS^{R2} provides a MOSFET configuration that lets the motor coast to avoid this problem. Omitting a proprietary motion controller, the developments at TRI were facilitated by reusing developments of m·ReS^{R2}.

The electronics were adapted to fit some special needs like a tilt sensor to detect the orientation of the motor. To reduce the prototype-like look of m·ReS^{R1}, the motor and the electronics were placed into a casing. m·ReS^{R2} is equipped with a stronger motor and a gear with a lower reduction gear ratio which should improve backdrivability. The actuator by Dunkermotoren is stronger than any of Faulhaber and also cheaper than a comparable one from the competitor. However, it turned out that also the quality was lower e.g. observed by the presence of higher friction.

In conclusion, the iterations helped to scout different issues and improve the second iteration in several aspects.

Chapter 5

Implementation of parametrizable actuated hand exoskeletons¹

This chapter presents the implementation of the exoskeleton based on the preliminary concepts in Chapter 3. After describing the system and its design, the parametrization of the computer-aided design (CAD) model is described. Then, actuation, sensing, and electronics are described before an extension module for the use of one actuator for four fingers is explained.

5.1 Introductory system description

The exoskeleton is worn by the patient and tendons, also called cables or wires, are attached to it exerting forces on the exoskeleton that are transmitted to the fingers. Restricted to one actuator per finger, only unidirectional movements are possible within one training session. The force of the actuator is transferred via the cable-transmission to the exoskeleton. Several attachment points are feasible to allow different exercises and during them, the force can be adapted by use of the microcontroller and electronics. They also read sensors to measure the joint angles that are placed within the exoskeleton. The two iterations of the exoskeletons m·ReS^{X1} and m·ReS^{X2} were partially developed in a diploma thesis [64] and a bachelor thesis [116], respectively.

5.2 Mechanical design

The exoskeleton is manufactured by means of rapid prototyping using a 3D printer. This removes limitations of traditional production techniques. Due to the additive manufacturing technique, indentations do not have to be avoided. Very complex geometries can directly be created from digital CAD data, which are not feasible to be manufactured traditionally in the workshop. The used printer is an EOS Formiga P100 that applies selective laser sintering (SLS). The printing material is a fine powder based on polyamide-12 that has an elastic modulus of $1700 \pm 150 \text{ N mm}^{-2}$, low sliding friction coefficient, and excellent abrasion resistance.

¹Parts of this chapter have been published in [196, 197]

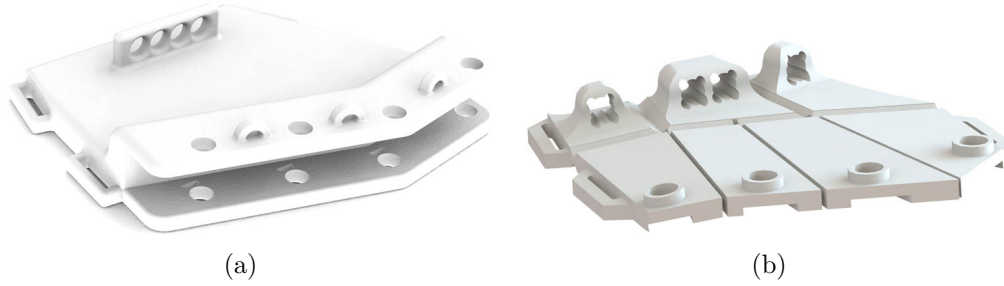


Figure 5.1: Comparison of the bases of the two iterations

5.2.1 Base

m·ReS^{X1} uses a plane simple base where the exoskeleton’s phalanges are attached. It is fixed at the back of the hand by using straps and velcro (Fig. 5.1a). m·ReS^{X2} has a more sophisticated base design to account for movements and to increase comfort. It is divided into three planes that are partially separated by slits and tapered to increase flexibility (Fig. 5.1b). A neoprene layer can be added, which distributes forces onto the hand increasing comfort.

5.2.2 Joints

The distal (DIP) and proximal interphalangeal (PIP) joints as well as the metacarpophalangeal (MCP) joint in m·ReS^{X1} are designed as revolute joints. These 1-DOF kinematic pairs have the major advantage that they have a simple design and require little space on the dorsal sides of the fingers. Still, the little space necessary to align the mechanical and the anatomical rotational axis leads, in the case of the PIP and DIP joint, to abduction. This disadvantage has been accepted to avoid placing the joint on the dorsal side. Alternative joints introducing passive DOFs consisting of several connected bars inevitably lead to bulky structure on the back of the hand [32]. Additionally, revolute joints are integrated, allowing for abducting/adducting the fingers. However, the size of the fingers of m·ReS^{X1} prevented the user from executing these movements. In m·ReS^{X2} the walls are thinner to reduce the abduction caused by the exoskeleton and making it more comfortable to wear.

In case of the MCP joint, lateral placement colinearly to the anatomic joint axis is not possible. Therefore, for m·ReS^{X1} the revolute joint has been shifted to the back of the hand. Additionally, a prismatic joint has been introduced to account the relative change of distance between the shifted MCP joint and the PIP joint (Fig. 5.2). However, jamming of the 3D printed prismatic joint caused unwanted forces on the fingers.

m·ReS^{X2} uses a more sophisticated MCP joint to align the mechanical and anatomical axes. This renders the prismatic joint unnecessary. It consists of two arcs gliding

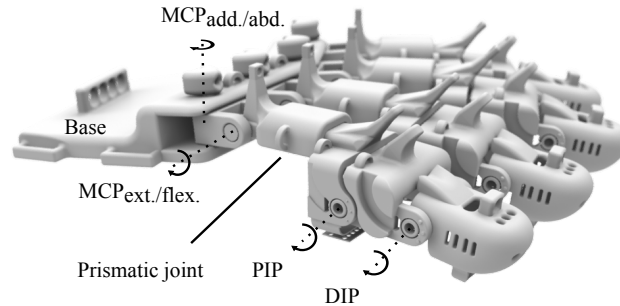


Figure 5.2: Joints of $m\text{-ReS}^{\text{X1}}$ drawn into a rendered image [196] ©IEEE

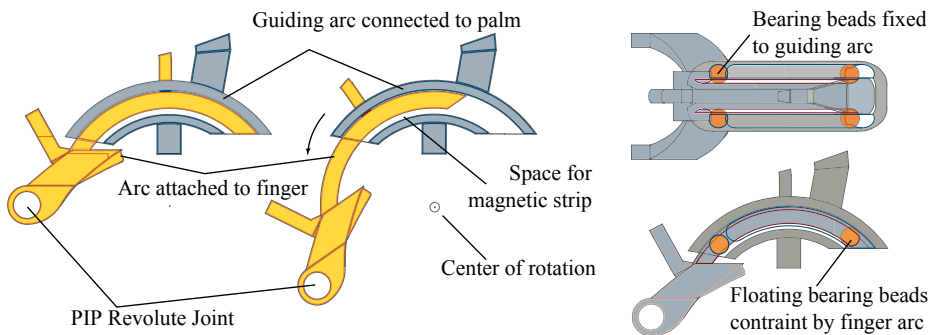


Figure 5.3: New design of MCP joint of $m\text{-ReS}^{\text{X2}}$ [197] ©Springer

into each other with their axes of rotation coinciding with the anatomy. The guiding arc is connected to the base and the other arc is attached to the exoskeleton's proximal phalanges. The arc structure is prone to jamming, since the force is not directed in the sliding direction. Ball bearings are integrated to guide the arcs and reduce friction. Two beads follow the guiding arc and are restraint from falling out by placing them into an indentation. At least two other beads run freely within a groove (Fig. 5.3). Increasing their amount improves stability, but causes more friction and reduces the joint's range of motion. The minimum required number of beads is four and the optimum was found to be six.

5.2.3 Preliminary thumb design

The unique function of the thumb is opposition to the other fingers, which is a prerequisite for the sophisticated use of the hand in humans [131]. This special role complicates the thumb's inclusion into an exoskeleton.

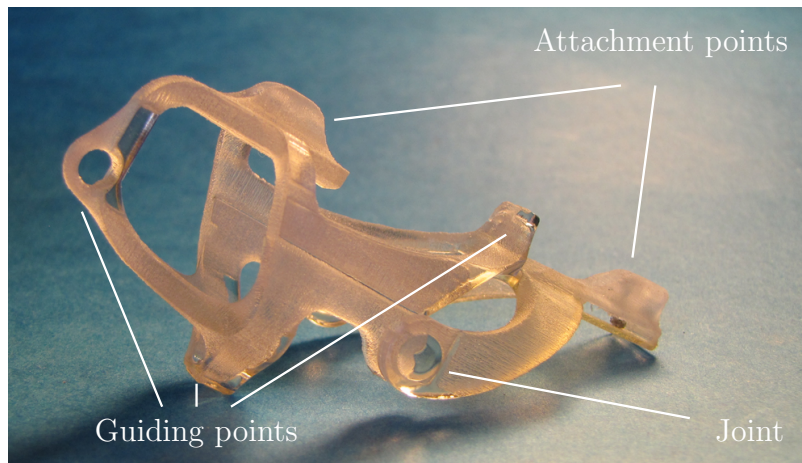


Figure 5.4: Preliminary design of the thumb module

Pinching training is the most important exercise that includes the thumb. Therefore, a module that focuses on this training was developed (Fig. 5.4). The design is simplified by omitting a mechanical connection to the base. The exercises are performed by connecting the actuating tendon over guides at the fingers to the thumb. This is described more in detail in the configurations section (Section 5.4.2). Apart from measuring the tendon displacement with the motor encoder, the thumb module is not equipped with angle sensors. The only measurement that remains is the relative displacement of the cable.

5.2.4 Assembly

One key feature of $m\text{-ReS}^{\text{X1}}$ is that the exoskeleton is printed in one piece including the joints. The advantage is that no assembly is necessary, increasing cost-efficiency, especially with regard to falling costs for 3D printers and printing material. A clearance of 0.3 mm kept the moving parts from melting together during the print process. However, the clearance causes translational movements in the joints, which potentially leads to problems with the sensors. This, together with the more complex MCP joint design, lead to printing the parts separately in $m\text{-ReS}^{\text{X2}}$. This allows to minimize the clearance to nominal dimensions improving sensor accuracy. The assembly effort is minimized by using a clip-in mechanism to connect the parts. Another advantage is that fingers and bases can be printed in generic sizes to create a set that fits different sized hands. Although the long-term goal is to achieve customized exoskeletons, during the development and for studies such a set can help to test the exoskeleton on more people. Images of the assembled exoskeletons in both iterations are shown in Fig. 5.5.

$m\text{-ReS}^{\text{X}}$ demonstrates the possibility to reduce assembly effort using rapid prototyping technology. Although the exoskeleton itself is complex, the impact on the

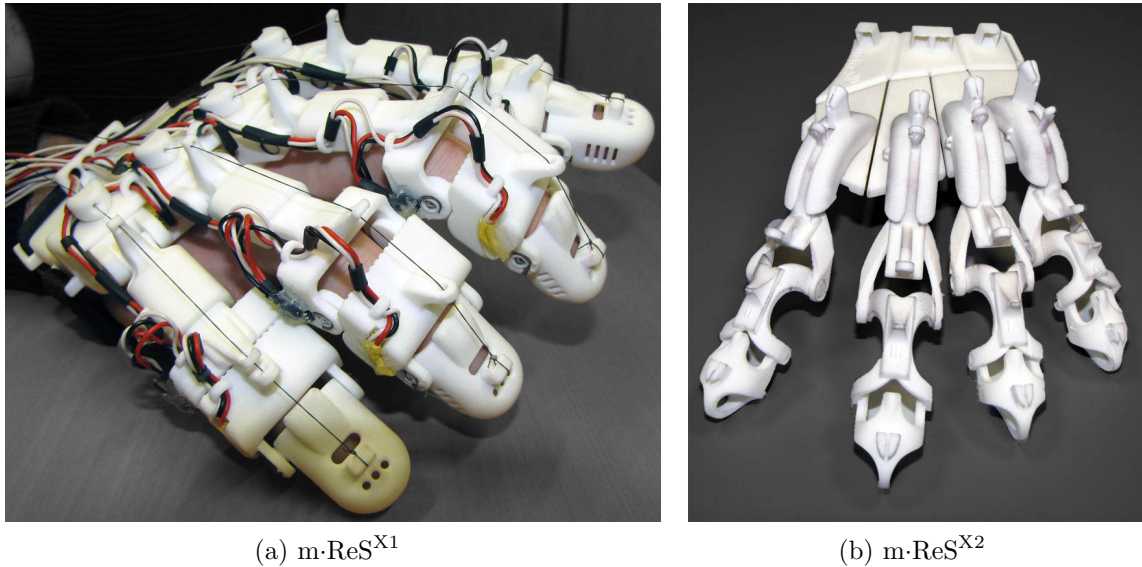


Figure 5.5: Both versions of m-ReS^X

cost is kept low. This is particularly important for customized exoskeletons that are individually adapted to each patient. The following Section 5.3 describes how the introduction of parameters into the CAD model allows for individualized exoskeletons.

5.3 Parameterization

Having joint axes in both the exoskeleton and the human fingers creates a redundant system, which requires matching the rotational centers. Misalignment with the anatomy belongs to one of the major problems of exoskeletons. It can cause unwanted reaction forces and makes the usage uncomfortable or even painful. A possible solution is to use adaptation mechanisms to fit different hands. This is, however, ruled out by one of the requirements (Section 3.4.3) due to increased weight and set up time. Besides, systems that offer discrete sizes (e.g. SaebFlex) are not ideally suitable for patients that would require intermediate sizes. Exoskeletons with self-aligning axes have been developed based on decoupling joint rotations and translations [175]. This is achieved at the cost of increased mechanical complexity [175], which is required to be kept low.

We address this issue by parameterizing the CAD model of the exoskeleton. The parameters adapt the link dimensions and part sizes, regarding conditions of the exoskeleton design. They are based on measurements of the user's hand dimensions. This approach is enabled by the use of rapid-prototyping manufacturing techniques. The adapted parts are transferred to a 3D printer that creates the individualized

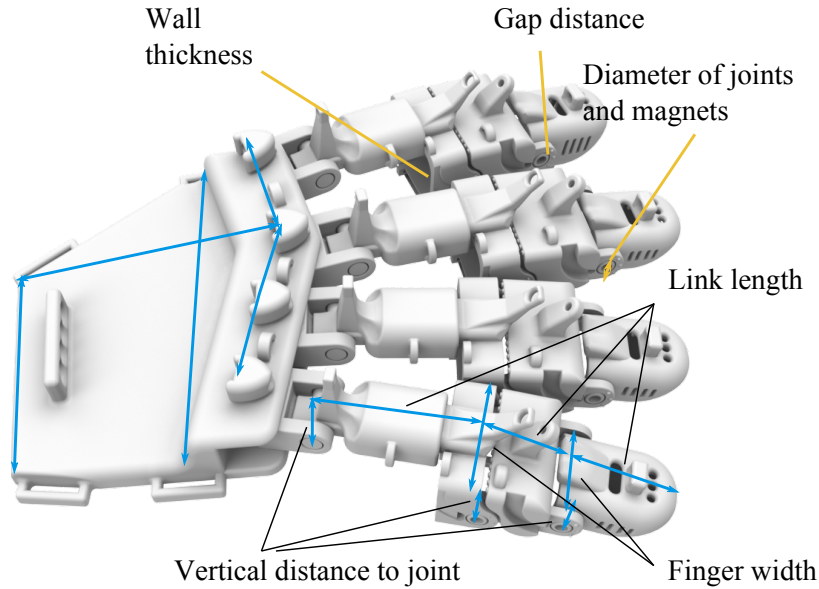


Figure 5.6: Blue lines: Parameters taken from anatomy. Orange lines: Additional general parameters where applicable. The parameters are sketched in for one finger only but are similar to the other fingers [196] ©IEEE.

exoskeleton. This means that each exoskeleton is fitted to each patient. This customization reduces misalignments without the need for adjustment mechanisms and avoids the problem with intermediate sizes.

m·ReS^{X1} incorporates 40 parameters in the CAD model; eight per finger for the dimensions, five at the base, the sensor size, wall thickness and joint gap distance (Fig. 5.6). In comparison to the previous prototype, m·ReS^{X2} is based on 44 measurements. One of the reasons for this increase lies in the more complex design of the back of the hand, which regards the transversal arc. Twelve of the parameters alone define the back of the hand to adapt it more comfortably. The exoskeleton is divided into three planes, which are controlled by parameters that assign dimensions and angles, such that the middle part sits on the back of the hand over the anatomical middle and ring finger's MCP joint. Figure 5.7 visualizes the parameters on a scanned image of the hand. Orange arrows show measurements for width and height, yellow ones the joint positions and link lengths. Further parameters that define the material strength and thickness of an additional neoprene layer are not depicted.

In the development stage, the parameters are measured by hand using a caliper. Inaccuracies are introduced by the presence of soft tissue. As a guideline, the width and height of fingers and base are taken without compression. Averaging several measurements can reduce inaccuracies.

An easy and fast transition from the measurements of the hand dimensions to the final model is important. The parameters are written in an Excel file that is imported by Solidworks. The 3D model is updated based on these parameters regarding the

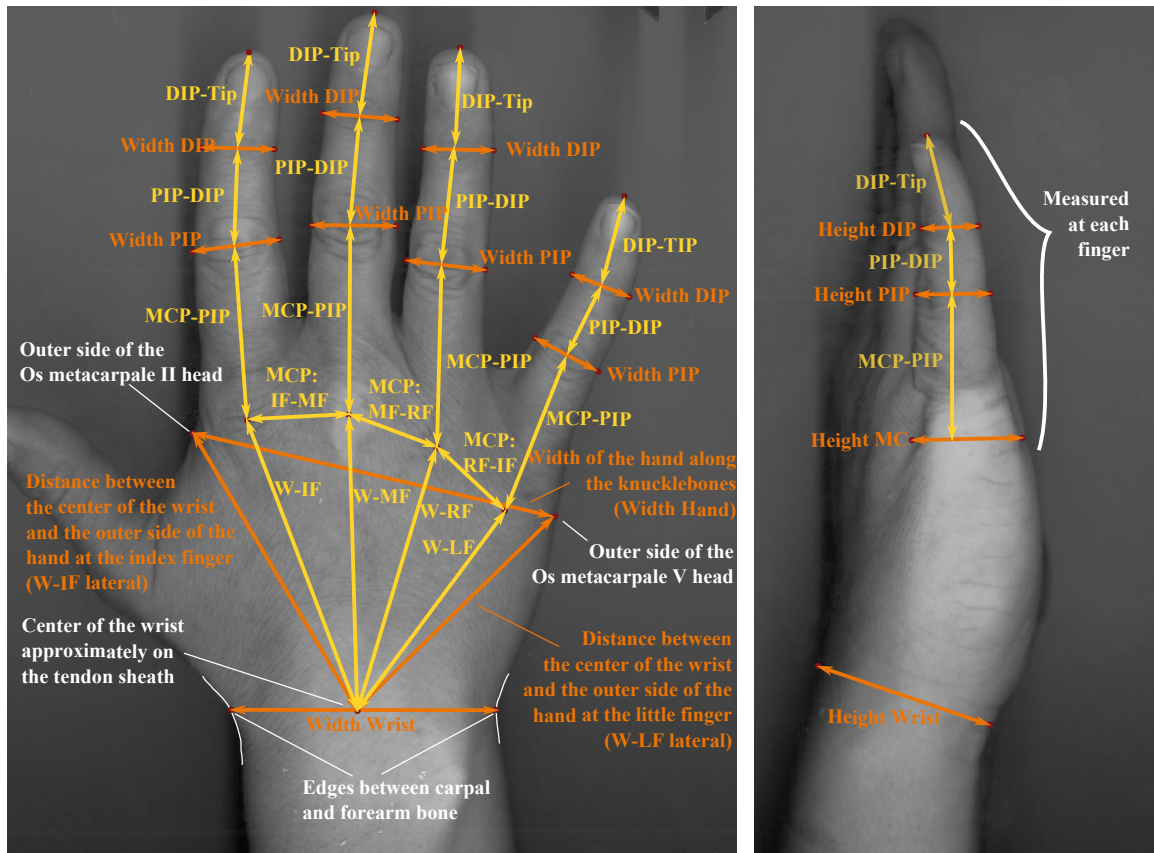


Figure 5.7: Orange arrows represent measurements for width and height, yellow ones the joint positions and link lengths [197] ©Springer

definitions of which sizes change and which are independent. Thus, the possibility remains to amend the design and the improvements, and extensions can be incorporated without touching the fitting. The final, customized parts are exported to the STL format, which is compatible to a vast majority of 3D printers. This CAD-CAM process exploits the advantages of rapid prototyping the exoskeletons and, due to dropping prices, 3D printing is expected to become economical even for single customized versions.

5.4 Actuation and transmission

Actuators enable supporting or counteracting forces onto the fingers, giving haptic feedback and enhancing the training possibilities. In the requirements, it was reasoned to reduce the number of actuators to one per finger. This section presents how the motors are used in conjunction with a tendon-based transmission and that, despite

the limitation of the number of motors, the training possibilities can be extended by changing the configuration.

5.4.1 Tendon-based transmission

Section 2.3.3.2 and 3.3.2 stated already major advantages of tendon-based transmission, also referred to as cable-drive, that justified to predetermine this method. In this section further advantages are given and the implementation in m·ReS^X is described.

One requirement is to minimize the weight of the exoskeleton in order to reduce limitations and strain while wearing. Since the motors account for the largest share of weight, they are placed separately. To transfer the forces over longer distances, cable-drives are a perfect fit. In contrast to gears, they have the advantage that under tension no backlash occurs due to the structural continuity of the cable [185]. Ultra strong polyethylene fibers (e.g. Dyneema®) offer very high tensile strength, stiffness, and low friction coefficient [120], making it well suitable for the application in exoskeletons. Equipping the motors with encoders, the displacement of the cable can be measured and used as a sensor input for joint angle measurements (Section 5.5.3). The parametrization adapts dimensions of the exoskeleton to the patient. The cable-transmission is convenient in this respect since no fixed distances have to be kept but changes in the size are encountered with a different tendon-lengths over the exoskeleton.

The motor torque is translated to force by the use of a simple 3D printed winder. The relation between motor torque τ_M and cable force F_C depends on the radius of the winder r_W :

$$F_C = \frac{\tau_M}{r_W} \quad (5.1)$$

Decreasing the size of the winder, increases the force exerted on the cable. At the same time this reduces backdrivability, since the fingers have to exert higher forces to exert the same torque on the motor than using a larger winder.

Longer distances between the actuator and the exoskeleton can be bridged with Bowden cables. The force-transmitting cable is lead through an hollow outer cable housing. It is flexible while it ought to keep a constant length. This way the exoskeleton can be moved with respect to the motor without having a major effect on the cable length. The outer tube is connected to the exoskeletons base and the cable is attached to the finger to transmit the forces from the motor.

Since the number of motors was set to be restricted to one per finger, not every joint can be actuated. When the motor pulls at the finger-tip the force acts on all three joints. The torque that is transmitted to the single finger joints depends on the force direction and magnitude. The magnitude is defined by the motor power and the direction by the routing. The tendon is routed according to guides arranged in the 3D model defining the lever arms, which determine the torques transmitted onto the fingers. Longer lever arms are preferred, since smaller motors are required to provide the same amount of torque on the finger. This is one reason why the CyberGrasp

has an overhead structure for the tendon guides. However, in a medical environment, enormous exoskeletons can appear intimidating on patients and shall be avoided. A balance should be found between small lever arms spiking out from the exoskeleton, and enough distance for the cable to touch only the guides over the whole range of movement. Only the DIP joint has an additional deflection point that is negligible, since the tendon is deflected, but not within the anatomical ROM. One side-effect of this approach is that a constant force on the cable does not result in a constant torque on the finger over the angle range. However, the flexibility in use is expected to compensate this disadvantage. The tendon-based transmission enables to change the routing and attachment point, which is described in detail in the next session.

5.4.2 Configurations to train different movements

m·ReS^X is developed for stroke survivors, and that accordingly, providing assistance in extension is the most important function. Therefore, the standard configuration is to attach the cables at the finger tips and pull from the back of the hand supporting the opening of the hand Fig. 5.9a. The use of a cable-drive offers the flexibility to change the application point and the direction of the force. For instance, by attaching the cables on the lower side of the fingers and guiding them to the back of the hand, pulling the tendons would lead to assistance in flexion. Several different attachment points have been included in the design where the cables can be attached. Applying the force at the MCP link leads to sole actuation of the MCP joint (Fig. 5.8b). Similar attachment points have been included for the other links or joints.

The change of the configuration has to be accomplished easily and swiftly. Metal beads are attached at the end of the cables that can be put into indentations (Fig. 5.8a). If force is applied on the tendon, the attachment is fastened. Otherwise, the bead can easily be removed and put swiftly into another attachment indentation.

The use of configurations allows for the simplification of the thumb module. To prevent excessive complexity, training of the thumb has been implemented by changing the guiding of the cable (Section 5.2.3). The endpoint is attached to the thumb module and guided over the tip of the finger that shall be opposed, enabling opposition to each single finger in different configurations. m·ReS^{X2} provides three guiding eyes per finger to allow different angles of opposition (Fig. 5.4). The cables may also be routed around an object, for instance a cylinder to train grasping of objects. This configuration only allows to support in the closing direction. To open the hand, the exoskeleton may be used in combination with a soft ball that supports in opening the hand (Fig. 5.9b).

This simplification comes with some disadvantages in comparison to a dedicated guiding structure. Without the use of an additional object, the force vector is always directed between the attachment and the guiding point and, thus, force can only be exerted in this direction. The fingers cannot be forced to follow other trajectories that might be closer to an anatomically natural path. Outweighing advantages and

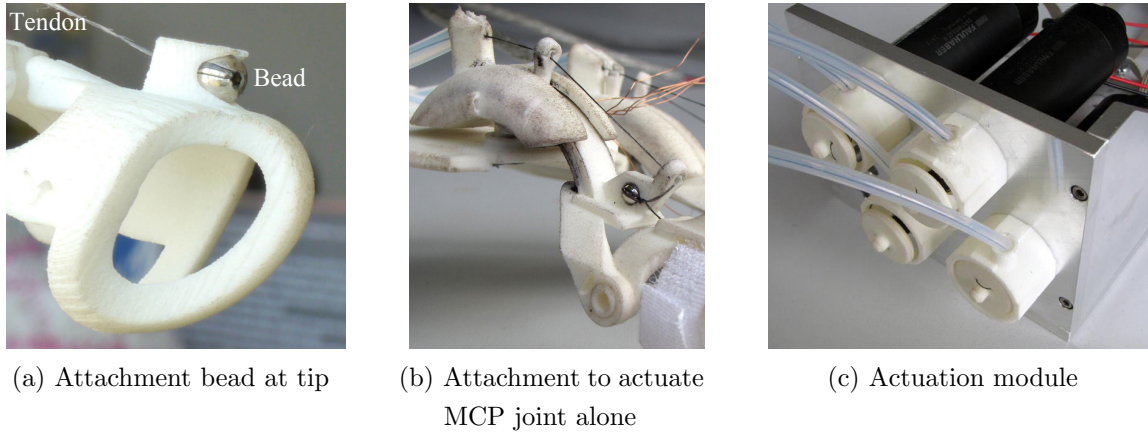


Figure 5.8: Attachment examples and actuation module

disadvantages, in the long-term a more elaborate thumb module is desired. Still, the present implementation already allows for pinching training based on the existing exoskeleton with minor additional costs and developments.

5.4.3 Motor selection

The dimensioning of the motor is mostly determined by the maximum torque that needs to be exerted. This depends on the necessary force and the relation to torque over the winder radius (eq. 5.1). $m\cdot\text{ReS}^{\text{X1}}$ is preliminary equipped with a Faulhaber 2342 CR brushed DC motor, achieving a nominal torque of 16 mNm and a planetary gear with a reduction ratio of 3.71:1. The low ratio ensures high backdrivability. Studies proved that haptic feedback can even be achieved with higher reduction gear ratios up to 23:1 [108, 174]. According to eq. 5.1, a winder radius of $r_{\text{W}}=3\text{ mm}$ results in a maximum tendon force of 19.78 N.

When the motors were extended for $m\cdot\text{ReS}^{\text{X2}}$, a new DC motor model with a higher continuous torque was available. It allows to omit a gear reducing friction, inertia, and other undesired effects like backlash. Moreover, the accuracy of actuation and sensing is inherently improved, high backdrivability can be achieved, and the weight is lower than a motor-gear combination with comparable nominal torque. The Faulhaber 2657 CR motor exerts a nominal torque of 44 mNm, which results in a force of 14.7 N with a winder radius of 3 mm. Although it exerts a lower torque than the geared motor, the corresponding forces on the cables are within the required range of 10 N to 15 N (Section 3.4.3), achieving higher forces than the CyberGrasp (12 N) [16].

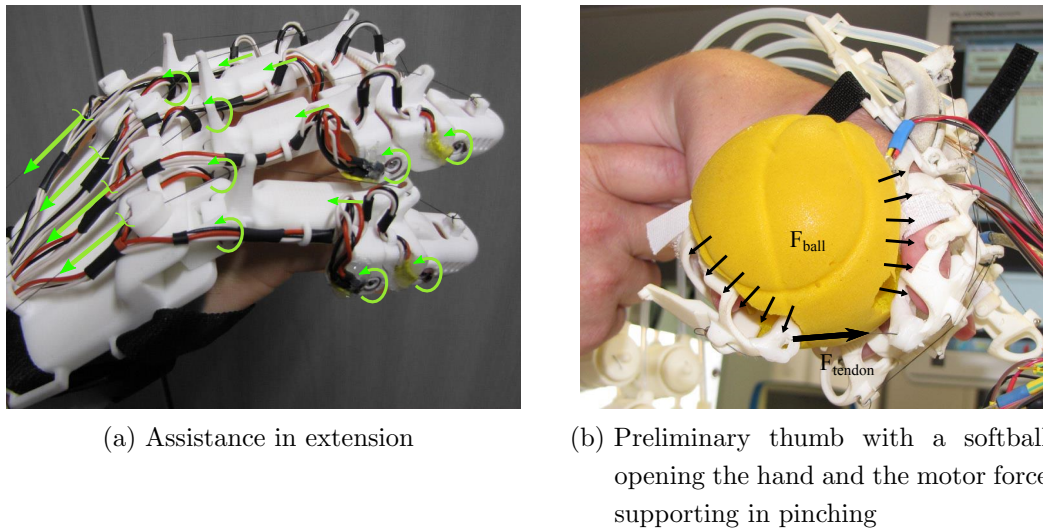


Figure 5.9: Example configurations with force vectors depicted with arrows

5.4.4 Actuation module

Three different major basic choices for the placement of the actuators are feasible:

1. On the hand
2. On the forearm
3. Remotely (e.g. on a table or in a backpack)

The advantage of the first possibility mounted on the hand is that no relative movements between the exoskeleton and the actuators occur. Therefore, no Bowden cables or similar transmission types are necessary. Apart from the power supply cable, the exoskeleton could be freely moved. However, the weight of the actuators lasts on the hand and barely enough space is available. More space is available on the forearm to place the motors. In this case a relative movement between the exoskeleton and the actuators occur when the wrist is moved. Similar to the hand, the arm can be freely used within the range of the power supply cable. However, also here the weight is a problem, which can cause fatigue, in particular due to the lever effect of the arm [16]. Commonly, stroke patients lack strength in the arm, which is why the requirements stated to keep the weight as low as possible. This leads to selecting the third possibility, namely placing the actuators remotely.

Following the modular approach, the motors are grouped in an actuation module (Fig. 5.8c). They are fastened to the aluminum front plate using the motors' screw threads. The forces are transmitted over Bowden cables (Section 5.4.1) to the

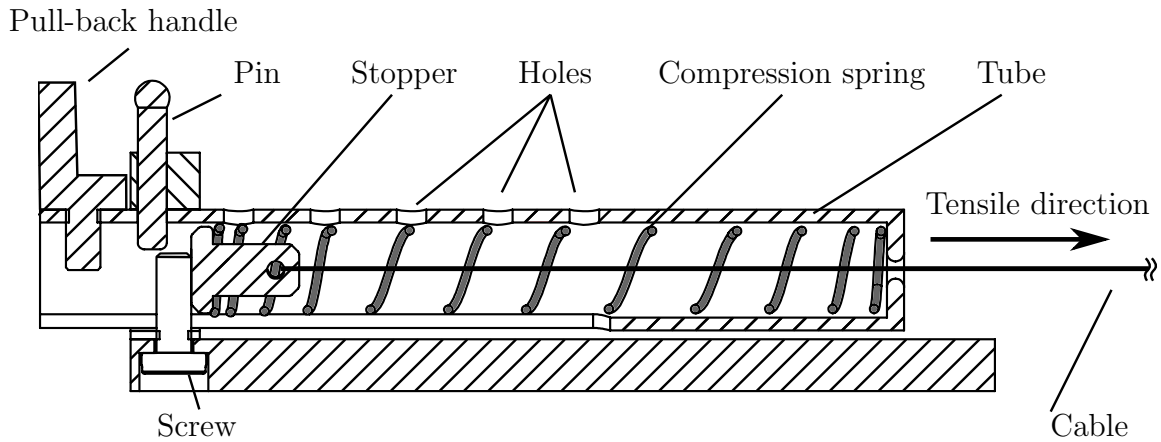


Figure 5.10: Spring mechanism for motor-less exercises with m·ReS^X

exoskeleton. The winders attached to the motor shafts are surrounded by casings, leaving through-holes for the cables with sockets for connecting the Bowden sheaths.

The actuation module incorporates a mechanism to use springs for force exertion as a cheap alternative to motors (Fig. 5.19). Compression springs are used that are guided in a tube, which is closed at one side, apart from a small through-hole. The cable goes through this opening and is attached to a stopper that is guided inside of the tube and presses against the spring from the other side. After applying a preload when the exoskeleton is in the fully extended position, the flexion leads to a compression of the spring and the force is increased linearly to the displacement according to Hooke's law. Two springs are available to vary the ratio between force and displacement (Spring constants: 0.169 N mm^{-1} and 0.249 N mm^{-1}).

A splint can be inserted into several holes in the tube to block it against the actuator module ground plate. Thus, the distance between the end of the tube and the screw, which both constrain the spring, can be adjusted. Depending on this length, the pitch of the spring and, thus, the preload can be adjusted.

5.5 Angle sensing

Accurate angle sensing is necessary to reliably evaluate movement impairments in a clinical context [206]. It also allows for interactive exercise applications, the study of rehabilitation paradigms and documentation of the training progress. m·ReS^X uses three different types of angle sensors applied depending on the joint type, the application, and the cost.

5.5.1 Hall-effect based angle sensing

Since additional friction of the sensors against the finger movement shall be avoided, potentiometers and similar sensors are ruled out. Accelerometers are an alternative that allow angle measurements by measuring the acceleration of gravity in comparison to a reference. Although frictionless, they are typically used for static gesture recognition due to noisy estimation caused by the superposition of the movement acceleration [84, 149]. Instead, we use Hall effect sensors for angle measurement allowing contactless measurements, so that no additional friction is caused.

5.5.1.1 Voltage-to-angle mapping

Based on the Hall effect, the sensor converts the surrounding magnetic field into a voltage that is measured by a microcontroller. The magnet is rotated with one link of the joint and the magnetic field is measured with the sensor in the second link of the joint. The amplitude and oscillation length of the magnetic field depends on the distance and the angle of the magnet to the sensor. The maximum and minimum values are at its poles and in between it follows a trigonometric curve, where one oscillation corresponds to one revolution.

Assembled, the joints of m-ReS^{X1} can only be turned with a maximum angle range of around 90°, which requires to do the calibration process before fixing the magnet in its final position. Figure 5.11 shows sensor outputs over the range of the joint with orientations of the magnet. It is positioned in a way that the inflexion point of the sine wave is in the middle of the rotational area. Thus, the orientations result in unambiguous voltages and the relation is more suitable for linearization. m-ReS^{X1} uses an inverse sine function for the angle estimation, which maps the hall sensor's voltage to an angle. A linear mapping between the voltages at the end-points and the angle range (based on measurements or the mechanical design) would allow for runtime calibration at the expense of inaccuracies due to deviations from the trigonometric curve. A comparison shown in Fig. 5.12 between a sine curve and a line going through $\sin(\pi)$ with a corresponding slope of -1 shows that a decent accuracy can be achieved over a range of about 60° ($\approx \pi \pm 0.5$). This would allow for good accuracy of the DIP joint, but the angle range of the PIP and MCP joints are above 90°, leading to high errors. Another disadvantage is that the initial one-time process of assembling and aligning the magnet is tedious and time-consuming. If recalibration is necessary, either reassembly is required or linear calibration has to be used. More details are given in [64].

In contrast, m-ReS^{R2} has the advantage that its PIP joint is turnable over 180° allowing for runtime calibration with high accuracy based on a trigonometric mapping. The magnet can be arranged such that U_{\max} and U_{\min} cover 180°. However, the most important position is extension corresponding to 0° that would be in an inaccurate region due to the low sensitivity at the minima and maxima. Therefore, the range is shifted approximately 30° to a region with a higher slope improving sensitivity.

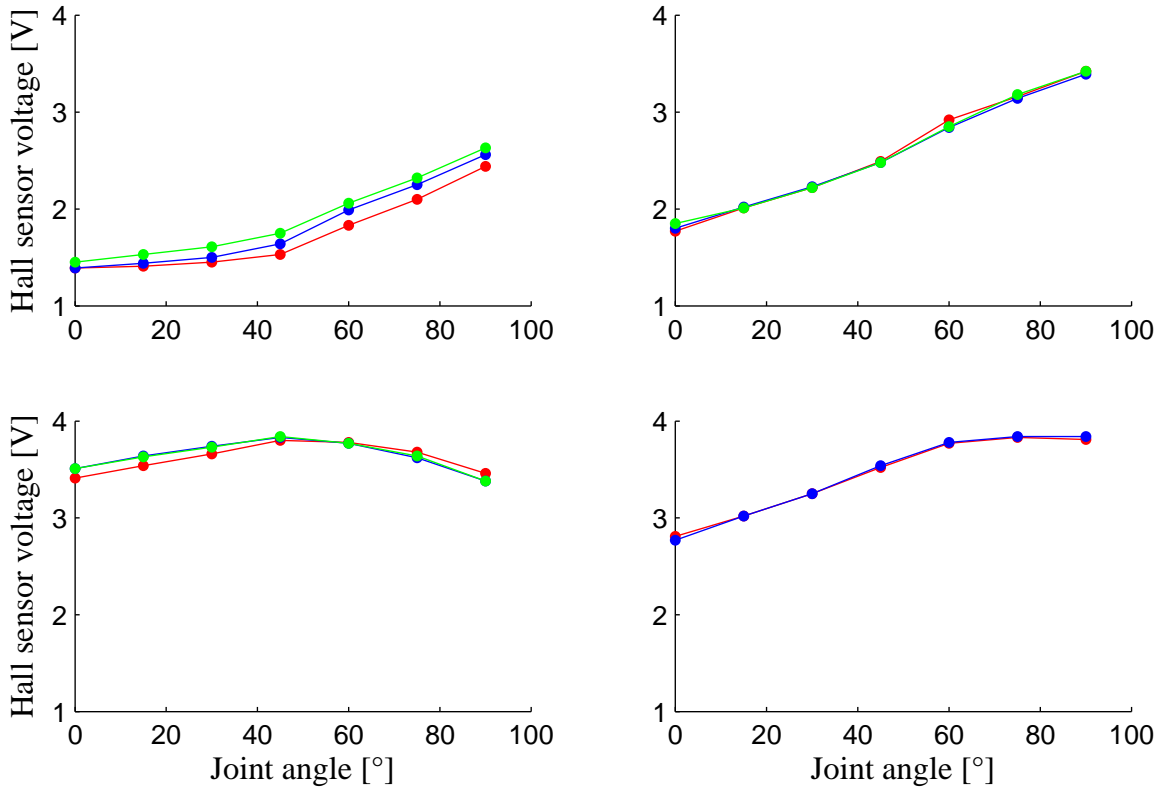


Figure 5.11: Different magnet orientations. Each curve represents another measurement. The upper right plot's orientation is 45° , the lower left one's 90° and the lower right one's 135° rotated in relation to the upper left one's orientation. The orientation used for m-ReS^{X1} corresponds to the sensor output in the upper right graph.

The method is depicted in Fig. 5.12. For the shifted calibration, first, the differences between the minimum voltage and the voltages at the end positions of the joint ΔU_{start} and ΔU_{end} are measured. The calibration is carried out such that the joint angle between θ_{start} and θ_{end} is 180° . Then $\Delta U_{\text{start}} + \Delta U_{\text{end}}$ equals ΔU_{max} , which corresponds to $U_{\text{max}} - U_{\text{min}}$. Having the minimum and maximum of a sine curve allows to establish the following equation

$$U(\theta) = \frac{U_{\text{max}} - U_{\text{min}}}{2} \cos(\theta) + \frac{U_{\text{max}} - U_{\text{min}}}{2} + U_{\text{min}} \quad (5.2)$$

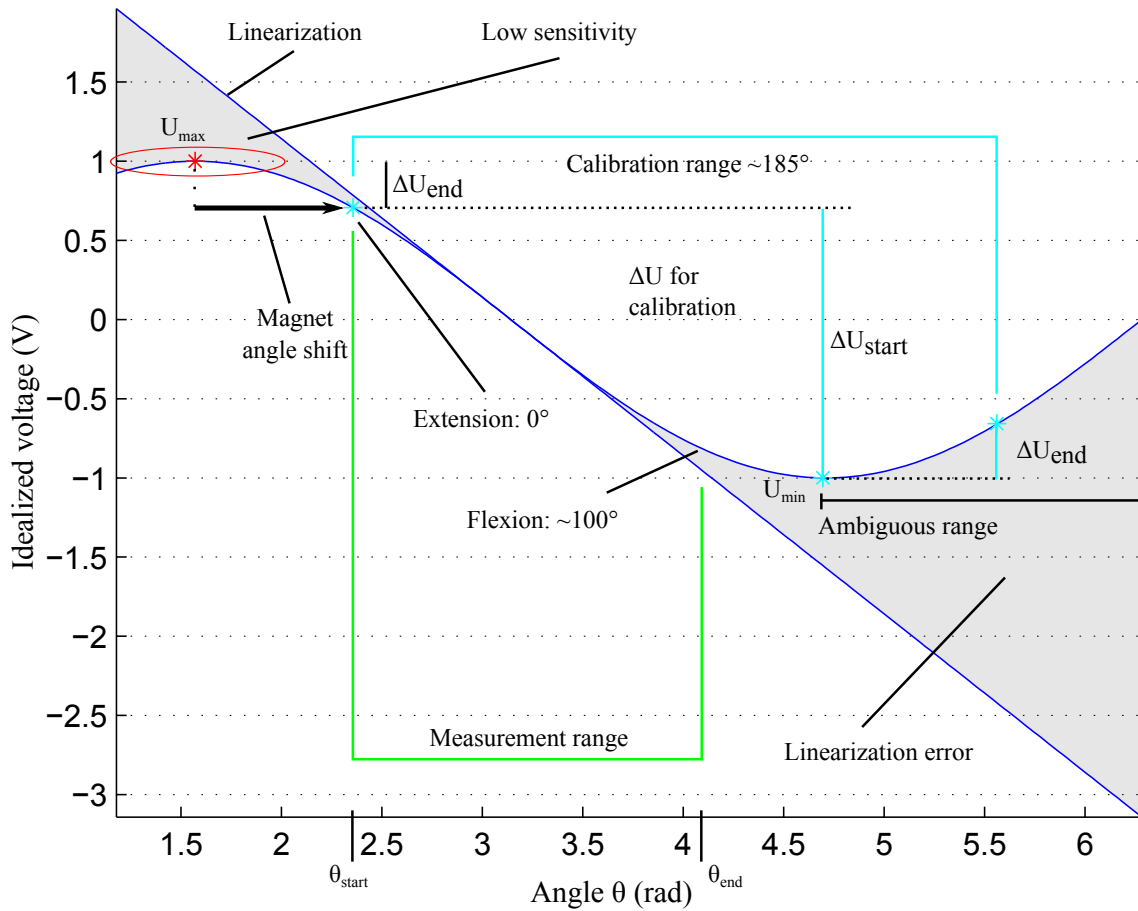


Figure 5.12: Angle shift, calibration, and linearization

The equation can be solved for θ to receive an angle as a function of $U(\theta)$:

$$\theta = \arccos\left(\frac{2U(\theta) - U_{\min} - U_{\max}}{U_{\max} - U_{\min}}\right) \quad (5.3)$$

5.5.1.2 Assembly

The exoskeleton accommodates space for the sensors and magnets, so that the assembly is standardized and facilitated. The signal-to-noise ratio (SNR) is inverse proportional to the distance between sensor and magnet. Therefore, the distance is kept close to the 3D printer-dependent minimum (Fig. 5.13a).

Due to availability sphere-shaped magnets were used for m-ReS^{X1}. Since it allows for rotation around two axis inside the joint, handling is difficult. With the help of another magnet with known pole orientation, they can be correctly aligned and fixed to the exoskeleton. The printing of m-ReS^{X1} in one piece required a clearance in the joints of 0.3 mm. This causes issues in the accuracy of the sensor, since relative

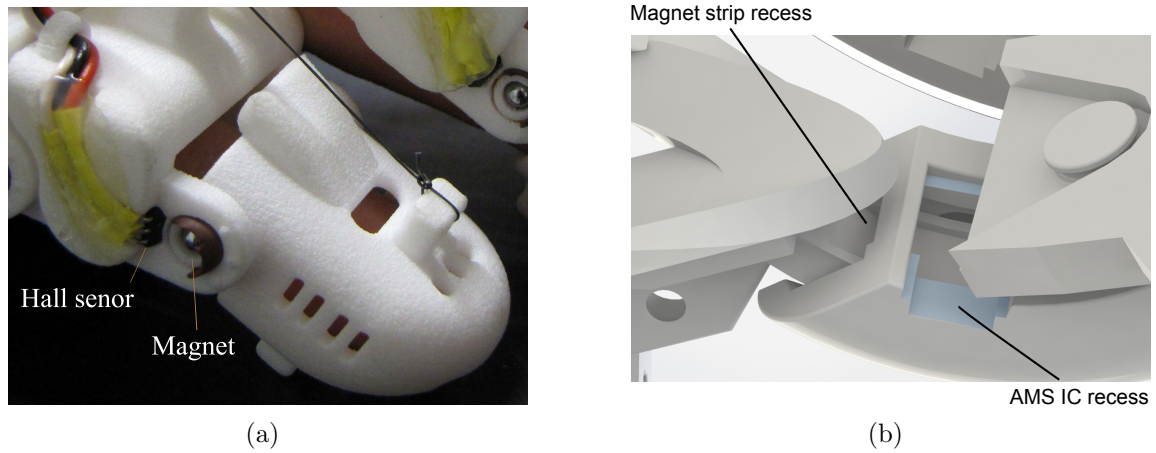


Figure 5.13: (a) Angle measurement based on Hall sensors that measure the magnetic field of a magnet in the joint of $m\text{-ReS}^{\text{X1}}$; (b) MCP joint sensor space.

movements between sensor and magnet lead to disturbances in the magnetic field, superimposing the wanted change of the field due to the rotation.

$m\text{-ReS}^{\text{X2}}$ uses cylinder-shaped magnets that only allows rotation around the axis of rotation. This makes the assembly faster and more accurate. Furthermore, it is not printed in one piece, allowing to minimize the clearance to nominal dimensions, which improves sensor accuracy.

5.5.2 Multi-pole magnet strip encoder for MCP joint angle sensing

$m\text{-ReS}^{\text{X2}}$ owns an MCP joint with its center of rotation being collinear to the anatomical joint. It replaces the combination of a non-collinear revolute joint with a prismatic joint in $m\text{-ReS}^{\text{X1}}$ (Section 5.2.2). The new joint design necessitate to use another sensing method instead of measuring the magnetic field of a rotating magnet inside the revolute joints. Flex and bend sensors are ruled out due to the low accuracy. A voltage divider in combination with resistor over the arc similar to a potentiometer gives an absolute angle. This possibility is not pursued since the electrical contact induces friction, and, more importantly, is prone to malfunction.

Therefore, we use a contactless sensor based on magnetic field measurements. The integrated circuit (AS5306 by AMS) owns Hall elements similar to the other sensing method. In contrast, they do not measure a rotating magnet, but sense a multi-pole magnetic strip. By counting the alternating magnetized poles on the strip a distance can be determined and by placing the strip on the arc a rotary motion can be detected. Friction is not increased due to the contactless measurement. Another advantage is

that the chip and the strip are small enough to integrate them into the joint. The chip sits in a recess of the outer arc and reads the magnetized strip placed in a groove on the inner arc (Fig. 5.13b).

The quadrature incremental output provides 40 pulses per pole pair and a resolution of 15 μm . The angular accuracy depends on the parameters of the customized exoskeleton. For instance, the angular resolution is 0.04° for a radius of 20.44 mm of the bent magnet strip, belonging to the exoskeleton of a female subject. Besides the two quadrature channels, the chip provides an analog signal of the magnetic field strength, and a channel to indicate pole transitions and loss of signal.

5.5.3 Motor encoder for angle estimation using Denavit-Hartenberg convention

The motor can be equipped with encoders offering an additional means of angle measurement. In the first place, the motor encoders incrementally capture the angular displacement of the motor. Over the winder the rotation is translated into a linear movement of the tendon. The tendon is guided over the finger to the attachment point at the tip. During the flexion and extension of the fingers, the tendon length changes, given that it is on tension. The displacement of the tendon can be used to measure the degree of flexion averaged over the three joints. This information alone can be taken as a means of assessment for the ROM. Alternatively, it can be used to replace sensors or to correct measurements of other sensors. Also malfunctions, e.g. ripping of the tendon, can be detected.

The resolution in tendon displacement is calculated by dividing the circumference by the number of pulses per revolution. Our exoskeleton uses a 3D printed winder with a 3 mm radius. m·ReS^{X2} uses an encoder with 1024 pulses per revolution resulting in a length per pulse of

$$l_p = \frac{2\pi \cdot 3\text{mm}}{1024} = 0.018 \frac{\text{mm}}{\text{pulse}}$$

or approximately 54 pulses per mm. However, the resolution does not reflect other influences like elasticity or irregular winding of the tendon.

The approach to determine a relation between the tendon displacement and the joint angles is exemplary shown for m·ReS^{X1}. The same principle can be applied to m·ReS^{X2}. The naming convention of the points and coordinate systems (COS) is depicted in Fig. 5.14.

The tendon length depends on the distances from the end of the bowden cable at the point 0P_0 over the deflection points 1P_1 , 2P_2 , 3P_3 to the fixation at the finger tip 4P_4 . The deflection points again depend on the joint angles and the linear joint. Therefore, if they are known, the tendon length can be calculated.

The links of the exoskeleton are serially connected with each other. In an absolute coordinate system, changes in the angle of a joint influences the position of the

deflection points in the following links of the kinematic chain. Therefore, the deflection points have to be transformed into one reference coordinate system. In the present case, it makes sense to use reference frame 0 connected to the exoskeleton's base as a reference. The Denavit-Hartenberg (DH) convention is used to formalize the mathematical transformation [40]. Coordinate frames are attached to the joints between two links in a defined way, such that four parameters per joint describe their relation using homogeneous coordinates.

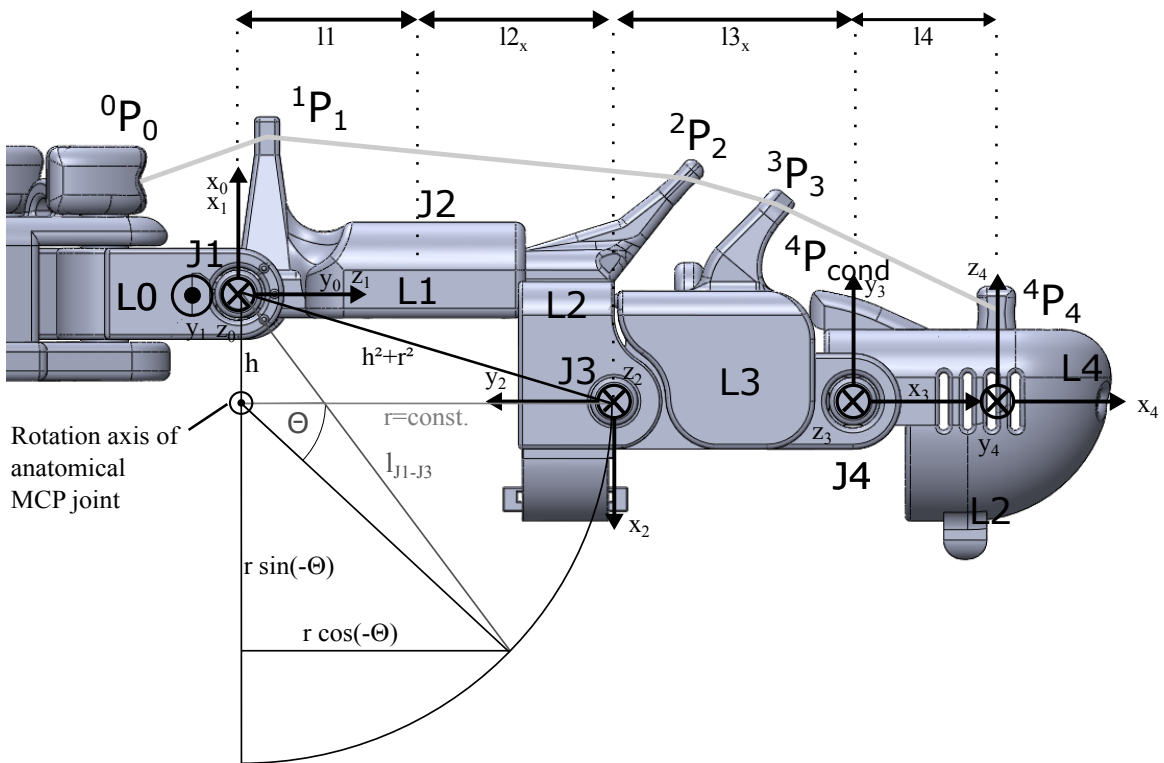


Figure 5.14: Frames, links, and joints according to Denaviat-Hartenberg parameters. 0P_0 to 4P_4 are the tendon's deflection points. The trigonometric relations show assumptions and convention for the calculation of the linear joint extension.

The coordinate frames with the associated links and joints according to the DH convention are shown in Fig. 5.14. Accordingly, the DH parameters are determined (Table 5.1).

i	α_i	a_i	d_i	θ_i
1	$-\pi/2$	0	0	θ_{MCP}^*
2	$-\pi/2$	l_{2y}	$l_1+l_{2x}+l_{lin}^*$	π
3	0	l_{3x}	0	$\theta_{PIP}^* - \pi/2$
4	$\pi/2$	l_4	0	θ_{DIP}^*

Table 5.1: DH parameters according to coordinate systems in Fig. 5.14. The asterisk marks variables.

The homogenous coordinates between the reference frames can be calculated using:

$${}^{i-1}A_i(\theta_i, d_i, a_i, \alpha_i) := \begin{pmatrix} \cos(\theta_i) & (-\sin(\theta_i)) \cos(a_i) & \sin(\theta_i) \sin(a_i) & a_i \cos(\theta_i) \\ \sin(\theta_i) & \cos(\theta_i) \cos(a_i) & (-\cos(\theta_i)) \sin(a_i) & a_i \sin(\theta_i) \\ 0 & \sin(a_i) & \cos(a_i) & d_i \\ 0 & 0 & 0 & 1 \end{pmatrix} \quad (5.4)$$

Inserting the parameters from Table 5.1 into equation 5.4 results in the transformation matrices ${}^0A_1(\theta_{MCP})$, ${}^1A_2(\theta_{MCP}, l_{lin})$, ${}^2A_3(\theta_{PIP})$ and ${}^3A_4(\theta_{DIP})$.

These matrices give a relation between adjacent deflection points and can be used to set up transformations as single functions of each of the joint angles. For setting up a general equation including all joints, every point needed to be calculated back into the same frame. The following matrix multiplications allow to calculate each position vector back of the respective frame into the reference frame 0 at the base:

$$\begin{aligned} {}^0A_2(\theta_{MCP}, l_{lin}) &= {}^0A_1 \cdot {}^1A_2 \\ {}^0A_3(\theta_{MCP}, \theta_{PIP}, l_{lin}) &= {}^0A_1 \cdot {}^1A_2 \cdot {}^2A_3 \\ {}^0A_4(\theta_{MCP}, \theta_{PIP}, \theta_{DIP}, l_{lin}) &= {}^0A_1 \cdot {}^1A_2 \cdot {}^2A_3 \cdot {}^3A_4 \end{aligned}$$

Then, the adjacent deflection position vectors can be subtracted and the distance is obtained using the Euclidean norm. This results in one equation for calculating the total length difference.

If only the tendon length is of interest, the equation can also be split up into functions for each joint angle, facilitating the implementation on a microcontoller. Either only the adjacent deflection points belonging to the joint are transformed into one frame attached to the joint based on the corresponding transformation ${}^{i-1}A_i$. Alternatively, the law of cosines can be solved for the angle of the single joint

$$\theta = \arccos\left(\frac{r_1^2 + r_2^2 - d_0^2}{2r_1r_2}\right) - \alpha_0 \quad (5.5)$$

where r_1 and r_2 are the radii around the joint axis to the deflection points, d_0 is the distance between the deflection points for $\theta = 0^\circ$ and α_0 is the angle between the deflection points for $\theta = 0^\circ$.

The tendon length is a function of θ_{MCP} , θ_{DIP} , θ_{PIP} and the linear joint extension l_{lin} . Whereas, the joint angles may be measured, the extension of the prismatic joint is based on a estimation developed in the next paragraph.

5.5.3.1 Linear joint displacement

The linear joint displacement between L1 and L2 is not measured by sensors. The exoskeleton is parameterized, so that the linear joint is not extended when all three rotational joints are at 0 degree (extended pose). We assume that the joint extends in such a way that the PIP and DIP joint of the exoskeleton remains aligned with the respective anatomical joints. This implies that the distance between the anatomical MCP joint and the PIP joint l_{J1-J3} is constant and that l_{lin} is a trigonometric function of θ_{MCP} (Fig. 5.14).

$$\begin{aligned} l_{J1-J3} &= \sqrt{(r \cdot \sin \theta_{MCP} + h)^2 + (r \cdot \cos \theta_{MCP})^2} \\ &= \sqrt{r^2 + 2 \cdot r \cdot h \cdot \sin \theta_{MCP} + h^2} \end{aligned}$$

The extension of the linear joint is determined by the difference to the joint distance for $\theta_{MCP} = 0^\circ$

$$l_{lin} = l_{J1-J3} - \sqrt{h^2 + r^2}$$

In the application friction, jamming, and misalignment of the anatomical joints can lead to deviations from the model. It helps, however, to improve the estimation without having sensors available.

5.5.3.2 Conditional deflection point

Due to the exoskeleton's design an additional deflection point occurs after a certain angle of the PIP joint (Fig. 5.16a). Before reaching the limit angle, the deflection is disregarded but for wider angles an increased tendon displacement occurs. To setup a conditional function, the threshold angle has to be found first by means of simulation.

The simulation treats the conditional deflection point as an additional waypoint even for small DIP joint angles where no additional deflection occurs. Therefore, the length at the limit angle, where just no deflection occurs and the points 3P_3 , ${}^4P_{cond}$, and 4P_4 are arranged in line, is the minimum length. Then, the difference between the lengths with and without the additional deflection points equals zero (Fig. 5.15 center).

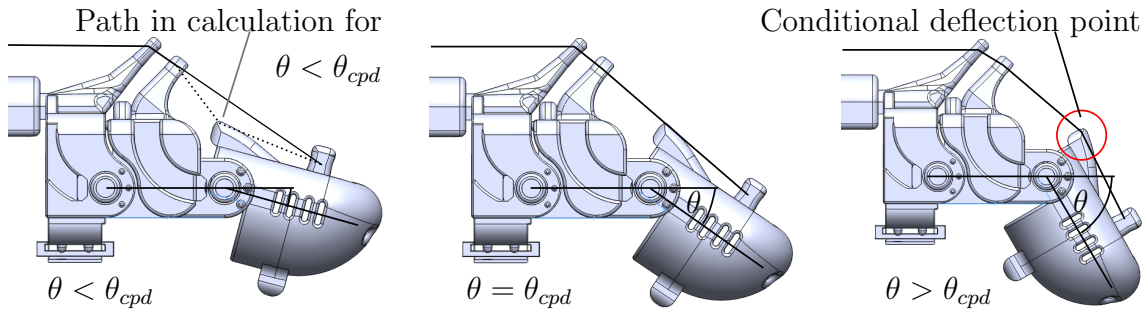


Figure 5.15: No additional deflection point (left); threshold angle (center).; additional deflection point (right)

The distances between the points in relation to the DIP angle, once with the additional deflection point and once without it, has to be compared to calculate the threshold angle. The DH transformations are used to bring 3P_3 , ${}^4P_{cond}$, and 4P_4 into the same coordinate system and calculate the lengths differences as a function of θ_{DIP} . The plot based on this function is shown in Fig. 5.16a. By deriving the function, equating it to zero, and solving for the angle, the conditional deflection limit angle was calculated to be $\theta_{cdp} = 0.658$ rad for m·ReS^{X1}.

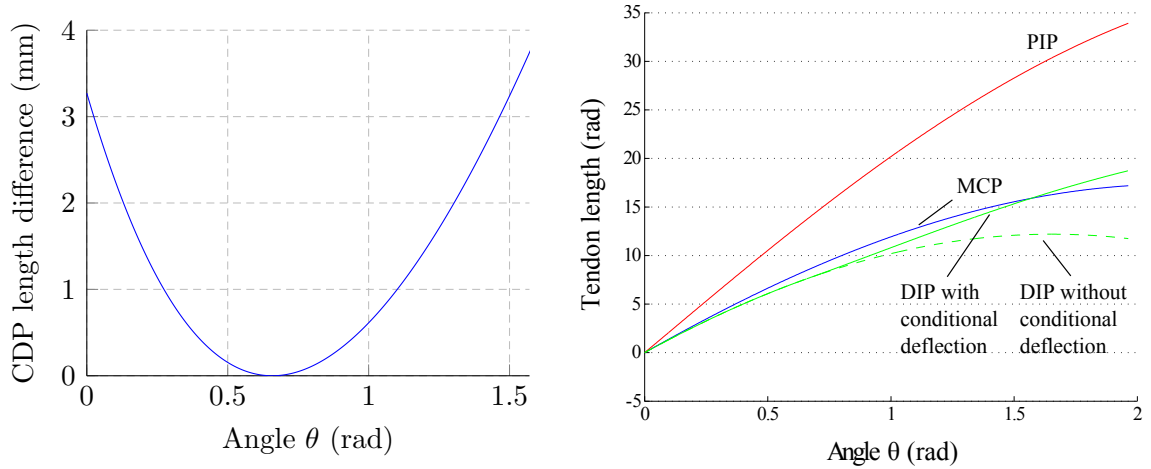
The angles as a function of the tendon length have to be unambiguous over the range of application. Figure 5.16b shows the simulated tendon length displacement as a function of the angles of MCP, PIP, and DIP. A maximum angle of 2 rad is shown in the graph, since the range of motion of m·ReS^{R1} exceeds limits of human joints. The function has to continuously rise over the angle range. Otherwise, the inverse function would return two angles for one tendon length. This occurs for the dashed line which decreases at around $\pi/2$. The additional length of the conditional deflection extends the unambiguous range.

5.6 Current limiting for force control

In this section, first, the current sensing method is discussed before its application is described together with a circuit for limiting the current in the second part.

5.6.1 Current sensing

Shunt resistors are used to measure the armature current of the motors in m·ReS^X. The resistive method is the simplest, most inexpensive, accurate, and linear one in comparison to all other ways. The drawbacks are that it introduces additional resistance into the electrical circuit. It furthermore increases the output impedance, which can lead to reduced terminal voltage or in extreme cases interruption of the circuit from the ground plane. These problems can be alleviated by reducing the shunt



- (a) Plot of the difference of the lengths with and without the additional PIP deflection point as a function of the DIP angle (rad)
- (b) Angle to tendon length difference for joint angles of DIP (green), PIP (red) and MCP (blue). The green dashed line shows the curve for DIP without regarding the conditional deflection point at $\theta = 0.658$.

Figure 5.16: Influence of the conditional deflection point (CDP)

resistance. However, the voltage measured over very low resistance shunts becomes comparable to circuit offset voltages, compromising accuracy. A balance therefore has to be found. A resistor of $0.5\ \Omega$ is used that offers a high voltage drop over it, so that noise does not strongly affect the measurement. The voltage is amplified with a non-inverting operational amplifier circuit to fit the measurement range of the microcontroller's ADC.

In contrast to this method, $m\cdot\text{ReS}^{\text{R2}}$ uses a Hall-effect sensor to measure the current (Section 4.3). First, because $m\cdot\text{ReS}^{\text{X}}$ requires five current sensors instead of one. Therefore, cost and complexity play a stronger role. Second, $m\cdot\text{ReS}^{\text{R2}}$ needs to detect the direction of the current through the motor, which would require to extend the simple shunt circuit. Since tendon-drives inherently can only pull, information about the direction is not required to be detected. Third, the motor in $m\cdot\text{ReS}^{\text{R2}}$ uses higher currents. The shunt resistance can be reduced to achieve the same output differential voltage $U = R \cdot I$. Still, the power dissipation of the resistor depends on the squared current, which is why stronger resistors are required. Together with the requirement of high-accuracy resistors, the selection is strongly limited.

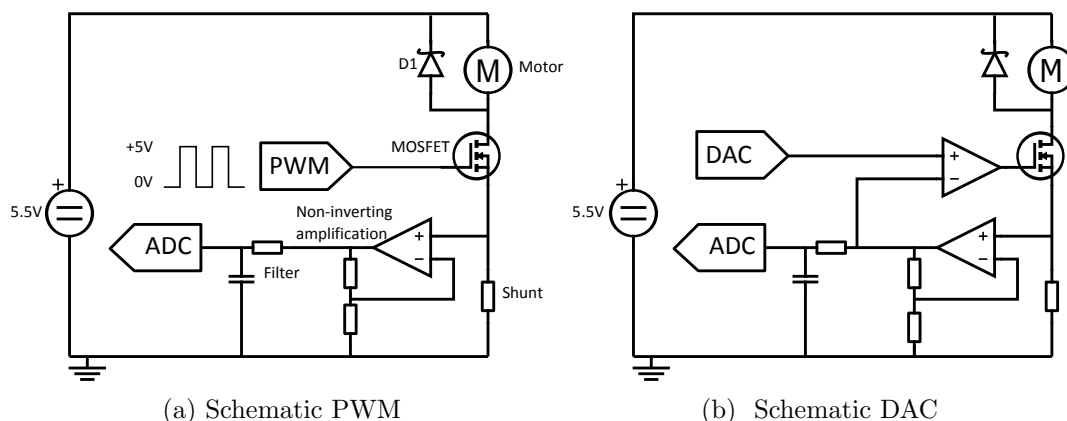


Figure 5.17: Simplified schematics for current measurement and limiting

5.6.2 Current limiting

Three different circuits were observed. The first one is based on a patent, the second one is based on amplifying the pulse-width modulation (PWM) signal of the microcontroller, and the third one uses an operational amplifier as a comparator with a digital-to-analog converter (DAC).

The first method is based on a modified version of a patented circuit that is specifically designed for torque control of electrical motors [192]. It incorporates two transistors to switch the power depending on an operational amplifier comparing the filtered feedback of the motor current with a comparison voltage (Fig. 5.18). More details on the implementation for $m\cdot\text{ReS}^{\text{X1}}$ is given in [64]. To avoid conflicts or cost using a patented circuit, this version serves only for comparison purposes to other developed circuits.

The second method works similar to the circuit used for $m\cdot\text{ReS}^{\text{R2}}$ but only needs one transistor instead of a motor driver due to unidirectional drive. The voltage on the motor is limited by switching a metal-oxide-semiconductor field-effect transistor (MOSFET). The PWM signal is applied to the gate so that the conductivity between the source and drain is altered, which affects the serially connected motor. The fly-back diode D1 eliminates the voltage spike induced by the motor in case of sudden reductions of its supply voltage. The current through the motor and the MOSFET is determined using a shunt. The voltage over the shunt resistor is amplified by a non-inverting amplifier circuit and filtered before it is sampled by the ADC (Fig. 5.17a).

The third method is a simplified version of the patented circuit. Similar as before, this circuit uses an operational amplifier that compares the voltage from a DAC with the amplified and filtered shunt voltage. Advantageously, it only requires one MOSFET to drive the motor (Fig. 5.17b).

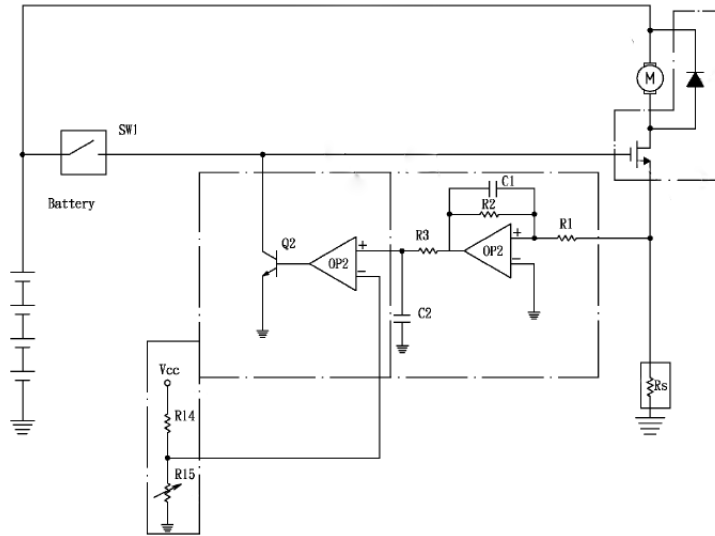


Figure 5.18: Patented circuit for torque control. Adapted from [192]

The PWM circuit requires the microcontroller to control the current to a certain level similar to $m\cdot\text{ReS}^{\text{R2}}$ (Section 4.3). The second method has the advantage that the loop is closed without the need of a microcontroller. The operational amplifier works as a comparator, resembling a proportional controller with unlimited gain. Since the microcontroller measures the current and controls the DAC-voltage, it may be used as a second layer of control. Further details can be found in [116].

5.7 Two-stage differential gear for force distribution of one motor

The major cost-drivers of $m\cdot\text{ReS}^{\text{X}}$ are the actuators. In the requirements the number of motors has been restricted to one per finger to limit the cost. However, further cost reduction by optionally using a single actuator was stated to be desired. An additional module has been developed, which allows to use one actuator only for the training of four fingers. Since the module is optional, the potential client can choose the version closest to the patients' needs. This section describes the development of the module which has been submitted for patenting.

A common method to simplify finger training by reducing the number of actuator is to use a shared shaft for all fingers [45, 47]. In the case of a cable-driven system, the cable displacement differs due to different lengths of the fingers. This leads to more strain for the finger with the longest closing trajectory. As a countermeasure the winder radii may be adjusted accordingly. Still, another issue with this solution remains. Since the fingers are still coupled with each other over the shaft, the fingers'

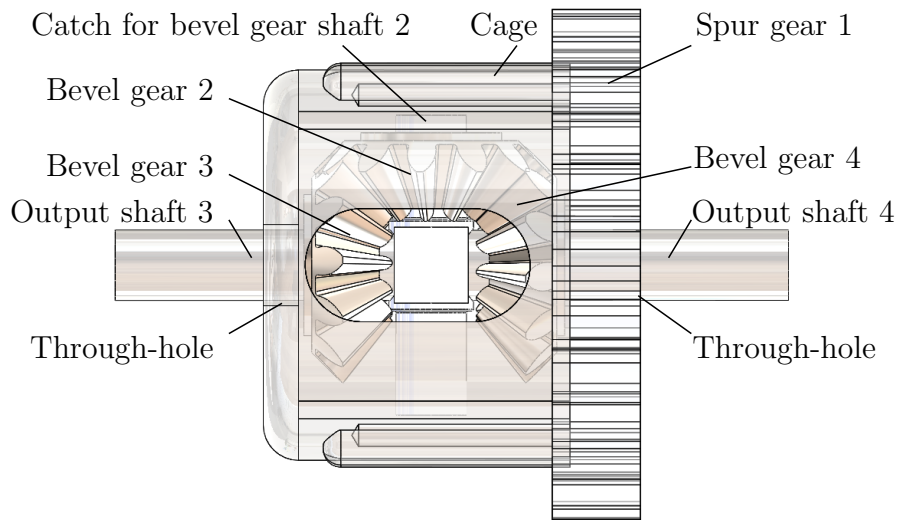


Figure 5.19: Look inside of a single differential gear. Output and input torque can also be reversed.

performances influence each other. For instance, in a hand closing exercise against the motor, the strongest finger would facilitate the closing movement of the other fingers.

We propose another approach that achieves to balance the input torque of one actuator on four output shafts, while allowing independent rotations. The invention is based on a multistage differential gear. In normal operation, the notation is as follows: the shaft or gear that is engaged with the motor shaft is referred to as input. The output shaft or gears are the ones that are connected to the fingers. However, any of these shafts can serve as input or output due to backdrivability.

For better understanding, first, a single differential gear is observed. Spur gear 1 is connected to the cage, which has a groove, where the shaft of bevel gear 2 sits. Its rotational axis is normal to the output shaft axis. It intersects with the two bevel gears 3 and 4, which are connected to two independent collinear output shafts (Fig. 5.19).

This configuration allows three basic modes of operation:

Differential Gear 1 distributes the input torque over gear 2 onto gear 3 and 4. Different angular velocities of the output gears result in gear 2 to spin. If the gears 3 and 4 turn in opposite directions only gear 2 rotates while gear 1 stays put. In general, gear 2 spins when speed difference between gear 3 and 4 occur.

Reduction If one of the gears 3 or 4 is blocked, the other gear turns with half the torque and double angular velocity as gear 1.

Reversal If gear 1 is blocked, a spinning of gear 3 lets gear 4 turn in opposite direction and vice versa (Gear train ratio $R_G = -1$)

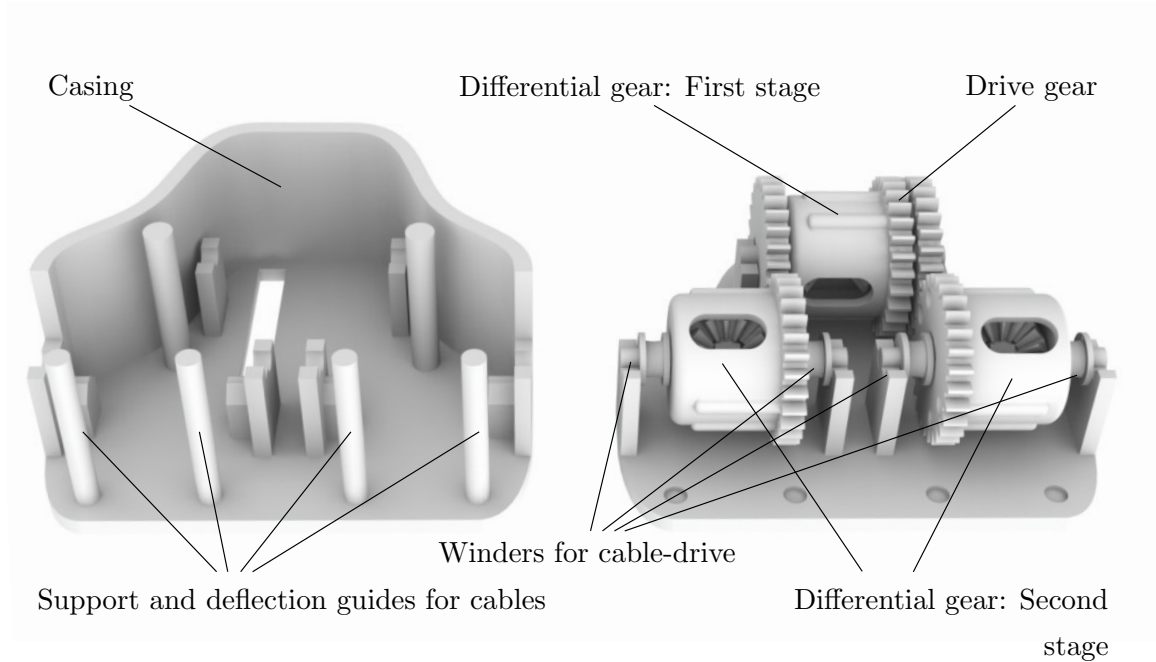


Figure 5.20: Differential gear. Drive gear refers to normal mode of operation.

In the differential mode of operation, its major function is to maintain a constant torque ratio between the output torque shafts, while allowing for different rotation rates. The ratio of angular velocity between the shafts depends on gear ratios inside the differential gearbox:

$$A n_3 + B n_4 - C n_1 = 0. \quad (5.6)$$

Two constants are required while the third one is redundant. Commonly A equals B and C=2. The respective torque ratios are:

$$\frac{\tau_3}{\tau_4} = -\frac{A}{B} \quad \frac{\tau_3}{\tau_1} = -\frac{A}{C} \quad \frac{\tau_4}{\tau_1} = -\frac{B}{C}. \quad (5.7)$$

The indexes refer to the numbering of the gears in Fig. 5.19.

This principle is extended to a second stage. The output shafts of the first stage are equipped with spur gears, which engage with the input spur gears of two differential gears in the second stage (Fig. 5.20). The torque is, thus, distributed on four output shafts. The modes of operation of the single differential gear trains can be combined, multiplying the possible modes in the second stage.

This special kind of gearbox allows modes of operation that are interesting for rehabilitation. Two possible configurations are exemplarily depicted in Fig. 5.21.

Driving both stages in differential configuration leads to an equal distribution of the torque onto the four output shafts. The first stage distributes the input torque onto the second stage such that

$$\tau_{S_1} = \tau_{S_2} = -\frac{\tau_S}{2}. \quad (5.8)$$

This torque is then again divided in a way such that the four output shaft torques are equal according to

$$\tau_{11} = \tau_{12} = \tau_{21} = \tau_{22} = \frac{\tau_{S_1}}{2} = \frac{\tau_{S_2}}{2} = -\frac{\tau_S}{4}. \quad (5.9)$$

The angular velocity of the output shafts depends on the input shaft's speed such that

$$n_{S_1} = -2n_S - n_{S_2} \quad (5.10)$$

and

$$n_{11} = 2n_{S_1} - n_{12}. \quad (5.11)$$

Inserting equation 5.10 into 5.12 results in

$$n_{11} = -2n_{S_2} - 4n_S - n_{12}. \quad (5.12)$$

The same applies for n_{S_2} , n_{12} , n_{21} and n_{22} , accordingly.

A second configuration is shown in Fig. 5.21b where two former output shafts as well as the previous input shaft are blocked and one of the second stage shafts serves for actuation. This mode of operation is interesting when no motor is available, since one finger can be mobilized by pulling at the strings with the healthy hand. The torque and angular velocity transmitted to the first stage are determined by applying the reduction mode of operation in the other direction. This means that gear_{S2} turns with half the speed but double amount of torque:

$$n_{S_2} = \frac{n_{22}}{2} \quad (5.13)$$

$$\tau_{S_2} = 2\tau_{22}. \quad (5.14)$$

The first stage operates in reversal mode since gear_S is blocked. Therefore,

$$n_{S_1} = -n_{S_2} \quad (5.15)$$

and

$$\tau_{S_1} = -\tau_{S_2}. \quad (5.16)$$

The other side of the second stage works in non-reversed reduction mode, dividing the torque in half and doubling the angular speed. This leads to a torque and speed on the output shaft of

$$\begin{aligned} \tau_{11} &= \frac{\tau_{S_1}}{2} \\ &= -\tau_{22} \end{aligned} \quad (5.17)$$

and

$$\begin{aligned}n_{11} &= 2 n_{S_1} \\ &= -n_{22}\end{aligned}\tag{5.18}$$

The developed prototype is able to show the functioning of the approach. However, it is a proof of concept, which was quickly developed using rapid prototyping technology. Therefore, it is not optimized for high backdrivability and force and torque measurements with the prototype will deviate from the theoretical considerations established above.

Typically worn on the back of the hand, the motor torque can be distributed equally to the four fingers independent of the displacement the single fingers have covered. The cable displacement is independent for each finger so that the tendon remains tightened also if single fingers are stronger or faster. Even without a motor the device is functional. By blocking the motor, the torque is transferred between the fingers. This makes it possible to grasp cables with the hand and transmit the force over the gear train to the fingers. The gearbox can also be placed on a table with the hand put on it. Then the motor works against extension of the hand. By integrating a motor and its controller into the module, the exoskeleton can be omitted. This stand-alone version was submitted to the patent office, where the application is pending.

5.8 Discussion on iteration improvements

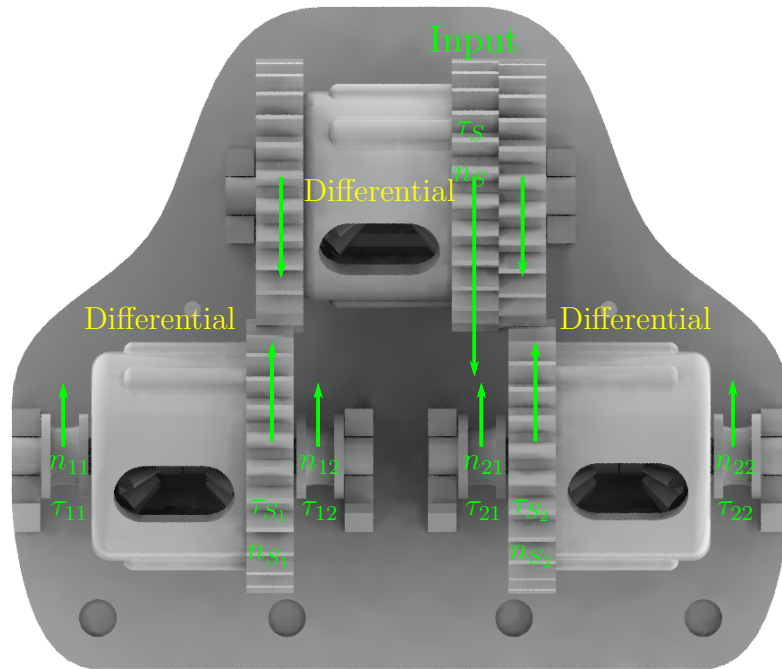
Several differences between the iterations exist. Most strikingly, the mechanical design evolved. The MCP joint is completely redesigned to align its rotational axis with the anatomical one. Thus, the prismatic joint can be omitted and unwanted forces during the MCP rotation can be reduced. However, the design is more complex and requires bearing beads to reduce friction, which increases proness to malfunction as well as assembly effort. The exoskeleton can, therefore, not be printed in one piece anymore. This increased assembly effort contradicts the achievements from the first prototype but also brings advantages. First, the gap in the joint can be reduced, which improves the Hall effect sensor measurements. Second, a set of generic sized parts can be printed to fit different hands without parametrization. This is convenient for testing and development, although eventually the exoskeleton shall be printed in one piece.

The exoskeleton's base is more complex incorporating slits and taperings to achieve compliance with the hand's dorsum. For this more parameters are taken to account for the arcs of the hand. The number is increased from 40 in m·ReS^{X1} to 44 in m·ReS^{X2}.

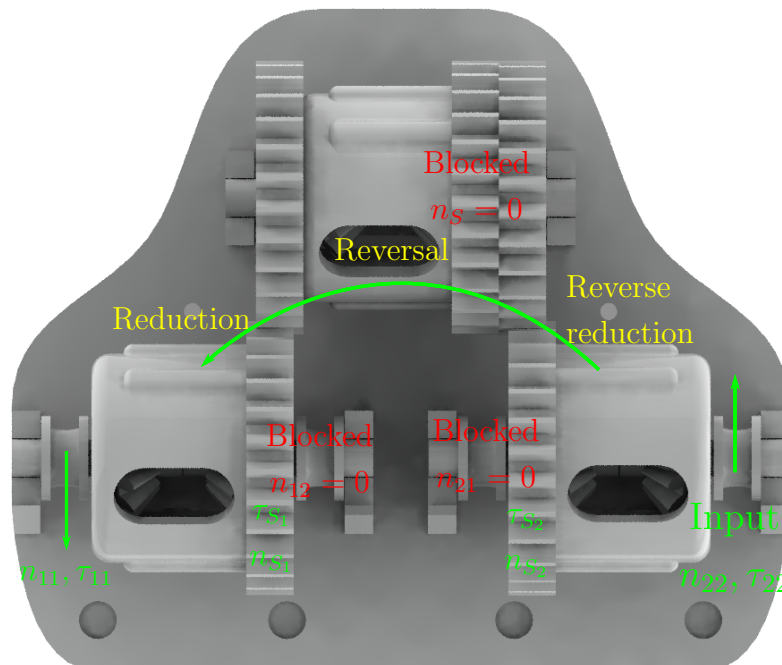
The actuation works very similar. Due to availability of a stronger motor, the gear could be omitted in m·ReS^{X2}. The maximum torque is however reduced from 59.36 mN m to 44 mN m. The method for torque measurement and control is the same

in both versions. A shunt measures the current and is limited with an operational amplifier circuit that compares the voltage over the shunt with a DAC controlled setpoint.

The angle sensing in both versions employs Hall effect sensors and motor encoder measurements to estimate the angle from the tendon displacement. m·ReS^{X2} requires a new sensor for the MCP joint due to the changed design. Different sensor combinations are feasible that depend on availability of a motor encoder, total cost of the glove, and which joint angles are necessary to be measured.



(a) Standard differential configuration. The input torque τ_S is equally distributed on the output shafts.



(b) Reversal configuration. The first-stage input gear is blocked as well as the second-stage shaft₂₁ and shaft₂₂. The torque of a tendon-force on shaft₂₁ is transferred to shaft₁₁.

Chapter 6

Software and communication

The different modules use a similar software and communication structure to reduce the programming effort and maintenance. Therefore, the developments are not placed within the implementation chapters of the modules but are described together in this chapter.

First, the communication hardware and architecture are described, which take care of the information exchange between the low-level and the high-level software (Fig. 6.1). The low-level part runs on a microcontroller, which, for instance, controls the motor and acquires the sensor data. It is described in the second section. The user interacts with the high-level software, which is described in the third section.

6.1 Communication architecture

6.1.1 Communication hardware

The communication architecture takes care of sending information between the hardware-near microcontroller program and the high-level graphical user interface (GUI).

The requirements demand the communication architecture to be flexible to apply it to different modules. The wide distribution of serial communication in the automation industry as well as in the microcontroller and electronics community makes it well suitable.

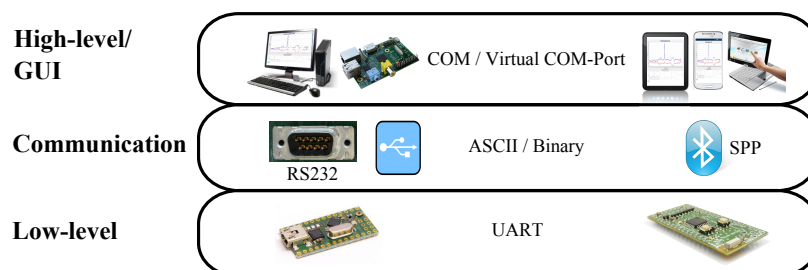


Figure 6.1: Communication architecture

m·ReS^{R1} uses an industrial motion controller that comes along with the Faulhaber motor. It uses RS-232, a widespread standard for serial transmission of data. Its circuit board includes a D-sub connector, which can be plugged into ports equipped in most personal computers. Otherwise, the functionality can be extended using a USB-to-RS-232 converter. The microcontroller code of the industrial motion controller is proprietary and low-level functions are not accessible.

m·ReS^{R2} and m·ReS^X own more possibilities of connection due to the customized hardware and the use of accessible microcontrollers. They establish communication either over USB or Bluetooth. For the tethered USB connection, an integrated circuit (IC) on the microcontroller board bridges between UART (Universal Asynchronous Receiver Transmitter) and USB. It creates a virtual COM port relieving from the necessity to have a physical one, as in case of the motion controller in m·ReS^{R1}. Bluetooth in conjunction with the serial port profile (SPP) allows similar functionality with a wireless connection. This architecture unbinds the low-level program from any specific operating system or program. The only requirement is that serial communication compatible to the hardware is provided depending either on the USB-to-UART IC, an external USB to RS232 converter, or SPP with Bluetooth. Figure 6.2 shows which system connects how to which hardware.

m·ReS^{R2}-based Toronto Rehabilitation Institute extension The communication for the extension module developed at the Intelligent Assistive Technology and Systems Lab (IATSL), Toronto Rehabilitation Institute (TRI) for their upper limb reaching robot (Section 4.7) is based on the groundwork of m·ReS^{R2} in terms of the communication architecture and commands. The implementation on another system underlines the advantage of the chosen architecture. Although the systems were developed independently from each other, the effort of establishing the communication is low.

The TRI system offers two ways of communication using serial interface commands:

- The microcontroller board of the hand extension can be connected to the computer to communicate with a Java GUI or
- the COM-port can be forwarded from the computer to the robot to implement the communication in Simulink.

For the proof-of-concept the system is connected to the computer and controlled via a Java interface independently from the main software. In the longterm the hand module should be connected directly to the robot offering extended possibilities in the interaction.

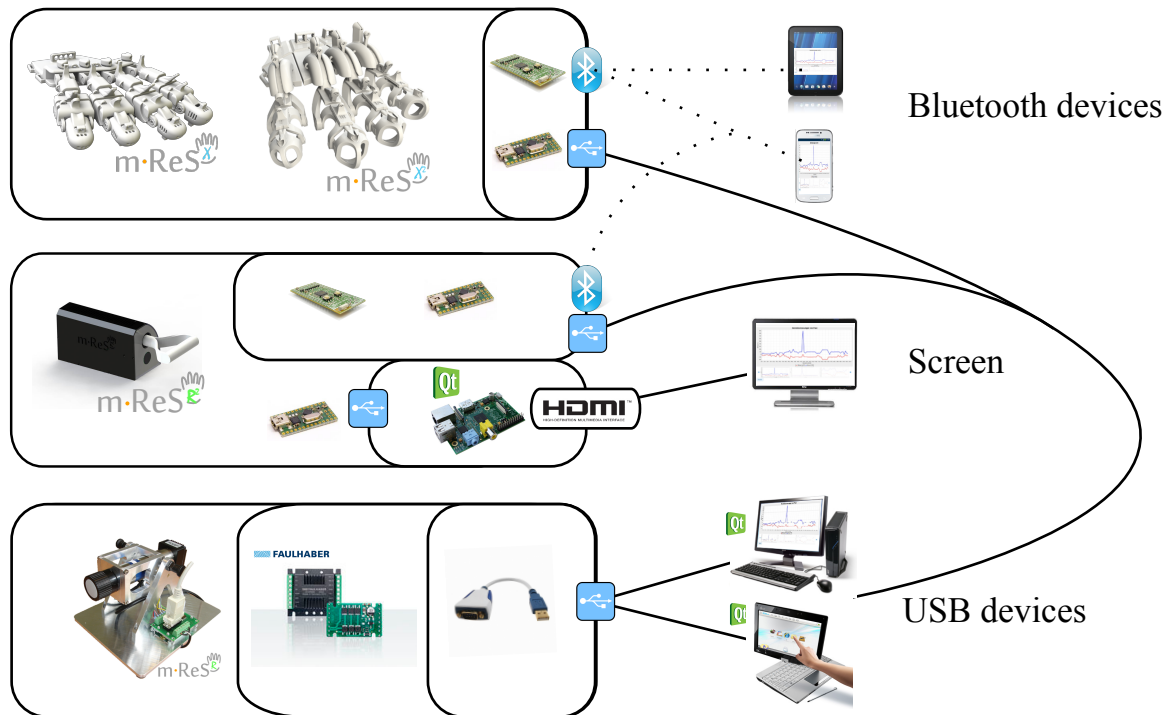


Figure 6.2: Interfaces of the different modules for communication between hardware and software. The Qt symbol indicates for which systems the framework has been implemented.

6.1.2 Data transmission

The communication is either based on ASCII (American Standard Code for Information Interchange) commands or on a custom binary protocol. Sending and receiving data encoded as ASCII has the advantage that it is in a human-readable format. This type of communication is, however, inefficient because each character is stored in an 8-bit byte. Transmitting, for instance, the output of a 10-bit ADC sample (0-1024) would take four bytes (one for each symbol) and possibly an additional byte for an identifier to assign the meaning of the value. Using a binary format, the same information could be included into two bytes where 10 bit are used to transmit the ADC value and 6 bit can be used for the transfer protocol and data identification. We use both encodings for communication depending on the amount of data sent and which hardware is used.

m·ReS^{R1} mostly relies on ASCII commands that set and read-out the functionalities of the motion controller such as positioning or angle sensor acquisition. Besides, a binary interface allows to trace certain measurements with an increased update rate. The command set is fixed and not expandable. Functions that are not provided by the motion controller can only be implemented with a sequence of commands over the

serial interface. For instance in current control, one pass including sensor data acquisition, computing a setpoint of the armature current on the computer, and sending it to the motor takes 16 ms in average. This rate corresponds to a frequency of 62.5 Hz, which is sufficient for applications in stroke rehabilitation, since the presence of friction in the system provides stability, and the human motion achieves only low mechanical bandwidth of around 7 Hz and 2 Hz for normal speed movements [45]. However, this interface reaches its limits for more sophisticated control schemes like friction and inertia compensation. Also the virtual spring mode cannot be implemented with the functionality provided by the motion controller.

m·ReS^{R2} and m·ReS^X The low-level code implemented on the microcontrollers in m·ReS^{R2} and m·ReS^X provide a similar communication protocol as Faulhaber's motion controller. It involves a set of commands that control low-level functions such as motor control or sensor data acquisition. The controllers and real-time computations are implemented on the microcontroller to relieve the communication bottleneck over the serial interface. Infrequently, the rehabilitation mode has to be changed, having a minor influence on the transmission rate. These settings are set using ASCII commands, facilitating debugging and extending the command set. m·ReS^{R2} transmits some information continuously like torque, position, and velocity during exercises. Still, the speed of ASCII transmission is sufficient for the amount of data.

In cases where more data has to be transmitted continuously, binary transmission is beneficial. Especially in case of m·ReS^X, where capturing the finger poses and forces requires several measurements. A maximum of 36 measured values have to be transmitted (16 angular positions and their velocities from the angle sensors and one force value per finger from the motors). Transmitting every value for presenting the finger poses and forces in the GUI with an acceptable refresh rate requires a high transmission rate. Here, the ASCII format is not advised but binary transmission is used. In the binary format the data length is known, and by specifying a protocol, the overhead is reduced. The protocol has been implemented as part of a bachelor thesis and revised in a second one [170, 187].

The high-level access to these functions can be easily implemented in different programming language, and on several operating systems and devices. For debugging, an ordinary terminal program such as HTerm can be used to send commands and receive data.

m·ReS^{R2}-based Toronto Rehabilitation Institute extension For the sake of reusability and compability, the m·ReS^{R2} interface is implemented on the microcontroller with adapted parameters and commands. However, it differs in the direction of the communication. Due to compability with the existing software, the extension module's GUI is implemented in Java. The programming language requires a virtual machine to run the code. This additional layer causes issues with hardware close functions like serial communication. The lower speed in receiving and processing UART

messages from the microcontroller can lead to lags. Furthermore, the system shall be designed such that extensions in functionality can be achieved only by changing the Java code without touching the microcontroller code. These two arguments lead to the decision to solely use GUI-driven communication. This means that no data is sent by the microcontroller without request by the GUI. The disadvantages are the larger overhead causing more traffic and slower refresh rates. The command-driven access to many functions and process variables offers the flexibility to increase the functionality from the GUI-side alone. This coincides with the motion controller of m·ReS^{R1} where access to the microcontroller code is prohibited and, therefore, a large list of commands is available to access the low-level functions. One exception is the data stream mode where angular position and velocity, torque are sent with a fixed rate.

6.1.3 Command set

Between the systems, many commands overlap with each other. The command set can be divided into three major blocks. First, "Get"-commands to acquire measurements like the angular position, speed or torque. Second, the "Set"-commands specify parameters like the home position or the maximum allowed current. Third, a special kind of "Set"-commands defining the training mode, e.g. virtual spring or passive mode.

For the TRI reaching robot an extension of the command set was required to adapt the functionality to the requirements for an upper-limb extension system. One example is a command to temporarily fix the motor in a position according to the therapists wishes stabilizing the patient's posture for reaching exercise with the UL robot. For easier syncing of the send data and compatibility with available code at IATSL, the measurements are prefixed with a letter indexing the kind of measurement. The commands are listed in the appendix (Appendix B).

6.2 Low-level microcontroller program

The low-level program takes care of the communication, sensor acquisition with the ADCs and interrupt pins, and the control of armature current or position amongst other things.

The communication is based on UART. Each symbol sent over the serial interface causes an interrupt. The received letters are stored in a buffer until the symbol for carriage return (0x0D) or line feed (0x0A) are received. Then the combined letters are checked against the existing commands and in case of a match, the corresponding code is executed.

The analog digital converters (ADC) read in the analog sensor values and code them into a 10-bit value. m·ReS^{R2} only requires one ADC to measure the Hall sensor voltage, which is proportional to the armature current through the motor. For m·ReS^X the

number of sensors exceeds the available ADCs of the ATmega328P, which is why an additional 8-channel ADC is added to the circuit, which is read-out via SPI (Serial Peripheral Interface). Also the digital-to-analog converter (DAC) that limits the current in m·ReS^{X2} is controlled via SPI.

The rotary incremental encoders that track the angular displacement of the motors and the IC measuring movements of the multi-pole magnet strip of m·ReS^{X2}'s MCP joints provide two quadrature outputs, which are 90° out of phase allowing for the determination of the relative position and the direction of motion. They are connected to interrupt pins so that rising and falling edges can be captured. The relative encoder samples have to be constantly tracked to get an absolute angle.

An interrupt-based timer accounts for isochronal samples and executions. This is important for the implemented PID controller. In each time step (normally 10 ms) the setpoint is compared to a process value and the control value is adapted according to the proportional, integral, and derivative parameters. A position and a current controller have been implemented. For both the manipulated variable is the PWM value ranging from 0 to 255. Anti-windup for the integral controller is included and the cumulated integral error is reset passing the home position. This needs to be done for the virtual spring, since the torque direction is switched, which would otherwise disturb the control due to the delay of the integral error.

Due to the use of compatible hardware and communication protocol, wide parts of the developments can be used interchangeably. The ATmega168 is compatible to the ATmega328P except for minor deviations in some registers. A different current sensor and motor driver were used but also in this case the necessary amendments were rather marginal. Preprocessor statements are used to develop the code within one project, and defines are used to fit the compiled version to the hardware.

6.3 High-level software and graphical user interface

As stated in the requirements, a graphical user interface is necessary. It provides several functions:

- Easy access to the low-level functions
- Visualization of sensor feedback
- Implementation of visual feedback distortion
- Guidance on how to use the program and how to perform the exercises
- Set permissions and restrictions of functions for user groups (patient, therapist, administrator)

Section 6.1 about the communication shows that the access to the hardware functions is not limited to one specialized program or operating system. The flexible and expendable architecture leads to many possibilities in implementing the high-level graphical user interface. Details about the selection and the implementation of the software is described in the following subsections.

6.3.1 m·ReS GUI with C++ and Qt

The programming language was selected based on the requirements in subsection 3.4.1.3. C++ runs inherently fast as native executable machine code without the need of a virtual machine. Being closer to the hardware level is beneficial for the communication with the microcontroller. In contrast, the popular alternative programming language Java uses the Comm-API which is prone to several issues both in the official SUN version and the RXTX library.

6.3.1.1 Qt framework

The functionality of C++ is extended by using Qt - a cross-plattform application and user interface framework. Qt is open source, maintained by Digia and free to use in commercial applications thanks to the LGPL license. It runs on Windows, Mac OS and Linux but also on devices based on Embedded Linux, Windows CE/Mobile, Symbian and the newly coming Meego without modification of the code. This improves reusability of the software for future developments. The requirements suggest the use of the single-board computer Raspberry Pi. The Qt code is runnable on the Raspberry Pi using the QtonPi project. Qt's GUI designer is another advantage.

An important extension of C++ native functionality is Qt's unique signal & slot mechanism. Signals are messages sent under certain conditions or explicit calls. If a slot is connected to the signal, it receives the emitted message and executes code accordingly. This facilitates communication between objects in an easy and type-safe manner. Despite the additional functionality, the code is compiled to native binaries remaining the advantage of C++.

For the serial communication with the hardware, the QextSerialPort library is used [163]. It provides an interface to serial ports for Qt-based applications. Distributed under the MIT licence, the code can be included into commercial products.

6.3.1.2 Irrlicht 3D engine

For m·ReS^X, a 3D engine is used to visualize the exoskeleton with the angle of the joints. The Irrlicht 3D engine is an easy to implement, flexible, and stable library and used due to several further advantages that overlap with the ones for C++ and Qt. It is open source, platform independent and, additionally, API independent supporting, inter alia, OpenGL and Direct3D devices. It is, furthermore, not dependent on other

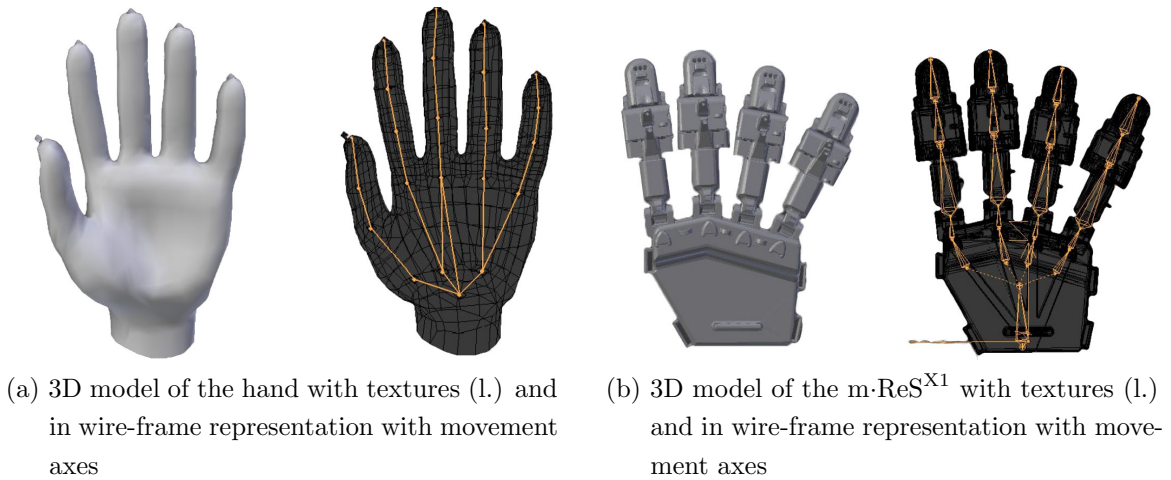


Figure 6.3: 3D model in Blender

libraries. It is distributed under zlib/libpng license, which has even lower requirements than the GPL or LGPL for redistributing it in other projects or commercial products.

Finally, a strong argument for the use is that it interacts flawlessly with the open source 3D graphics and animation software Blender. To visualize the sensed joint angles with the 3D models, rotation axes have to be defined. This is done in Blender and the exported model is imported to Irrlicht. This allows to set the angles in the model according to the sensor measurements. A hand model and a downsampled exoskeleton model of m-ReS^{X1}, exported from Solidworks, has been included (Fig. 6.3). Parts of the m-ReS^{X1} software and the Irrlicht integration were developed as part of a bachelor thesis [187].

6.3.1.3 Software structure

The software follows a modular structure in order to increase code reusability, especially with regard to the different hardware used. The helper classes play a key-role, which allow for cross-class communication without each others' knowledge. Thus, classes can be added or removed without influencing the functioning. The communication with the hardware runs exclusively over the helper classes. This gives a better overview concerning the access to the safety relevant hardware and facilitates to add or amend restrictions. For example, the maximum angle the motor turns must not exceed the patient's range of motion under any circumstance. A distributed access to the motor functions makes a violation more probable compromising safety.

Furthermore, the helper class abstracts the communication from the hardware, facilitating the integration of different kinds of systems. Each m-ReS module has its dedicated helper class, which is loaded at program startup. The correct system is automatically recognized after performing a software-handshake. The helper class

translates certain functionality demanded by other classes to a specific command. For instance, the command to apply voltage to the motor is based on an ASCII command for $m\cdot\text{ReS}^{\text{R}2}$, whereas $m\cdot\text{ReS}^{\text{X}}$ uses the binary format. However, the class that demands to apply voltage is not aware of the difference. Furthermore, the helper class contains several get and set methods, information about the exercise mode, and hardware-specific constants and conversions. The program structure, class interaction parts of the GUI for $m\cdot\text{ReS}^{\text{R}}$ were developed as part of a bachelor thesis, which gives more details on the implementation [205].

6.3.1.4 Exercises and modes

In this section exercises and modes are described that are used with $m\cdot\text{ReS}^{\text{R}}$ and $m\cdot\text{ReS}^{\text{X}}$.

Progress evaluation Before the exercises are performed, it is important to determine the patient's passive (with motor assistance) maximum range of motion as a rotation limit for the motor (Fig. 6.4a). Afterwards, the actively reachable maximum range of motion (ROM) and torque are measured to provide a reference value for the following exercises (Fig. 6.4b). These measurements are also stored to compare them over several sessions (Fig. 6.4c). Also the trajectories are stored to give the therapists the possibility to have a closer look at how the exercises were achieved. Further progress evaluation values can be extracted depending on the therapists wishes.

Visual feedback distortion Visual feedback distortion of force/torque or (angular) position can be applied to most exercises. Either in a dedicated view for studies (Fig. 6.5a), in progress evaluation screens or during games. Several settings have been implemented that can only be accessed in therapist view (Fig. 6.5b). Before, the setting was done locally, but it is shifted to settings that can be changed remotely with the tele-rehabilitation functionality.

Passive training Passive or assisted exercises include the actuators supporting the patient in performing different movements. $m\cdot\text{ReS}^{\text{R}}$ supports the rotational movement either by using the passive mode cube (Section 4.6.1) or in automatic mode. The limits in ROM are based on the initial assessment and may be altered. In automatic mode, the repetition frequency, and the maximum torque can be set.

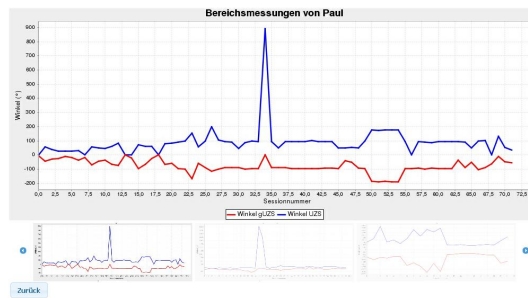
In the standard configuration of the cable-guiding of $m\cdot\text{ReS}^{\text{X}}$, the actuators assist in opening the hand. They work against the commonly occurring increased muscle tone in flexion and potentially improves mobilization.

Active training Depending on the abilities of the patient, the support of the motors can be reduced. In $m\cdot\text{ReS}^{\text{R}}$, the friction and inertia compensation includes a parameter for the difficulty, defining to which extent the support is reduced. The



(a) Passive maximum range of motion

(b) Maximum achieved torque evaluation



(c) Graph of the maximum values over several sessions

 Figure 6.4: m·ReS^R GUI screens: Performance tests and progress evaluation

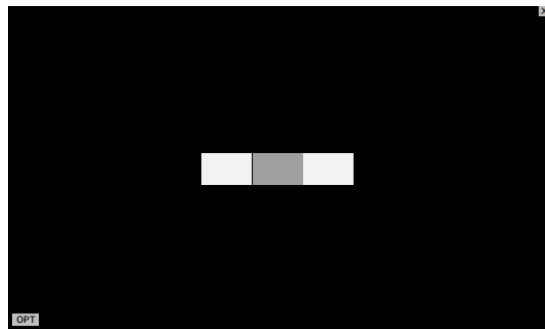
virtual spring exercise available for m·ReS^{R2} increases countertorques with the displacement from the home position.

In m·ReS^X, the force on the cables can be adapted. Either a constant force or a variable force depending on the amount of flexion is applied on the tendon. The latter mode resembles the virtual spring mode from m·ReS^R.

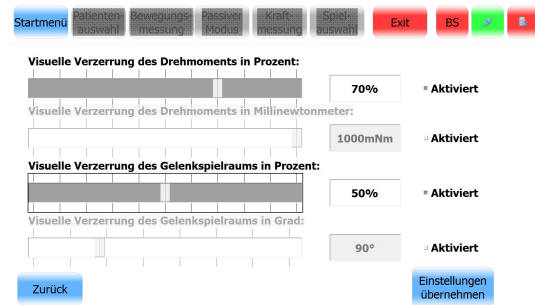
Independence of finger movements The independence of finger movements or fractionation is an indicator for the fine motor skills. In an exercise for m·ReS^X, the patient is asked to move one specific finger and the degree to which the other fingers move is measured (Fig. 6.6a). The fractionation is determined with the following formula:

$$F_F = \left(1 - \frac{ROM_O}{ROM_F}\right) \cdot 100\% \quad (6.1)$$

where F_F is the finger fractionation, ROM_F is the averaged range of motion of the finger to be moved individually, and ROM_O is the averaged range of motion over the other fingers and joint angles. This metric may serve for progress evaluation, tracking its course over several sessions.

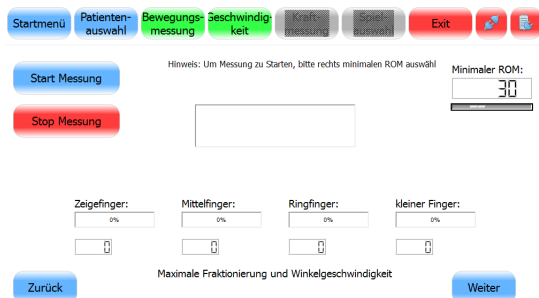


(a) Form used in the experiment with $m\text{-ReS}^{\text{R1}}$ to determine the just noticeable difference between either two angles or two torques

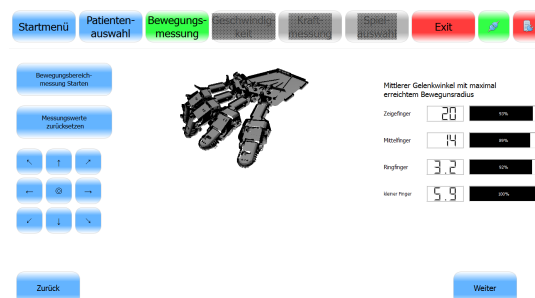


(b) Visual feedback distortion settings for $m\text{-ReS}^{\text{R}}$

Figure 6.5: Visual feedback distortion related views



(a) $m\text{-ReS}^{\text{X}}$ finger independence test



(b) 3D representation of $m\text{-ReS}^{\text{X1}}$ in the GUI

Figure 6.6: $m\text{-ReS}^{\text{X}}$ GUI screens of different exercises

3D graphics window The 3D representation is very useful for testing the angle sensors, since malfunctions can be recognized in one glance. This view gives immediate feedback and comprehensible information about the joint angles. Unnatural finger poses or jerky movements show inaccurate or uncalibrated sensors. The 3D view is suitable for demonstration purposes (Fig. 6.6b).

Moreover, the maximum reached joint angles are determined in 3D view. The actual angle is shown together with a percentage of a normal ROM of a healthy hand. The angles of each finger are summarized into one number to avoid overwhelming and not comprehensible amount of information. Still, the whole data set is stored and can be accessed if desired.

Rehabilitation games Three simple games for $m\text{-ReS}^{\text{R}}$ have been implemented to demonstrate how the hardware can be used (Fig. 6.7). Either the torque or the

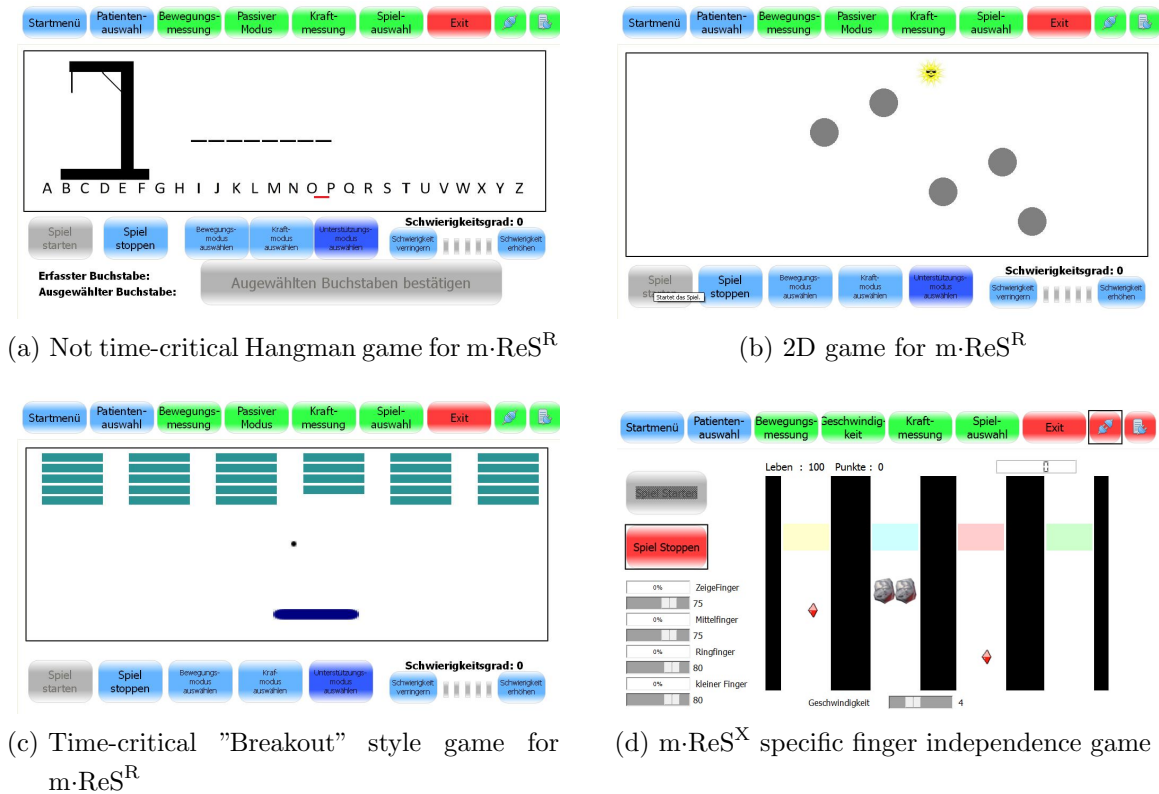


Figure 6.7: Simple rehabilitation games. The first three games have been developed for $m\cdot ReS^R$, but $m\cdot ReS^X$ can also be used as an input device.

range of motion can be used as a game variable (for instance the position in the game). The games differ in the dynamics of the game play. The "hangman" game is not time-critical in order to avoid pressure on the patient or decreasing motivation of more impaired stroke sufferers. "Breakout" requires to block the flying ball before it reaches the ground, forcing patients to get there in time. The 2D game is not time-critical again, however, it requires higher cognitive skills to control the second dimension with the passive mode cube as an additional input.

Thanks to the modular class structure, abstracting the input from the functionality, $m\cdot ReS^X$ can be used to play the same games with only minor modifications. The averaged joint angles are mapped to the movements in the game. Additionally, a game specific for $m\cdot ReS^X$ has been included. On four tracks, representing the fingers, symbols occur and move from one end to the other. In a certain area on each track, the symbols can be caught by moving the corresponding finger over an averaged angle threshold. This exercise trains the independence of fingers (Fig. 6.7d).

The games were intended for demonstration purposes. Against expectations, therapists as well as older patients were satisfied. More complicated games or more effects

often overexert patients that have to struggle with physical as well as cognitive impairments. Younger patients raised with the presence of computer games probably may demand more sophisticated games.

6.3.1.5 Telerehabilitation functionality

Patients using m·ReS at home should still be supervised by a therapist in their training, which is why remote access is an important aspect of the system. The necessary telerehabilitation functionality is developed parallelly in another work. In the present state of development, several training parameters are logged and securely transmitted over the internet to a server and can be accessed from there. Key data like maximum achieved ROM or torque as well as whole trajectories of each session are stored and can be examined by the therapists in a web-based GUI. If no internet connection is available, the data is stored locally and transmitted as soon as the device is connected. The web front-end is based on the JavaServer Faces component suite PrimeFaces and JavaEE 6 and connects to a JavaDB database. The application is hosted on a GlassFish application server.

6.3.1.6 Raspberry Pi

The Raspberry Pi is a perfect fit to complement the system. It is cheap, Qt-compatible, and small enough to be integrated into m·ReS^{R2} to provide an out-of-the-box solution for potential customers. Several open-source operating systems exist. We use Debian Wheezy, which works together with QtonPi allowing to natively compile Qt programs on the Raspberry Pi. The m·ReS^R program has been ported, and a running GUI on the Raspberry Pi demonstrated the functioning. The software of m·ReS^X includes Irrlicht libraries, which should be compatible with the Raspberry Pi but have not been implemented and tested yet.

6.3.1.7 Navigation and user interface

The navigation leading through the steps of the training is kept easy. Exercises that require previous steps are restricted. For instance, the games cannot be played before the maximum range of motion and torque are determined. It is possible to go to prior steps and repeat the measurement. The actual, done, and restricted steps are coded in color in a bar at the upper side of the screen. Preferences are blue, performed tasks are green, unavailable exercises grey, and red for exit and if the telerehabilitation server or the hardware is not available (Fig. 6.6).

m·ReS^{R1} uses the eeePC's touchscreen capabilities for user interaction. Whereas, the feedback of colleagues and healthy subjects was positive, the clinical use showed flaws of the GUI. Since stroke occurs more probable in older ages, also visual and cognitive constraints have to be regarded. In use, an elderly woman did not know whether to focus on the hand or on the interface. Especially the passive joint range

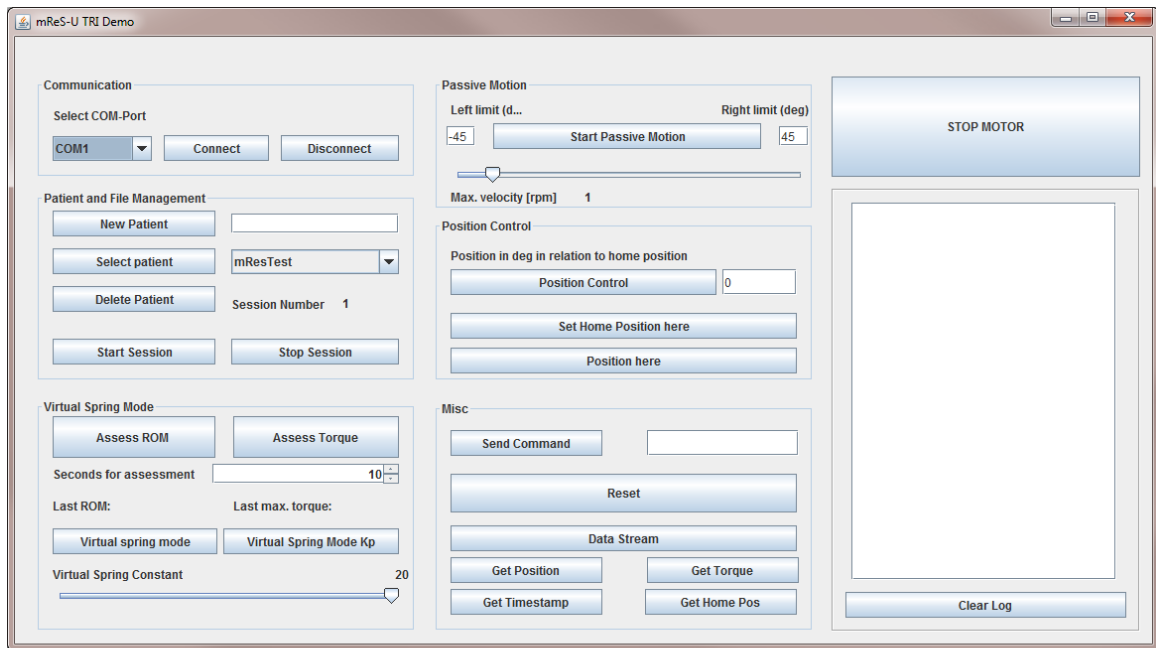


Figure 6.8: The graphical user interface developed for the TRI rehabilitation robot extension to be used in studies by the researchers

of motion assessment was unpractical for elderlies, since the focus had to be switched between the hand and the motor control button on the touchscreen. This can cause confusion where to focus and what to do. For the given reasons, the user interface of m-ReS^{R2} was facilitated. The focus distance between the training hand and the GUI is kept shorter by including a five-buttons cursor panel, which is placed within the vicinity of the handle. Due to the flexible communication structure and software, also the eeePC can be used, alternatively.

6.3.2 Toronto Rehabilitation Institute extension GUI in Java

A dedicated GUI was created for the m-ReS^{R2} sub-module for the reaching robot at TRI. It gives access to the training modes and data acquisition implemented on the microcontroller. Compatibility to the existing software of the upper-limb rehabilitation system shall be remained. Accordingly, the GUI is based on Java, facilitating the integration of the new code into the existing software. It, foremost, focuses on providing an interface that gives access to the hardware functions by non-technical staff without much prior knowledge about its operation. The GUI is tailored to the use of the system in studies since this is the most important application of the system at TRI in the near future. The GUI is shown in Fig. 6.8.

An event-based method together with a 64-bit package of the RXTX Java library has been used to establish communication. It allows access to the training modes and store data such as position, speed, and torque, which is provided by the microcontroller. The data of each patient is permanently stored in a serialized form and loaded at startup of the program. For each patient a text file is created on the first session. Depending on the patient and the session number the respective file is then extended in the follow-up sessions. Not only training data but also the use of the program is documented, allowing for conclusions about how important the single functionalities are. The sampling data is processed by the program in such a way that it can be easily plotted. The plots may help to evaluate the training sessions, to observe the rehabilitation progress of the patients, and performance analysis for studies.

Chapter 7

Evaluation and studies¹

This chapter provides performance evaluations and demonstrates the application of the systems in preliminary studies. The devices use inexpensive hardware to provide actuation and sensing. The performance evaluation quantifies the accuracy of actuators, sensors, and control, and determines whether it is sufficient for applications in rehabilitation. The description of the experiments is structured according to the modules.

7.1 Evaluation of m·ReS^R

First, friction and inertia compensation are evaluated. Then, the accuracy of sensors and actuators is examined. This indicates the suitability for the application from a technical point of view. Angle measurements are not assessed since the encoders offer by far more accurate measurements than the limiting factor, namely the gear. The backlash is below 1° for m·ReS^{R1} and is not stated in the datasheet for m·ReS^{R2}. m·ReS^{R1} has been applied on a preliminary study to test the just noticeable difference. The experiment and the results are described in Section 7.1.3. The section closes with describing experiences in application.

7.1.1 Friction and inertia compensation with m·ReS^{R1}

The gear of m·ReS^{R1} has a reduction ratio of 43:1 to provide sufficient torque to work against the muscles of the forearm. However, a high gear ratio leads to lower backdrivability. Therefore, a friction and inertia compensation algorithm has been implemented that reduces the backdriving torque without the additional use of expensive force-torque sensors. The following experiments evaluate the compensation by observing the torque on a force/torque (FT) sensor with and without the friction and inertia compensation while varying the velocity.

Method A possible experimental scenario is to have a human subject driving the motor while measuring the torque. The resulting data is, however, not objective and

¹Parts of this chapter have been published in [193, 194, 196, 197, 198]

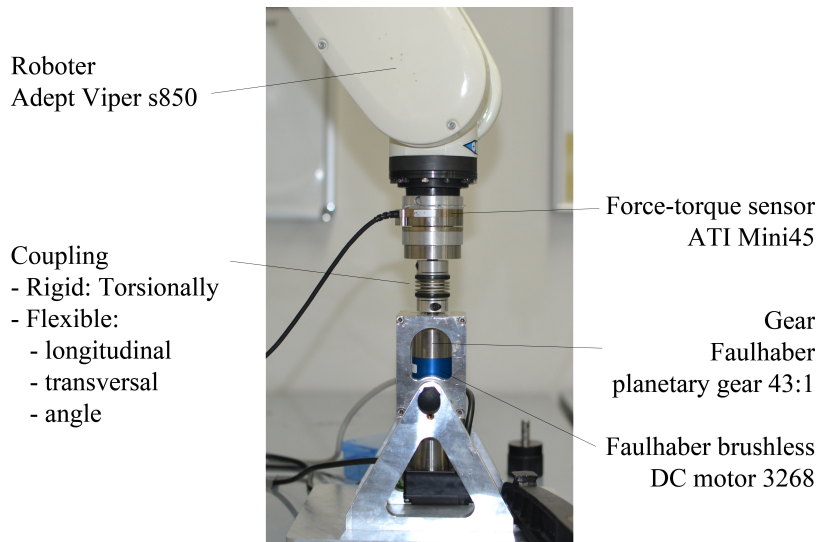


Figure 7.1: Experimental setup of the robot-driven evaluation of friction and inertia compensation [198] ©IEEE

repeatable, since the profiles differ from each other and are poorly comparable. For more reliable results, we used an Adept s850 robot to apply different acceleration and velocity profiles on the motor and measure the response. The robot is equipped with a force-torque sensor and is connected to the motor over a metal bellow-type coupling. The coupling is torsionally rigid to uncompliantly transmit the torques but flexible in longitudinal and transversal direction. It has angular flexibility to prevent forces caused by non-concentric alignment, from disturbing the measurement. A FT sensor is mounted between the robot and the motor. It measures the counter torque of the motor resulting from the robot input with and without compensation with an average sampling rate of 70 Hz. The experimental setup is shown in Fig. 7.1.

$m\cdot\text{ReS}^{\text{R1}}$ uses an extended version of the software that frequently samples the measurements and writes them to a file. The robot is programmed using scripts in the Adept programming language V+. The accelerations and decelerations are quantified in the percentage of the maximum the robot can perform. According to the data sheet 100 % velocity equals $600\text{ }^\circ\text{s}^{-1}$, whereas the maximum acceleration was not stated. Driving the motor of $m\cdot\text{ReS}^{\text{R1}}$ with the robot while sampling the encoder showed that 100 % acceleration is about $550\text{ }^\circ\text{s}^{-2}$.

The robot drives different profiles, which were repeated ten times with the same velocity and acceleration. The data sets were then synchronized and merged by determining the time when the motor starts moving in the different repetitions and shifting the data correspondingly. A position threshold of 5° had to be passed so that noise is not interpreted as the beginning of the profile.

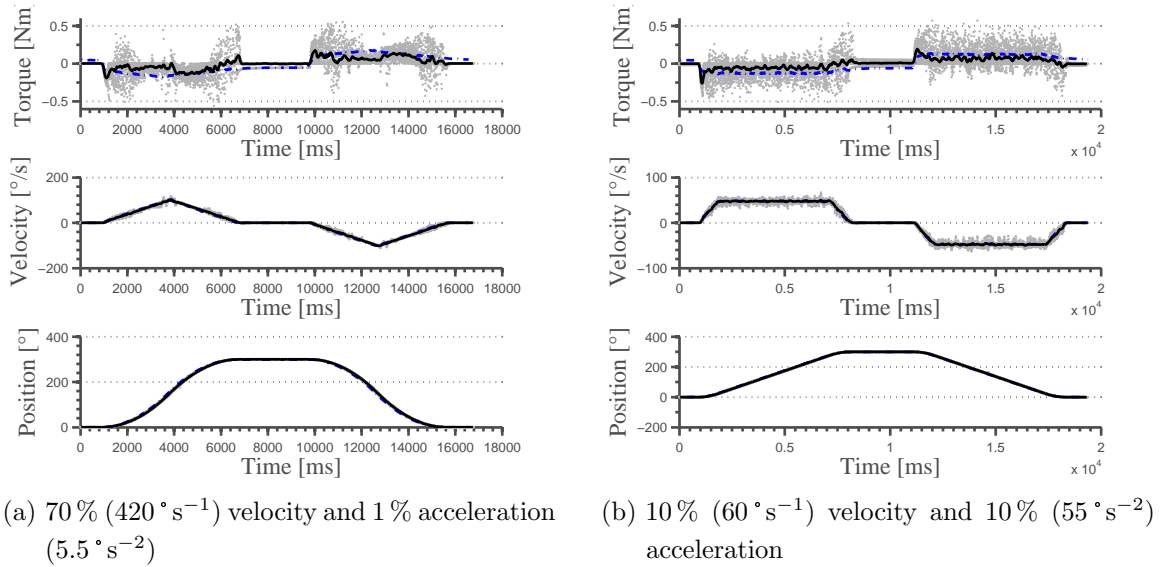


Figure 7.2: Synchronized and merged data set of torque, velocity and position. Blue dash-dot line: Moving average without compensation; Grey points: Measuring points with friction and inertia compensation; Black solid line: Moving average of the friction and inertia compensation measuring points [198] ©IEEE.

Results The synchronized and merged datasets are illustrated as grey dots in Fig. 7.2. The figures show the validity of the merging process since no outliers can be observed in the velocity and position graphs. Synchronization between the motor and the force-torque measurements is not required, since the same time stamp is used. The measurements with compensation, visualized in bright gray, were filtered by using central moving average over 100 data points to clarify the underlying course.

In order to further clarify the results, we generated boxplots that include all tests with $v_{max} = 10 \%$ (see figure 7.3a) and $v_{max} = 70 \%$ (Fig. 7.3b) and the whole range of accelerations ($a_{max} = 1 \%, 10 \%, 25 \%$). They give a summary of the findings and allow to distinguish between no compensation, both friction and inertia compensation, and each one separately. The absolute value of every measurement with $v \neq 0$ is taken into account. The values during standstill are filtered out, in order to avoid influences on the result. In addition to the standard boxplot comprising of the smallest observation, lower quartile, median, upper quartile, and largest observation, the arithmetic means in form of the black dots are included (Fig. 7.3).

Discussion The influences of the kinetic and inertia compensation on the backdriving torque of a motor was examined. The robot-based evaluation allows to accurately repeat different profiles of velocity and acceleration, providing objective results.

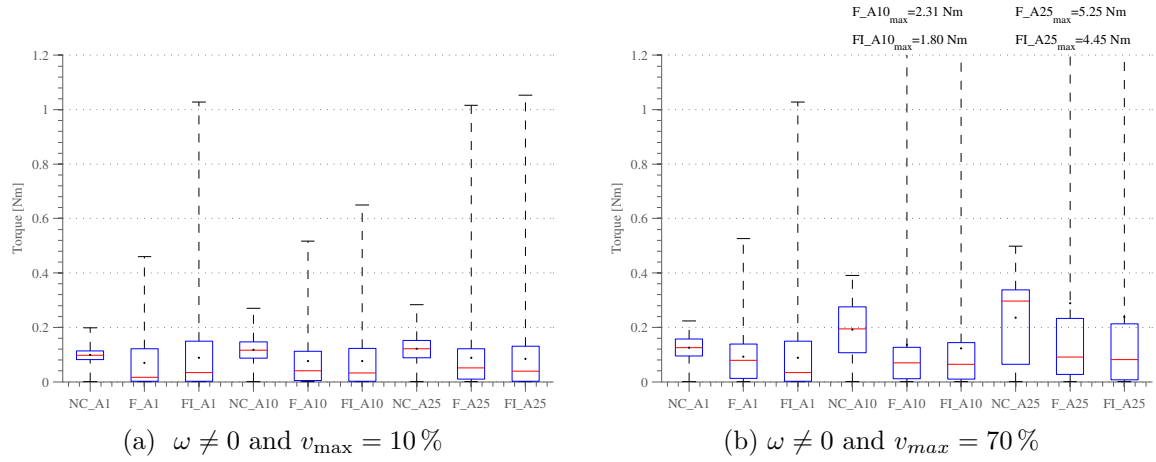


Figure 7.3: Boxplots of the absolute difference of the torque over all measurements. A= acceleration (%); NC = no compensation; F = with friction compensation; FI = with friction and inertia compensation [198] ©IEEE

The velocity graphs of the two figures illustrate why different speeds and accelerations were observed. Having higher accelerations and lower velocities leads to a shorter acceleration phase and a longer plateau of constant velocity. In the opposite case, no plateau phase exists since the robot calculates a bang-bang trajectory. The kinks between accelerating and decelerating induces additional torque peaks.

The figures allow first conclusions about the influence of the friction compensation. Whereas the position graph is uniform, the velocity graph shows outliers for measurements with compensation. They are triggered in cases of over- or under-compensation, resulting in fluctuations of the torque. Although the variance is higher, the averaged graph with compensation shows in both figures lower torques in comparison to the uncompensated one.

Comparing the boxplots with and without compensation (F_Ax, FL_Ax and NC_Ax in Fig. 7.3) for the different accelerations shows consistently that median and average of the data with compensation (friction and inertia) performs better than without. An overall value was obtained by averaging the differences between FL_Ax and NC_Ax, and F_Ax and NC_Ax, respectively, from both boxplots. In average, kinetic + friction compensation reduced the median values of the backdriving torques by 66.67 % and the average values by 23.58 % (62.75 % of the median values and 20.74 % of the average for kinetic compensation only). However, the variance and maximum values are higher, which coincides with the plots against time (Fig. 7.2).

The comparison of boxplots with kinetic friction compensation only and kinetic + inertia compensation (F_Ax and FL_Ax) is inconclusive. For example, inertia compensation improves the results according to the median and average with $a_{\max} = 25\%$ for both velocities but causes higher torques for $a_{\max} = 1\%$ and $v_{\max} = 10\%$. The

average over all measurements shows an improvement of 3.92 % from the median and 2.84 % from the average values, indicating slight benefits of the inertia compensation.

The conducted experiments show that the compensations significantly reduced the backdriving torque for a wide range of accelerations and velocities, covering the requirements of rehabilitation applications. Both, kinetic friction compensation only and kinetic with inertia compensation, improved backdrivability. However, the experiments revealed only a slight advantage of the inertia over friction compensation only. They also show that the variance and torque peaks are increased, which has different reasons. First, the rigid coupling transmits the torque uncompliantly from the robot to the motor. In cases of overcompensation or lags, the motor works against the robot causing the torque to rise instantaneously. However, the human hand is much more compliant so that the measured torque peaks are not experienced by a user in that extent. Third, the voltage on the motor induces resistance until the compensation reacts. The lag of around 20 ms until the control increases the motor current causes the initial higher torques.

It is important to notice that this configuration represents a critical scenario with high reduction gear ratio (low backdrivability) and slow control. Still, the results show that compensation can work under these conditions. Implementing the control on a microcontroller would enable further improvements. The bottleneck of the RS-232 interface and the restricted set of commands of the motion controller could be avoided. Increasing the sample rate enables filtering of the velocity and, thus, achieving less noise in the acceleration. It seems promising that the result of the inertia compensation can be shifted further towards being beneficial over kinetic friction compensation alone.

7.1.2 Torque measurement and control

7.1.2.1 Torque measurement with m·ReS^{R1}

The limited access to the low-level functions of Faulhaber’s proprietary motion controller prevents the torque estimation to be based on current measurements. Instead, the torque is based on the control parameter in position control mode. Since no relation based on physical principles exists, the mapping between the torque and the position control parameter has to be measured.

Method The experimental setup to observe the relation between these two quantities uses the same FT sensor as the friction and inertia compensation experiments. However, the robot was not used since it is not capable of driving defined torque profiles. Instead, a human subject applies torques manually onto the FT sensor that is connected to m·ReS^{R1}. The position control output and the torque from the FT sensor are sampled and plotted against each other over the observed torque range from -1.5 N m to 1.5 N m . The relation between them is modeled with a polynomial fitting with a degree of 7, which showed a good fitting and higher degrees did not greatly

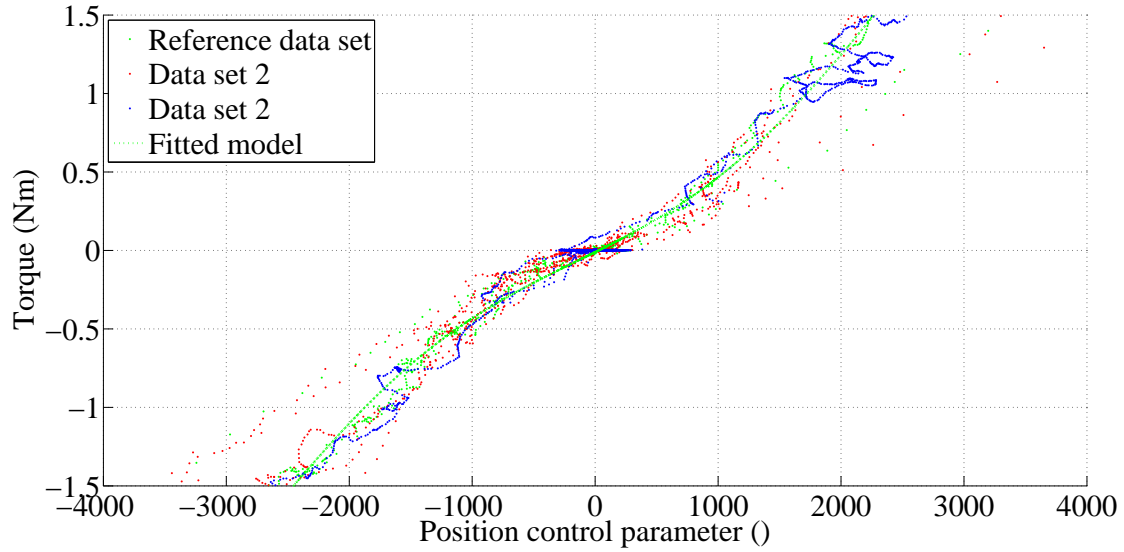


Figure 7.4: Mapping of the position control output to torque measurements. Green marker: Reference data; Green line: Fitted model; Red marker: Data set 2; Blue marker: Data set 3.

further improve. However, the mapping represents the optimized case to the fitted model, which is why the experiment is repeated with the old mapping applied on two further data sets. Finally, the root mean square errors (RMSE), are calculated.

Results The mapping between the position control parameter and the calibrated force-torque sensor based on the reference data set revealed a RMSE of 0.06 N m in the ± 1.5 N m range. Outside, less measurement points are available and the variance is higher making the model more inaccurate. Two other data sets were sampled and the model was applied on them. The RMSE is 0.1244 N m and 0.0906 N m for the second and third data set, respectively. Figure 7.4 shows the plots of the data sets including the fitted model.

Taking the fitting for all the measurements over the whole range (over 3 N m) results in RMSE of 0.0904 N m, 0.1609 N m, and 0.1207 N m for the reference, data set 2, and 3, respectively.

Discussion The limitations of the proprietary motion controller cause implications on the experiment to determine the accuracy. In contrast to $m \cdot \text{ReS}^{\text{R}2}$, the current or the torque cannot be successively increased. Therefore, a reverse load has to be exerted onto the motor. For this task, the robot is fairly suitable, since it does not support torque control but only position and time-dependent trajectories. The human hand is able to slowly increase the torque on the motor but not in an objectively accurate and repeatable way. Still, the representation of the results plotting the

torque estimation against the FT measurement supersedes the need to know the slope of the torque against the time.

The results reveal issues and limitations of this way of measurement. A hysteresis occurs revealing a difference in the mapping between rising and falling torques. The RMSE error summarizes the plot to one quantity facilitating the comparison to other measurements and offering an estimation of the accuracy. The results show that a fitted curve allows an acceptable amount of accuracy in the observed range with a RMSE between 2% and 4.133%. As expected, the transfer of the mapping to the other data sets exhibits higher errors. Restricting the range is acceptable since higher torques are rather used for passive training than for measurement purposes. However, the results are biased since the measurements are denser for lower torques that exhibit lower deviations and variance.

Torque control is not provided by the motion controller and the functionality is restricted to the measurement during position control. The results make clear that solutions from the automation industry are not well suitable for this special kind of application. Hardware is needed that allows for faster control and torque measurements without being restricted to position the motor. m-ReS^{R2} was developed to improve these shortfalls.

7.1.2.2 Torque measurement and control with m-ReS^{R2}

The microcontrolled, customized hardware of m-ReS^{R2} gives more possibilities in torque measurement. It is based on the linear relation between current and torque, which are controlled by a pulse-width modulation (PWM)-controlled motor driver. First, the open-loop response of the current to different PWM signals is observed before examining the closed-loop current-control with a FT sensor. Based on the second experiment the static friction is compensated to improve the measurement quality and control.

PWM Voltage to Current m-ReS^{R2} uses pulse width modulation, switching a MOSFET to control the current. The 8-bit PWM signal is created with the microcontroller using a quartz with 14 745 600 Hz, which results in a PWM frequency of 57.6 kHz. PWM inherently induces oscillations, which shall be observed in this experiment.

Method The motor is blocked in order to avoid influences from counter-electromotive forces (counter EMF). This corresponds to the later application, where the hand is mostly in a torque equilibrium with the motor, and rather less movements occur. Several steps with different pulse-widths are applied, and the response of the current is measured. This represents the open-loop relation between pulse width length and the current. The pulse width is increased in 13 steps in both directions ranging from 0 to 206. No current control is activated, which is why the PWM values are limited to keep the current below 4.9 A. Otherwise the torque goes above

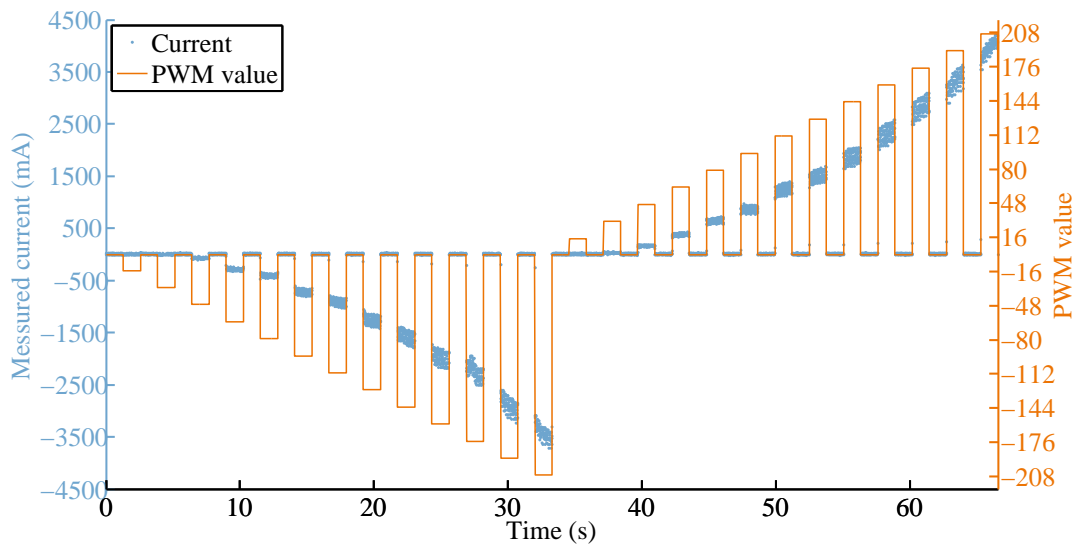


Figure 7.5: m·ReS^{R2} Step response of the control voltage and measurement of the resulting amplified voltage over the shunt.

the continuous rated allowance. Between the steps the PWM value is reset to zero in order to observe steps of increasing height. A 47 nF capacitor filters the current measurements but apart from that no averaging or filtering is applied.

Results The setpoint and the measured current are plotted against the time (Fig. 7.5). The results show that the relation between the PWM signal and the current is not linear. Moreover, the current shows asymmetric behavior with higher currents for positive values.

Discussion The oscillations, caused by a combination of the PWM signal, the motor driver, and the motor itself, are within an expected and acceptable range. A simple moving average may be applied to smoothen the current response. The current appears to be higher for positive values. However, the same could not be observed in a second run with switched directions. This lead to the conclusion that the difference is not caused by the direction but by a time-dependent factor. Since the temperature of the motor driver increased with the time it was expected to cause this asymmetry, which is why a heatsink was attached. A temperature increase in the motor may also cause this behavior but is operated under conditions rated to be continuous and no temperature increase could be observed.

Current-based torque measurement evaluated with a force-torque sensor

After the observation of the open-loop response, the current sensor is used to close the loop. This means that the PWM value is adapted by a PID controller depending

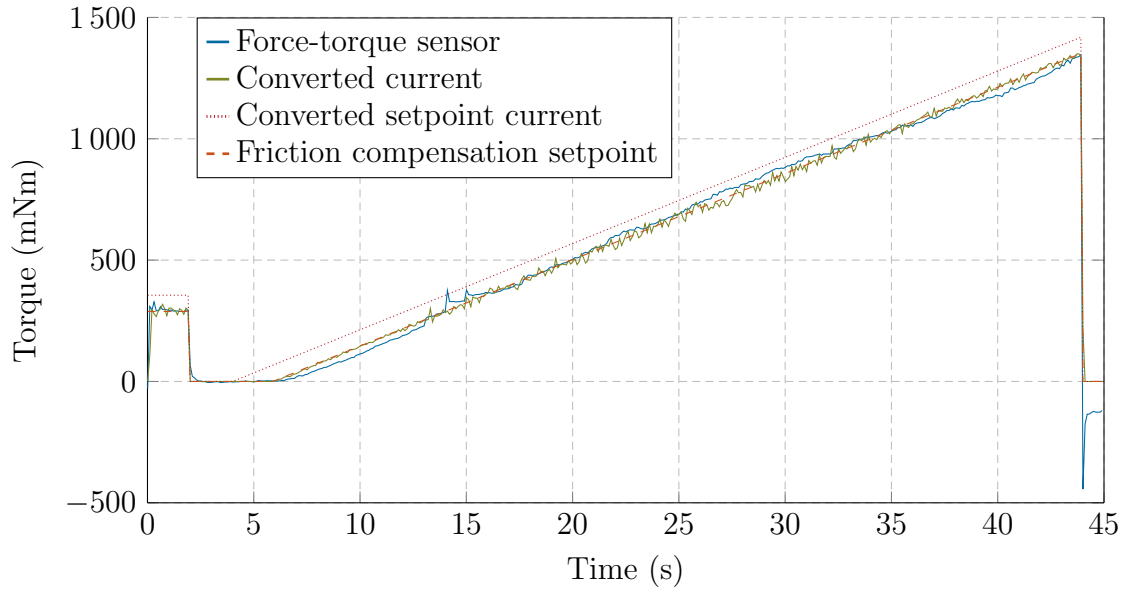


Figure 7.6: Comparison of force-torque to current measurements including the setpoint trajectory with and without regarding the static friction. All currents are converted with the torque constant determined by the force-torque test [194] © ICST

on the difference between the setpoint current and the actual current. A controller with integral behavior ($K_I = 1.7 \cdot T$) and a sample rate of $T = 10$ ms is used.

The experiment assesses the accuracy of the control of the current measurement-based torque estimation by comparing it to FT sensor measurements. The sensor is aligned with m·ReS^{R2} and the chuck is fastened so that the torque is transmitted. A current profile is applied on the end-effector and the estimated torque is compared to the measured one with the FT sensor. The experimental setup is similar to Fig. 7.1 except for using m·ReS^{R2}.

The current profile includes a step from zero to 1000 mA at the beginning and a drop from 4000 mA to zero at the end of the sampling period. These two prominent points are used for synchronization and scaling of the two sensors, which return samples with constant but different frequencies. Attaching the FT sensor to the device and the initial current increase influences the torque measurements. Therefore, the baseline is shifted to the average of the torque measurements after the initial step and before the setpoint current increases. The results are plotted in Fig. 7.6.

The dotted line represents the setpoint current according to the profile, which is converted into torque in order to compare it to the FT measurements. The conversion follows the motor's torque constant, which has been determined in this experiment.

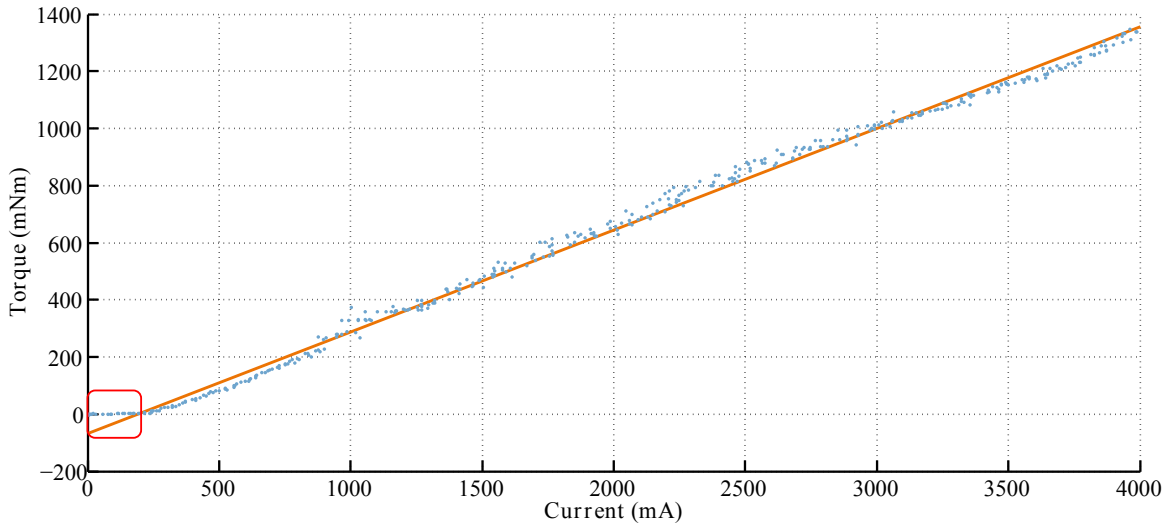


Figure 7.7: Current measurements plotted against the force-torque sensor samples without compensation of friction effects. The red box indicates where the torque does not rise with the current.

Static friction compensation The measurements in Fig. 7.6 reveal an increase of current without effect on the FT sensor at the beginning of the slope. Whereas in Fig. 7.6 the converted current and torque measurements are plotted against the time, a representation of plotting them against each other clarifies this issue. Figure 7.7 shows clearly that the torque does not rise with the current in the lower regions below 200 mA (red square) although a linear relation over the whole range is expected.

This observation indicates a disturbance in the conversion, which is typically caused by influences of the gear mostly due to friction. A slight movement is necessary to overcome backlash so that the cogs mesh with each other in order to transmit torque. Overcoming the torque to start a movement is impeded by static friction. We deem this responsible to most parts for the gap between current input and torque output.

One method to determine the static friction is to increase the current until movement occurs [132, 198]. We carried out this experiment by increasing the current setpoint in steps of 1 mA, with 30 passes per step before the setpoint is increased, until a movement occurs (encoder measurement $\neq 0$). Passing each step several times slows down the rise and prevents fast controller jumps and jerky movements that distort the result. The analog-to-digital converter (ADC) measurements of the current sensor are averaged over three samples but apart from that no filters are applied. If movement occurs, the current is stored and the procedure is repeated. After 100 runs, the measured threshold currents were averaged, which resulted in a breakaway current of 120 mA.

Ideally, this current determines threshold between a stalling and a continuously running motor. However, this result is an average and the boxplots in Fig. 7.8 show

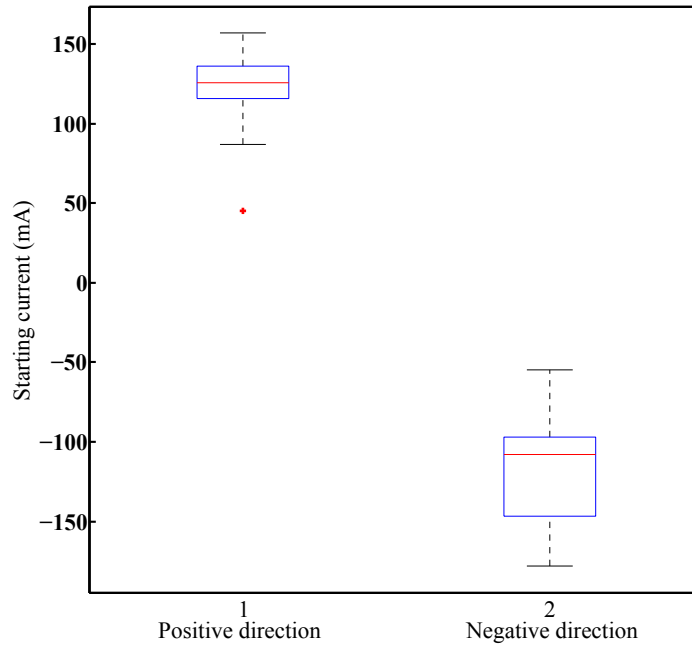


Figure 7.8: Boxplot of the static friction experiment with the starting current of 100 runs in positive (1) and negative (2) direction

that the threshold is fuzzy. Applying 120 mA on the motor does not result in a continuous movement of the motor. The reason is that small movements within the backlash of the gear require lower torques than continuous motion. The minimum detectable change of motion results in an underestimating threshold current. This raises the question where to set the optimal angle or speed threshold. Inherently, not one single true answer can be given, which is why we use the FT measurements (Fig. 7.6) to get a better estimate.

To compensate for this effect in the conversion, we iteratively approximated a relation between the measured current and the torque from the force/torque sensor. According to the assumption of a static friction model, we defined a constant i_f , below which, the torque estimation is defined to be zero. After overcoming the static friction, the torque rises fairly linear with the current. Therefore, we deem a linear model sufficient, which corresponds to the physical relation between current and torque. The model is used to convert the current measurements to a torque estimation with the following equation

$$\tau_{\text{FT}}(i) = \begin{cases} k_{\text{MFT}} (i - i_f) \cdot R_G \cdot \eta & i > i_f \\ 0 & i \leq i_f \end{cases}, \quad (7.1)$$

where τ_{FT} is the estimated torque, i is the measured current, k_{MFT} the torque constant based on the FT measurements, i_f is the constant threshold current, R_G the gear ratio, and η the efficiency factor.

i_f lies at the intersection between the abscissa and the linearly increasing part in Fig. 7.7. To determine it, we iteratively increase the static friction and crop the points below the threshold current measurements. Then, a line

$$\tau_{\text{temp}}(i) = k_{M_{\text{temp}}} \cdot R_G \cdot \eta (i - i_f) + b \quad (7.2)$$

is fitted onto the data starting from $i = i_f$. Then, i_f is increased and the fitting repeated until $b \approx 0$. The converted torque from currents below the threshold i_f are set to 0 mNm. The static friction was determined to be 188 mA or 67 mNm, respectively. The slope of the line represents the torque constant including to the reduction gear ratio of 7:1 and the efficiency of the gear of 0.9. Inserting these parameters into Eq. (7.2) and solving for the torque constant results in $k_{M_{FT}} = 56.41$.

We measured a root-mean-square error of 25.78 mNm for the model applied to the fitted current profile of Fig. 7.6. Tested on a second run, the error was only slightly higher with 30.08 mNm.

Discussion m·ReS^{R2} The usual method to determine the static friction torque, by increasing the current until movement occurs, results in a lower threshold current. We expect this to be influenced by the encoder's high sensitivity in conjunction with the gear's backlash. Since the application of the higher threshold current onto the motor does not lead to unwanted continuous movement, the higher value is valid. It can now be utilized to decrease the initial user induced torque and improve the accuracy of the torque estimation.

The measured torque constant $k_{M_{FT}}$ lies between the quotient of the starting current and the stall torque of 52.75 mNm A^{-1} and the torque constant $k_{M_{DS}} = 64 \text{ mNm A}^{-1}$ both taken from the data sheet. The difference can be explained with the gear efficiency and the torque constant both depending on the working point. This means that the parameters from the data sheet can be used as a good estimate but the FT measurement allows to regard gear effects and to tune the accuracy.

7.1.2.3 Discussion of torque measurement and control evaluation

Comparing the RMSE of the experiments between m·ReS^{R1} (between 2 % and 4.133 % over $\pm 1.5 \text{ Nm}$ range) and m·ReS^{R2} (2.15 % over 1.4 Nm range) does not exhibit tremendous improvements. However, due to limitations of m·ReS^{R1} in the experimental design, manual torque exertion was used. Inherently, the torques are not equally distributed over the torque range. More measurement points are found around lower torques that show lower variances biasing the result towards lower RMSE. m·ReS^{R2} shows a more objective experimental setup with a static rise over the whole torque range. Comparing Fig. 7.4 and 7.6 reveals on first sight that the variance is strongly increased for higher torques in the case of m·ReS^{R1} whereas m·ReS^{R2} shows comparably low variance around the setpoint over the whole torque range. This underlines that the torque measurement has been significantly improved. Furthermore, torque

control has been implemented, which did not only improve the quality of the evaluation but also extends the use of the system for rehabilitation exercises.

As expected, the accuracies of both iterations of m·ReS^R are around one order of magnitude below force-torque sensor accuracy. However, prices of suitable commercial sensors alone start from €6000 and the bulky sensor has to be integrated into the design counteracting portability. m·ReS^{R1} and m·ReS^{R2}, have both a total material cost of under €1000, justifying the lower accuracy for the intended application.

7.1.3 Preliminary study on the just noticeable difference with m·ReS^{R1}

This preliminary study demonstrates how the system can be applied for studying rehabilitation paradigms. It determines the just noticeable difference (JND) of healthy subjects with m·ReS^{R1}. More studies including stroke patients are intended to be carried out by the cooperating neurologists.

The JND is the amount of increase between two stimuli to reliably distinguish them. It is defined as the percentage of distortion, where 75 % of the trials have been correctly discriminated [145]. Like described in Section 2.3.3.3 the JND has been determined for finger movement and force in a rehabilitation context [18]. We use m·ReS^{R1} to determine the JND for range of motion and for torque of the supination / pronation motion with 13 healthy participants aged between 19 and 31. The parameters of the experiment are kept close to experiments by Matsouka et al. for a better comparison of the results [123]. The study was conducted as part of a bachelor thesis [190], however, the data analysis was amended.

7.1.3.1 Setup and precondition

The setup consists of three basic components: m·ReS^{R1}, a screen for visualizing sensor data and a keyboard for the subjects to give feedback. m·ReS^{R1}'s motor is oriented horizontally to study the JND on supination / pronation. The handle's initial position at the beginning of each trial is parallel to the work surface. The robot stands under a visual cover on a table facing to the edge, which is around 45 cm away from the robot's base. The cover occludes the wrist, reducing a visual bias from observing the handle's position directly. This position is sufficient to keep the study participants' elbows on the table while grasping the handle of the robot with the hand. The screen shows a bar giving feedback about the torque and position level. It consists of three squares showing whether the level is below (left square), within (middle) or above (right) the designated range (Fig. 6.5a). It is kept simple to reduce distractions from the task that could influence the JND.

In the study, the subjects have to keep the position or torque level over a period of time. A tolerance window has to be defined so that human imprecision and noise do not impede the process of remaining at the designated level. However, an increase of

the tolerance interval makes the determination of the JND more inaccurate. Based on measurements of the accuracy of the device, we set the tolerance to $\pm 4\%$. The noise has a stronger relative influence for lower torques. Therefore, also an absolute minimum tolerance interval of 8 mN m was introduced. The tolerance for the position runs is set to $\pm 4\%$ as well.

The base torque and position varies over the trials. The maximum levels for range of motion and torque have to be limited to stay within the range of human capabilities. Furthermore, the accuracy of the torque measurement has to be regarded which depends on the exerted torque. The limits for the torque trials are set to 100 mN m and 1075 mN m, respectively, to stay within a range with an acceptable accuracy. In an experiment with a constant weight attached to the motor, over 95 % of the samples lay within the tolerance interval. To improve torque measurement accuracy, a variable-length moving average filter has been implemented, which is described in [190].

The range of motion has to be limited so that the anatomical limits are not exceeded. The limit is defined by the maximum target position together with the maximum distortion, which has been set to 55 % before. From the semi-pronated pose the anatomical limits are above 90° [171]. Therefore, we define the maximum target position to 50° leading to a maximum distorted target position $\theta_{d,max} = 50^\circ * 1.55 = 77.5^\circ$ and, thus, under the anatomical limits. The minimum angular position is set to 10° so that the difference in angle after the lowest distortion of 10 % is over the maximum inaccuracy of the gear due to backlash of 1° .

7.1.3.2 Procedure

For determining the JND, the participants of the study carried out two experiments for position and for torque each consisting of 100 runs with two samplings each. The first target is the reference torque, which serves as a comparison value. The second sampling was either the same target value or was increased by 10 %, 25 %, 30 %, 40 %, or 55 %. Each of the distortion factors was applied 10 times and the remaining 50 runs were undistorted. The program allocated the order pseudo-randomly. When the subject reaches the designated position or torque, the program highlights the middle square on the screen. After staying within the tolerance range for 2 seconds, a pop-up indicates that the measurements can be terminated by pressing the space key. This ensures that the subject perceives the position or torque with a sufficient amount of time. It was permitted and encouraged to take more time. After the first measurement, the second one is initiated and thereafter a dialog box prompts to enter whether the subject thinks both samplings were similar or not and to state the level of the confidence ranging from 1 to 5. A rating of 1 means that the subject was completely unsure, whereas a rating of 5 means absolutely sure about the guess. If the subject was not able to constantly stay in the position or torque range, the investigator can instruct to skip the trial. It is then excluded from the evaluation.

The position JND is the percentage of difference in angle due to distortion that is reliably determinable. The user moves the end-effector from the semi-pronated base position to two target positions. The first one is the reference and the second one is either distorted or the reference position again. After each of both samplings the motor moves the end-effector back to the base position.

The torque JND is the difference between two torque levels that the subjects can reliably differentiate. It is determined in base position without change in angle. The position is controlled by the motor controller and the torque is determined by a mapping to the position control parameter.

During the runs, the program writes several parameters into a file. The basic information are the number of the run, starting time, distortion factor, and torque or position experiment, answer whether similar or distorted, and the confidence value. Additionally, the trajectory consisting of time and position is sampled with 32 Hz. It may provide more information about how the subject made a decision or which tactic they used. After the first as well as after the second sampling of the position experiment, the robot moves the end-effector back to the base position.

7.1.3.3 Results

The evaluation is based on correctly recognized distorted runs (correct-positive) and incorrectly identified undistorted runs (false-positive). Furthermore, only runs with a confidence level equally or higher than 3 are observed. This decreases the number of random guesses. The JND is calculated as the percentage increment in position or torque that led to a sensitivity index of 1, which occurs at 75 % correct discrimination [10]. For its computation, the ratio between correct-positive and false-positives to the total amount of guesses with a confidence level above 2 is plotted against the percentage of distortion d . To approximate the distortion in percent that was discriminated in 75 % of the runs, an exponential functions (according to [123]) is fitted to the results, where f states the percentage of answers claimed distorted for the relative angular position

$$f_{P,rel}(d) = 1700 - 1480 * e^{-\left(\frac{0.97*d}{100}\right)} \quad (7.3)$$

and, accordingly, the function for the relative torque

$$f_{T,rel}(d) = 7660 - 7648 * e^{-\left(\frac{0.01*d}{100}\right)}. \quad (7.4)$$

The relative distortion that could be reliably discriminated lies at the intersection between the fitted function and the horizontal 75 % line. We computed a JND for the angular position of 46.2 % and a torque JND of 56.3 %.

Based on the same data, we, furthermore, determine the absolute JNDs. First, the reference value is multiplied with the relative distortion. This results in a variety of different distortions. The data is then reorganized in a way such that the absolute distortion can be calculated as a ratio of recognized distorted to total number of

valid guesses. For this, the absolute results are grouped in intervals of 30 mN m or 5°, respectively. Accordingly, the absolute JNDs were determined. The exponential function for angular position is

$$f_{P,abs}(d) = 137 - 115 \cdot e^{-\left(\frac{4.88 \cdot d}{100}\right)} \quad (7.5)$$

and for torque:

$$f_{T,abs}(d) = 141 - 140 \cdot e^{-\left(\frac{0.47 \cdot d}{100}\right)} \quad (7.6)$$

The absolute JNDs for the angular position and the torque are 12.6° and 160 mN m, respectively. Plotted together with the standard deviation, the results of the relative torque and the absolute position are plotted in Fig. 7.9.

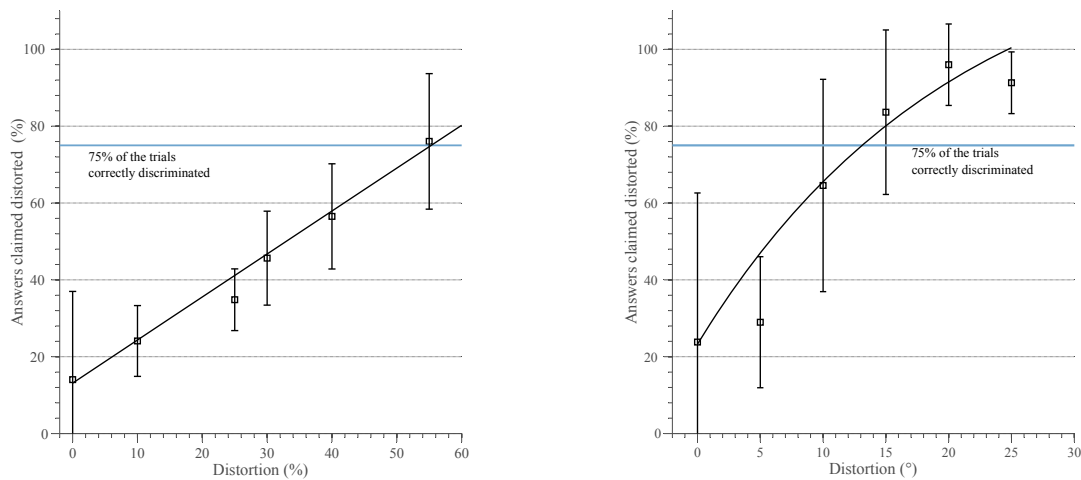
Additionally, the sampling time has been measured. The median is used to compare the times between the two samplings. The average is less suitable, since outliers caused by pauses within the sessions have a stronger influence. The average of the medians over all subjects of the time needed for the first sampling in torque mode is 9.6 s and for the second sampling is 6.9 s. The average for the first sampling in position mode is 11.6 s and for the second sampling is 10.8 s.

7.1.3.4 Discussion

As expected, the results for the relative JNDs show that the two stimuli could be discriminated more accurately for higher distortions. The obtained JNDs have a comparable magnitude but are higher than the results of Brewer et al. 2008, who computed a force JND for young unimpaired subjects of 19.7% for the flexion of the index finger in the metacarpophalangeal joint [18]. Two differences in the study setup may explain the deviation in the results. First, different movements exerted by different muscles were observed. Finger flexion is expected to be more accurate in comparison to supination and pronation which are executed by muscles of the forearm. Additionally, position and torque are studied independently from each other whereas Matsuoka et al. had a combined movement by applying linearly increasing force with the deviation using a haptic device. Furthermore, the tolerance range influences the result and may be responsible for an increase.

The study has been designed for relative distortions. However, the absolute deviations also play a role. Therefore, a study dedicated to measure the absolute values would increase the amount of samples over the whole range of distortions and clarify the interpretations.

The experiment was intentionally kept simple to avoid distractions from the task. Rehabilitation games, more demanding tasks, sounds, and other diversions potentially increase the JND. Furthermore, the study participants were young healthy subjects aged between 19 and 31. Older and also impaired subjects have a higher threshold for discriminating stimuli [18]. Therefore, higher values can probably be used in a rehabilitation setup.



(a) Relative just noticeable difference of torque discrimination

(b) Absolute just noticeable difference of angular position discrimination

Figure 7.9: Distortion as a function of the percentage of the answers that claimed distorted.

The sampling period comparison showed that the participants took more time for the first sampling than for the second one. The first run gives an estimate of the target value, which helps to find the level around the base level faster in the subsequent runs.

7.1.4 Clinical study with the extension module for the TRI rehabilitation robot

The rehabilitation robot for shoulder and elbow-based exercises developed at the Toronto Rehabilitation Institute has been extended with a m-ReS^{R2}-based module for pronation/supination training (Section 4.7). The extension module is being tested in an in-depth case study involving stroke patients, therapists, and healthy participants. Mobility data, including position, velocity, and torque measurements, is sampled during the use of the extension module to draw comparisons between the performance of healthy participants and stroke survivors. During the session, stroke survivors and therapists who test the prototypes are encouraged to describe their opinion. After finishing the exercises, Likert scale questionnaires and semi-structured interviews are carried out. The gathered details about the participants' perceptions help to assess the usability and possibilities of improvements of the device, and provide paramount information for a user-centered design of further developments.

7.1.5 Application experience

The torque control can be applied in different exercises. We implemented a mode called virtual spring where the torque is linearly increased with the angular difference to a neutral position. Figure 7.10 shows a representative short session of a healthy subject in this mode. The data is sampled every 10 ms. The graph shows that the torque against the hand increases with the deviation of the angle from the neutral 0° position.

The passive mode is tested in four different runs: without a user (no external force on the handle), with a healthy subject whose hand is moved passively without working against the motor, and a stroke sufferer who tries to do the same. Furthermore, a session with the same stroke patient using the passive mode cube was carried out. In case of the sessions without the passive mode cube, the motor followed a sinusoidal trajectory with a frequency of 0.2 Hz and an amplitude ranging from -60° to 60° where 0° is the semi-pronated position. The trajectory is plotted together with the torque that indicates the amount of resistance introduced by the user. The plots are grouped in Fig. 7.11.

The plots exhibit that the controller achieves a smooth sinusoidal trajectory without abrupt movements, following the specified ROM and frequency. The torque measurements allow to draw conclusions about the resistance implied by the user. The first plot without external forces on the handle shows the lowest torque. Slightly higher torques can be observed in the second plot where the hand of the healthy subject is placed on the handle. The motor has to overcome the additional external forces in order to keep following the trajectory. The plot of the passive mode with a stroke patient shows the highest torques and asymmetric resistance between movements towards supination and towards pronation. This can be explained with spasticity, which is a symptom that commonly occurs after stroke. The increased muscle tone forces the hand towards a pronated position. Therefore, the motor has to overcome higher torques turning the hand into the supinated position, which is reflected in the plots. The same can be observed for the stroke sufferer using the bilateral passive mode cube. It can be seen that the torque peaks are not as high which corresponds to the lower angular displacements. The torque measurements during the passive modes demonstrate that they may be used to observe spasticity and estimate the degree of the impairment [194].

7.2 m·ReS^X

This section, first, evaluates the accuracy of using the cable-drive to estimate the angles of different joints of the exoskeleton. Then, the accuracies of the other kinds of angle sensors are assessed with some assessments being based on a comparison to the first method. Then, a performance evaluation of the force control is evaluated

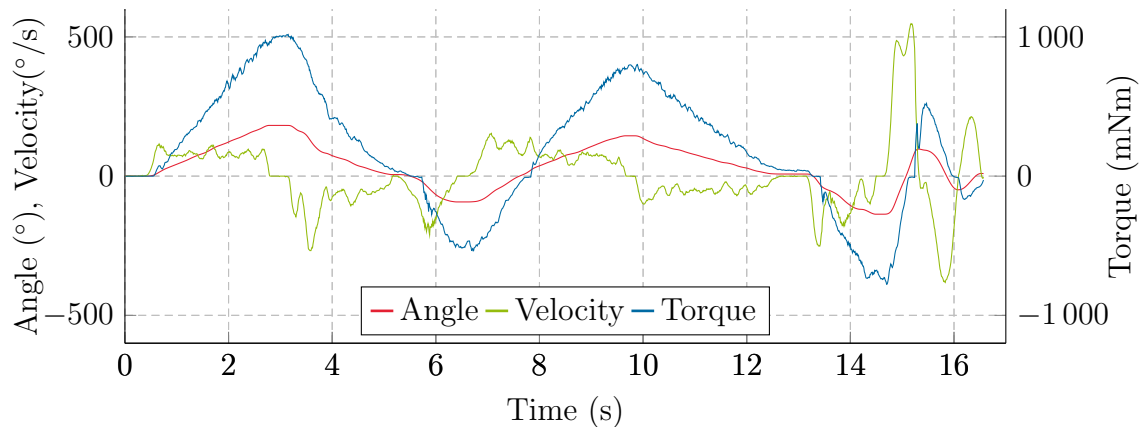


Figure 7.10: Representative short session in virtual spring mode. [194] ©ACM

followed by an assessment of the parametrization and a qualitative analysis of the application experience.

7.2.1 Tendon displacement measurements for angle estimation

The actuators of m·ReS^X rotate winders, which pull cables that are attached to the fingers. Although the primary function is to exert forces onto the fingers, the motor encoder can be used as an additional sensor. In this section, the accuracy of the method, presented in Section 5.5.3 shall be evaluated. It also forms the basis for the evaluation of other sensors.

7.2.1.1 Comparison of the model to manual angle measurements

First, the validity of the model has to be determined. For this, we manually adjust the exoskeleton to different angles and compare this reference to the angles computed from the tendon displacement based on our model. The single joints of the exoskeleton are set to angles in 10° steps with the help of a pattern with angles sketched in (Fig. 7.12). The joint to be assessed remains movable while the other two joints are blocked. After the joint was positioned, the corresponding encoder values were sampled for each 10° step. Since the relation between tendon displacement over a joint and angle is solvable for one joint, the relation between the values can be compared. The results are plotted in Fig. 7.13.

The RMS error between metacarpophalangeal (MCP), proximal interphalangeal (PIP), and distal interphalangeal (DIP) joint angle measurements and the converted tendon length displacement is $RMSE_{MCP} = 0.22$ mm, $RMSE_{PIP} = 0.962$ mm, and $RMSE_{DIP} = 0.5482$ mm, respectively. The results demonstrate the functioning of the method and the implemented model.

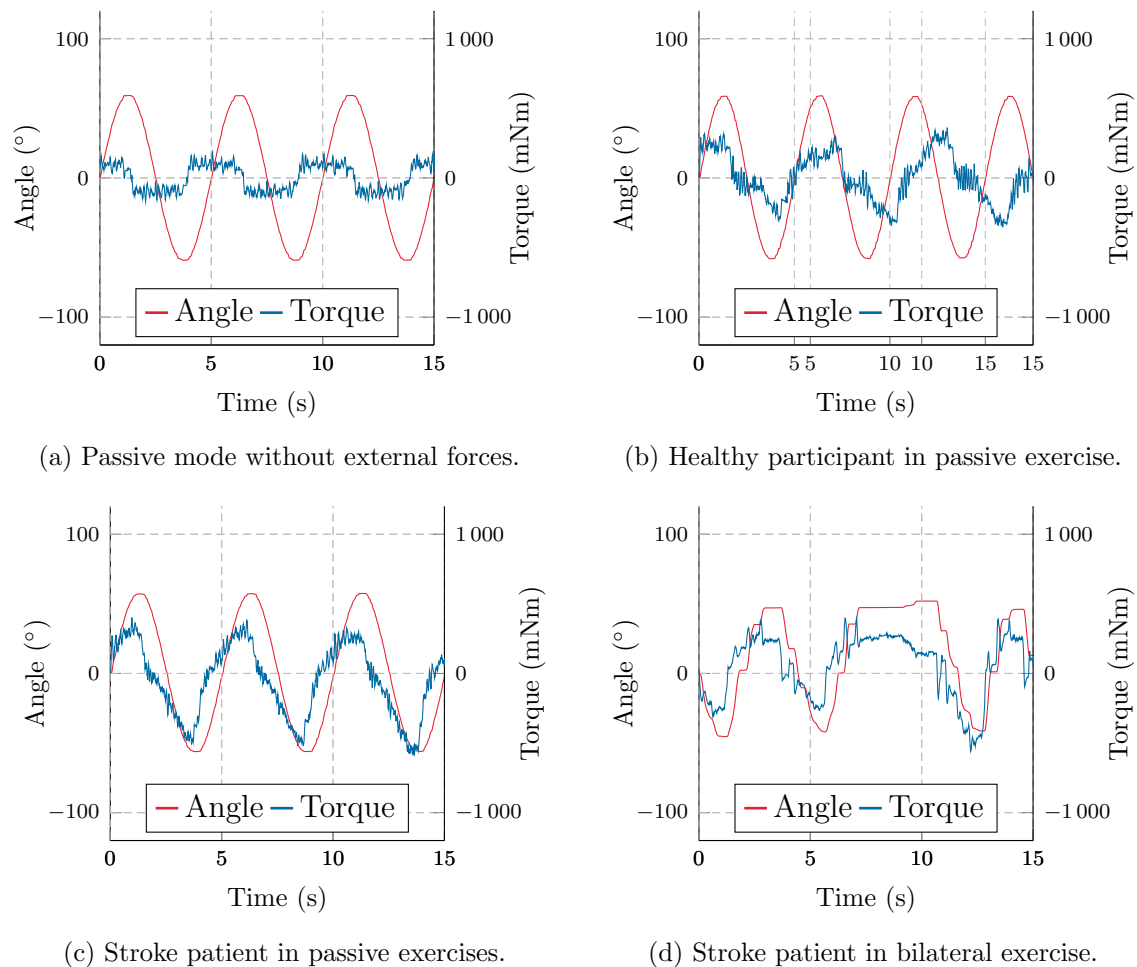


Figure 7.11: Automatic passive mode and bilateral exercise using the passive mode cube [195] ©Springer

7.2.1.2 Influence of lateral shifts of joints

The following simulation observes the extend to which inaccuracies in the manufacturing influence the comparison between angle and motor encoder measurements. The Denavit-Hartenberg parameters (Section 5.5.3) are based on rotations around the joints' centers of motions taken from the CAD model of $m\text{-ReS}^{X1}$. However, due to the manufacturing process, a lateral shift of the joint can occur. $m\text{-ReS}^{X1}$ is 3D printed in one piece which requires a gap in the joint so that the rotating parts do not melt together. For the used printer, the gap distance has to be higher than 0.3 mm. This gap results in errors in the computation of the cable length. Therefore, the following simulation compares the tendon displacement length with ideal conditions and a shift in the joint.

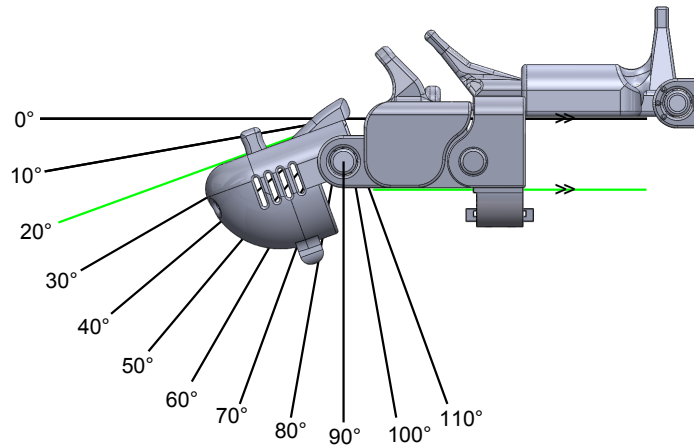


Figure 7.12: Angle pattern

Since in use the tendon is under tension, we expect a shift in the same direction towards the base. Therefore, this simulation computes the difference in cable-length between the ideal concentric and shifted coordinates of 0.3 mm in negative y_0 , positive y_2 and negative x_3 direction (Fig. 7.15). The difference is calculated for each angle and plotted in Fig. 7.14. The initial error (0.17 mm) for $\theta_{MCP,PIP,DIP} = 0^\circ$ is set to zero since only the relative deviation from the starting position is relevant.

The graph shows that the gap shift can increase as well as decrease the tendon displacement depending on the joint angle. The maximum combined error over the three joint angles is 0.1 mm. Depending on the combination of angles, the shortening and extension of the displacement cancels each other out, which is why the error is expected to stay well below the maximum deviation. Therefore, the gap shift will not be regarded in the following experiments.

7.2.1.3 Discussion of tendon displacement based angle estimation

The application of the Denavit-Hartenberg convention establishes the relation between a measured tendon length difference and the corresponding joint angle.

To evaluate the validity, the computed angles have to be compared to ground truth. The comparison with the angle measurements based on the pattern is not without errors due to the manual alignment process. Still, the correlation indicates the validity of the model. The manual measurements coincide to a high degree with the model. Especially DIP and MCP are well-aligned whereas slight deviations exist for the PIP joint.

The gap shift simulation underlines the validity of disregarding the gap shift in the joint. The additional input provided by the motor encoder can be used in various ways. It allows to replace one angle sensor or to give a combined measurement over

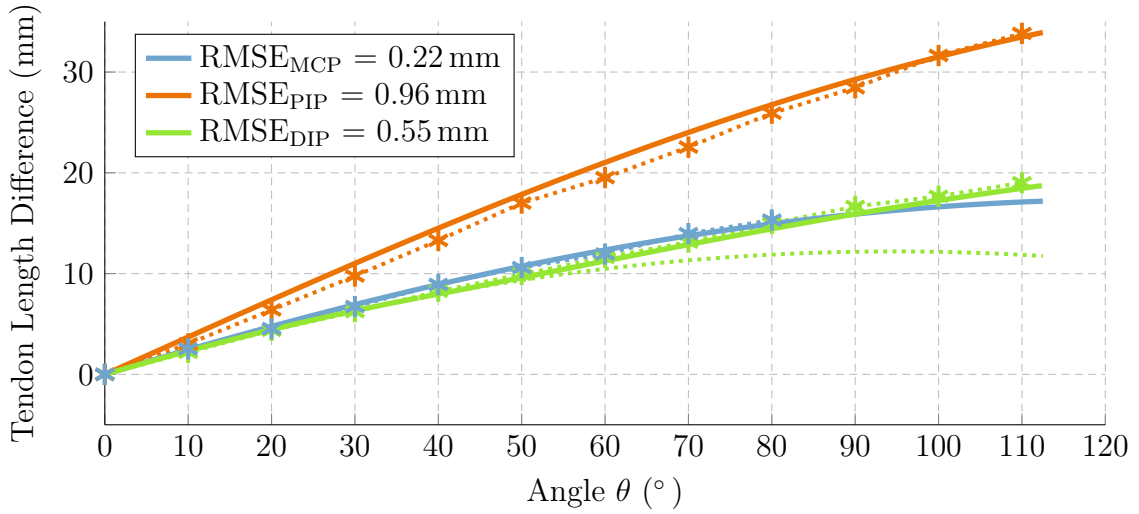


Figure 7.13: Measurements (dotted lines) of DIP (green), PIP (red) and MCP (blue) aligned to a pattern with 10° steps are compared to computed angles based on motor encoder measurements (solid lines)

two or three joints. Moreover, it can be used for assessing the accuracy of angle sensors, which will be applied in the following sections.

7.2.2 Finger joint angle measurement accuracy using Hall effect based sensor

The Hall effect based sensor method works by measuring the magnetic field of a diametrically magnetized magnet in the joint (Section 5.5.1). In this section the accuracy is tested, first, with a goniometer for $m\text{-ReS}^{X1}$ and then with the above described method based on tendon displacement for $m\text{-ReS}^{X2}$.

7.2.2.1 $m\text{-ReS}^{X1}$ angle sensors evaluated with goniometer

$m\text{-ReS}^{X1}$ was adjusted to different orientations using a goniometer. The output of the implemented angle estimation algorithm, based on the Hall effect sensor, was measured. For this experiment only the proximal joint of the PIP joint was observed using a goniometer to adjust different angles. The joint offers more space on the connecting links to apply the goniometer. Due to the flat planes on the top side of each joint, the adjustment process seems to be exact, which is why we consider it as an accurate comparison value. Slight force was applied on the tendon in order to simulate realistic application conditions. The manufacturing process required gaps in the joint of 0.3 mm, which were reduced using heat shrink tubings with a wall thickness of 0.25 mm.

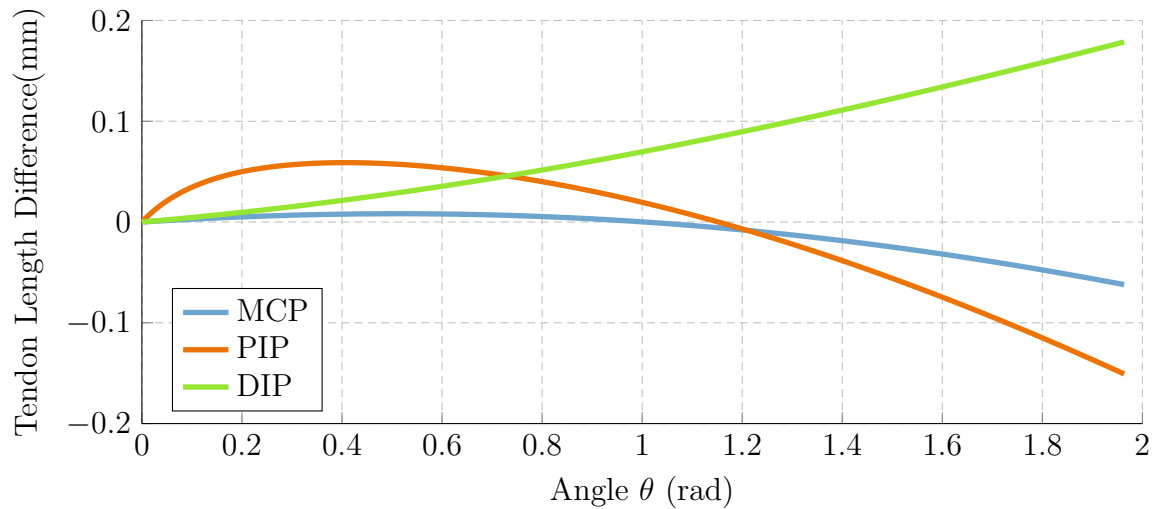


Figure 7.14: Tendon length deviation between ideal and shifted coordinates (each joint axis 0.3 mm towards the base) for each joint angle of the index finger of m·ReS^{X1} with the initial error (0.17 mm) for $\theta_{MCP,PIP,DIP} = 0^\circ$ set to zero

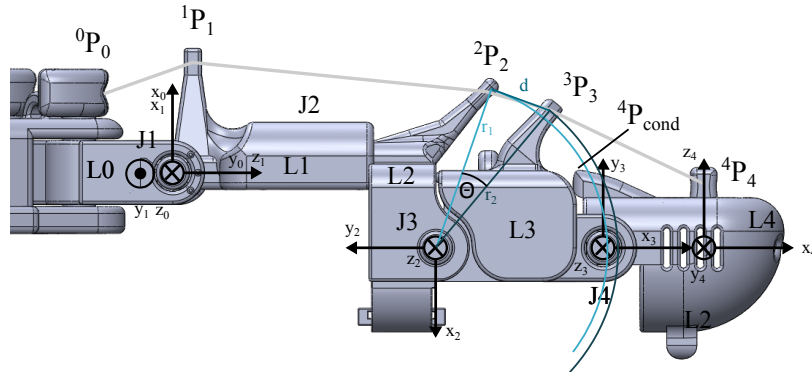
Angles from 0° to 90° in steps of 22.5° were adjusted by using the goniometer. For each step, the computed angle from the microcontroller based on the Hall effect sensors were sampled a 100 times and averaged. This was repeated ten times for each angle, re-adjusting the goniometer for each measurement. The results are shown in table 7.1. The RMSE is 1.57° with a standard deviation (SD) of 0.58° .

Table 7.1: Angle measurement accuracy

Goniometer ($^\circ$)	0	22.5	45	67.5	90
Microcontroller ($^\circ$)	-0.28	19.64	44.12	69.26	90.47
Mean Error ($^\circ$)	-0.28	-2.86	-0.88	1.76	0.47
SD ($^\circ$)	0.2150	0.7970	0.4472	1.047	0.4146
Root mean square error: 1.57°					
Average standard deviation: 0.5842°					

Table 7.2: Hall effect based sensor evaluated with goniometer

To confirm the results, further measurements were conducted by another subject with one run of each joint of the fingers (4 runs DIP, 4 runs PIP, 4 runs MCP). The

Figure 7.15: Definition of coordinate systems of $m\cdot\text{ReS}^{\text{X1}}$

RMS errors were 1.22° for the four DIP joints, 1.73° for the PIP joints and 2.03° for the MCP joint resulting in a total RSME of 1.69° .

7.2.2.2 $m\cdot\text{ReS}^{\text{X2}}$ angle sensors evaluated with image-based angle comparison

The exoskeleton's links in $m\cdot\text{ReS}^{\text{X2}}$ are printed as separate parts allowing for lower tolerances in the joints. Furthermore, cylinder-shaped magnets are used that facilitate assembly. This section describes the experiment to assess the accuracy of the Hall-effect based angle sensors in $m\cdot\text{ReS}^{\text{X2}}$. Since the goniometer cannot be applied well at the new shape of $m\cdot\text{ReS}^{\text{X2}}$, an image-based approach was used. The experiments using this method were conducted as part of a bachelor thesis [134]. A camera was pointed onto the joint such that the image plane is normal to the joint axis. Then, the joint of the index finger's PIP joint was adjusted to 31 different angles ranging from 0° to $\approx 160^\circ$. For each angle, an image was taken and 100 Hall effect-based angle measurements were sampled by the microcontroller.

The angle is manually determined in the images after importing them into Solidworks drawings. Two lines are drawn into the image over straight, clearly visible structures of the two parts that are connected by the joint. In the next step, the angle between these lines can get calculated by Solidworks (Fig. 7.16). The samples of each angle from the microcontroller are averaged and compared to the manually determined angles.

The Hall effect measurements are plotted against the image-based angles (Fig. 7.17). The ideal curve with a slope of 1 is represented by the yellow line. For higher angles, the minimum of the Hall sensor voltage sine curve is passed so that ambiguous Hall sensor-based voltages occur (compare Fig. 5.12). The threshold angle, calculated from the calibration, is drawn into the plot (blue solid line) demonstrating that it fits to the measurements. Since the ambiguous range lies beneath the maximum angle of the anatomical PIP joint [171](green dashed line), the deviations are not relevant in

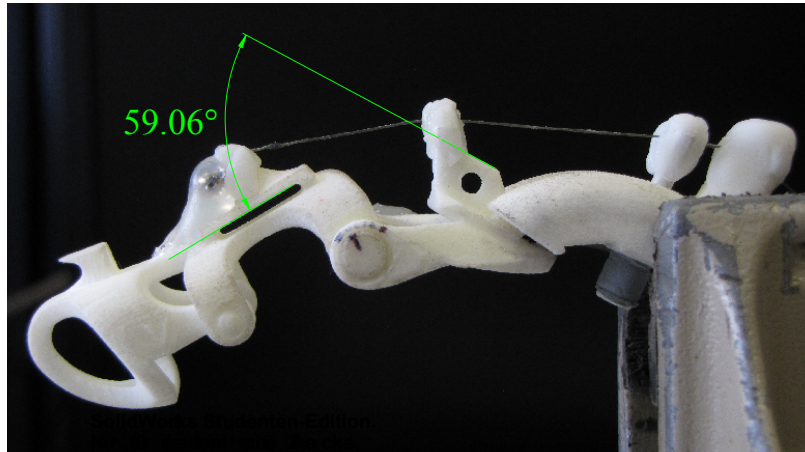


Figure 7.16: Evaluation of the Hall effect angle sensor with an image-based comparison

application. Two RMS errors are calculated. Over the unambiguous range a RMSE of 2.286° was found, and over the relevant range of the DIP joint a RMSE of 1.87° . Errorbars with their associated standard deviation are drawn into Fig. 7.17 but they are in most cases too small to be visible. To quantify the variance over the 100 samples, the SD for each angle is averaged resulting in $SD_{\text{avg}} = 0.67^\circ$.

7.2.2.3 Discussion

The Hall-effect sensor measurements of the DIP joint showed promising results with a low RMS error of 1.57° . The experiment was extended to the other joint angles measured by another subject confirming the former measurements. The higher RMSE of the MCP is strongly influenced by an outlier of 7.75° deviation. This was probably caused by the lateral shifts in the joints.

The joint had to be centered with a tubing to close gaps caused by the manufacturing process. Without the centering, the gap permits lateral shifts disturbing the magnetic field measurements and leading to high errors in double-digit range. Moreover, it was statically measured and the results are, therefore, considered as ideal. Movements may cause the error to increase. Therefore, these good results can only be achieved under ideal experimental conditions.

The application of the goniometer is prone to errors. Whereas the DIP joint of the outer finger in the first trial can be easily reached, the other joints in the second experiment offered less contact surface and lower reachability impeding the application of the goniometer at the other joints. Therefore, the image-based method has been introduced to assess the Hall effect sensor with cylinder-shaped magnets in m·ReS^{X2}. Problems in setting specific angles were avoided since arbitrary angles can be used for comparison. Thus, this method is expected to get closest to ground truth. The RMSE of 1.87° lies within the same region as the former results indicating the valid-

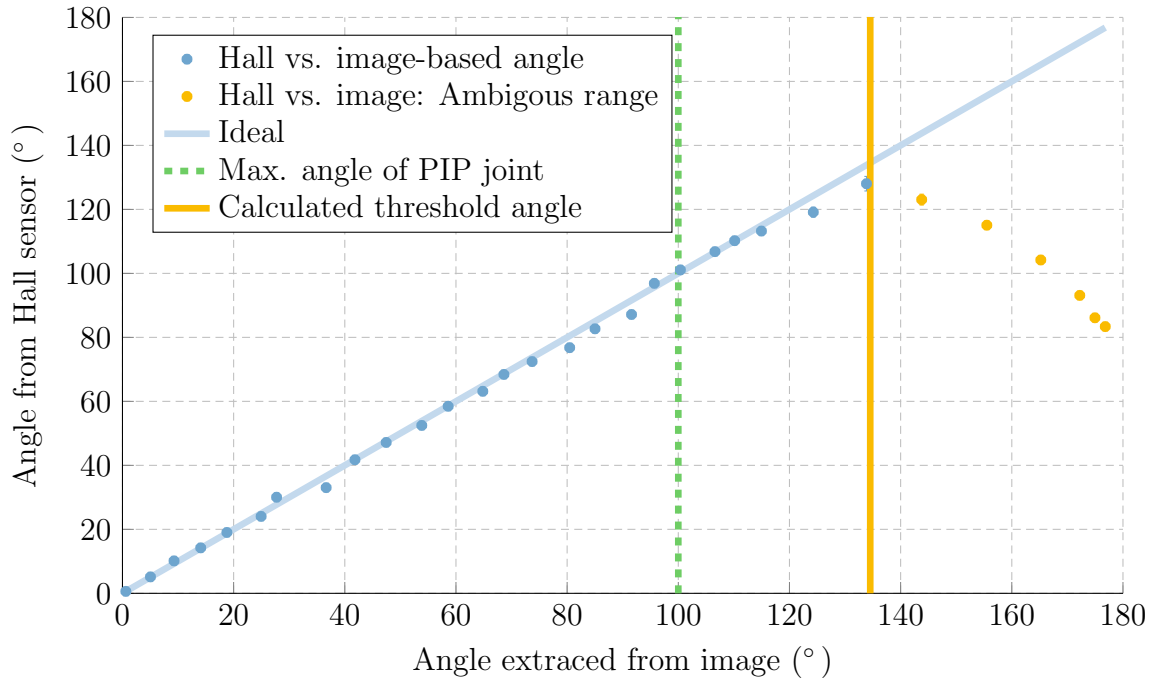


Figure 7.17: Comparison of Hall effect to image-based angle measurements

ity of the other methods. Although the results appear to not have improved, the big advance is that no outliers due to lateral shifts occur and that this accuracy can be achieved in application without the need for a tubing.

7.2.3 MCP joint angle measurement accuracy using a multi-pole magnetic strip encoder

The MCP joint of m·ReS^{X2} uses an arc-shaped joint so that the axis of rotation coincides with the anatomical one. This requires to use another kind of sensors: a multi-pole magnetic strip encoder.

7.2.3.1 Experimental setup and results

The evaluation of the accuracy is based on a comparison to the method presented in Section 7.2.1. The converted measurement of the cable-drive displacement with the motor encoder is a reliable means to evaluate the angle measurement accuracy given that the radii of the guiding points can be accurately determined, and that the starting and end position are consistent and not disturbed by mechanical effects.

A finger of the exoskeleton is fixed in a bench vise and the tendon is connected to a motor fixed in a second vise keeping the distance between them constant. The DIP and PIP joints are fixed in a fully extended pose such that only the MCP joint

	Plotted run (Fig. 7.18)		Avg. over four runs	
	RMSE (°)	Max. Error (°)	RMSE (°)	Max. Error (°)
Linear	1.89	3.11	1.8	3.24
Trigonometric	1.36	2.81	1.38	2.98

Table 7.3: Root-mean square error (RMSE) and maximum error of the angular accuracy experiment.

remains movable. At the beginning of the experiment, the MCP is fully flexed. Then, the motor pulls at the cable while sampling the motor encoder and the AS5306 simultaneously until the MCP is completely extended. Both sensors are of incremental type and set to zero at the beginning of the experiment so that the comparison gives the relative angular accuracy. The experiment was repeated four times.

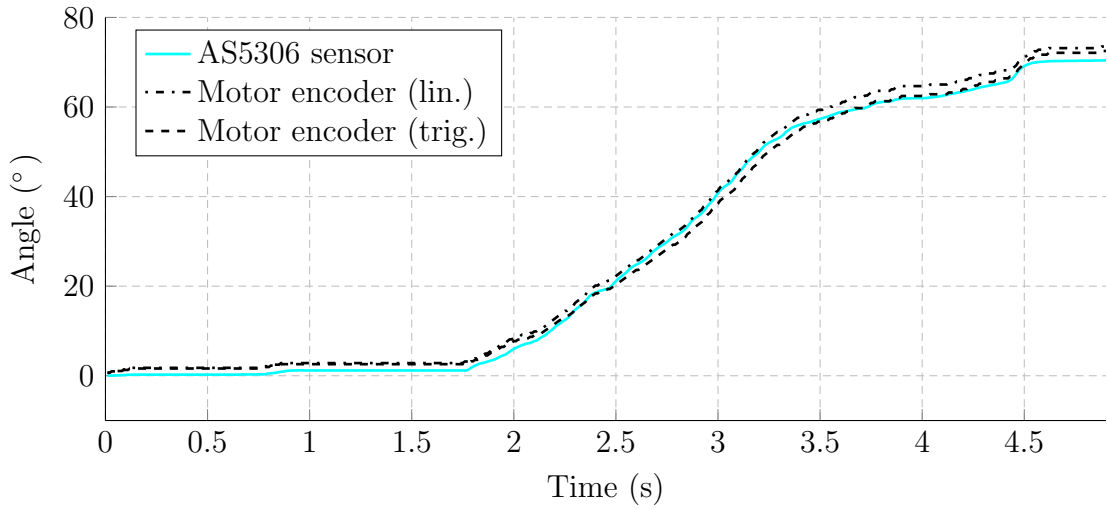
Given that only one joint is moved, the angle can be calculated from the motor encoder values by two methods. Either the law of cosines can solve the relation between the tendon displacement, which is equal to the change of the distance d between the guiding points with the radii r_1 , r_2 and the joint angle θ (Fig. 7.15). The parameters are extracted from the CAD drawing. Or the calculation is based on the end positions of the joint and their respective tendon displacements in the form of motor encoder values. In between, the angle is linearly interpolated. The angle of the sensor is plotted against the converted angle from the motor encoder (Fig. 7.18).

The root-mean-square error (RMSE) and maximum error were computed for the linear and the trigonometric approach of the plotted run and averaged over all four runs (Table 7.3).

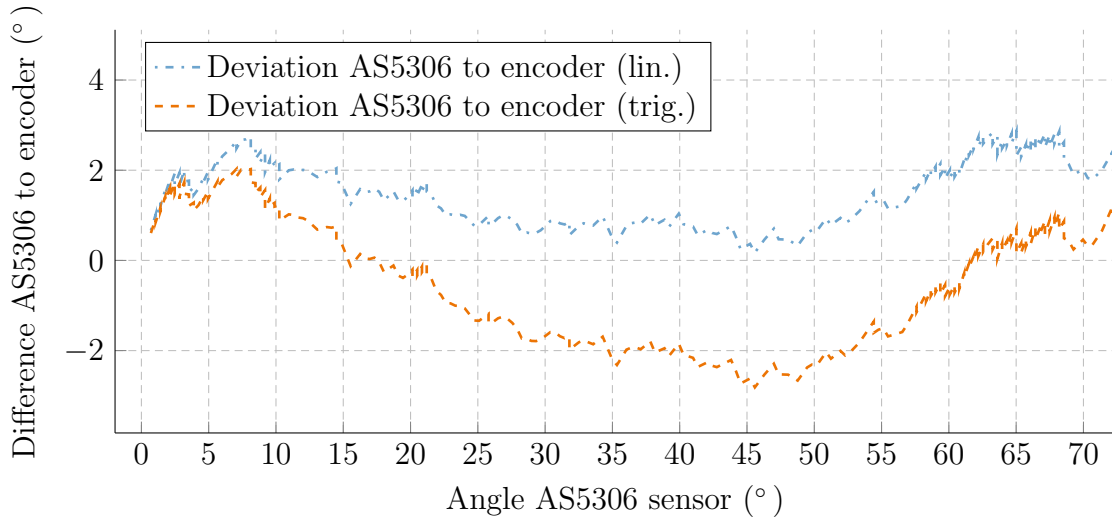
7.2.3.2 Discussion

The evaluation of the MCP angle sensor uses the method described in Section 7.2.1. Using the motor encoder allows for a faster sampling process than for, e.g., using a goniometer. More samples may give further insights on the accuracy of the angle estimation. Repeating the experiment resulted in comparable plots speaking for the validity of the method.

The winder radius has an influence on the estimated angle so that the change of diameter due to the winded cable can cause errors. Therefore, a second estimation with linear approach is included, which depends on the mechanical range of motion. Although the second approach is not without errors either, the source of errors is independent from the first method, which confirms the validity of the evaluation. It cannot clearly be determined, which way is the most accurate one, but the correlation between all three results speak for the functioning of the method and low errors in either case. This method only observes the relative angular accuracy. An absolute



(a) Angle as a function of the time



(b) Difference between the AS5306 sensor and each of the two methods of the angle estimation over the tendon length displacement measurement

Figure 7.18: Exemplary plot of one of four runs of the angular accuracy experiment assessing the MCP joint sensor

error occurs if the two output channels of the quadrature encoder cannot be sampled fast enough, or if the magnetic field of the magnetized strip is lost while the joint is moved. The first case is not expected to occur while the latter one might happen due to play in the joint that reduces the magnetic field.

The highest total RMSE of both calculation methods of 1.89° is well below the requirement of 5° (Section 3.4.3). This is a good result especially regarding the

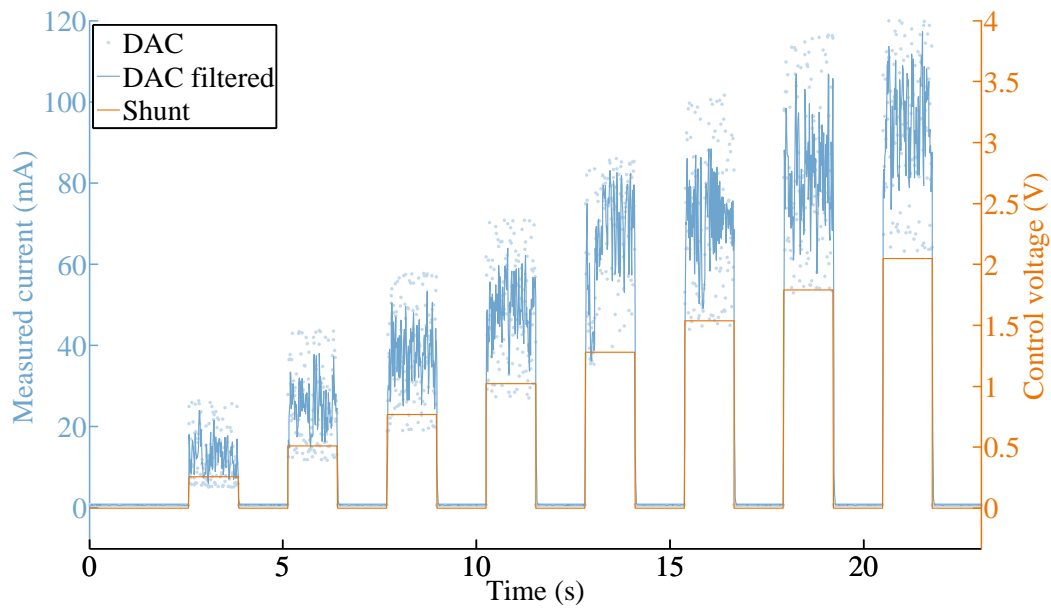


Figure 7.19: Step responses of a patented current limiter circuit

inexpensive hardware and the low manufacturing accuracy and strength of the 3D printing material. The results are better compared to an experiment where even a specialized goniometer for joint angle measurements of the finger achieved a standard error not below 3° [173].

7.2.4 Current Limiting for Force Control

Besides accurate angular measurements, it is required to control the forces that act on the fingers. The following experiments determine how accurate the force that acts on the fingers can be controlled. The experiments in this subsection were conducted as part of two Bachelor theses [64, 116].

7.2.4.1 Open-loop step responses

These experiments evaluate the step response of the output on sudden increases of the control signal. The results show the linearity and variance of the output response and whether the current can be limited with an open-loop approach.

Three circuits are observed:

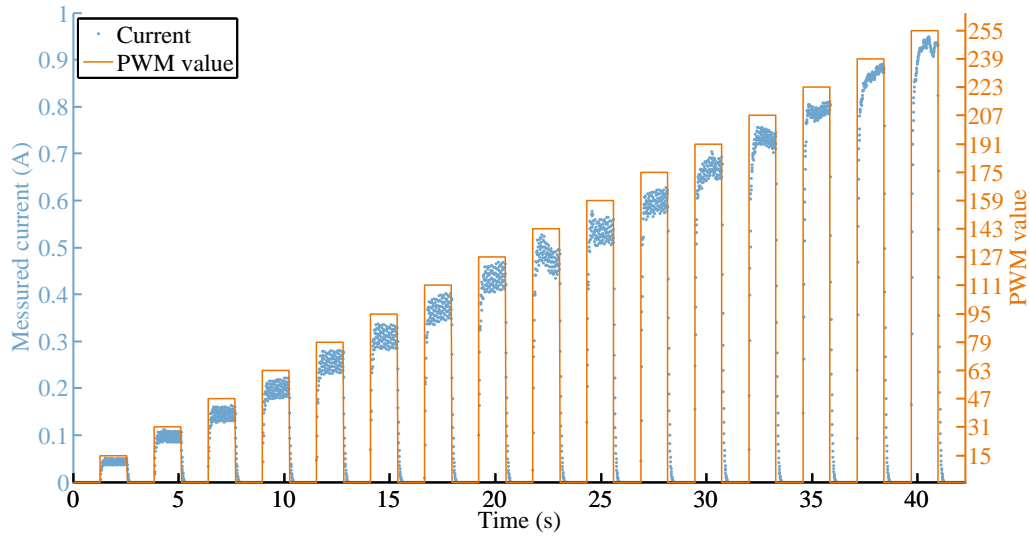


Figure 7.20: Step responses of pulse width modulation-based circuit

- An operational amplifier-based circuit that compares the DAC with the shunt voltage ([64, 192])
- An amplified PWM signal is applied on the motor (Fig. 5.17a) similar to $m\cdot\text{ReS}^{\text{R}2}$
- A simplified version of the first circuit (Fig. 5.17b) applied on $m\cdot\text{ReS}^{\text{X}2}$.

The first method is applied on $m\cdot\text{ReS}^{\text{X}1}$ and, therefore, a Faulhaber 2342 CR motor with 18 mNm and a gear ratio of 3,71:1 is used. The DAC control voltage determines the switching of two MOSFETs limiting the current through the motor. The motor shaft is fixed to mimic application in simplified force control without counter EMF. In contrast to the following circuits, no low-pass filter has been used. For better comparison, the current measurement has been processed with a first-order low-pass filter with a cut-off frequency of 14.6 Hz according to the RC network used for the PWM-based circuit. Then, 8 voltage steps in different heights are applied and the current is measured over a shunt of $0.5\ \Omega$. The measurement are plotted in Fig. 7.19.

The subsequent circuits were tested on $m\cdot\text{ReS}^{\text{X}2}$ with a Faulhaber 2657 CR motor. The PWM-based circuit incorporated an RC network with a cutoff frequency of 14.6 Hz and was supplied with 4 V. The samples were taken in 10 ms steps. The plot is shown in Fig. 7.20.

The same experiment was applied on the simplified DAC circuit. It uses a RC network with a cutoff frequency of 1.4 kHz. The results are shown in Fig. 7.21.

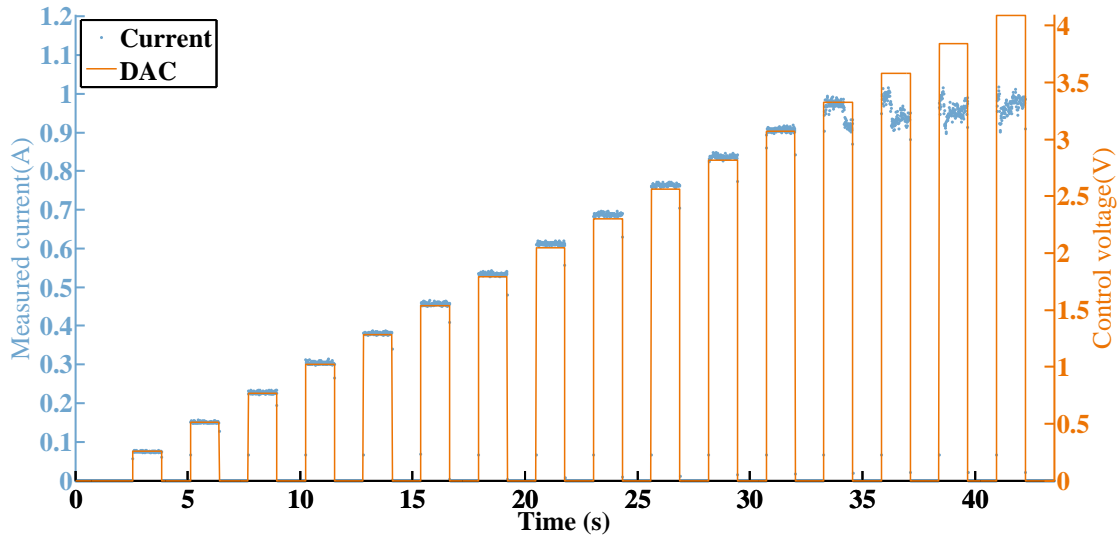


Figure 7.21: Step responses of the simplified DAC-controlled operational amplifier circuit

7.2.4.2 Force/torque sensor measurements

The following experiment examines the relation between the current measured by the ADC and the exerted force of the motor on a cable using the patent-derived circuit from m·ReS^{X1}. It allows for conclusions about the accuracy of the current-based force estimation and limiting by comparing the estimated value with force-torque sensor measurements.

A winder was mounted onto the motor, transforming the torque into a force with a lever arm of $r = 2.5$ mm. The tendon on the winder was connected to a force-torque sensor (ATI mini 45). The term "force" used in the evaluation is the Euclidean norm of the forces in x, y, and z-direction measured by the force/torque sensor (F in Fig. 7.22). 100 force measurements per step were sampled and averaged. The results can be seen in Fig. 7.23. They are compared to the motor's torque-current relation from the data sheet, which is converted into a force over the same lever arm of $r = 2.5$ mm.

The graph shows linear behavior with an RMSE of 0.5537 N to the best-fit line and only slightly worse RMSE of 0.5937 N in comparison to the converted torque constant's slope. The points in gray are not included in the error calculation since the maximum current has been reached and the force cannot further increase and follow the linear behavior. A maximum force of 22.5 N could be reached. Using a smaller winder radius of 1.5 mm, we achieved a maximum force of 36.1 N.

The experiment was repeated with m·ReS^{X2} in an improved experimental setup, which was conducted as part of a bachelor thesis [46]. A C# program to sample the force-torque sensor was extended with a serial communication interface to read out the microcontroller measurements. Therefore, torque measurements and current can

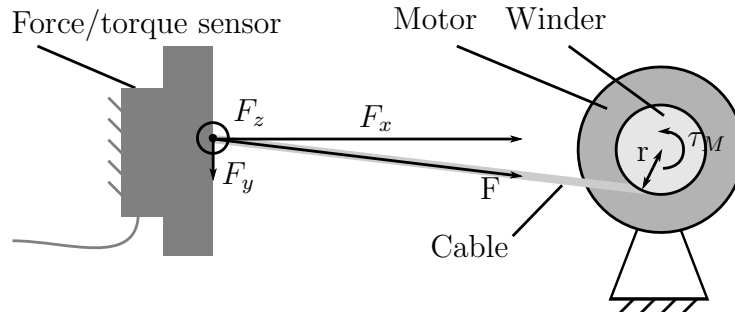


Figure 7.22: Experimental setup of the force control evaluation [196]

be compared with a higher sampling rate and in a synchronized way. The current was linearly increased from 0 V on until the maximum DAC voltage of 4 V is reached. To reduce temperature dependence of the shunt, a constantan resistor is used with a resistance of $0.54\ \Omega$. The torque was generated with a winder radius of 4 mm. Due to the greater winder radius and the weaker motor-gear combination, the maximum force is lower than in the experiment with $m\cdot\text{ReS}^{\text{X1}}$.

Figure 7.24 shows the current and the torque as a function of the time. To observe linearity and compare the results to the motor's torque constant from the datasheet, the current is plotted against the torque in Fig. 7.25. The higher amount of data gives more insights into the relation between current and torque. The overall accuracy is good with a RMSE of 0.3 N between the torque constant from the datasheet and the measured relation.

7.2.4.3 Discussion

The comparison of the open-loop step responses reveals that the different methods differ in the variance around the set point. The first method based on a patent [192] shows the highest fluctuations (Fig. 7.19) even with low-pass filtering with a similar cutoff frequency than the PWM method. It must be noted that the conversion factor between current and torque for the motor-gear combination in $m\cdot\text{ReS}^{\text{X1}}$ is higher than for $m\cdot\text{ReS}^{\text{X2}}$ with $183.2\ \text{mN m A}^{-1}$ and $34.8\ \text{mN m A}^{-1}$, respectively. Therefore, the torque would even fluctuate more. The PWM circuit (Fig. 7.20) shows better results than the first circuit. By far the best results are achieved with the third method, which is a simplified version of the first one. It shows an excellent open-loop response with very low variance around the setpoint. This is especially remarkably since the filter's cutoff frequency is around a hundred times higher. Although showing better behavior, the circuit needs less components than the patented one. However, both circuits were not optimized. With the use of electronic filters the difference in quality of the output signal is expected to decrease. The PWM circuit requires filtering for good results. This is more critical for $m\cdot\text{ReS}^{\text{X}}$ since the smaller motor and gear do not act as strong as a filter than for $m\cdot\text{ReS}^{\text{R2}}$, where this method is applied as well. Therefore, the third circuit is used for $m\cdot\text{ReS}^{\text{X}}$. Due to the quality and linearity, it

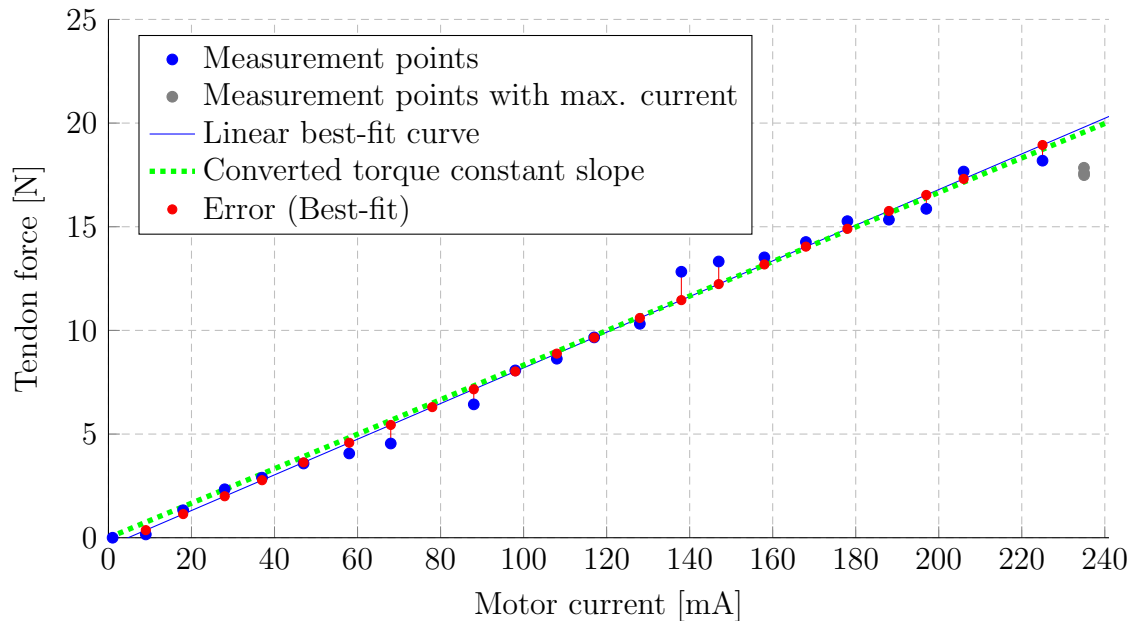


Figure 7.23: Relation between the armature current and the force on a FT sensor produced by the motor with the patented circuit [192]

may even be used in open-loop configuration without feedback of the current to the microcontroller. However, a software control of the DAC voltage may be used to influence the behavior of the plant.

Then it was observed, how the controlled current applied to the motor affected the force. The first patent-based circuit was used to test the force that is exerted of the controlled motor. The RMSE of 0.5937 N (3.3% of the 18 N range) or in comparison to the linear torque constant's slope is an acceptable error. Whereas in this experiment the current measurements were sampled a 100 times and averaged, which was not done in the second experiment with m·ReS^{X2}. Still, it achieved a RMSE of 0.306 N, which is around the same relative error (3.6% of the 8.5 N range). Furthermore, the higher amount of data points gives more information about the relation between current and torque. The maximum force can be adapted by changing the winder radius. However, decreasing the winder size, the disturbance caused by winding the tendon on the lever arm is higher. Several other variables influence the outcome of the experiment. For instance, the shunt resistor has a tolerance range, the circuit itself influences the measurement, and the motor's torque constant may deviate from the datasheet and also depends on the temperature. Despite many influencing factors, good measurement accuracy has been achieved, which justifies to omit an expensive, commercial force-torque sensor in this application.

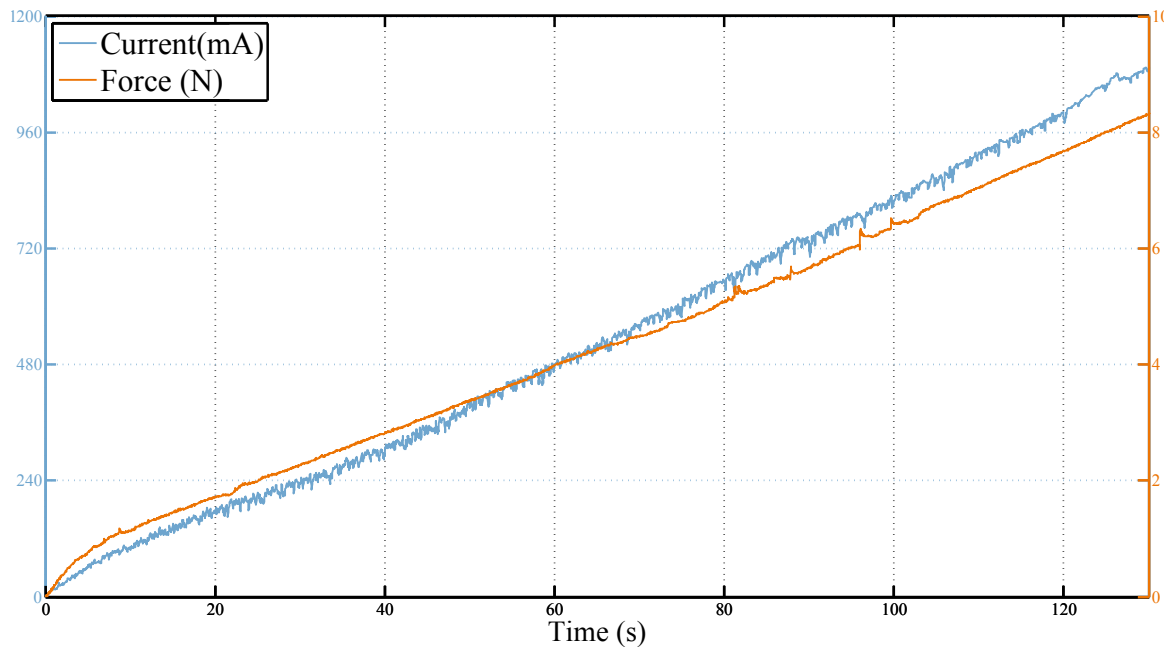


Figure 7.24: Current and force against the time to test the force control with $m\cdot\text{ReS}^{\text{X}2}$

7.2.5 Parametrization

This section evaluates the parametrization, which is used to create customized exoskeletons that fit to the user's hand. The parameters are taken manually by using a goniometer. The errors in the measurements and its influence on the parameterized exoskeleton shall be assessed. The parametrization is evaluated with $m\cdot\text{ReS}^{\text{X}2}$, which was parametrized to a female patient who suffered stroke in 2004. The hemiparesis lead to a loss of motor functions of the left upper limb. The functionality of her hand is impeded and muscle tone is increased. Especially, the little finger is affected. Additionally, the parametrization is tested on a healthy male subject.

The parametrization was evaluated in three different ways. First, a quantitative analysis of the parameters itself allows for conclusions about the error in the measurements itself. Then, the parameterized model was compared to a scan of the hand before printing. Finally, the print was qualitatively evaluated. Parts of the evaluation of the parametrization was conducted as part of a bachelor thesis [116].

7.2.5.1 Quantitive analysis of the parameter measurement

Two subjects obtained sets of parameters both from the healthy and the impaired hand of a stroke survivor. The average of both measurements of the impaired hand is used for the parametrization.

The standard deviation (SD) between the two subjects over all measurements allows for conclusions about the accuracy of the sampling process. The squared deviation

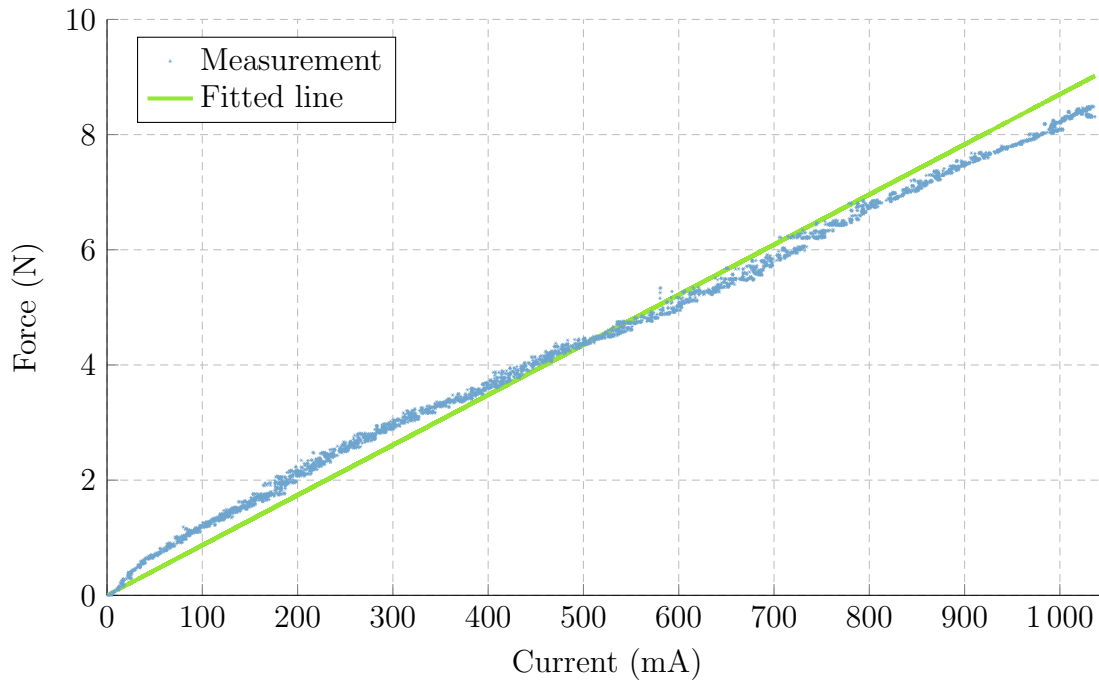


Figure 7.25: Force control experiment with m·ReS^{X2}: Force plotted against the current with a fitted line compared to the motor’s torque constant from the datasheet

from the mean for each pair of measurements was summed up and divided by the samples for both subjects resulting in SDs of 1.44 mm and 0.3 mm of the impaired hand and of the healthy hand, respectively.

Table 7.4 contains the measured values related to the base and table 7.5 measurements from the index finger of the impaired hand. The other fingers showed comparable or better results with lower SDs. The complete table including the measurements of the other fingers can be found in Appendix C.1.2. The measurements of the right unimpaired hand are stated in Appendix C.1.1.

The parameters of the exoskeleton for the healthy person are based on the same parameter measurements taken by five subjects. The boxplots in Fig. 7.26 visualize the deviations from the mean, summarized for the measurements of the dorsum, the fingers, and the thumb.

7.2.5.2 Qualitative evaluation using a visual 2D model overlay

Before printing the exoskeleton, a visual comparison between a projected 2D representation of the model and an image of the hand was used to estimate the functioning of the parametrization.

Table 7.4: Measured values in millimeters from the back of the hand of the left impaired hand of the stroke survivor. SD= standard deviation, W = wrist, IF = index finger, MF = middle finger, RF = ring finger, LF = little finger. The measurements with their abbreviations are visualized in Fig. 5.7.

	W-IF	W-MF	W-RF	W-LF	MCP: IF-MF	MCP: MF-RF	MCP: RF-LF	Width Wrist	Height Wrist	Width Hand	W-IF ulnar	W-LF radial
Back of the hand												
Subject 1	78.2	75.0	64.8	65.5	25.1	21.6	20.5	53.0	35.7	72.9	78.5	67.0
Subject 2	71.1	69.2	66.4	63.6	23.2	18.9	16.3	50.4	35.6	70.3	75.1	68.6
SD	3.55	2.9	0.8	0.95	0.95	1.35	2.1	1.3	0.05	1.3	1.7	0.8

The healthy hand was scanned, which was not possible for the impaired hand due to increased muscle tone. Therefore, an image was taken with a common digital camera from a top-down perspective manually pointed perpendicularly onto the impaired hand. A reference is necessary to resize the image to the same scale as the model. Therefore, a caliper with a known length between the tips placed next to the hand. Since the reference is close to the the hand, camera image distortion, tilts, and pans are expected to be marginal and, therefore, are neglected. The image was imported into the CAD program Solidworks laid under the 2D-drawing of the parameterized exoskeleton. Then, a line was drawn with the length of the caliper reference and the image was scaled until the caliper opening in the image corresponds to the length of the line. The overlay is shown in Fig. 7.28 for the stroke patient and for the healthy subject.

7.2.5.3 Discussion of the pre-print parametrization

Three ways of evaluation for the parametrization are presented. The first two, namely the quantitative analysis of the measurements and the visual overlay of a 2D representation of the model onto an image, give the possibility to assess the quality of the fitting before printing the exoskeleton. After the print, the exoskeleton can be donned to test the final fitting, which is described in the following section about the application experience.

The quantitative analysis of the stroke patient and the healthy subject widely overlap. For both, the standard deviations of the parameter measurements are acceptable, which was confirmed in the visual comparison. The strongest differences were found in the measurements of the dorsum. There, the measurement points to be gauged are not as clear to identify as the ones for the fingers. The center point of the wrist has to be determined by the subjects. The difference in this point is propagated to several measurements, increasing the deviations. In particular, the subjects interpreted the

Table 7.5: Measured values of the left impaired hand in millimeters. This table only exemplary states the parameters of the index finger (highest deviations compared to other fingers). The complete table with all measurements can be found in Appendix C.1.2. S1/S2 = measurements by subject 1/2, SD= standard deviation, W = wrist, IF = index finger, MF = middle finger, RF = ring finger, LF = little finger. The measurements with their abbreviations are visualized in Fig. 5.7.

	MCP-PIP	PIP-DIP	DIP-Tip	Width PIP	Height PIP	Width DIP	Height DIP	Height MCP
Index finger								
Subject 1	39.0	23.0	20.8	14.4	13.2	11.7	10.1	23.0
Subject 2	29.4	20.8	19.1	16.9	13.9	12.9	9.8	21.3
Mean	34.2	21.9	19.95	15.65	13.55	12.3	9.95	22.15
SD	4.8	1.1	0.85	1.25	0.35	0.6	0.15	0.85

position of the outer side of the metacarpal base differently. The boxplot representation of the measurements of the five subjects measuring the healthy person shows clearly that the dorsum showed the strongest deviations (Fig. 7.26). However, these parameters, responsible for the adaption of the exoskeleton's base, are not as critical as, for instance, the parameters for the joint distances.

The qualitative observation provides an additional evaluation of the functioning of the parametrization before printing the exoskeleton. It shows for both parametrizations that the parameter resulted in an exoskeleton that seems to fit. However, the method has some limitation due to the 2-dimensional representations. For instance, it is hardly visible that the little finger on the image was not completely extended due to increased tone. The strong deviations in comparison to the model seems to reveal a misfit. Moreover, the comparison reveals a shortcoming of the exoskeleton design. Although the new design reduced the material between the finger, the exoskeleton's middle and ring finger overlap. This means that the exoskeleton will still cause slight abduction of the fingers. Except for the little finger of the stroke patient, no apparent deviations could be recognized approving the exoskeletons to be printed.

7.2.6 Application Experience

This section describes successful elements of the design but also issues that were encountered during the use. This part inherently lacks quantitative measurements and is kept in descriptive form.

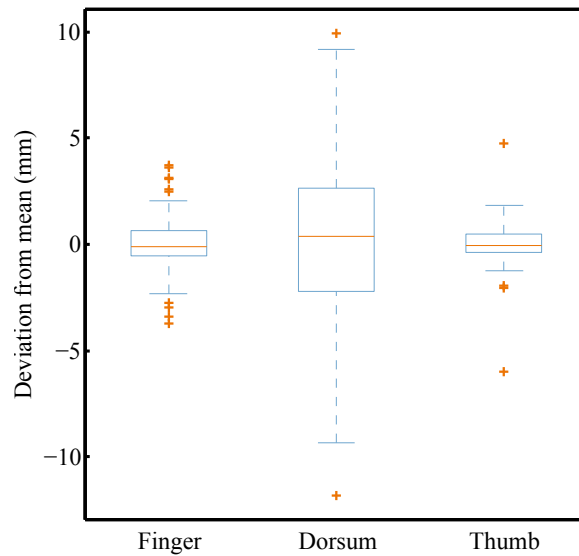


Figure 7.26: Boxplot of the deviation from the mean between five subjects measuring the parameters of a healthy subject

The parameterized exoskeleton was tried on a stroke patient (Fig. 7.27). In general, the good fit reconfirmed the pre-evaluation with the visual overlay and showed the functioning of the parametrization. One exception is the little finger, which did not fit as well as the other fingers and tended to slip out of the exoskeleton. The increased muscle tone, which was most prominent at this finger, is deemed to be most responsible for this misfit. This impeded both the measurement and the use.

The rerouting of the tendon over the index finger to the thumb module enabled the motors to support in pinching, which worked fairly well. However, it does not allow for extending the fingers, which is more important for most stroke patients including the one who tested it. Therefore, we used a soft ball for opening the hand and the motor to close it. The motor of m·ReS^{X2} was able to show the functioning, although it was slightly too weak to work against the softball. The motor-gear combination of m·ReS^{X2} is capable of exerting more torque and is expected to be sufficient. After the exercise, the patient noted that the opening distance between the fingers should be greater.

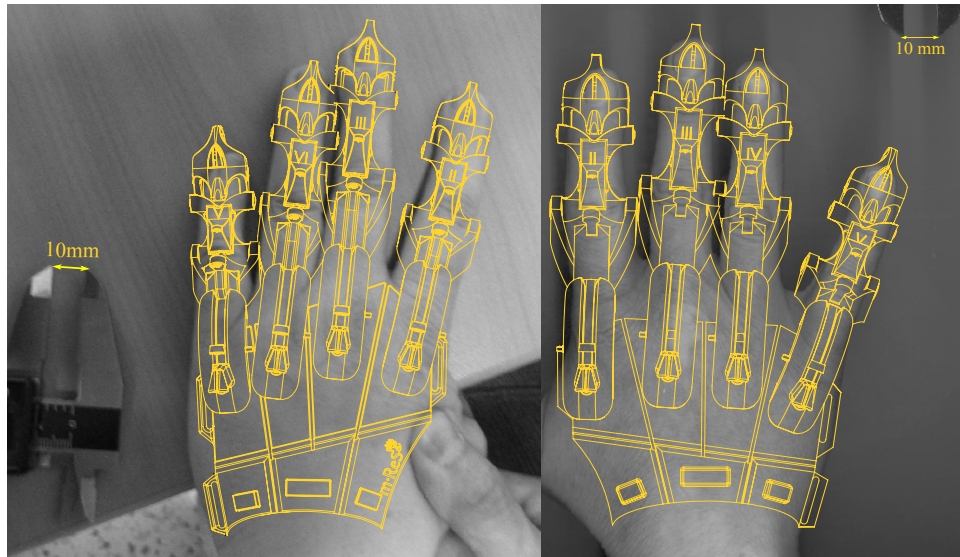
Without previous practice, the patient was asked to don the glove. Without giving help, she was able to do so in under four minutes. It is noteworthy that the glove used a preliminary velcro strap design in the test. Although the needed time is already low, improved fastening and practice in donning are expected to reduce the period.

The material of m·ReS^{X2} is reduced in comparison to m·ReS^{X1} in order to avoid interferences between the fingers and a bulky design. This must not cause breaking parts or bad structural integrity. In a short test, force was applied manually on the tendon until the hand of the patient was completely opened. High forces are necessary to work against the increased tone of the fingers but the exoskeleton did

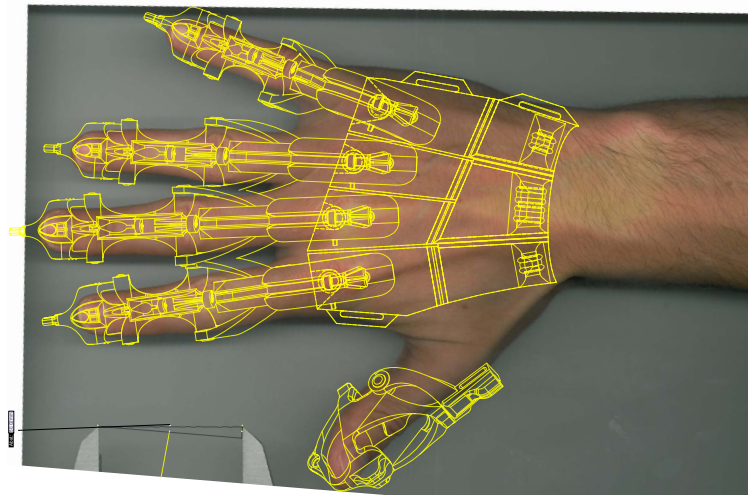


Figure 7.27: Patient wearing parameterized exoskeleton

not break. Only the guiding structures were not strong enough, which is why they have to be fortified for future versions. The test was repeated with the maximum forces of the motor with the same positive result. The weight including the sensors is below 100 g which is considered very lightweight [16].



(a) Left impaired hand © Springer (b) Right healthy hand of the stroke patient© Springer.



(c) Right hand of a healthy subject.

Figure 7.28: Comparison of the parametrized 2D model to an image of the impaired hand (a), to a scan of the right health hand of the stroke subject (b), and to the right hand of a healthy subejct including the thumb (c)

Chapter 8

Conclusion and future work

8.1 Conclusion

This thesis presents a rehabilitation system for training of forearm, wrist, and hand functions after stroke. The work encompasses the concept of the modular structure, the mechanical and hardware design, the electronics, the graphical user interface and low-level software, and the communication between them.

The literature review showed the benefits of robotic stroke rehabilitation but also revealed a lack of cost-effective systems and devices suitable for home rehabilitation. Since stroke leads to several different impairments of hand functions, a training system requires the training of different movements and exercises, which stands in contrast to the need for simpler, inexpensive systems [11]. In this work, the gap between multifunctional expensive devices and simple but limited device is bridged by proposing a modular approach. The proposed system distributes movement exercises on different components, which allows for the reduction of mechanical complexity of single modules, better serving customers' needs by providing optional components, and enabling simultaneous usage by different patients in a clinical setup. Furthermore, by changing the configuration of the devices, the training possibilities can be extended without additional cost. The modular approach and design of the system are unique and represent a valuable contribution to the field of rehabilitation robotics.

Despite different functionality, the modules show similarities and synergies. There are vast overlaps in software and communication architecture between both modules. The software is separated into a high-level part, which can run for instance on a PC, and a low-level code, flashed on a microcontroller. The high-level software, based on C++ and using the framework Qt, provides, among other things, the graphical user interface (GUI), exercises and games, and functionality for the rehabilitation paradigm visual feedback distortion. The low-level part includes sensor acquisition, actuation, and control. The communication architecture in between allows versatile access via serial commands and provides the freedom to use different software on almost any operating system that provides serial communication, either tethered or wireless via Bluetooth. The software incorporates telerehabilitation functionality, which is being developed parallelly in another work, giving therapists remote access to the measure-

ment data, and allowing them to change training parameters. To avoid the necessity for the end-user to provide a PC or other access device, the Raspberry Pi - a credit card-sized computer - represents an inexpensive and small alternative. The high-level software has been successfully compiled on a Raspberry Pi. This allows to provide an all-in-one bundle that only needs a screen to get started. Alternatively, potential clients can choose to use their own available computer and connect it to a less expensive version without a Raspberry Pi. This high flexibility may improve prospects of commercialization, but still has not been emphasized in the systems from related works.

Sensors are employed allowing for interactive applications, the study of rehabilitation paradigms, and the documentation of the training progress. In general, the measurements are range of motion (ROM) of joint angles and torque measured without expensive additional sensors. Actuators allow passive, active assisted, and active resistive training. By reusing the actuators of each module in different configurations, the training possibilities are extended without an increase in cost and complexity. The concept lead to a separation of the system into two major modules with several submodules, which are summarized in the following sections.

8.1.1 Training of rotational movements with the module

m·ReS^R

The first module (m·ReS^R) trains supination/pronation, dorsiflexion, and fine finger functions. It is designed as an end-effector with one degree of freedom (DOF) that is provided by a motor, assisting or resisting the patient's movements depending on the training mode. Its orientation relative to the forearm and the chosen handle determine the movement to be trained.

The module was developed in two iterations. The first iteration uses industrial motion solutions to quickly build a prototype to gain application experience as well as clinical and patient feedback. This version helped to provide new insights into friction and inertia compensation that improved the backdrivability of the device to facilitate patient-induced movements. Furthermore, it was applied to a study to test the just noticeable difference, which is an important property for the rehabilitation paradigm visual feedback distortion.

Based on feedback and experience, the second prototype was developed. The major improvements were the use of custom-made electronics for optimized sensing and actuation, and the implementation of low-level software on a microcontroller for faster control and more direct hardware access. Expensive force/torque sensors that diminish cost-efficiency and commercialization prospects were omitted. Torque measurement and control is based on the motor-inherent linear relation to the armature current. The performance evaluation revealed that the torque can be measured and controlled with a relative root-mean-square error of 2.15% in a range from 0 N m to 1.4 N m. This is a good result considering the reduction in cost by omitting a force-torque

sensor, which can cost several thousand euros. Therefore, it is feasible to replace expensive torque sensors with motor measurements without relinquishing torque control and measurement. However, closed-loop force control, necessary for admittance devices, is not possible.

Based on former work, m·ReS^R has been used to extend a haptic rehabilitation robot for shoulder and elbow reaching exercises developed at the Toronto Rehabilitation Institute (TRI), Canada. The extension derived from m·ReS^{R2} allowed for supination/pronation exercises and positioning of the wrist to improve the posture during reaching exercises. This extension demonstrates several benefits of the system. First, it exhibits modular properties since the m·ReS^{R2} module is not only useful as a stand-alone version, but can also be incorporated into another training device as a submodule. Second, the flexibility of the communication structure is underlined since no significant modifications on the microcontroller code were necessary, but still the system worked flawlessly together with a new high-level software.

The modularity of the system spans across several further submodules and optional components. As desired by therapists, a multitude of different handles can be attached, which are suited for specific training and allow adaption for the difficulty of grasping. A safety handle, which transmits torque around the motor axis but releases the grip when pulled back, has been developed at TRI and can also be employed for m·ReS^R. An additional component, called the Passive Mode Cube, can be plugged in to control the position of the motor. This is useful for hemiparetic patients, who can use their healthy hand to passively move the impaired one for mobilization.

m·ReS^R provides a cost-effective less complex rehabilitation system with functionality for use in home rehabilitation. It was designed for commercialization where a robust design with minimal moving parts plays an important role in affordability and life-cycle cost [150]. The design correlates with the current state of knowledge about rehabilitation robotics, which states that machines may have benefits in research, but highly sophisticated robotic devices may not yet be needed [148]. It is more portable than any device found in related works, which allows for the same exercises. The submodules allow for customization to fit the functionality to the users' needs. In contrast to most other systems, the cost is kept low for better commercialization prospects, for instance by replacing expensive force/torque sensors with optimized armature current-based torque measurements. These advantages underline the contributions of the design to the field of rehabilitation robotics.

8.1.2 Grasping and pinching trained with the exoskeleton m·ReS^X

The second module (m·ReS^X), in contrast to the above described device, is designed as an exoskeleton. The human hand is comprised of a multitude of joints and DOFs, making an exoskeleton inherently complex. Still, this work shows solutions for reducing the assembly effort, setup time, and potential cost. We apply 3D printing

to manufacture complex parts cost-effectively, particularly in small series, and with regard to the continuously falling prices of 3D printing.

One of the major problems of exoskeletons is misalignment with the anatomy. Other systems use either adaptation mechanisms that require a tedious fitting process [33, 181, 188], expensive aluminum or steel parts for each size to manufacture [201], or self-aligning systems that increase complexity, weight, and cost [30]. The application of 3D printing enables the introduction of parameters in the CAD model that control the dimensions of the single parts. Thus, the exoskeleton can be adapted to the patient's hand based on measurements of the anatomy. An exoskeleton was parameterized to a stroke patient and a healthy subject. To assess the parametrization before printing the exoskeleton, a novel two-fold pre-print evaluation has been developed. First the measurements of the hand size are compared quantitatively. Then, the visual 2D-overlay of the model is placed onto an image of the hand to examine the fitting qualitatively. Apart from minor misalignments of the little finger, the pre-evaluation was successful so that the exoskeleton was printed. The functionality of the parameterization was confirmed after the exoskeleton was tried on by the stroke patient. Only the little finger did not fit sufficiently and sometimes slipped out of the exoskeleton. However, this finger showed the strongest spasms which impeded both measurement and use. The patient was able to don the glove within five minutes without prior practice or help. This demonstrates self-dependent use, which is especially essential for home rehabilitation. The parametrization is unique and contributes to the design of exoskeletons. Although parametrization has been used before to some extent [25, 26], the parameters and other aspects are not described, and it has never been evaluated to this extent.

Actuators enable supporting or counteracting forces onto the fingers, providing haptic feedback and enhancing training possibilities. However, little space is available for actuators and their weight has a strong effect on performance and ergonomics. Therefore, tendon-based transmission is used to place the actuators remotely. This gives more flexibility in the way force is transmitted and exerted on the exoskeleton. Similar to m-ReS^R, the actuators are reused in different configurations. Instead of actuating each joint, the attachment point can be changed. This method simplifies the design, but requires additional effort to change the training modes and does not provide bi-directional movements within a session. This limitation is justified by the main focus of stroke therapy being on assistance in extension. The rerouting of the tendon over one of the fingers to the thumb allows for preliminary training of pinching movements, disregarding the complex anatomy of the thumb. The actuators assist in closing the grip by pulling the fingers together. A soft ball or similar objects can be used to assist in extension.

Three different types of sensors in m-ReS^X capture the joint angles and force on the fingers. Two types of joint angle sensors are based on the Hall-effect, either mapping the magnetic field of a rotating magnet in the joint to the respective angle, or measuring the rotary motion in combination with a multi-pole magnetic strip. Furthermore, the displacement of a cable guided over a joint can be measured with the

motor encoders and translated into a rotary motion. If a motor encoder is available, this technique can be used as an angle sensor, or it may be used to assess the accuracy of the other sensors. Potential customers can choose a combination of these sensors according to their needs and available funds. In several experiments with the different sensors, the highest root-mean square error observed was below 1.89° (MCP magnetic strip sensor: 2.7% in a range from 0° to 70°). To put this into perspective, even a specialized goniometer for joint angle measurements of the finger achieved a standard error of the measurement not below 3° at the PIP joint, and in the same study the traditional goniometer's minimum measurement error was 4.3° at the MCP joint [173]. These results are even biased towards lower errors since the standard error takes the sample size into account twice. More importantly, our results are below the 5° mean error limit accepted by the American Medical Association to consider the measurements reliable for the evaluation of movement impairments in a clinical context [206]. This good result is especially noteworthy regarding the relatively inexpensive hardware and the low manufacturing accuracy and strength of the 3D printing material.

The sensors may be employed for objective rehabilitation progress evaluation performed automatically and throughout the whole therapy. In comparison to traditional measurements, the sampling time is reduced drastically, since the application of a goniometer is omitted and the fingers can be measured simultaneously.

To reduce the number of the expensive motors but still allow independent finger training, a two-stage differential gear has been developed. A prototype demonstrated the functionality of the invention. After approval by the University of Lübeck and by the affiliated patent exploitation company, a patent application was submitted, which is pending.

8.2 Future Work

This work has proposed approaches and systems that extend the possibilities of robotic rehabilitation. The feasibility has been shown, but more extensive user tests and patient studies are yet to be carried out. Usability and applicability should be studied in the clinical as well as the home environment. We proposed to use the sensor data for objective progress evaluation. Correlation between robot-assisted measurements and standard clinical measures has been shown [29, 98]. Still, studies are necessary to translate the large quantities of sampled data into useful, consistent, reliable, and comprehensible information, and to evaluate the correlation with other scales (Section 2.3.4).

The technical side offers further space to extend and continue the project. The electronics of m-ReS use microcontrollers and sensor boards that facilitated the prototyping. The board could be redesigned, incorporating all the basic components on one board, and modularizing the circuit boards for optional components. For a com-

mercial product, the design has to be developed with regard to applicable regulations and norms.

The adaptation of $m\text{-ReS}^{\text{R2}}$ that extends Toronto Rehabilitation Institute upper limb robot has been incorporated into a study, which will provide valuable information about patient and therapist experiences in a clinical setting. This is particularly interesting since the results are transferable to $m\text{-ReS}^{\text{R2}}$. They provide valuable information about usability, issues in use, effectiveness of rehabilitation, and ideas for improvements.

Software functionality has been implemented to carry out studies on long-term rehabilitation success. A preliminary study with $m\text{-ReS}^{\text{R1}}$ identified the just noticeable difference (JND) between two stimuli of torque and angle, respectively, for supination/pronation movements of healthy subjects. Next, the study can be extended to the other movements trainable with $m\text{-ReS}$, and the JND of stroke patients can be identified and applied to the distortion of the visual feedback to verify the prospects of this rehabilitation paradigm. A future study would benefit from the higher accuracy and extended possibilities of $m\text{-ReS}^{\text{R2}}$.

The telerehabilitation functionality is planned to be further enhanced, allowing for more possibilities of interaction between therapists and patients. The motivation of the patients could be increased by giving them the possibility to compare their progress with other patients. The implementation of such a feature would be a valuable addition to the functionality. The system's capabilities have to be further evaluated, ideally by deploying devices in the home environment.

The complexity of $m\text{-ReS}^{\text{X}}$ offers possibilities for alternative designs and extensions of the functionality. The parametrization offered several advantages. However, the measurement process for parameter generation is time-consuming. The consequent step will be to automate this process, for instance, by using 3D scanners, or 2D scanners and a model to determine the missing parameters. Sanchez-Reillo et al. proposed biometric identification through hand geometry measurements [165]. The technique based on CCD camera images could be applied for parametrization. Magnetic resonance imaging scans would be more accurate due to direct measurements inside the anatomy and not indirect ones from the surface. Cost and availability is, however, an issue. The parametrization provides customized fitted exoskeletons for each patient, reducing misalignment, and omitting adaptation mechanisms. For studies and testing purposes, a set of parts based on generic hand sizes could avoid the need for customization for each user.

The design of the thumb has been rudimentarily implemented by attaching the cable at the thumb and routing it over the finger. No sensors are equipped but the tendon displacement could be used for getting a rough estimate on the performance. For this, it has to be calibrated, for instance, by measuring the displacement for the completely extended and the opposed position. Although a soft ball was used to assist in opening the hand, a stroke patient commented that the grasp was not opened enough. To overcome this issue and increase the training possibilities, the approach should be extended through the use of dedicated actuators, sensors, and

guiding structures. Modifications in the mechanical design could enable a configuration for assisting extension by pulling at the thumb from the palmar side of the hand. The functioning of the rerouting and application of forces has to be tested more intensively on patients with increased muscle tone to further assess the suitability of this approach.

The prototype of the patented differential gear demonstrated the functioning of the torque distribution of one motor onto four fingers. The mechanical design is built upon rapid prototyping for the proof of concept. Introducing bearings and the replacing of some of the plastic parts with metal would improve backdrivability and lead to a more functional device. Quantitative measurements could then examine the torque transfer behavior and the efficiency of the gear.

The graphical user interface allows access to the functionality of the system and gives exemplary games and exercises. However, it can be extended in many ways, including further training modes, games, and rehabilitation paradigms. Further exercises may particularly address activities of daily living, or apply recent findings about serious games [24].

The system can also be extended to other impairments such as tendon injuries of the hand. Continuous Passive Motion (CPM) systems may help to prevent the development of stiffness and edema, to reduce pain, and to improve range of motion following orthopedic surgery [77, 138, 191]. m·ReS^X limitation in actuating each joint may constrain the use in this application, while m·ReS^R provides CPM and may be suitable.

Appendix A

Abbreviations

ASCII American Standard Code for Information Interchange

CAD Computer-aided design

COM Communication port

CPM Continuous passive motion

DIP Distal interphalangeal joint

EMG Electromyography

FT Force/torque (sensor)

GPL GNU General Public License

GUI Graphical User Interface

IC Integrated circuit

LGPL GNU Lesser General Public License

MCP Metacarpophalangeal joint

PIP Proximal interphalangeal joint

OT Occupational therapist

PT Physical therapist

ROM Range of motion

sEMG surface electromyography

SLA Stereolithography

SPI Serial Peripheral Interface

SPP Serial Port Profile

UART Universal Asynchronous Receiver Transmitter

UL Upper limb

Appendix B

Command set for communication

Command	Function
BS	Enable/disable binary stream
CW+PWM	Rotate clockwise (PWM 0-255)
CCW+PWM	Rotate counterclockwise (PWM 0-255)
CCM	Current control mode
CCS	Calibrate current sensor
DI	Disable motor
DS	Data stream
EN	Enable motor
EXP	Mode for temporary experiments
GCC	Get parameters for current control
GDS	Get position, speed, torque, and timestamp sent together
GH	Get home position
GHD	Get home position in degree
GI	Get actual motor current
GIA	Get average motor current over five samples in ampere
GIL	Get current limit
GMS	Get max speed
GS	Get actual speed in degree per second
GSP	Get setpoint position
GP	Get actual position in encoder steps
GPD	Get actual position in degree
GT	Get actual torque
GV	Get voltage of current sensor
GVA	Get average voltage over five samples of current sensor
HS	Set home position
PH	Position here
PLL	Set position limit left
PLR	Set position limit right
PMM	Set passive motion mode
PMC	Set passive motion cube mode
PMF	Set passive motion frequency/speed

Command	Function
POM	Set position mode
POS	Set setpoint position in degree
PX	Get angular position and send it in the format t+position in degree+\n so that it can be filtered in the TRI upper limb reaching robot Java software
R	Reset
S	Stop
SIL	Set current limit
SMC	Set motor to coast
SMB	Set motor to brake
SP	Set setpoint position in encoder steps
SPD	Set setpoint position in degree
SPLD	Set position limits
SPLA	Activate position limits
SPLD	Deactivate position limits
T	Get timestamp
TX	Get torque and send it in the format t+ torque in mNm +\n, so that it can be filtered in the TRI upper limb reaching robot Java software
VS	Set virtual spring mode with current control with current setpoint depending on position displacement
VSC+number	Set virtual spring constant
VSP	Set virtual spring mode with a proportional controller of voltage (PWM) depending on the position deviation

Appendix C

Parametrization measurements

Abbreviations used in this chapter: W = wrist, IF = index finger, MF = middle finger, RF = ring finger, LF = little finger. The measurements with their abbreviations are visualized in Fig. 5.7. All measurements are in millimeters.

C.1 Stroke patient

C.1.1 Unimpaired right hand

Table C.1: Measured values from the back of the hand of the right unimpaired hand in millimeters of the stroke patient.

	W-IF	W-MF	W-RF	W-LF	MCP: IF-MF	MCP: MF-RF	MCP: RF-LF	Width Wrist	Height Wrist	Width Hand	W-IF ulnar	W-LF radial
Subject 1	62.0	57.0	55.6	55.3	25.1	20.5	22.7	55.5	33.8	77.6	69.1	57.6
Subject 2	67.7	62.0	61.5	61.2	24.5	21.1	22.0	57.7	37.4	78.0	72.2	61.8
Mean	64.8	59.5	58.5	58.2	24.8	20.8	22.3	56.6	35.6	77.8	70.6	59.7
Standard deviation	4.03	3.53	4.17	4.17	0.42	0.45	0.49	1.55	2.54	0.28	2.19	2.96

Table C.2: Measurements of the right unimpaired hand.

	MCP-PIP	PIP-DIP	DIP-Tip	Width PIP	Height PIP	Width DIP	Height DIP	Height MCP
Index finger								
Subject 1	39.0	21.7	21.3	15.9	14.9	13.7	12.1	23.1
Subject 2	46.7	25.0	22.3	16.5	15.0	14.6	11.4	23.6
Mean	42.8	23.3	21.8	16.2	14.9	14.1	11.7	23.3
Standard deviation	5.44	2.33	0.71	0.42	0.07	0.64	0.49	0.35
Middle finger								
Subject 1	43.8	28.0	20.3	15.5	14.9	13.3	11.3	23.5
Subject 2	46.2	26.2	22.8	16.1	15.2	14.2	11.3	25.8
Mean	45.0	27.1	21.5	15.8	15.0	13.7	11.3	24.6
Standard deviation	1.73	1.30	1.77	0.38	0.21	0.64	0.04	1.63
Ring finger								
Subject 1	42.0	26.3	24.0	14.7	14.1	13.1	10.8	21.9
Subject 2	39.4	22.9	23.7	15.2	14.2	13.5	11.0	21.6
Mean	40.7	24.6	23.8	14.9	14.1	13.3	10.9	21.7
Standard deviation	1.84	2.40	0.21	0.35	0.07	0.25	0.14	0.21
Little finger								
Subject 1	27.4	18.7	20.8	13.2	11.6	11.7	9.3	19.3
Subject 2	30.8	18.9	21.2	13.2	11.9	12.0	9.3	20.5
Mean	29.1	18.8	21.0	13.2	11.7	11.8	9.3	19.9
Standard deviation	2.37	0.11	0.29	0.00	0.21	0.18	0.00	0.85

C.1.2 Impaired left hand

Table C.3: Measured values of the left impaired hand in millimeters.

	MCP-PIP	PIP-DIP	DIP-Tip	Width PIP	Height PIP	Width DIP	Height DIP	Height MCP
Index finger								
Subject 1	39.0	23.0	20.8	14.4	13.2	11.7	10.1	23.0
Subject 2	29.4	20.8	19.1	16.9	13.9	12.9	9.8	21.3
Mean	34.2	21.9	19.95	15.65	13.55	12.3	9.95	22.15
Standard deviation	4.8	1.1	0.85	1.25	0.35	0.6	0.15	0.85
Middle finger								
Subject 1	42.4	25.2	21.8	14.7	13.2	12.5	10.6	22.7
Subject 2	44.0	26.5	17.9	15.8	14.4	13.3	12.6	22.0
Mean	43.2	25.8	19.8	15.2	13.8	12.9	11.6	22.3
Standard deviation	0.8	0.65	1.95	0.55	0.6	0.4	1	0.35
Ring finger								
Subject 1	37.6	21.4	21.6	14.4	13.0	12.4	10.0	20.4
Subject 2	41.5	25.0	23.6	14.9	12.6	12.1	9.2	22.2
Mean	39.5	23.2	22.6	14.6	12.8	12.2	9.6	21.3
Standard deviation	1.95	1.8	1	0.25	0.2	0.15	0.4	0.9
Little finger								
Subject 1	29.6	17.0	18.2	12.9	11.8	11.0	9.6	13.5
Subject 2	30.9	17.3	15.6	13.5	12.6	12.4	8.7	19.2
Mean	30.25	17.15	16.9	13.2	12.2	11.7	9.15	16.35
Standard deviation	0.65	0.15	1.3	0.3	0.4	0.7	0.45	2.85

C.2 Healthy subject

Table C.4: Measured values of the fingers of the right hand of a healthy subject in millimeters.

	MCP-PIP	PIP-DIP	DIP-Tip	Width PIP	Height PIP	Width DIP	Height DIP	Height MCP
Index finger								
Subject 1	41	26	22.5	18.65	19.9	14.6	11.45	26.8
Subject 2	47.8	28.5	22.2	18.6	17	14.7	11.4	26.2
Subject 3	45.17	27.27	20.71	20.03	17.17	16.02	12.82	27.48
Subject 4	45.37	27.26	20.93	17.93	16.2	14.37	10.93	25.29
Subject 5	44.35	23.84	19.95	19.04	16.38	14.99	10.93	26.84
Mean	44.738	26.574	21.258	18.85	17.33	14.936	11.506	26.522
Middle finger								
Subject 1	52.5	32.8	24.15	18.35	16.5	15.15	11.85	27.1
Subject 2	49.3	33.4	23.3	19.1	17.8	15.5	12.7	27.5
Subject 3	53.5	31.76	23.68	18.95	16.48	15.99	12.39	26.29
Subject 4	50.71	30.9	20.58	17.99	15.88	13.69	11.77	26.21
Subject 5	51.15	29.97	22.4	18.38	16.04	14.75	11.64	27.07
Mean	51.432	31.766	22.822	18.554	16.54	15.016	12.07	26.834
Ring finger								
Subject 1	49.25	31.6	22.9	17.5	14.75	12.15	10.7	24.65
Subject 2	51.5	32.6	23.6	19.1	15.2	14.4	10.9	25.8
Subject 3	46.47	29.3	23.23	18.5	16.2	14.72	12.33	25.33
Subject 4	45.53	30.28	22.16	17.4	16.07	12.68	10.43	23.89
Subject 5	46.58	26.69	20.58	17.53	14.49	13.71	10.8	24.87
Mean	47.866	30.094	22.494	18.006	15.342	13.532	11.032	24.908
Little finger								
Subject 1	39.2	25.85	21.85	15.05	13.5	12.95	10	22.1
Subject 2	36.1	23	20	15	13.6	13.2	10	25
Subject 3	35.47	21.59	20.43	14.75	14.06	14.15	10.91	23.97
Subject 4	34.12	21.01	19.78	14.07	13.48	12.1	9.52	22.91
Subject 5	35.59	19.17	19.66	14.65	13.22	13.7	9.51	23.11
Mean	36.096	22.124	20.344	14.704	13.572	13.22	9.988	23.418

List of Figures

2.1	Bones of the human hand [118]	10
2.2	Typical end-effector and exoskeleton. (a) End-effector Armeo Power [133] (b) Exoskeleton [141, 181]	13
4.1	Rendered image of the CAD draft of $m\cdot\text{ReS}^{\text{R1}}$	34
4.2	Horizontal and vertical orientation of the force-torque sensor	35
4.3	Relations between the motor current i , motor torque τ_{M} , torque constant k_{M} , gear ratio R_{G} , efficiency rate η , and torque output τ_{G}	38
4.4	$m\cdot\text{ReS}^{\text{R1}}$ motor suspension and electronics	40
4.5	Schematic for the motion controller with functionality for an extension module called Passive Motion Cube (Section 4.6.1)	41
4.6	Simplified schematic of the $m\cdot\text{ReS}^{\text{R2}}$ circuit focusing on the actuation. Connectors for the Passive Motion Cube, the motor encoder, power supply, and the navigation switch were omitted.	42
4.7	Mapping between current and velocity. The black curves were generated by increasing the velocity or current, respectively, and measuring the dependent variable and the grey curve by decreasing velocity or current [198] ©Springer.	44
4.8	Block diagram of the friction compensation	45
4.9	Image of $m\cdot\text{ReS}^{\text{R2}}$ in horizontal orientation for supination/pronation and vertical orientation for dorsiflexion and fine finger training.	46
4.10	$m\cdot\text{ReS}^{\text{R2}}$ input interface and connectors	47
4.11	Horizontal (l.) and vertical (r.) orientation of $m\cdot\text{ReS}^{\text{R2}}$ using the adjustable table	47
4.12	Extension modules and handles	48
4.13	$m\cdot\text{ReS}^{\text{R1}}$ motion controller	50
4.14	Bottom side and look inside of the extension module	52
4.15	(a) Final design of the extension module in use with the upper limb rehabilitation robot in the background; (b) Supination/pronation safety handle; (c) A close-up of the steel ball plunger release mechanism	53
5.1	Comparison of the bases of the two iterations	56
5.2	Joints of $m\cdot\text{ReS}^{\text{X1}}$ drawn into a rendered image [196] ©IEEE	57
5.3	New design of MCP joint of $m\cdot\text{ReS}^{\text{X2}}$ [197] ©Springer	57
5.4	Preliminary design of the thumb module	58
5.5	Both versions of $m\cdot\text{ReS}^{\text{X}}$	59

5.6	Blue lines: Parameters taken from anatomy. Orange lines: Additional general parameters where applicable. The parameters are sketched in for one finger only but are similar to the other fingers [196] ©IEEE. .	60
5.7	Orange arrows represent measurements for width and height, yellow ones the joint positions and link lengths [197] ©Springer	61
5.8	Attachment examples and actuation module	64
5.9	Example configurations with force vectors depicted with arrows . . .	65
5.10	Spring mechanism for motor-less exercises with m·ReS ^X	66
5.11	Different magnet orientations. Each curve represents another measurement. The upper right plot's orientation is 45°, the lower left one's 90° and the lower right one's 135° rotated in relation to the upper left one's orientation. The orientation used for m·ReS ^{X1} corresponds to the sensor output in the upper right graph.	68
5.12	Angle shift, calibration, and linearization	69
5.13	(a) Angle measurement based on Hall sensors that measure the magnetic field of a magnet in the joint of m·ReS ^{X1} ; (b) MCP joint sensor space.	70
5.14	Frames, links, and joints according to Denaviat-Hartenberg parameters. ⁰ P ₀ to ⁴ P ₄ are the tendon's deflection points. The trigonometric relations show assumptions and convention for the calculation of the linear joint extension.	72
5.15	No additional deflection point (left); threshold angle (center);; additional deflection point (right)	75
5.16	Influence of the conditional deflection point (CDP)	76
5.17	Simplified schematics for current measurement and limiting	77
5.18	Patented circuit for torque control. Adapted from [192]	78
5.19	Look inside of a single differential gear. Output and input torque can also be reversed.	79
5.20	Differential gear. Drive gear refers to normal mode of operation. . . .	80
5.21	Example configurations of the two-stage differential gear	84
6.1	Communication architecture	85
6.2	Interfaces of the different modules for communication between hardware and software. The Qt symbol indicates for which systems the framework has been implemented.	87
6.3	3D model in Blender	92
6.4	m·ReS ^R GUI screens: Performance tests and progress evaluation . . .	94
6.5	Visual feedback distortion related views	95
6.6	m·ReS ^X GUI screens of different exercises	95
6.7	Simple rehabilitation games. The first three games have been developed for m·ReS ^R , but m·ReS ^X can also be used as an input device. .	96
6.8	The graphical user interface developed for the TRI rehabilitation robot extension to be used in studies by the researchers	98

7.1	Experimental setup of the robot-driven evaluation of friction and inertia compensation [198] ©IEEE	102
7.2	Synchronized and merged data set of torque, velocity and position. Blue dash-dot line: Moving average without compensation; Grey points: Measuring points with friction and inertia compensation; Black solid line: Moving average of the friction and inertia compensation measuring points [198] ©IEEE.	103
7.3	Boxplots of the absolute difference of the torque over all measurements. A= acceleration (%); NC = no compensation; F = with friction compensation; FI = with friction and inertia compensation [198] ©IEEE	104
7.4	Mapping of the position control output to torque measurements. Green marker: Reference data; Green line: Fitted model; Red marker: Data set 2; Blue marker: Data set 3.	106
7.5	m·ReS ^{R2} Step response of the control voltage and measurement of the resulting amplified voltage over the shunt.	108
7.6	Comparison of force-torque to current measurements including the set-point trajectory with and without regarding the static friction. All currents are converted with the torque constant determined by the force-torque test [194] © ICST	109
7.7	Current measurements plotted against the force-torque sensor samples without compensation of friction effects. The red box indicates where the torque does not rise with the current.	110
7.8	Boxplot of the static friction experiment with the starting current of 100 runs in positive (1) and negative (2) direction	111
7.9	Distortion as a function of the percentage of the answers that claimed distorted.	117
7.10	Representative short session in virtual spring mode. [194] ©ACM	119
7.11	Automatic passive mode and bilateral exercise using the passive mode cube [195] ©Springer	120
7.12	Angle pattern	121
7.13	Measurements (dotted lines) of DIP (green), PIP (red) and MCP (blue) aligned to a pattern with 10° steps are compared to computed angles based on motor encoder measurements (solid lines)	122
7.14	Tendon length deviation between ideal and shifted coordinates (each joint axis 0.3 mm towards the base) for each joint angle of the index finger of m·ReS ^{X1} with the initial error (0.17 mm) for $\theta_{MCP,PIP,DIP} = 0^\circ$ set to zero	123
7.15	Definition of coordinate systems of m·ReS ^{X1}	124
7.16	Evaluation of the Hall effect angle sensor with an image-based comparison	125
7.17	Comparison of Hall effect to image-based angle measurements	126
7.18	Exemplary plot of one of four runs of the angular accuracy experiment assessing the MCP joint sensor	128
7.19	Step responses of a patented current limiter circuit	129

7.20	Step responses of pulse width modulation-based circuit	130
7.21	Step responses of the simplified DAC-controlled operational amplifier circuit	131
7.22	Experimental setup of the force control evaluation [196]	132
7.23	Relation between the armature current and the force on a FT sensor produced by the motor with the patented circuit [192]	133
7.24	Current and force against the time to test the force control with $m\cdot\text{ReS}^{\text{X}2}$	134
7.25	Force control experiment with $m\cdot\text{ReS}^{\text{X}2}$: Force plotted against the cur- rent with a fitted line compared to the motor's torque constant from the datasheet	135
7.26	Boxplot of the deviation from the mean between five subjects measur- ing the parameters of a healthy subject	138
7.27	Patient wearing parameterized exoskeleton	139
7.28	Comparison of the parametrized 2D model to an image of the impaired hand (a), to a scan of the right health hand of the stroke subject (b), and to the right hand of a healthy subejet including the thumb (c) . .	140

List of Tables

3.1	Overview of movements to be trained with the device	22
4.1	Absolute maximum forces and torques acting on a sensor during different grasps performed by three healthy subjects	35
5.1	DH parameters according to coordinate systems in Fig. 5.14. The asterisk marks variables.	73
7.1	Angle measurement accuracy	123
7.2	Hall effect based sensor evaluated with goniometer	123
7.3	Root-mean square error (RMSE) and maximum error of the angular accuracy experiment.	127
7.4	Measured values in millimeters from the back of the hand of the left impaired hand of the stroke survivor. SD= standard deviation, W = wrist, IF = index finger, MF = middle finger, RF = ring finger, LF = little finger. The measurements with their abbreviations are visualized in Fig. 5.7.	136
7.5	Measured values of the left impaired hand in millimeters. This table only exemplary states the parameters of the index finger (highest deviations compared to other fingers). The complete table with all measurements can be found in Appendix C.1.2. S1/S2 = measurements by subject 1/2, SD= standard deviation, W = wrist, IF = index finger, MF = middle finger, RF = ring finger, LF = little finger. The measurements with their abbreviations are visualized in Fig. 5.7. . .	137
C.1	Measured values from the back of the hand of the right unimpaired hand in millimeters of the stroke patient.	153
C.2	Measurements of the right unimpaired hand.	154
C.3	Measured values of the left impaired hand in millimeters.	155
C.4	Measured values of the fingers of the right hand of a healthy subject in millimeters.	i

Bibliography

- [1] ADAMOVICH, SERGEI V, GERARD G FLUET, ABRAHAM MATHAI, QINYIN QIU, JEFFREY LEWIS and ALMA S MERIANS: Journal of NeuroEngineering and Rehabilitation. Journal of neuroengineering and rehabilitation, 6:28, 2009.
- [2] AISEN, MINDY LIPSON, H IGO KREBS, NEVILLE HOGAN, FLETCHER MCDOWELL and BRUCE T VOLPE: The effect of robot-assisted therapy and rehabilitative training on motor recovery following stroke. Archives of Neurology, 54(4):443–446, 1997.
- [3] AKOSILE, CHRISTOPHER OLUSANJO, BABATUNDE AO ADEGOKE, OE JOHNSON et al.: Effects of Proprioceptive Neuromuscular Facilitation Technique on the Functional Ambulation of Stroke Survivors. Journal of Nigeria Society of Physiotherapy, 18(1-2):22–27, 2012.
- [4] ALLIN, SONYA, YOKY MATSUOKA and ROBERTA KLATZKY: Measuring just noticeable differences for haptic force feedback: implications for rehabilitation. In Haptic Interfaces for Virtual Environment and Teleoperator Systems, 2002. HAPTICS 2002. Proceedings. 10th Symposium on, pages 299–302. IEEE, 2002.
- [5] ALTMAN, JOSEPH: Are new neurons formed in the brains of adult mammals? Science, 135(3509):1127–1128, 1962.
- [6] ANDRINGA, AUKJE, INGRID VAN DE PORT and JAN-WILLEM MEIJER: Long-term use of a static hand-wrist orthosis in chronic stroke patients: a pilot study. Stroke research and treatment, 2013, 2013.
- [7] ANDRINGA, AUKJE S, INGRID GL VAN DE PORT and JAN-WILLEM G MEIJER: Tolerance and effectiveness of a new dynamic hand-wrist orthosis in chronic stroke patients. NeuroRehabilitation, 33(2):225–231, 2013.
- [8] ANG, KIAM HEONG, GREGORY CHONG and YUN LI: PID control system analysis, design, and technology. Control Systems Technology, IEEE Transactions on, 13(4):559–576, 2005.
- [9] ATES, SERDAR, JOAN LOBO-PRAT, PIET LAMMERTSE, HERMAN VAN DER KOOIJ and AH STIENEN: SCRIPT Passive Orthosis: Design and technical evaluation of the

- wrist and hand orthosis for rehabilitation training at home. In IEEE International Conference on Rehabilitation Robotics, volume 2013, pages 1–6, 2013.
- [10] BAHEUX, KENJI, MAKOTO YOSHIKAWA, AKIRA TANAKA, KAZUNORI SEKI and YASUNOBU HANDA: Diagnosis and rehabilitation of hemispatial neglect patients with virtual reality technology. *Technology and Health Care*, 13(4):245–260, 2005.
- [11] BALASUBRAMANIAN, SIVAKUMAR, JULIUS KLEIN and ETIENNE BURDET: Robot-assisted rehabilitation of hand function. *Current opinion in neurology*, 23(6):661–670, 2010.
- [12] BARRY, JONI G, SANDY A ROSS and JUDY WOEHRLE: Therapy incorporating a dynamic wrist-hand orthosis versus manual assistance in chronic stroke: A pilot study. *Journal of Neurologic Physical Therapy*, 36(1):17–24, 2012.
- [13] BENOWITZ, LARRY I and S THOMAS CARMICHAEL: Promoting axonal rewiring to improve outcome after stroke. *Neurobiology of disease*, 37(2):259–266, 2010.
- [14] BOHANNON, RICHARD W and MELISSA B SMITH: Interrater reliability of a modified Ashworth scale of muscle spasticity. *Physical therapy*, 67(2):206–207, 1987.
- [15] BONITA, R, AW STEWART and R BEAGLEHOLE: International trends in stroke mortality: 1970-1985. *Stroke*, 21(7):989–992, 1990.
- [16] BOUZIT, M., G. BURDEA, G. POPESCU and R. BOIAN: The Rutgers Master II-new design force-feedback glove. *Mechatronics, IEEE/ASME Transactions on*, 7(2):256–263, 2002.
- [17] BREWER, BAMBI R, MATTHEW FAGAN, ROBERTA L KLATZKY and YOKY MATSUOKA: Perceptual limits for a robotic rehabilitation environment using visual feedback distortion. *Neural Systems and Rehabilitation Engineering, IEEE Transactions on*, 13(1):1–11, 2005.
- [18] BREWER, BAMBI R., ROBERTA KLATZKY and YOKY MATSUOKA: Visual feedback distortion in a robotic environment for hand rehabilitation. *Brain Research Bulletin*, 75(6):804–813, 2008.
- [19] BREWER, BAMBI R., ROBERTA L. KLATZKY and YOKY MATSUOKA: Feedback distortion to overcome learned nonuse: A system overview. In Engineering in Medicine and Biology Society, 2003. Proceedings of the 25th Annual International Conference of the IEEE, volume 2, pages 1613–1616. IEEE, 2003.

-
- [20] BREWER, BAMBI R., ROBERTA L. KLATZKY and YOKY MATSUOKA: Visual-feedback distortion in a robotic rehabilitation environment. Proceedings of the IEEE, 94(9):1739–1751, 2006.
- [21] BROEREN, JURGEN, ANN BJORKDAHL, LISBETH CLAESSON, DANIEL GOUDE, A LUNDGREN-NILSSON, HANS SAMUELSSON, CHRISTIAN BLOMSTRAND, KATHARINA STIBRANT SUNNERHAGEN and MARTIN RYDMARK: Virtual rehabilitation after stroke. Studies in health technology and informatics, 136:77, 2008.
- [22] BROEREN, JURGEN, MARK DIXON, KATHARINA STIBRANT SUNNERHAGEN and MARTIN RYDMARK: Rehabilitation after stroke using virtual reality, haptics (force feedback) and telemedicine. Studies in health technology and informatics, 124:51, 2006.
- [23] BROEREN, JURGEN, MARTIN RYDMARK and KATHARINA STIBRANT SUNNERHAGEN: Virtual reality and haptics as a training device for movement rehabilitation after stroke: a single-case study. Archives of physical medicine and rehabilitation, 85(8):1247–1250, 2004.
- [24] BURKE, JAMES WILLIAM, MDJ MCNEILL, DARRYL K CHARLES, PHILIP J MORROW, JACQUI H CROSBIE and SUZANNE M McDONOUGH: Optimising engagement for stroke rehabilitation using serious games. The Visual Computer, 25(12):1085–1099, 2009.
- [25] BURTON, THOMAS MW, RAVI VAIDYANATHAN, STUART C BURGESS, AJ TURTON and CHRIS MELHUISH: Sensitivity Analysis of a Parametric Hand Exoskeleton Designed to Match Natural Human Grasping Motion. In Advances in Autonomous Robotics, pages 390–401. Springer, 2012.
- [26] BURTON, TMW, R VAIDYANATHAN, SC BURGESS, AJ TURTON and C MELHUISH: Development of a parametric kinematic model of the human hand and a novel robotic exoskeleton. In Rehabilitation Robotics (ICORR), 2011 IEEE International Conference on, pages 1–7. IEEE, 2011.
- [27] BÜTEFISCH, CATHRIN, HORST HUMMELSHEIM, PETRA DENZLER and KARL-HEINZ MAURITZ: Repetitive training of isolated movements improves the outcome of motor rehabilitation of the centrally paretic hand. Journal of the neurological sciences, 130(1):59–68, 1995.
- [28] CASE, LAUREN C and MARC TESSIER-LAVIGNE: Regeneration of the adult central nervous system. Current biology, 15(18):R749–R753, 2005.

- [29] CELIK, OZKAN, MARCIA K O'MALLEY, CORWIN BOAKE, HARVEY S LEVIN, NURAY YOZBATIRAN and TIMOTHY A REISTETTER: Normalized movement quality measures for therapeutic robots strongly correlate with clinical motor impairment measures. *Neural Systems and Rehabilitation Engineering, IEEE Transactions on*, 18(4):433–444, 2010.
- [30] CEMPINI, MARCO, STEFANO MARCO MARIA DE ROSSI, TOMMASO LENZI, MARIO CORTESE, FRANCESCO GIOVACCHINI, NICOLA VITIELLO and MARIA CHIARA CARROZZA: Kinematics and design of a portable and wearable exoskeleton for hand rehabilitation. In Rehabilitation Robotics (ICORR), 2013 IEEE International Conference on, pages 1–6. IEEE, 2013.
- [31] CHARNNARONG, JAIN, NEVILLE HOGAN, HERMANO I KREBS and ANDRE SHARON: Interactive robotic therapist, November 14 1995. US Patent 5,466,213.
- [32] CHIRI, AZZURRA, MARCO CEMPINI, STEFANO MARCO MARIA DE ROSSI, TOMMASO LENZI, FRANCESCO GIOVACCHINI, NICOLA VITIELLO and MARIA CHIARA CARROZZA: On the design of ergonomic wearable robotic devices for motion assistance and rehabilitation. In Engineering in Medicine and Biology Society (EMBC), 2012 Annual International Conference of the IEEE, pages 6124–6127. IEEE, 2012.
- [33] CHIRI, AZZURRA, FRANCESCO GIOVACCHINI, NICOLA VITIELLO, EMANUELE CATTIN, STEFANO ROCCELLA, FABRIZIO VECCHI and MARIA CHIARA CARROZZA: HANDEXOS: towards an exoskeleton device for the rehabilitation of the hand. In Intelligent Robots and Systems, 2009. IROS 2009. IEEE/RSJ International Conference on, pages 1106–1111. IEEE, 2009.
- [34] COHEN, STANLEY, RITA LEVI-MONTALCINI and VIKTOR HAMBURGER: A nerve growth-stimulating factor isolated from sarcom as 37 and 180. *Proceedings of the National Academy of Sciences of the United States of America*, 40(10):1014, 1954.
- [35] COLLIN, C and DT WADE: Assessing motor impairment after stroke: a pilot reliability study. *Journal of Neurology, Neurosurgery & Psychiatry*, 53(7):576–579, 1990.
- [36] COLLIN, C, DT WADE, S DAVIES and V HORNE: The Barthel ADL Index: a reliability study. *Disability & Rehabilitation*, 10(2):61–63, 1988.
- [37] CROSBIE, JH, S LENNON, JR BASFORD and SM MCDONOUGH: Virtual reality in stroke rehabilitation: still more virtual than real. *Disability & Rehabilitation*, 29(14):1139–1146, 2007.

-
- [38] CRUZ, EG, HC WALDINGER and DG KAMPER: Kinetic and kinematic workspaces of the index finger following stroke. *Brain*, 128(5):1112–1121, 2005.
- [39] DE WIT, LIESBET, KOEN PUTMAN, BIRGIT SCHUBACK, ARNOŠT KOMÁREK, FELIX ANGST, ILSE BAERT, PETER BERMAN, KRIS BOGAERTS, NADINE BRINKMANN, LOUISE CONNELL et al.: Motor and Functional Recovery After Stroke A Comparison of 4 European Rehabilitation Centers. *Stroke*, 38(7):2101–2107, 2007.
- [40] DENAVIT, JACQUES: A kinematic notation for lower-pair mechanisms based on matrices. *Trans. of the ASME. Journal of Applied Mechanics*, 22:215–221, 1955.
- [41] DESROSIERS, JOHANNE, RÉJEAN HÉBERT, ELISABETH DUTIL and GINA BRAVO: Development and reliability of an upper extremity function test for the elderly: the TEMPA. *Canadian Journal of Occupational Therapy*, 60(1):9–16, 1993.
- [42] DICKERSON, LORI M, PETER J CAREK and ROBERT GLEN QUATTLEBAUM: Prevention of recurrent ischemic stroke. *American family physician*, 76(3):382–388, 2007.
- [43] DIMYAN, MICHAEL A and LEONARDO G COHEN: Neuroplasticity in the context of motor rehabilitation after stroke. *Nature Reviews Neurology*, 7(2):76–85, 2011.
- [44] DOBKIN, BRUCE H: Rehabilitation after stroke. *New England Journal of Medicine*, 352(16):1677–1684, 2005.
- [45] DOVAT, LUDOVIC, OLIVIER LAMBERCY, ROGER GASSERT, THOMAS MAEDER, TED MILNER, TEO CHEE LEONG, ETIENNE BURDET et al.: HandCARE: a cable-actuated rehabilitation system to train hand function after stroke. *IEEE transactions on neural systems and rehabilitation engineering: a publication of the IEEE Engineering in Medicine and Biology Society*, 16(6):582, 2008.
- [46] EHLEBEN, IRA: Modularisierung der Steuereinheit eines haptischen Handschuhs zur Schlaganfallrehabilitation. Bachelor thesis, University of Lübeck, 2014. In preparation.
- [47] FISCHER, H.C., K. STUBBLEFIELD, T. KLINE, X. LUO, R.V. KENYON and D.G. KAMPER: Hand rehabilitation following stroke: a pilot study of assisted finger extension training in a virtual environment. *Topics in Stroke Rehabilitation*, 14(1):1–12, 2007.
- [48] FLUET, M-C, OLIVIER LAMBERCY and ROGER GASSERT: Upper limb assessment using a virtual peg insertion test. In *Rehabilitation Robotics (ICORR), 2011 IEEE International Conference on*, pages 1–6. IEEE, 2011.

- [49] FRISOLI, ANTONIO, FABRIZIO ROCCHI, SIMONE MARCHESCHI, ANDREA DETTORI, FABIO SALSEDO and MASSIMO BERGAMASCO: A new force-feedback arm exoskeleton for haptic interaction in virtual environments. In Eurohaptics Conference, 2005 and Symposium on Haptic Interfaces for Virtual Environment and Teleoperator Systems, 2005. World Haptics 2005. First Joint, pages 195–201. IEEE, 2005.
- [50] FUGL-MEYER, AXEL R, L JÄÄSKÖ, INGEGERD LEYMAN, SIGYN OLSSON and SOLVEIG STEGLIND: The post-stroke hemiplegic patient. 1. a method for evaluation of physical performance. Scandinavian journal of rehabilitation medicine, 7(1):13–31, 1974.
- [51] GLADSTONE, DAVID J, CYNTHIA J DANELLS and SANDRA E BLACK: The Fugl-Meyer assessment of motor recovery after stroke: a critical review of its measurement properties. Neurorehabilitation and Neural Repair, 16(3):232–240, 2002.
- [52] GOWLAND, CAROLYN, PAUL STRATFORD, MAUREEN WARD, JULIE MORELAND, WENDY TORRESIN, SANDRA VAN HULLENAAR, JULIE SANFORD, SUSAN BARRECA, BERNADETTE VANSPALL and NANCY PLEWS: Measuring physical impairment and disability with the Chedoke-McMaster Stroke Assessment. Stroke, 24(1):58–63, 1993.
- [53] GREGSON, JANINE M, MICHAEL LEATHLEY, A PETER MOORE, ANIL K SHARMA, TUDOR L SMITH and CAROLINE L WATKINS: Reliability of the Tone Assessment Scale and the modified Ashworth scale as clinical tools for assessing poststroke spasticity. Archives of physical medicine and rehabilitation, 80(9):1013–1016, 1999.
- [54] GRICE, KIMATHA OXFORD, KIMBERLY A VOGEL, VIET LE, ANA MITCHELL, SONIA MUNIZ and MARY ANN VOLLMER: Adult norms for a commercially available Nine Hole Peg Test for finger dexterity. American Journal of Occupational Therapy, 57(5):570–573, 2003.
- [55] HAMANN, G.F., MARIO SIEBLER and WOLFGANG VON SCHEIDT: Schlaganfall: Klinik-Diagnostik-Therapie Interdisziplinäres Handbuch. Ecomed Verlagsgesellschaft, 2002.
- [56] HAMILTON, B and C GRANGER: Guide for the use of the uniform data set for medical rehabilitation. Buffalo (NY): Research Foundation of State University of New York, 1990.
- [57] HANKEY, GRAEME J, KONRAD JAMROZIK, ROBYN J BROADHURST, SUSANNE FORBES and CRAIG S ANDERSON: Long-term disability after first-ever stroke and related prognostic factors in the Perth Community Stroke Study, 1989–1990. Stroke, 33(4):1034–1040, 2002.

-
- [58] HEISE, KIRSTIN-FRIEDERIKE, GIANPIERO LIUZZI, MAXIMO ZIMERMAN, CHRISTIAN GERLOFF and FRIEDHELM HUMMEL: Intensive orthosis-based home training of the upper limb leads to pronounced improvements in patients in the chronic stage after brain lesions. WCNR Vienna, A165, 2010.
- [59] HENDERSON, AMY, NICOL KORNER-BITENSKY and MINDY LEVIN: Virtual reality in stroke rehabilitation: a systematic review of its effectiveness for upper limb motor recovery. *Topics in stroke rehabilitation*, 14(2):52–61, 2007.
- [60] HESSE, S, C WERNER, M POHL, S RUECKRIEM, J MEHRHOLZ and ML LINGNAU: Computerized Arm Training Improves the Motor Control of the Severely Affected Arm After Stroke A Single-Blinded Randomized Trial in Two Centers. *Stroke*, 36(9):1960–1966, 2005.
- [61] HESSE, STEFAN, H KUHLMANN, J WILK, C TOMELLERI and STEPHEN GB KIRKER: Journal of NeuroEngineering and Rehabilitation. *Journal of neuroengineering and rehabilitation*, 5:21, 2008.
- [62] HESSE, STEFAN, GOTTHARD SCHULTE-TIGGES, MATTHIAS KONRAD, ANITA BARDELEBEN and CORDULA WERNER: Robot-assisted arm trainer for the passive and active practice of bilateral forearm and wrist movements in hemiparetic subjects. *Archives of physical medicine and rehabilitation*, 84(6):915–920, 2003.
- [63] HEUSCHMANN, PU, O BUSSE, M WAGNER, M ENDRES, A VILLINGER, J RÖTHER, PL KOLOMINSKY-RABAS and K BERGER: Schlaganfallhäufigkeit und Versorgung von Schlaganfallpatienten in Deutschland. *Akt Neurol*, 37:333–340, 2010.
- [64] HEYER, LARS: Entwicklung eines haptischen Handschuhs zum Training von Handfunktionen für die Schlaganfallrehabilitation. Master's thesis, University of Lübeck, 2012.
- [65] HOFFMAN, HENRY B and GLYN L BLAKEY: New design of dynamic orthoses for neurological conditions. *NeuroRehabilitation*, 28(1):55–61, 2011.
- [66] HOMETELEMED: ReJoyce. <http://www.hometelemed.com/rejoyce-workstation/>, 2014. Accessed: 2014-07-04.
- [67] HU, XIAO LING, KAI-YU TONG, RONG SONG, XIU JUAN ZHENG and WALLACE WF LEUNG: A comparison between electromyography-driven robot and passive motion device on wrist rehabilitation for chronic stroke. *Neurorehabilitation and Neural Repair*, 23(8):837–846, 2009.

- [68] HUQ, RAJIBUL, ELAINE LU, ROSALIE WANG and ALEX MIHAILIDIS: Development of a portable robot and graphical user interface for haptic rehabilitation exercise. In Biomedical Robotics and Biomechatronics (BioRob), 2012 4th IEEE RAS & EMBS International Conference on, pages 1451–1457. IEEE, 2012.
- [69] IN, HYUNKI, KYU-JIN CHO, KYURI KIM and BUMSUK LEE: Jointless structure and under-actuation mechanism for compact hand exoskeleton. In Rehabilitation Robotics (ICORR), 2011 IEEE International Conference on, pages 1–6. IEEE, 2011.
- [70] IQBAL, J., N. TSAGARAKIS and D. CALDWELL: Design of a Wearable Direct-driven Optimized Hand Exoskeleton Device. In ACHI 2011, The Fourth International Conference on Advances in Computer-Human Interactions, pages 142–146, 2011.
- [71] JACK, DAVID, RARES BOIAN, ALMA S MERIANS, MARILYN TREMAINE, GRIGORE C BURDEA, SERGEI V ADAMOVICH, MICHAEL RECCE and HOWARD POIZNER: Virtual reality-enhanced stroke rehabilitation. Neural Systems and Rehabilitation Engineering, IEEE Transactions on, 9(3):308–318, 2001.
- [72] JOHANSSON, RS and G WESTLING: Coordinated isometric muscle commands adequately and erroneously programmed for the weight during lifting task with precision grip. Experimental Brain Research, 71(1):59–71, 1988.
- [73] JOHNSON, MICHELLE J, XIN FENG, LAURA M JOHNSON and JACK M WINTERS: Potential of a suite of robot/computer-assisted motivating systems for personalized, home-based, stroke rehabilitation. Journal of NeuroEngineering and Rehabilitation, 4:6, 2007.
- [74] JOHNSON, MICHELLE J, RUI CV LOUREIRO and WILLIAM S HARWIN: Collaborative tele-rehabilitation and robot-mediated therapy for stroke rehabilitation at home or clinic. Intelligent Service Robotics, 1(2):109–121, 2008.
- [75] JONES, C.L., F. WANG, C. OSSWALD, X. KANG, N. SARKAR and D.G. KAMPER: Control and kinematic performance analysis of an Actuated Finger Exoskeleton for hand rehabilitation following stroke. In Biomedical Robotics and Biomechatronics (BioRob), 2010 3rd IEEE RAS and EMBS International Conference on, pages 282–287. IEEE.
- [76] JOO, LOH YONG, TJAN SOON YIN, DONALD XU, ERNEST THIA, PEI FEN CHIA, CHRISTOPHER WEE KEONG KUAH and KONG KENG HE: A feasibility study using interactive commercial off-the-shelf computer gaming in upper limb rehabilitation in patients after stroke. Journal of rehabilitation medicine, 42(5):437–441, 2010.

-
- [77] KAISER, R.T., G. TELEPKO, V. RICCI, R.J. DROZDOWSKI and B.C. KALUSTYAN: Continuous passive motion orthosis device for a limb, July 20 1993. US Patent 5,228,432.
- [78] KAMPER, DG and WZ RYMER: Impairment of voluntary control of finger motion following stroke: role of inappropriate muscle coactivation. *Muscle & nerve*, 24(5):673–681, 2001.
- [79] KAWASAKI, HARUHISA, S ITO, Y ISHIGURE, Y NISHIMOTO, T AOKI, T MOURI, H SAKAEDA and M ABE: Development of a hand motion assist robot for rehabilitation therapy by patient self-motion control. In Rehabilitation Robotics, 2007. ICORR 2007. IEEE 10th International Conference on, pages 234–240. IEEE, 2007.
- [80] KAWSAKI, HARUHISA, SATOSHI ITO, YUTAKA NISHIMOTO, HIROKI KIMURA and HIROYUKI HAYASHI: Hand rehabilitation support system based on self-motion-control. In Robotics and Automation, 2004. TExCRA'04. First IEEE Technical Exhibition Based Conference on, pages 55–56. IEEE, 2004.
- [81] KELLER, THIERRY and JOEL PERRY: Rehabilitation Robotics: From Expensive Tools for Specialized Hospitals towards Home and Tele-Rehabilitation Use. 2009.
- [82] KELLER, THIERRY, JOEL C PERRY, IGONE IDIGORAS LEIBAR, JUANMA BELDA and LLORENÇ SERVERA: TeleREHA: Investigation and development of rehabilitation platform for home use and tele-rehabilitation. In AALIANCE Conference, Malaga, Spain, 2010.
- [83] KERN, THORSTON A: Engineering haptic devices. Springer, 2009.
- [84] KIM, J.H., N.D. THANG and T.S. KIM: 3-d hand motion tracking and gesture recognition using a data glove. In Industrial Electronics, 2009. ISIE 2009. IEEE International Symposium on, pages 1013–1018. IEEE, 2009.
- [85] KINGSTON, BERNARD: Understanding joints: a practical guide to their structure and function. Nelson Thornes, 2000.
- [86] KOLLEN, BOUDEWIJN J, SHEILA LENNON, BERNADETTE LYONS, LAURA WHEATLEY-SMITH, MARK SCHEPER, JAAP H BUURKE, JOS HALFENS, ALEXANDER CH GEURTS and GERT KWAKKEL: The effectiveness of the bobath concept in stroke rehabilitation what is the evidence? *Stroke*, 40(4):e89–e97, 2009.

- [87] KOLOMINSKY-RABAS, PL, C SARTI, PU HEUSCHMANN, C GRAF, S SIEMONSEN, B NEUNDOERFER, A KATALINIC, E LANG, KG GASSMANN and TR VON STOCKERT: A prospective community-based study of stroke in Germanythe Erlangen Stroke Project (ESPRO) incidence and case fatality at 1, 3, and 12 months. *Stroke*, 29(12):2501–2506, 1998.
- [88] KOWALCZEWSKI, JAN, SU LING CHONG, MARY GALEA and ARTHUR PROCHAZKA: In-home tele-rehabilitation improves tetraplegic hand function. *Neurorehabilitation and neural repair*, 25(5):412–422, 2011.
- [89] KRAKAUER, JOHN W: Arm function after stroke: from physiology to recovery. In *Seminars in neurology*, volume 25, pages 384–395. [New York]: Thieme-Stratton Inc.,[c1981-, 2005.
- [90] KRAKAUER, JOHN W: Motor learning: its relevance to stroke recovery and neurorehabilitation. *Current opinion in neurology*, 19(1):84–90, 2006.
- [91] KREBS, H IGO, NEVILLE HOGAN, MINDY L AISEN and BRUCE T VOLPE: Robot-aided neurorehabilitation. *Rehabilitation Engineering, IEEE Transactions on*, 6(1):75–87, 1998.
- [92] KREBS, HERMANO IGO, BRUCE T VOLPE, DUSTIN WILLIAMS, JAMES CELESTINO, STEVEN K CHARLES, DANIEL LYNCH and NEVILLE HOGAN: Robot-aided neurorehabilitation: a robot for wrist rehabilitation. *Neural Systems and Rehabilitation Engineering, IEEE Transactions on*, 15(3):327–335, 2007.
- [93] KWAKKEL, GERT: Impact of intensity of practice after stroke: issues for consideration. *Disability & Rehabilitation*, 28(13-14):823–830, 2006.
- [94] KWAKKEL, GERT, BOUDEWIJN J KOLLEN, JEROEN VAN DER GROND and ARIE JH PREVO: Probability of regaining dexterity in the flaccid upper Limb Impact of severity of paresis and time since onset in acute stroke. *Stroke*, 34(9):2181–2186, 2003.
- [95] KWAKKEL, GERT, BOUDEWIJN J KOLLEN and HERMANO I KREBS: Effects of robot-assisted therapy on upper limb recovery after stroke: a systematic review. *Neurorehabilitation and neural repair*, 22(2):111–121, 2008.
- [96] KWAKKEL, GERT, ROLAND VAN PEPPEN, ROBERT C WAGENAAR, SHARON WOOD DAUPHINEE, CAROL RICHARDS, ANN ASHBURN, KIMBERLY MILLER, NADINA LINCOLN, CECILY PARTRIDGE, IAN WELLWOOD et al.: Effects of augmented exercise therapy time after stroke a meta-analysis. *Stroke*, 35(11):2529–2539, 2004.

-
- [97] LAMBERCY, O., L. DOVAT, R. GASSERT, E. BURDET, C.L. TEO and T. MILNER: A haptic knob for rehabilitation of hand function. *Neural Systems and Rehabilitation Engineering*, IEEE Transactions on, 15(3):356–366, 2007.
- [98] LAMBERCY, OLIVIER, LUDOVIC DOVAT, HONG YUN, SENG KWEE WEE, CHRISTOPHER KUAH, KAREN CHUA, ROGER GASSERT, THEODORE MILNER, TEO CHEE LEONG and ETIENNE BURDET: Robotic assessment of hand function with the HapticKnob. In Proceedings of the 4th International Convention on Rehabilitation Engineering & Assistive Technology, page 33. Singapore Therapeutic, Assistive & Rehabilitative Technologies (START) Centre, 2010.
- [99] LANGE, BELINDA, CHIEN-YEN CHANG, EVAN SUMA, BRADLEY NEWMAN, ALBERT SKIP RIZZO and MARK BOLAS: Development and evaluation of low cost game-based balance rehabilitation tool using the Microsoft Kinect sensor. In Engineering in Medicine and Biology Society, EMBC, 2011 Annual International Conference of the IEEE, pages 1831–1834. IEEE, 2011.
- [100] LANGHORNE, PETER, FIONA COUPAR and ALEX POLLOCK: Motor recovery after stroke: a systematic review. *The Lancet Neurology*, 8(8):741–754, 2009.
- [101] LEE, JOHANNA H VAN DER: Constraint-induced therapy for stroke: more of the same or something completely different? *Current opinion in neurology*, 14(6):741–744, 2001.
- [102] LEE, JOHANNA H VAN DER, VINCENT DE GROOT, HELEEN BECKERMAN, ROBERT C WAGENAAR, GUSTAAF J LANKHORST and LEX M BOUTER: The intra- and interrater reliability of the action research arm test: a practical test of upper extremity function in patients with stroke. *Archives of physical medicine and rehabilitation*, 82(1):14–19, 2001.
- [103] LI, JITING, SHUANG WANG, JU WANG, RUOYIN ZHENG, YURU ZHANG and ZHONGYUAN CHEN: Development of a hand exoskeleton system for index finger rehabilitation. *Chinese journal of mechanical engineering*, 25(2):223–233, 2012.
- [104] LIN, K-C, C-Y WU, T-H WEI, CHANG GUNG, C-Y LEE and J-S LIU: Effects of modified constraint-induced movement therapy on reach-to-grasp movements and functional performance after chronic stroke: a randomized controlled study. *Clinical Rehabilitation*, 21(12):1075–1086, 2007.
- [105] LLOYD-JONES, DONALD, ROBERT ADAMS, MERCEDES CARNETHON, GIOVANNI DE SIMONE, T BRUCE FERGUSON, KATHERINE FLEGAL, EARL FORD, KAREN FURIE, ALAN GO, KURT GREENLUND et al.: Heart disease and stroke statistics 2009

- update a report from the American Heart Association Statistics Committee and Stroke Statistics Subcommittee. *Circulation*, 119(3):e21–e181, 2009.
- [106] LLUCH, ALBERTO: Intrinsic causes of stiffness of the interphalangeal joints. Coopeland SA, Gschwend N, Landi A, Saphar Ph (eds). *Joint stiffness of the upper limb*. S Louis: Mosby, pages 259–64, 1997.
- [107] LO, ALBERT C, PETER D GUARINO, LORIE G RICHARDS, JODIE K HASELKORN, GEORGE F WITTENBERG, DANIEL G FEDERMAN, ROBERT J RINGER, TODD H WAGNER, HERMANO I KREBS, BRUCE T VOLPE et al.: Robot-assisted therapy for long-term upper-limb impairment after stroke. *New England Journal of Medicine*, 362(19):1772–1783, 2010.
- [108] LONGNION, J., J. ROSEN, M. SINANAN and B. HANNAFORD: Effects of geared motor characteristics on tactile perception of tissue stiffness. *Studies in health technology and informatics*, pages 286–292, 2001.
- [109] LOUREIRO, RUI, FARSHID AMIRABDOLLAHIAN, MICHAEL TOPPING, BART DRIESSEN and WILLIAM HARWIN: Upper limb robot mediated stroke therapy GENTLE/s approach. *Autonomous Robots*, 15(1):35–51, 2003.
- [110] LU, ELAINE C, ROSALIE WANG, RAJIBUL HUQ, DON GARDNER, PAUL KARAM, KARL ZABJEK, DEBBIE HÉBERT, JENNIFER BOGER and ALEX MIHAILIDIS: Development of a robotic device for upper limb stroke rehabilitation: A user-centered design approach. *Paladyn*, 2(4):176–184, 2011.
- [111] LU, ELAINE C, ROSALIE H WANG, DEBBIE HEBERT, JENNIFER BOGER, MARY P GALEA and ALEX MIHAILIDIS: The development of an upper limb stroke rehabilitation robot: Identification of clinical practices and design requirements through a survey of therapists. *Disability & Rehabilitation: Assistive Technology*, 6(5):420–431, 2011.
- [112] LUCAS, LENNY, MATTHEW DiCICCO and YOKY MATSUOKA: An EMG-controlled hand exoskeleton for natural pinching. *Journal of Robotics and Mechatronics*, 16:482–488, 2004.
- [113] LUM, PETER S, CHARLES G BURGAR, PEGGY C SHOR, MATRA MAJMUNDAR and MACHIEL VAN DER LOOS: Robot-assisted movement training compared with conventional therapy techniques for the rehabilitation of upper-limb motor function after stroke. *Archives of physical medicine and rehabilitation*, 83(7):952–959, 2002.

-
- [114] LUO, XUN, TIFFANY KLINE, HEIDI C FISCHER, KATHY A STUBBLEFIELD, ROBERT V KENYON and DEREK G KAMPER: Integration of augmented reality and assistive devices for post-stroke hand opening rehabilitation. In Engineering in Medicine and Biology Society, 2005. IEEE-EMBS 2005. 27th Annual International Conference of the, pages 6855–6858. IEEE, 2005.
- [115] MACIEJASZ, PAWEŁ, JÖRG ESCHWEILER, KURT GERLACH-HAHN, ARNE JANSEN-TROY, STEFFEN LEONHARDT et al.: A survey on robotic devices for upper limb rehabilitation. Journal of neuroengineering and rehabilitation, 11(3), 2014.
- [116] MÄNNEL, GEORG: Further Development of a Haptic Glove for the Rehabilitation of Hand function After Stroke. Bachelor thesis, University of Lübeck, 2014.
- [117] MARCHAL-CRESPO, L. and D.J. REINKENSMEYER: Review of control strategies for robotic movement training after neurologic injury. Journal of neuroengineering and rehabilitation, 6(1):20, 2009.
- [118] MARIANA RUIZ VILLARREAL, RETOUCHES BY NYKS: Scheme human hand bones (English). http://en.wikipedia.org/wiki/Hand#mediaviewer/File:Scheme_human_hand_bones-en.svg, 2014. Accessed: 2014-10-17.
- [119] MARIEB, ELAINE NICPON and KATJA HOEHN: Human anatomy & physiology. Pearson Education, 2007.
- [120] MARISSSEN, ROELOF et al.: Design with ultra strong polyethylene fibers. Materials Sciences and Applications, 2(05):319, 2011.
- [121] MASIA, L, HERMANO IGO KREBS, P CAPPÀ and N HOGAN: Design and characterization of hand module for whole-arm rehabilitation following stroke. Mechanics, IEEE/ASME Transactions on, 12(4):399–407, 2007.
- [122] MATHIOWETZ, VIRGIL, KAREN WEBER, NANCY KASHMAN and GLORIA VOLLAND: Adult norms for the Nine Hole Peg Test of finger dexterity. Occupational Therapy Journal of Research, 1985.
- [123] MATSUOKA, YOKY, SONYA ALLIN and ROBERTA KLATZKY: The tolerance for visual feedback distortions in a virtual environment. Physiology & behavior, 77(4-5):651–655, 2002.
- [124] MCDONNELL, MICHELLE: Action research arm test. Australian Journal of Physiotherapy, 54(3):220, 2008.

- [125] METZGER, J-C, OLIVIER LAMBERCY, DOMINIQUE CHAPUIS and ROGER GSSERT: Design and characterization of the ReHapticKnob, a robot for assessment and therapy of hand function. In Intelligent Robots and Systems (IROS), 2011 IEEE/RSJ International Conference on, pages 3074–3080. IEEE, 2011.
- [126] MICHAELSEN, STELLA MARIS, RUTH DANNENBAUM and MINDY F LEVIN: Task-specific training with trunk restraint on arm recovery in stroke randomized control trial. *Stroke*, 37(1):186–192, 2006.
- [127] MORROW, KIRA, CIPRIAN DOCAN, GRIGORE BURDEA and ALMA MERIANS: Low-cost virtual rehabilitation of the hand for patients post-stroke. In Virtual Rehabilitation, 2006 International Workshop on, pages 6–10. IEEE, 2006.
- [128] MULAS, MARCELLO, MICHELE FOLGHERAITER and GIUSEPPINA GINI: An EMG-controlled exoskeleton for hand rehabilitation. In Rehabilitation Robotics, 2005. ICORR 2005. 9th International Conference on, pages 371–374. IEEE, 2005.
- [129] MURRAY, CHRISTOPHER JL and ALAN D LOPEZ: Alternative projections of mortality and disability by cause 1990–2020: Global Burden of Disease Study. *The Lancet*, 349(9064):1498–1504, 1997.
- [130] NAKAYAMA, HIROFUMI, HE&K STIG JGTGENSEN, HANS OTTO RAASCHOU and TOM SKYHUJ OLSEN: Recovery of upper extremity function in stroke patients: the Copenhagen Stroke Study. *Age (SD)*, 74:11–2, 1994.
- [131] NAPIER, JOHN R: The prehensile movements of the human hand. *Journal of bone and joint surgery*, 38(4):902–913, 1956.
- [132] NEF, TOBIAS and PETER LUM: Improving backdrivability in geared rehabilitation robots. *Medical & biological engineering & computing*, 47(4):441–447, 2009.
- [133] NEF, TOBIAS and ROBERT RIENER: Three-Dimensional Multi-Degree-of-Freedom Arm Therapy Robot (ARMin). In Neurorehabilitation Technology, pages 141–157. Springer, 2012.
- [134] NGUYEN, MAI LINH EDITH: Integration, Optimization, and Evaluation of Sensors of a Parameterizable Exoskeleton. Bachelor thesis, University of Lübeck, 2014.
- [135] NOWAK, D.A.: The impact of stroke on the performance of grasping: usefulness of kinetic and kinematic motion analysis. *Neuroscience & Biobehavioral Reviews*, 32(8):1439–1450, 2008.

-
- [136] NOWAK, D.A.: The impact of stroke on the performance of grasping: usefulness of kinetic and kinematic motion analysis. *Neuroscience & Biobehavioral Reviews*, 32(8):441, 2008.
- [137] NOWAK, DENNIS A.: Handfunktionsstörungen in der Neurologie. SpringerLink : Bücher. Springer, 2011.
- [138] O DRISCOLL, SHAWN W and NICHOLAS J GIORI: Continuous passive motion (CPM): theory and principles of clinical application. *Journal of rehabilitation research and development*, 37(2):179–188, 2000.
- [139] OBLAK, JAKOB, IMRE CIKAJLO and ZLATKO MATJACIC: Universal haptic drive: A robot for arm and wrist rehabilitation. *Neural Systems and Rehabilitation Engineering, IEEE Transactions on*, 18(3):293–302, 2010.
- [140] OCCUPATIONAL THERAPISTS, CANADIAN ASSOCIATION OF. <https://www.caot.ca/default.asp?pageid=294>, 2014. Accessed: 2014-07-02.
- [141] OCKENFELD, C, RK TONG, EA SUSANTO, SK HO and XL HU: Fine finger motor skill training with exoskeleton robotic hand in chronic stroke: Stroke rehabilitation. In *IEEE International Conference on Rehabilitation Robotics*, volume 2013, 2013.
- [142] ORGANIZATION, WORLD HEALTH: World Health Report 2002: World Health Report: Reducing Risks to Health Noncommunicable Diseases. World Health Organization, 2002.
- [143] OTTENBACHER, KENNETH J, YUNGWEN HSU, CARL V GRANGER and ROGER C FIEDLER: The reliability of the functional independence measure: a quantitative review. *Archives of physical medicine and rehabilitation*, 77(12):1226–1232, 1996.
- [144] OTTENBACHER, KENNETH J, PAM M SMITH, SANDRA B ILLIG, RICHARD T LINN, GLENN V OSTIR and CARL V GRANGER: Trends in length of stay, living setting, functional outcome, and mortality following medical rehabilitation. *Jama*, 292(14):1687–1695, 2004.
- [145] PANG, XIAO-DONG, HONG Z TAN and NATHANIEL I DURLACH: Manual discrimination of force using active finger motion. *Attention, Perception, & Psychophysics*, 49(6):531–540, 1991.
- [146] PASCUAL-LEONE, ALVARO, AMIR AMEDI, FELIPE FREGNI and LOTFI B MERABET: The plastic human brain cortex. *Annu. Rev. Neurosci.*, 28:377–401, 2005.

- [147] PATOGLU, VOLKAN, GURDAL ERTEK, OZGUR OZ, DENIZ ZOROGLU and GUL KREMER: Design Requirements for a tendon rehabilitation robot: results from a survey of engineers and health professionals. In ASME 2010 International Design Engineering Technical Conferences and Computers and Information in Engineering Conference, pages 85–94. American Society of Mechanical Engineers, 2010.
- [148] PATTON, JAMES, STEVEN L SMALL and WILLIAM ZEV RYMER: Functional restoration for the stroke survivor: informing the efforts of engineers. Topics in stroke rehabilitation, 15(6):521–541, 2008.
- [149] PERNG, J.K., B. FISHER, S. HOLLAR and K.S.J. PISTER: Acceleration sensing glove (ASG). In Wearable Computers, 1999. Digest of Papers. The Third International Symposium on, pages 178–180. IEEE, 1999.
- [150] PERRY, JOEL C, HARITZ ZABALETA, AITOR BELLOSO and THIERRY KELLER: ARMassist: A low-cost device for telerehabilitation of post-stroke arm deficits. In World Congress on Medical Physics and Biomedical Engineering, September 7-12, 2009, Munich, Germany, pages 64–67. Springer, 2009.
- [151] PIGNOLO, L.: Robotics in neuro-rehabilitation. Journal of Rehabilitation Medicine, 41(12):955–960, 2009.
- [152] QUANSER: Rapid Control Prototyping software QuaRC. <http://www.quanser.com/QUARC>, 2014. Accessed: 2014-07-27.
- [153] RASHEDI, E, A MIRBAGHERI, B TAHERI, F FARAHMAND, GR VOSSOUGH and M PARNIANPOUR: Design and development of a hand robotic rehabilitation device for post stroke patients. In Engineering in Medicine and Biology Society, 2009. EMBC 2009. Annual International Conference of the IEEE, pages 5026–5029. IEEE, 2009.
- [154] REEVES, ALEXANDER G: Disorders of the nervous systems; a primer. 1981.
- [155] REHA-STIM: Bi-Manu-Track. <http://www.reha-stim.de/cms/index.php?id=60>, 2014. Accessed: 2014-09-04.
- [156] REINKENSMEYER, DAVID J, JEREMY L EMKEN and STEVEN C CRAMER: Robotics, motor learning, and neurologic recovery. Annu. Rev. Biomed. Eng., 6:497–525, 2004.
- [157] RINGELSTEIN, E BERND and DARIUS G NABAVI: Der ischämische Schlaganfall: eine praxisorientierte Darstellung von Pathophysiologie, Diagnostik und Therapie. W. Kohlhammer Verlag, 2007.

- [158] RIZZO, A., M. McLAUGHLIN, Y. JUNG, W. PENG, S.C. YEH and W. ZHU: Virtual therapeutic environments with haptics: An interdisciplinary approach for developing post-stroke rehabilitation systems. In International Conference on Computers for People with Special Needs (CPSN 05), 2005.
- [159] RIZZO, ALBERT and GERARD KIM: A SWOT analysis of the field of virtual reality rehabilitation and therapy. *Presence*, 14(2):119–146, 2005.
- [160] ROSENBAUM, DAVID A, CAROLINE M VAN HEUGTEN and GRAHAM E CALDWELL: From cognition to biomechanics and back: The end-state comfort effect and the middle-is-faster effect. *Acta psychologica*, 94(1):59–85, 1996.
- [161] ROSENBAUM, DAVID A, RUUD J MEULENBROEK, JONATHAN VAUGHAN and CHRIS JANSEN: Posture-based motion planning: applications to grasping. *Psychological review*, 108(4):709, 2001.
- [162] ROSENSTEIN, LIBBY, ANGELA L RIDGEL, ANIL THOTA, BRIDGETTE SAMAME and JAY L ALBERTS: Effects of Combined Robotic Therapy and Repetitive Task Practice on Upper-Extremity Function in a Patient With Chronic Stroke. *Therapy*, 62:000–000, 2008.
- [163] ROTH, WAYNE, STEFAN SANDER, MICHAL POLICHT, BRANDON FOSDICK, LIAM STASKAWICZ and DEHAO ZHANG: QextSerialPort. <http://code.google.com/p/qextserialport/>, 2014. Accessed: 2014-04-17.
- [164] RUFF, RONALD M and STEPHEN B PARKER: Gender-and age-specific changes in motor speed and eye-hand coordination in adults: normative values for the Finger Tapping and Grooved Pegboard Tests. *Perceptual and motor skills*, 76(3c):1219–1230, 1993.
- [165] SANCHEZ-REILLO, RAUL, CARMEN SANCHEZ-AVILA and ANA GONZALEZ-MARCOS: Biometric identification through hand geometry measurements. *Pattern Analysis and Machine Intelligence, IEEE Transactions on*, 22(10):1168–1171, 2000.
- [166] SAPOSNIK, GUSTAVO, MINDY LEVIN et al.: Virtual reality in stroke rehabilitation a meta-analysis and implications for clinicians. *Stroke*, 42(5):1380–1386, 2011.
- [167] SARAKOGLU, IOANNIS and SOPHIA KOUSIDOU: Exoskeleton-based exercisers for the disabilities of the upper arm and hand. *na*, 2007.
- [168] SCHABOWSKY, C.N., S.B. GODFREY, R.J. HOLLEY, P.S. LUM et al.: Development and pilot testing of HEXORR: hand EXOskeleton rehabilitation robot. *Journal of neuroengineering and rehabilitation*, 7(1):36, 2010.

- [169] SCHAECHTER, JUDITH D: Motor rehabilitation and brain plasticity after hemiparetic stroke. *Progress in neurobiology*, 73(1):61–72, 2004.
- [170] SCHILD, KATRIN: Zusammenführung und Erweiterung der grafischen Benutzeroberfläche des mRes-Projektes für die robotergestützte Schlaganfallrehabilitation. Bachelor thesis, University of Lübeck, 2014. In preparation.
- [171] SCHÜNKE, MICHAEL, ERIK SCHULTE and SCHUMACHER: Prometheus Anatomical Atlas for Students. General anatomy and musculoskeletal system. Thieme Medical Publishers, 2010.
- [172] SONODA, SHIGERU, EIICHI SAITOH, SHOTA NAGAI, MINAKO KAWAKITA and YOSHIKIYO KANADA: Full-time integrated treatment program, a new system for stroke rehabilitation in Japan: comparison with conventional rehabilitation. *American journal of physical medicine & rehabilitation*, 83(2):88–93, 2004.
- [173] STAM, HJ, MS ARDON, AH DEN OUDEN, TAR SCHREUDERS and ME ROEBROECK: The compangle: a new goniometer for joint angle measurements of the hand. *Eura Medicophys*, 42:37–40, 2006.
- [174] STERGIOPOULOS, P., P. FUCHS and C. LAURGEAU: Design of a 2-finger hand exoskeleton for VR grasping simulation. *Eurohaptics*, Dublin, Ireland, pages 80–93, 2003.
- [175] STIENEN, A.H.A., E.E.G. HEKMAN, F.C.T. VAN DER HELM and H. VAN DER KOOIJ: Self-aligning exoskeleton axes through decoupling of joint rotations and translations. *Robotics, IEEE Transactions on*, 25(3):628–633, 2009.
- [176] STRONG, K., C. MATHERS and R. BONITA: Preventing stroke: saving lives around the world. *The Lancet Neurology*, 6(2):182–187, 2007.
- [177] TAKAHASHI, C.D., L. DER-YEGHIAIAN, V. LE, R.R. MOTIWALA and S.C. CRAMER: Robot-based hand motor therapy after stroke. *Brain*, 131(2):425, 2008.
- [178] TAKAHASHI, CD, L DER-YEGHIAIAN, VH LE and SC CRAMER: A robotic device for hand motor therapy after stroke. In Rehabilitation Robotics, 2005. ICORR 2005. 9th International Conference on, pages 17–20. IEEE, 2005.
- [179] TAUB, EDWARD: Overcoming learned nonuse a new approach to treatment in physical medicine. In Clinical applied psychophysiology, pages 185–220. Springer, 1994.

-
- [180] TAUB, EDWARD and DAVID M MORRIS: Constraint-induced movement therapy to enhance recovery after stroke. *Current atherosclerosis reports*, 3(4):279–286, 2001.
- [181] TONG, KY, SK HO, PMK PANG, XL HU, WK TAM, KL FUNG, XJ WEI, PN CHEN and M CHEN: An intention driven hand functions task training robotic system. In *Engineering in Medicine and Biology Society (EMBC), 2010 Annual International Conference of the IEEE*, pages 3406–3409. IEEE, 2010.
- [182] TYROMOTION: Amadeo. <http://tyromotion.com/en/products/amadeo/overview>, 2014. Accessed: 2014-07-04.
- [183] TYROMOTION: Pablo. <http://tyromotion.com/en/products/pablo/overview>, 2014. Accessed: 2014-07-04.
- [184] TYSON, SARAH F and RUTH M KENT: The effect of upper limb orthotics after stroke: a systematic review. *NeuroRehabilitation*, 28(1):29–36, 2011.
- [185] VENEMAN, JAN FREDERIK: Design and evaluation of the gait rehabilitation robot LOPES. PhD thesis, Enschede, December 2007.
- [186] VOLPE, B.T., P.T. HUERTA, J.L. ZIPSE, A. RYKMAN, D. EDWARDS, L. DIPIETRO, N. HOGAN and H.I. KREBS: Robotic devices as therapeutic and diagnostic tools for stroke recovery. *Archives of neurology*, 66(9):1086, 2009.
- [187] VOOGD, JOCHEN: Weiterentwicklung eines haptischen Handschuhs mit Fokus auf der Implementierung einer Rehabilitationssoftware. Bachelor thesis, University of Lübeck, 2013.
- [188] WANG, JU, JITING LI, YURU ZHANG and SHUANG WANG: Design of an exoskeleton for index finger rehabilitation. In *Engineering in Medicine and Biology Society, 2009. EMBC 2009. Annual International Conference of the IEEE*, pages 5957–5960. IEEE, 2009.
- [189] WARD, NICK S and LEONARDO G COHEN: Mechanisms underlying recovery of motor function after stroke. *Archives of neurology*, 61(12):1844–1848, 2004.
- [190] WATTENBERG, MAXIMILIAN: Visual Feedback Distortion on Robotic Stroke Rehabilitation, 2013.
- [191] WEGE, ANDREAS, KONSTANTIN KONDAK and GÜNTER HOMMEL: Mechanical design and motion control of a hand exoskeleton for rehabilitation. In *Mechatronics and*

- Automation, 2005 IEEE International Conference, volume 1, pages 155–159. IEEE, 2005.
- [192] WEI, CHEN-KU: Torque control circuit for electrical motor, May 3 2011. US Patent 7,936,140.
- [193] WEISS, P., M. HELDMANN, T. MÜNTE, A. SCHWEIKARD and E. MAEHLE: A Rehabilitation System for Training Based on Visual Feedback Distortion. In Converging Clinical and Engineering Research on Neurorehabilitation, pages 297–302. Springer, 2013.
- [194] WEISS, PATRICK, ALEXANDER GABRECHT, M HELDMANN, T MÜNTE, A SCHWEIKARD and E MAEHLE: A Low Cost Tele-Rehabilitation Device for Training of Wrist and Finger Functions After Stroke. In 2nd ICTs for improving Patient Rehabilitation Research Techniques Workshop (8th International Conference on Pervasive Computing Technologies for Healthcare). 2013.
- [195] WEISS, PATRICK, ALEXANDER GABRECHT, MARCUS HELDMANN, ACHIM SCHWEIKARD and ERIK MAEHLE: A Cost-efficient Tele-Rehabilitation Device for Training Distal Upper Limb Functions After Stroke. In Communications in Computer and Information Science. Springer, 2014. To be published.
- [196] WEISS, PATRICK, LARS HEYER, THOMAS F MUNTE, MARCUS HELDMANN, ACHIM SCHWEIKARD and ERIK MAEHLE: Towards a parameterizable exoskeleton for training of hand function after stroke. In Rehabilitation Robotics (ICORR), 2013 IEEE International Conference on. IEEE, 2013.
- [197] WEISS, PATRICK, GEORG MÄNNEL, THOMAS MÜNTE, ACHIM SCHWEIKARD and ERIK MAEHLE: Parametrization of an Exoskeleton for Robotic Stroke Rehabilitation. In Replace, Repair, Restore, Relieve—Bridging Clinical and Engineering Solutions in Neurorehabilitation, pages 833–843. Springer, 2014.
- [198] WEISS, PATRICK, PATRICK ZENKER and ERIK MAEHLE: Feed-forward friction and inertia compensation for improving backdrivability of motors. In Control Automation Robotics & Vision (ICARCV), 2012 12th International Conference on, pages 288–293. IEEE, 2012.
- [199] WITYK, R.J. and R.H. LLINAS: Stroke. ACP key diseases series. American College of Physicians, 2007.

- [200] WOLF, STEVEN L, CAROLEE J WINSTEIN, J PHILIP MILLER, EDWARD TAUB, GINTENDRA USWATTE, DAVID MORRIS, CAROL GIULIANI, KATHYE E LIGHT, DEBORAH NICHOLS-LARSEN, EXCITE INVESTIGATORS et al.: Effect of constraint-induced movement therapy on upper extremity function 3 to 9 months after stroke: the EXCITE randomized clinical trial. *Jama*, 296(17):2095–2104, 2006.
- [201] WORSNOPP, TT, MA PESHKIN, JE COLGATE and DG KAMPER: An actuated finger exoskeleton for hand rehabilitation following stroke. In Rehabilitation Robotics, 2007. ICORR 2007. IEEE 10th International Conference on, pages 896–901. IEEE, 2007.
- [202] YAMAURA, HIROSHI, KOJIRO MATSUSHITA, RYU KATO and HIROSHI YOKOI: Development of hand rehabilitation system for paralysis patient—universal design using wire-driven mechanism—. In Engineering in Medicine and Biology Society, 2009. EMBC 2009. Annual International Conference of the IEEE, pages 7122–7125. IEEE, 2009.
- [203] YEONG, CHE FAI, ALEJANDRO MELENDEZ-CALDERON, ROGER GASSERT and ETIENNE BURDET: ReachMAN: a personal robot to train reaching and manipulation. In Intelligent Robots and Systems, 2009. IROS 2009. IEEE/RSJ International Conference on, pages 4080–4085. IEEE, 2009.
- [204] YOUNG, JAMES A and MARGARITA TOLENTINO: Neuroplasticity and its applications for rehabilitation. *American journal of therapeutics*, 18(1):70–80, 2011.
- [205] ZENKER, PATRICK: Implementierung einer Motoransteuerung mit visuellem Feedback und Reibungskompensation für den Einsatz in der Schlaganfallrehabilitation. Bachelor thesis, University of Lübeck, 2012.
- [206] ZHENG, HUIRU, NORMAN D BLACK and ND HARRIS: Position-sensing technologies for movement analysis in stroke rehabilitation. *Medical and biological engineering and computing*, 43(4):413–420, 2005.
- [207] ZIEGLER, JG and NB NICHOLS: Optimum settings for automatic controllers. *trans. ASME*, 64(11), 1942.